PHOSPHORUS AND SULFUR COSMOCHEMISTRY:

IMPLICATIONS FOR THE ORIGINS OF LIFE

by

Matthew Adam Pasek

_____

A Dissertation Submitted to the Faculty of the

DEPARTMENT OF PLANETARY SCIENCE

In Partial Fulfillment of the Requirements
For the Degree of

DOCTOR OF PHILOSOPHY

In the Graduate College

UNIVERSITY OF ARIZONA

2 0 0 6

THE UNIVERSITY OF ARIZONA
GRADUATE COLLEGE

As members of the Dissertation Committee, we certify that we have read the dissertation

prepared by Matthew Adam Pasek entitled Phosphorus and Sulfur Cosmochemistry:

Implications for the Origins of Life and recommend that it be accepted as fulfilling the

dissertation requirement for the Degree of Doctor of Philosophy

_____ Date: 04/11/2006
Dante Lauretta

_____ Date: 04/11/2006
Timothy Swindle

_____ Date: 04/11/2006
Alexander Pavlov

_____ Date: 04/11/2006
Neville Woolf

_____ Date: 04/11/2006
William Boynton

Final approval and acceptance of this dissertation is contingent upon the candidate's
submission of the final copies of the dissertation to the Graduate College.

I hereby certify that I have read this dissertation prepared under my direction and
recommend that it be accepted as fulfilling the dissertation requirement.

_____ Date: 04/11/2006
Dissertation Director:  Dante Lauretta

## STATEMENT BY AUTHOR

This dissertation has been submitted in partial fulfillment of requirements for an advanced degree at The University of Arizona and is deposited in the University Library to be made available to borrowers under rules of the Library.

Brief quotations from this dissertation are allowable without special permission, provided that accurate acknowledgment of source is made.  Requests for permission for extended quotation from or reproduction of this manuscript in whole or in part may be granted by the head of the major department or the Dean of the Graduate College when in his or her judgment the proposed use of the material is in the interests of scholarship.  In all other instances, however, permission must be obtained from the author.


SIGNED: _____
                        Matthew Adam Pasek

ACKNOWLEDGEMENTS

TABLE OF CONTENTS

TABLE OF CONTENTS- *Continued*

TABLE OF CONTENTS- *Continued*

LIST OF FIGURES

LIST OF TABLES

ABSTRACT

Phosphorus is a key element for life. This work reviews the role of phosphorus in life. Theories on the origin of life are confounded by a lack of reactive phosphorus, and attempts to overcome the dearth of reactive phosphorus must employ unrealistic phosphorus compounds, energetic organic compounds, or unusual physical conditions.

Meteoritic schreibersite provided an abundant source of reactive phosphorus for the early Earth. Water corrodes schreibersite to form a mixed valence series of phosphorus compounds. Schreibersite corrosion was studied by a variety of techniques, including NMR, MS, XRD, and EPR. Reduced phosphorus in schreibersite corrodes through release of phosphite radicals which react with other radicals to form the phosphorus compounds observed. These radicals are also capable of phosphorylating simple organic compounds to form P-C and P-O-C linkages.

The meteoritic mass flux was calculated using the mass frequency distribution of several meteorite collections. Much of the meteoritic mass that falls to the Earth is composed of metallic material which supplies abundant reactive phosphorus. Meteorites are a comparatively poorer source of carbon. Craters concentrate both reduced phosphorus and organic compounds through geomorphologic processes.

Phosphorus and sulfur biochemistry are intricately linked in metabolism. The cosmochemistry of sulfur was studied in depth using changing C/O ratios, sulfide formation kinetics, and gas diffusion. The results have implications for meteorites, studies of Jupiter, and of protoplanetary disks.

CHAPTER 1

INTRODUCTION

Phosphorus is the 15$^{th}$ element of the periodic table and was the first element to be discovered in modern times (1669) by the alchemist Hennig Brandt (Emsley 2000). Phosphorus has only one stable isotope with 15 protons and 16 neutrons, and its usual oxidation state is +5 on the surface of the Earth. The average crustal abundance of phosphorus is 750 ppm (Weaver and Tarney 1984, Wedepohl 1995) and its cosmochemical abundance is ~1000 ppm in CI chondrites and in the Sun (Wolf and Palme 2001). The nucleus of phosphorus has a spin of +½ and a strong dipole moment making nuclear magnetic resonance (NMR) spectrometry an effective method of chemical analysis for phosphorus and its salts. Phosphorus is referred to by its chemical symbol, P, throughout the remainder of this text, except where it is referred to at the beginning of a sentence.

Phosphorus is synthesized through stellar nuclear reactions, namely carbon burning:

$$^{12}C + {}^{12}C \rightarrow {}^{24}Mg^* \rightarrow {}^{23}Na + p \rightarrow {}^{23}Na\ (\alpha,p)\ {}^{26}Mg\ (\alpha,\gamma)\ {}^{30}Si\ (p,\gamma)\ {}^{31}P \qquad (1)$$
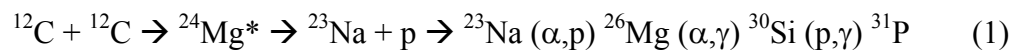
where * denotes an excited nuclear state, $\alpha$ is an alpha particle, p is a proton, and $\gamma$ is a gamma ray, and the nuclear processes are simplified by stating the particle added first followed by the particle lost in parentheses. Oxygen burning may form $^{31}P$:

$$^{16}O + {}^{16}O \rightarrow {}^{31}P + p \tag{2}$$

(Clayton 1988, Maciá et al. 1997), although O burning is followed by a host of secondary processes that remove P from the system.

In models of the early Solar System, P is present in the gas phase at temperatures above 1250 K for canonical Solar Nebula conditions. It forms a solid solution with Fe-Ni metal at lower temperatures. Finally phosphate minerals can form through subsequent oxidation of this metal. To summarize, the chemical history of P is complex and the oxidation states varies.

Throughout this dissertation I shall reference four different varieties of P that occur frequently in experimental systems: orthophosphate, reduced P compounds, condensed P compounds, and metallic P alloys.

The first compound, orthophosphate, $H_xPO_4^{-3+x}$, is the most abundant form of P on the surface of the Earth (species I, figure 1). When x is equal to 3, the compound is known as phosphoric acid, $H_3PO_4$. At a pH of 7, orthophosphate consists of nearly equal proportions of both $H_2PO_4^-$ and $HPO_4^{2-}$, and sodium salts of these two species are frequently used as a buffer to keep solutions at the physiologic pH of 7. The term "phosphate" is also used in this text and more generally refers to a $PO_4$ group, with linkages to other species (i.e., organophosphate). This compound is also referred to as "Pi".

The formal oxidation state of P in the reduced P compounds is less than 5. Examples include: hypophosphate, $P_2O_6^{4-}$ (P is +4), phosphite, $HPO_3^{2-}$ (P is +3), and hypophosphite, $H_2PO_2^-$ (P is +1). These species are shown as species II of figure 1.

Figure 1.  Molecular diagrams of phosphorus compound classes.

I.  Orthophosphate
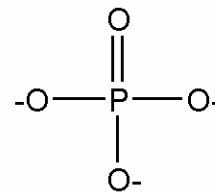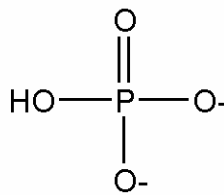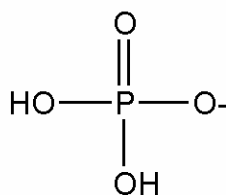


II.  Reduced Phosphorus Compounds
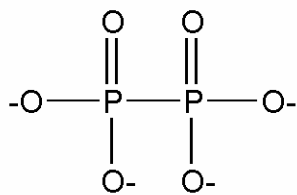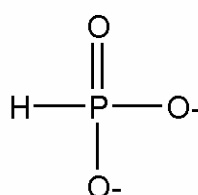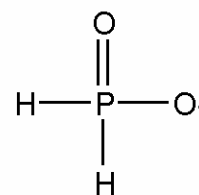


Hypophosphate        Phosphite        Hypophosphite

III.  Condensed Phosphorus Compounds
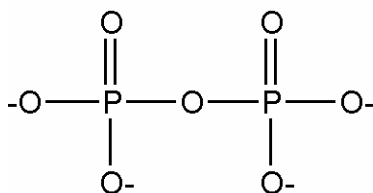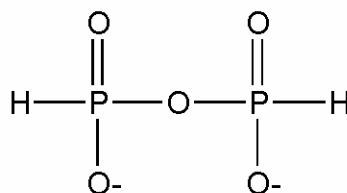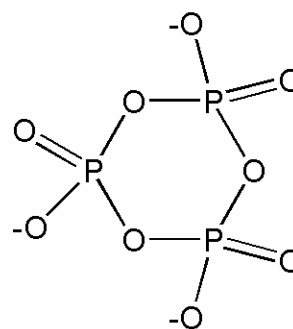


Pyrophosphate        Diphosphite        Trimetaphosphate
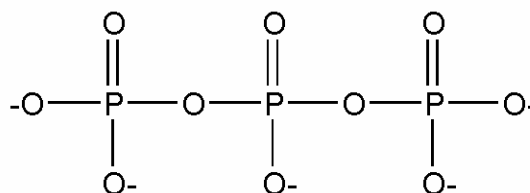


Triphosphate

Reduced P compounds are very rare on the surface of the Earth, though some are formed

through cellular biological reactions. Hypophosphate may also be referred to as "P4",

and phosphite referred to as "P3", following the nomenclature of Spikakov et al. (1999).

Note that this dissertation does not follow the recommendation of Spikakov et al. (1999)

for the compound $HPO_3^{2-}$. Spikakov et al. (1999), speaking as the voice of IUPAC, term

this compound H-phosphonate, whereas historically this compound is known as

phosphite (e.g., Van Wazer 1958). I follow the historic convention, and the term

"phosphonate" is reserved for compounds with C-P linkages.

Condensed P compounds are formed through the dehydration of protonated P

oxyacids. The P groups of condensed P compounds may consist of orthophosphate

and/or reduced P, depending on the starting material. An example of the synthesis of a

condensed phosphorus compound is the production of pyrophosphate from

orthophosphate:

$$O_3POH^{2-} + HOPO_3^{2-} \rightarrow O_3POPO_3^{4-} + H_2O \tag{3}$$
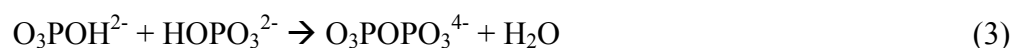
Examples of condensed P compounds are shown as species III of figure 1.

Pyrophosphate is also referred to as "PPi" in this text.

Metallic P alloys are a significant component of many meteorites and the main

mineral form of metallic P is schreibersite, $(Fe,Ni)_3P$. Other naturally occurring metallic

P alloys have different ratios of P to metal. Some have sulfur and silicon substituting for

P and others have titanium and chromium substituting for iron and nickel. The oxidation

state of P in metallic P alloy minerals is 0.

Other forms of naturally occurring P compounds include the gas phosphine, $PH_3$, which occurs in high pressure environments like Jupiter's atmosphere and perhaps in brown dwarfs (Fegley and Lewis 1980, Bjoraker et al. 1986), and biologic organic P compounds, which are detailed in this chapter. Still other forms of P molecules, including solid elemental P, do not occur naturally and are beyond the scope of this dissertation.

1.1 Phosphorus and Prebiotic Chemistry

Phosphorus is a key element in biology and understanding the chemistry of P on the early Earth provides insight into the origin of early biochemistry. This chapter will discuss the role of P in the origin of life and the "Phosphorus problem" as it relates to prebiotic chemistry. The phosphorus problem is especially problematic because phosphate and phosphorus have chemical properties that make them ideal for biochemistry. Phosphorus is ubiquitous in biochemistry due to these properties, and merits an overview of P biomolecules in modern biochemistry. Finally, this chapter will review and critique proposals regarding the prebiotic production of P biomolecules.

One of the most clearly elucidated pre-DNA biochemistries in the development of life is the so-called "RNA World." In the prebiotic chemistry / origins of life research community, "world" defines a biochemistry centered around a specific class of biomolecule or key inorganic component. Other "worlds" include the sugar world (Weber 2001), the thioester world (De Duve 1998), the iron-sulfur world

(Wachtershauser 1992), and the PAH (polycyclic aromatic hydrocarbon) world (Hazen 2005).  I will focus this discussion on the RNA world.

1.1.1 The RNA World

The RNA world refers to the biochemical world in which RNA was the genetic and catalytic molecule of life.  The RNA world comes in a two major forms, but has as its main premise that RNA preceded DNA and proteins as the genetic and catalytic material. The RNA world, like most prebiotic chemical models, suffers from a lack of reactive P, the so-called "phosphorus problem".  Reactive P is any P compound that is not in thermodynamic equilibrium with its surroundings, and on the surface of the Earth, P compounds other than orthophosphate may be considered to be reactive.  This phosphorus problem results from the geochemical behavior of P on the surface of the Earth.

The theoretical foundations of the RNA world consist of studies of ribozymes, or RNA enzymes, and genetic information transfer.  Drawing on analogies to the anthropic principle, there are two broad divisions in the origins of life community regarding the RNA world: the "weak" RNA world and the "strong" RNA world.  The first acknowledges that the RNA world preceded the DNA world, whereas the second states that the origin of life corresponds to the origin of the first self-replicating RNA molecule.

1.1.1.1 The "Weak" RNA World

The foundation of the weak RNA world is that RNA preceded DNA in biology and is based on the functions that RNA serves in modern biochemistry. Ribosomal peptide synthesis is a ribozyme catalyzed reaction (Kruger et al. 1982; Guerrier-Takada et al. 1983) and highlights the fact that certain RNA sequences can both catalyze biochemical reactions, essentially playing a similar role to proteins in modern biochemistry, and store genetic information (Cech et al. 1981). These discoveries have led many researchers to support the RNA-world model where early life used RNA for both its catalytic and informational functions (Crick 1968; Orgel 1968; Gilbert 1986). Furthermore, RNA replication is much simpler than DNA replication, involving fewer types of molecules. Cells produce DNA nucleotides from RNA nucleotides and RNA primers are required for initiation of DNA replication whereas enzymes that produce copies of RNA sequences do not require a primer. Based on these observations an RNA world is thought to have preceded the modern-day RNA / DNA / protein world that is the central dogma of molecular biology.

1.1.1.2 The "Strong" RNA World

The strong RNA world takes a more aggressive stance, arguing that the appearance of RNA or a related information-containing polymeric molecule signaled the origin of life. Under this hypothesis, the synthesis of an RNA strand proceeded through prebiotic

chemical reactions. Once formed, RNA strands provided the catalytic capabilities

necessary for rudimentary metabolism, and acted as the reproductive informational

macromolecule capable of natural selection and evolution, thus meeting the conditions

for being "alive" by most classical definitions. This view is popular because it offers a

simplified solution to the origin of life reducing to one the number of macromolecules

necessary to synthesize from prebiotic chemistry. It very clearly provides a definitive

starting point for the origin of life.

Orgel (2004) outlines the major steps that are required to establish a strong RNA-

world biotic system. The first step is synthesis of sugars, followed closely by the

formation of purine and pyramidine nucleoside bases. Then, nucleoside synthesis occurs

by linking the sugars, preferably ribose, with the nucleoside bases. Phosphorylation of

nucleosides must follow, forming the critical $P - O - C$ bond sequence, which links a

phosphate ion to the ribose molecule. Next, nucleotides are activated and subsequently

form long single-stranded polynucleotides. Some of these polynucleotides are then

converted to complementary double strands by template-directed synthesis. Ultimately

one of these double-stranded polynucleotides had to separate and copy itself and its

complement, yielding a second ribozyme molecule. Repetition of this process would lead

to an exponentially growing population, culminating in a system controlled by natural

selection.

The two steps in the RNA world that require phosphate include the initial

phosphorylation of nucleosides and the subsequent activation in preparation for

polymerization. Activated nucleotides consist of nucleotides with triphosphate groups

and drive polymerization to form RNA in vivo.   However, both steps involving

phosphate are especially complex chemical processes and require a variety of high-

energy intermediates.  Ultimately the prebiotic synthesis of these phosphorylated

compounds is difficult.  The difficulties associated with prebiotic phosphorylation are

detailed in the next section.

1.1.2 The "Phosphorus Problem"

Phosphorus is the limiting nutrient in most ecosystems (table 1).  In the rare ecosystem

where P is abundant, N is usually the limiting nutrient, followed by metal salts.  In the

marine ecosystem, C, N, and P are related to each other by the Redfield (1958) ratio, with

values of 106:16:1, respectively.  Phosphorus is much more prevalent in metabolic

processes, with a C:N:P ratio of 9.5:2:1, (Srinivasan and Morowitz 2004).  The metabolic

core of Srinivasan and Morowitz (2004) is the sum of metabolic processes common to all

organisms.  On the surface of the Earth P is limited by the geologic environment.  In most

ecosystems it predominantly forms orthophosphate minerals due to the significant

difference in energy between orthophosphate and all other varieties of condensed and

reduced P compounds.

Table 1.  Relative abundances of the biologic elements.  Abundances are normalized to 1 P atom. Cosmic abundances for H, N, S, and P are taken from Grevesse and Sauval (1998), with the C and O abundances from Prieto et al. (2001, 2002). Oceanic data are adapted from Lodders and Fegley (1998). Dry mass bacterial data is from Lange and Heijnen (2001). Metabolic core data is from Srinivasan and Morowitz (2004). Phospholipid data assumes a simple phospholipid species with two long chain carbon molecules minimal nitrogen.  RNA data assumes equal proportions of adenine, guanine, cytosine, and uracil.

| | Cosmic | Oceans | Bulk Bacteria | P-lipid | RNA | Metabolic Core |
|---|---|---|---|---|---|---|
| H | $2.8 \times 10^6$ | $4.9 \times 10^7$ | 203 | 90 | 10 | 15.4 |
| O | 1400 | $2.5 \times 10^7$ | 71.7 | 8 | 7 | 9 |
| C | 680 | 974 | 116 | 46 | 9.5 | 9.5 |
| N | 230 | 633 | 15.5 | 1 | 3.75 | 2 |
| S | 43 | 12,400 | 0.19 | 0 | 0 | 0.05 |
| P | 1 | 1 | 1 | 1 | 1 | 1 |

Phosphate mineralogy on Earth is best summarized as "apatite and variations thereof." Apatite is by far the most common orthophosphate mineral, with a chemical formula of $Ca_5(PO_4)_3(OH, F, Cl, HCO_3)$. Apatite is a ubiquitous mineral in all rock types, typically occurring at a fraction of a weight percent of the bulk rock. Other common phosphate minerals in the crust include vivianite, $Fe_3(PO_4)_2 \cdot 8H_2O$, which is formed primarily in aqueous systems, whitlockite, $Ca_9Mg(PO_4)_6OH$, and monazite, $ZPO_4$, where $Z$ is a trivalent rare earth element (Valsami-Jones 2004), both in pegmatites.

Most orthophosphate minerals are highly insoluble with very low solubility products ($K_{sp}$ values). Low $K_{sp}$ values imply that the concentration of P resulting from the dissolution of a mineral is minimal. The $K_{sp}$ of apatite is approximately $10^{-60}$ at a pH of 7 and temperature of 25°C, and the resulting dissolved orthophosphate concentration is $\sim 10^{-6}$ M. All other phosphate minerals are similarly insoluble, with phosphate concentrations approximately this order of magnitude. The orthophosphate concentration of some systems may be altered by addition of chelating agents (Schwartz 1972) or by decreasing the pH through addition of $CO_2$ (Kakegawa et al. 2002). In such systems, the total orthophosphate concentration may reach as high as $10^{-2}$ M, barring other influences.

Even with concentrations of orthophosphate as high as $10^{-2}$ M, the phosphorylation of organic compounds does not occur readily with orthophosphate. As an example, consider the phosphorylation of sugars, which is a fairly stable, low energy reaction. In order to phosphorylate a sugar to a yield of ~0.01% sugar-phosphate in water, an orthophosphate ($HPO_4^{2-}$) concentration of 0.1 M is necessary, higher than any geochemically plausible concentration.

Modern microorganisms overcome the low solubility of phosphate minerals by using acids on their environment to extract orthophosphate (e.g., Frossard et al. 1998) and utilize enzymes and metabolic reactions designed to incorporate P into biomolecules.

Early life did not have evolutionary adaptations and would have either depended on pre-existing organophosphates, or on reactive P capable of generating organophosphates. Given the dominance of P in the metabolic cycle (see table 1), in genetic material, and in membranes, it is unlikely that early life would completely "change horses" midway through, going from P-free life to P-dependent life. Accordingly there must have been prebiotic organophosphorus compounds or reactive P on the surface of the early Earth. The "phosphorus problem" is thus summarized as: Phosphorus is insoluble and unreactive on the Earth. How then did earliest life incorporate P into its biochemistry? Determining the origin of these compounds, guided by the constraints of geochemistry, is the "phosphorus problem."

1.2 Why Phosphorus?

Why are phosphate and P so important to life? What are the special characteristics of P that make it so suitable for biochemical molecules and reactions? What are some of the alternatives to P in biochemistry or in the origin of life? These issues have been explored by in depth by Westheimer (1987). Here I summarize Westheimer's argument, and discuss additional facets of P biochemistry.

1.2.1 Characteristics of Phosphorus and Phosphate

*Solubility.* Phosphate is water soluble in the absence of divalent cations.  Water is the most abundant solvent on the surface of the Earth and is the substance in which nearly all metabolic reactions must take place, hence all metabolic reactants must be water-soluble. Many organic compounds are phosphorylated upon entry into the cell membrane to increase solubility by adding a charged functional group.  For instance, adenine and adenosine are much less soluble in water than the phosphorylated equivalent of these molecules (table 2).  This is due primarily to the ionic character of the phosphate group in organophosphates.

*Ionization.*  Organophosphates are always negatively charged.  Ionization is necessary for biochemistry as ionic compounds do not diffuse through a membrane and are retained by the cell.  Negative ionization also serves a second purpose by preventing hydrolysis.  Hydrolysis occurs as the nucleophilic, or positive-charge seeking, oxygen in water bonds to an electrophilic, or negative-charge seeking center, which splits the molecule into two parts.  The charge on phosphate in organophosphates is localized around the phosphorus atom, and localized negative charges deter the negative oxygen in water from hydrolyzing the organophosphate bond.  Phosphate functional groups have the most negative charge of any functional group employed in biology, minimizing hydrolysis.

Table 2. Compound solubility in water.

| Compound | Solubility (mols/L) |
|---|---|
| Adenine[1] | 0.009 |
| Adenosine[1] | 0.020 |
| ATP[2] | 0.082 |

[1]Data from Rytting et al. (2005)
[2]Data from Roche Applied Science (2005/2006)

The acid-base characteristics of orthophosphate are related to the benefits of being ionized. Orthophosphate loses its first proton at a pH of ~2 but retains a proton up to a pH of ~13, which is superior to many organic acids. By retaining a proton, orthophosphate is active in dehydration reactions, encouraging phosphorylation.

*Energetics.* Organophosphates are ideal metabolic molecules due to the distinct electronic configuration of the phosphate group of organophosphates. Phosphorus biomolecules are typically thermodynamically unstable and will degrade to release energy. Much of this energy comes from the resonance stabilization of the two distinct molecules when an energetic P biomolecule is hydrolyzed. Metabolic reactions involving P biomolecules release intermediate amounts of energy. Compare the energy of hydrolysis of ATP with that of acetic anhydride (table 3). Acetic anhydride hydrolysis is very energetic, about three times as energetic, and not particularly useful for life.

As a side note, some P biomolecules are very energetic, like phosphoenol pyruvate. Others have very low energy, like the sugar phosphates. With an energy intermediate between these two biomolecules, ATP is particularly well-suited to its role as the energy currency of life. The metabolic breakdown of food takes place over several chemical steps. If the metabolic currency of life was a high-energy compound like phosphoenol pyruvate, then very few of these breakdown steps would provide the energy necessary to phosphorylate pyruvate. Conversely, if the metabolic currency was a low-energy compound like a sugar phosphate, the amount of energy extracted from each step would be low and catabolism would be a wasteful process. ATP is the happy intermediate between these two extremes, maximizing the energy extracted from each

Table 3.  Standard free energy of assorted compounds. With the exception of those species marked in bold, all reactions consist of loss of a $PO_3$ group.

| Name | Class | $\Delta G'^0$ (kJ/mol) |
| --- | --- | --- |
| Phosphoenol pyruvate | Phosphoenol | -61.9 |
| 1,3-bisphosphoglycerate | Phosphoacid Anhydride | -49.3 |
| Phosphocreatine | P-N compound | -43.0 |
| ADP | Condensed Phosphate | -32.8 |
| ATP | Condensed Phosphate | -30.5 |
| **ATP--> AMP + Pyrophosphate[1]** | Condensed Phosphate | -45.6 |
| AMP | Stable P Compound | -14.2 |
| Pyrophosphate | Condensed Phosphate | -19.2 |
| Glucose 1-phosphate | Stable P Compound | -20.9 |
| Fructose 1-phosphate | Stable P Compound | -15.9 |
| Glucose 6-phosphate | Stable P Compound | -13.8 |
| Glycerol 1-phosphate | Stable P Compound | -9.2 |
| **Acetyl CoA[2]** | Thioester | -31.4 |
| **Acetic Anhydride[3]** | Acid Anhydride | -91.1 |

Data from Nelson and Cox (2005) and references therein.  [1]This reaction is the loss of a pyrophosphate group from ATP.  [2] Acetyl-CoA has a S-C linkage which is hydrolyzed to form SH and HO-C; this reaction is discussed in chapter 5 of this dissertation.  [3]The hydrolysis of acetic anhydride forms two acetate groups.

step.  This preference for ATP is likely an evolutionary, post-origin-of-life adaptation due

to the complexity and specificity of ATP.  This issue is revisited in chapter 5.

*Kinetics.*  Despite the thermodynamic instability of many P biomolecules,

organophosphates are long-lived, or kinetically stable.  The kinetic stability of P

biomolecules is due to the hydrolysis-resistant negatively charged P group which repels

water, as discussed before.  Additionally, P biomolecules are resonance- stabilized which

allows for the sharing of electrons, increasing stability.  Finally, many P biomolecules are

stabilized by the presence of divalent cations, like $Mg^{2+}$.  Magnesium bonds to

orthophosphate and polyphosphate groups and reduces the space available for water to

attack the phosphate groups.

*Reactivity.*  Many metabolic reactions use phosphate groups to synthesize novel

compounds.   Reactions using phosphate groups are typically either substitution

reactions, in which phosphate is lost and replaced with another compound, or elimination

reactions, in which phosphate is lost and removes nearby functional groups in the

process.  Westheimer (1987) provides a few examples of both reactions, including the

decarboxylation (elimination) below:

$$
\begin{array}{ccc}
\underset{\underset{\underset{\underset{H_2C-O-P_2O_6^{4-}}{|}}{CH_2}}{\overset{\overset{\overset{\overset{COO^-}{|}}{CH_2}}{|}}{^{2-}O_3PO-C-CH_3}}} & \xrightarrow{\quad CO_2,\ PO_4^{3-}\quad} & \underset{\underset{\underset{\underset{H_2C-O-P_2O_6^{4-}}{|}}{CH_2}}{\overset{\overset{\overset{CH_2}{\parallel}}{C-CH_3}}{}}}{}
\end{array}
\tag{4}
$$
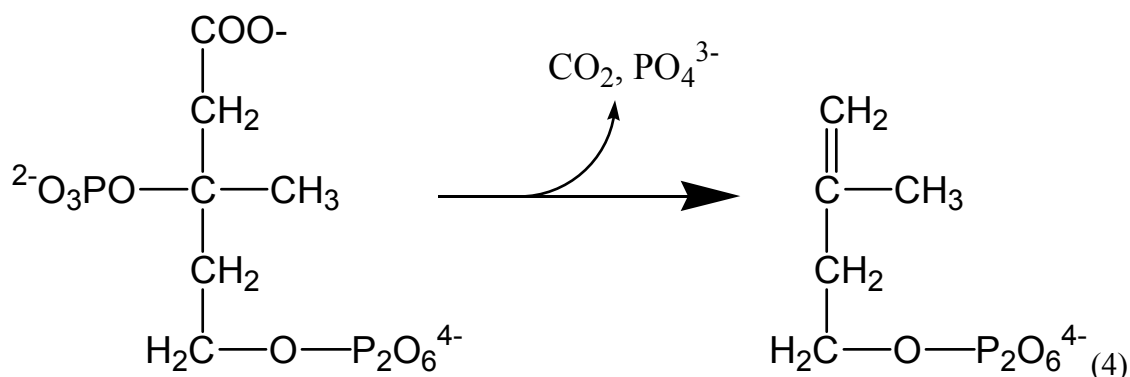
Reactions such as these demonstrate that phosphate is the leaving group for many metabolic reactions. Thus phosphate is used in biosynthetic pathways to change the chemical characteristics of molecules.

*Site Specificity*. Phosphate groups are easily recognized by enzymes since they bond strongly to divalent cations like $Mg^{2+}$. Enzymes that act on phosphates incorporate $Mg^{2+}$ into their structure and use the Mg/phosphate linkage as a spatial point of reference from which a chemical reaction occurs.

*Bridges*. The bridging capability of P is especially important to DNA and RNA. Orthophosphate is capable of forming two C-O-P linkages while still retaining a charge. This ensures that the genetic material is kept within a specific biologic location, like the nucleus, in the case of eukaryotes. Repeating these bridges forms a large polymer which contains the information necessary for life's functions.

*Achirality*. The orthophosphate functional group is achiral even when bound to one or two organic groups. Achiral fuctional groups minimize the information necessary for the construction or destruction of an organic molecule. With RNA and DNA, it is unimportant how the orthophosphate groups are connected, which is advantageous given the stereospecificity of the ribose and nucleobase. A lower information requirement for metabolic reactions is always advantageous as it minimizes the variation needed for enzymes and decreases the side products from biochemical reactions.

*Uniform Oxidation State*. P is nearly always $P^{5+}$ on the surface of the Earth, with the minor exception of the P-C organic compounds. Other elements change oxidation state depending on atmospheric composition, ocean depth, fluid composition, and

temperature.  Phosphorus is uniformly +5 below temperatures of about 1000 K and in the presence of water when the system is in thermodynamic equilibrium.  This is true even under mildly reducing conditions like those hypothesized on the early Earth (and used by Miller and Urey in 1953 to form organics from the atmosphere).

*Terrestrial distribution.* The only readily available compound with the chemical characteristics described above is orthophosphate.  As previously stated, P is the limiting nutrient for life and the terrestrial prebiotic system.  However, orthophosphate in all its forms is the most abundant species with the features described above.  Due to the centrality of P in biochemistry, many modern microorganisms have evolved to extract P from their surroundings, frequently at the cost of metabolic energy.  Since P is an ubiquitous minor element in most rocks, life is not limited to specific localities and is capable of diversifying.

Other elements and molecules may be similar or even superior to P for a specific feature, but the sum of the beneficial characteristics of P far outweighs those of its competitors.  Alternatives to P in biology are discussed by Westheimer (1987) and have been further discussed by other more recent works.  I will now address the alternatives to P in biology.

1.2.2 Alternatives to Phosphorus in Biological Systems

Hypothetical alternatives to P have traditionally taken two approaches. One approach specifically seeks to replace phosphate in genetic material like RNA and DNA. The other approach seeks to remove P from other biomolecules by mimicking its chemical characteristics.

Genetic alternatives to P seek to replace either the phosphate portion of the sugar-phosphate backbone of DNA/RNA, or seek to replace the whole of sugar-phosphate backbone. An example of the first type of substitution is glyoxylate replacement of phosphate (species I, figure 2). Glyoxylate will bridge ribose molecules like phosphate, and the carboxylic acid moiety provides a negative charge analogous to phosphate. Additionally, glyoxylate will spontaneously form such linkages, unlike phosphate which requires the addition of energy (Bean et al 2006). However, glyoxylate bridges introduce another chiral stereocenter into the genetic material, which necessitates more chemical synthetic information. Furthermore, glyoxylate is an uncommon molecule in biosystems, implying little biochemical activity.

Peptides have been proposed as a precursor to the sugar-phosphate backbone (e.g., Bohler et al. 1995, species II, figure 2). Peptide nucleic acid (PNA) consists of peptides that bond directly to nucleobases. Such peptides have no chiral centers, which is superior to ribose- or deoxyribose-based genetic material. However, PNA also lacks charge, meaning that it will readily diffuse through membrane materials, and has much less replicative fidelity than phosphate-based genetic material.

Figure 2. Alternatives to phosphate and phosphorus.

Species I

Glyoxylate
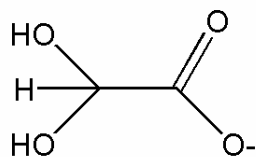
Glyoxylate-RNA
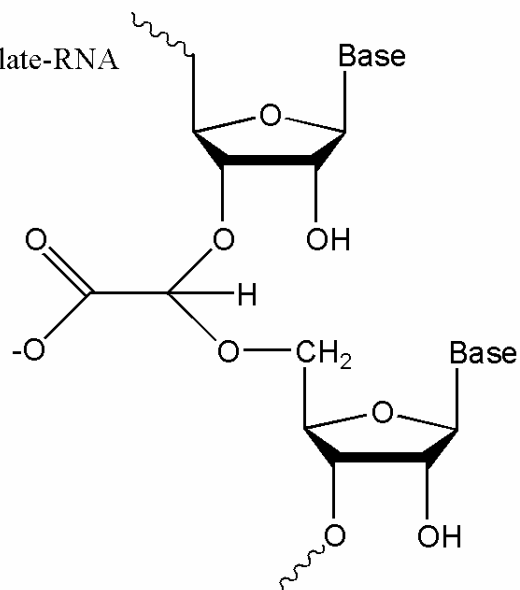
Species II

PNA
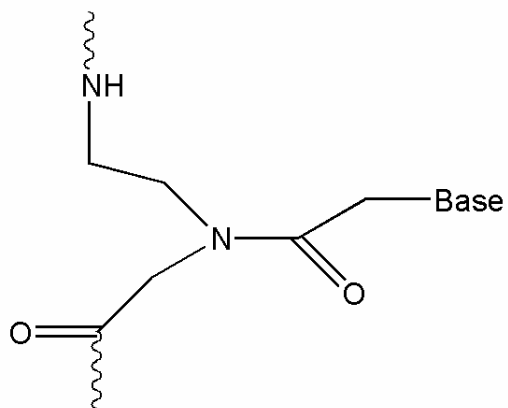
Species III
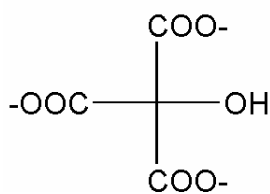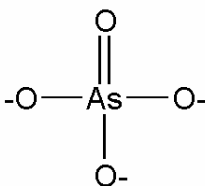
Citrate        Arsenate        Silicic Acid        Vanadate
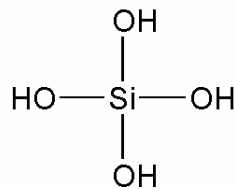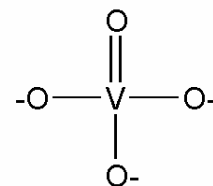
Neither glyoxylate nor peptides could serve as alternatives to phosphate outside of the genetic material. They lack the specialized characteristics necessary for metabolism or other biochemical functions.

General alternatives to P in biochemistry include species with three or more charges. Westheimer (1987) discusses three alternatives to phosphate: citric acid, arsenate, and silicic acid. I add vanadate to this list (species III, figure 2). Citric acid is an organic alternative with three negative charges. However, the charges are not closely localized but are spread over a much larger molecule. In addition, citric acid is a large, bulky molecule that is to use as a metabolic intermediate. Arsenate shares many chemical similarities with phosphate as arsenic lies just beneath P on the periodic table. However, $As^V$ will reduce to $As^{III}$ under mildly reducing conditions, which diminishes the adaptability of As compared to P. At first glance, silicic acid is a promising replacement as Si always has a +4 oxidation state on the surface of the Earth, and Si is many more times abundant than P. However, silicic acid is fully protonated to a pH of about 9, so silicic acid alternatives to phosphate lack a negative charge. Organosilicates are also unable to serve as energetic metabolic intermediates as they store minimal chemical energy. Vanadate inhibits phosphate enzymes due to its similarity in size and charge. However, vanadate is much rarer than phosphate in most systems, and V also exists in other oxidation states, similar to As.

To summarize, there are no compounds that could adequately substitute for phosphate with all of its various functions. Those compounds that have been proposed to substitute for P successfully mimic only a few specific biochemical functionalities.

Phosphorus is unique in its ubiquitous placement in modern biology. No substitute for P can mimic orthophosphate across its range of functions, from metabolism, to genetic material, to structure, to molecular signaling. The ubiquity of P in biochemistry is demonstrated in the following section.

1.3 Phosphorus in Biology- a Biochemical Survey

The most common oxidation state of P in living organisms is +5. Some exceptions exist and these rare molecules are detailed later. Phosphorus biomolecules are used in nearly every biochemical process. Phosphorus is critical to replication, information transfer, metabolism, structure, pH balancing, biosynthesis, signal transfer and chemical recognition, and is used in some catalytic (enzymatic) processes as a cofactor.

To begin the overview of P in biochemistry, it is first necessary to discuss the role of orthophosphate and orthophosphate minerals in life. Dissolved orthophosphate is the cellular source of P for phosphorylation reactions. Phosphorylation reactions are condensation reactions through which orthophosphate is added to an organic compound coupled with the loss of water:

$$HOPO_3^{2-} + R\text{-}OH \rightarrow R\text{-}OPO_3^{2-} + H_2O \tag{5}$$

Orthophosphate also functions as a buffer, keeping the pH relatively constant at ~7. Biogenic orthophosphate minerals include apatite, $Ca_5(PO_4)_3(OH,F,Cl)$ and struvite, $NH_4MgPO_4 \cdot 6H_2O$. The bones and teeth of vertebrates are composed of apatite, which is precipitated from solution using a complex series of proteins and intermediate calcium

minerals.  Struvite is more troublesome to biologic systems as it is the mineral precipitate that causes kidney stones, and it is the main P mineral of biological waste material (Ben Omar et al. 1998).

The structure, production, and reaction of P biomolecules are central to biochemistry.  I distinguish the varieties of P biomolecules by dividing them into two classes: the energetic P biomolecules and the stable P biomolecules.

1.3.1 Energetic Phosphorus Biomolecules

Energetic P biomolecules are primarily part of the metabolic process.  Examples of energetic P biomolecules are given in figure 3.  Metabolism is the set of chemical reactions that transfer energy from food sources to form molecules necessary for life.  The breakdown of complex molecules (food) is known as catabolism, the synthesis of biomolecules is anabolism, and combined the process is known as metabolism.

Central to all energetic P biomolecules is the moiety:
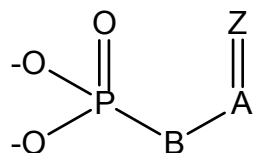


where A is either P or C, B is either O or N, and Z is O, $^{+}NH_2$, or $CH_2$.

The most energetic P biomolecule is phosphoenol pyruvate.  The phosphoacid anhydrides are next, followed by P-N compounds, and then

Figure 3. High energy phosphorus biomolecules.

I. Phosphoenol pyruvate
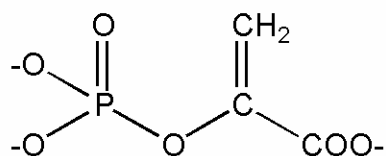
II. Acid Anhydrides (Acetyl Phosphate and 1,3-diphosphoglycerate)
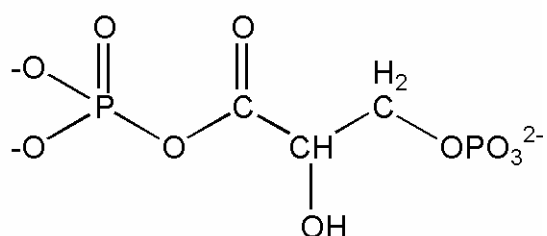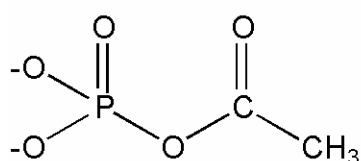
III. P-N Compounds (Phosphocreatine)
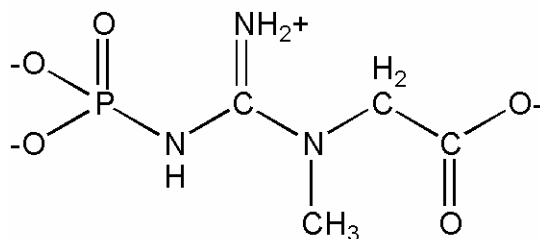
IV. Condensed Phosphates (ATP)
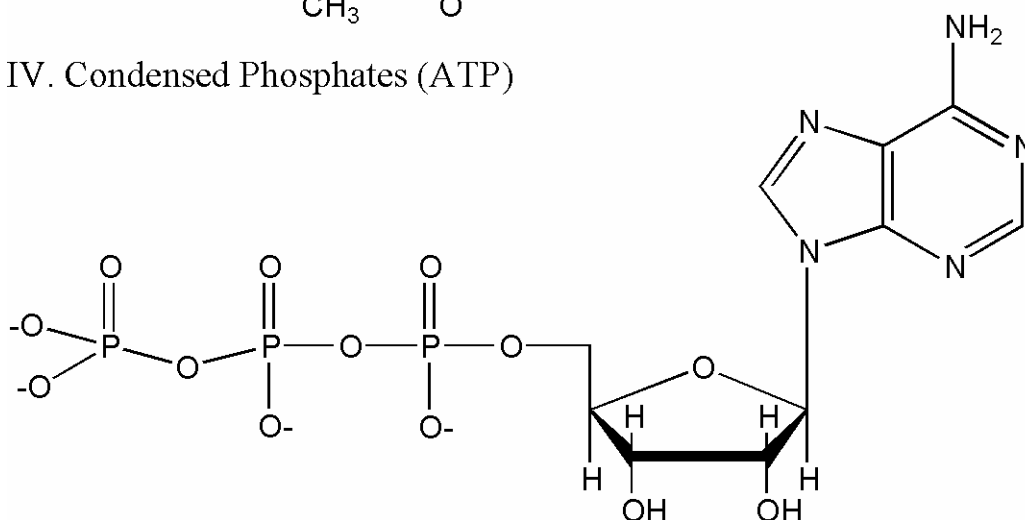
the condensed P compounds.  Table 3 (p. 28) summarizes the free energy associated with the hydrolysis of several compounds discussed in this dissertation.

Phosphoenol pyruvate (species 1, figure 3) is a very energetic P biomolecule due to the strained structure of the enol tautomer of pyruvate.  It is short-lived and is a high-energy intermediate of the catabolism of glucose.  Phosphoenol pyruvate transfers phosphate to ADP to form ATP during glycolysis.

Other energetic P biomolecules include phospho-acid anhydrides like acetyl phosphate and 1,3-bisphosphoroglycerate (species 2, figure 3).  Both compounds are primarily metabolic compounds, with the former playing a role in lipid synthesis and the latter an intermediate in glycolysis.   Phospho-acid anhydrides are very energetic and usually short-lived, acting primarily as reaction intermediates.  The dephosphorylation of these compounds is highly energetic because of the increase of available resonance states (i.e., electron sharing) of the two molecules compared to the single P molecule.

The final class of energetic P biomolecules is the P-N compounds, which have an unusual P-N linkage.  P-N bonds are not found naturally outside of biological systems.  Phosphocreatine (species 3, figure 3) is an example of a P-N compound.  P-N compounds serve primarily to store phosphate energy as they are stable and easily transfer phosphate to ADP.

The basic carrier of energy in all forms of life is adenosine triphosphate, or ATP.  Nearly all metabolic processes involve the synthesis or reaction of this molecule through transfer of a phosphate group.  Energy from the catabolism of biomolecules is used to add a phosphate group to adenosine diphosphate (ADP) to form ATP:

$$\text{ADP}^{2-} + \text{HPO}_4{}^{2-} + \text{catabolic energy} \rightarrow \text{ATP}^{4-} + \text{H}_2\text{O} \qquad (6)$$
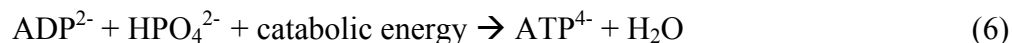
When energy is needed to make a new compound, a phosphate group is removed from

ATP to form ADP. The simple hydrolysis of ATP provides the energy for cellular

movement:

$$\text{ATP} + \text{H}_2\text{O} \rightarrow \text{ADP} + \text{HPO}_4{}^{2-} + \text{kinetic energy} \qquad (7)$$

Alternatively, ATP is used to phosphorylate organic compounds leading to a new

product:

$$\text{ATP} + \text{organic} \rightarrow \text{ADP} + \text{organic-PO}_3 \rightarrow \text{new organic} + \text{HPO}_4{}^{2-} + \text{ADP} \quad (8)$$
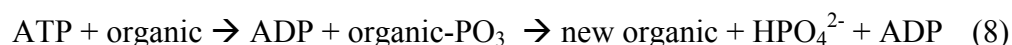
Note that ATP only transfers a $\text{PO}_3$ group to a compound, instead of an $\text{OPO}_3$ group.

ADP may also transfer a phosphate group with the release of energy, and ATP may

transfer a pyrophosphate group when more energy is necessary to perform an especially

thermodynamically unfavorable reaction. The P moiety in ATP and ADP is a condensed

phosphate group. Condensed phosphate groups are of moderate energeticity, making

them ideal for metabolic processes. Energetic condensed phosphates include other

nucleoside triphosphates like guanosine triphosphate, cytidine triphosphate, and

pyrophosphate (see species 4, figure 3).


1.3.2 Stable Phosphorus Biomolecules


While some of the P biomolecules described in the energetic P biomolecule section are

stable on long time scales, most notably the P-N compounds, the class of P biomolecules

in this section are referred to as "stable" because they serve functions other than the

metabolic transfer of chemical energy or its storage.  As such, these compounds must be kinetically stable.  Nearly all stable P biomolecules have the moiety:
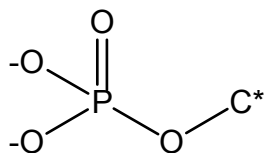


where C* is a carbon with an $sp^3$ hybridization.  This moiety is known as an "orthophosphate monoester".  Some stable P biomolecules have two linkages to carbon compounds through their oxygen atoms and these compounds are called orthophosphate diesters.  In addition to orthophosphate esters, some stable P-C compounds exist, and are detailed below.

Orthophosphate monoesters are stable P biomolecules in which there is only one P-O-C linkage.  These compounds include sugar-phosphates, 2,3-bisphosphoglycerate, and phospholipids (species 1, figure 4).  Sugar phosphates are the starting material for many metabolic processes, and "tagging" an organic compound with a phosphate group is a means by which many compounds, including sugars, are recognized by enzymes.  Some orthophosphate monoesters are catalytic cofactors, like 2,3-bisphosphoglycerate, which regulates the oxygen absorbing activity of hemoglobin and allows for rapid adaptation to changes in elevation.  Phospholipids consist of two long carboxylic acids attached to glycerol-1-phosphate.  The cellular membranes of most organisms consist of two layers of phospholipids with the long hydrocarbon chains of the outer layer pointing inwards, and the long hydrocarbon chains of the inner layer pointing outwards.  This bilayer is spontaneously formed from a concentrated solution of phospholipids.

Figure 4. Stable phosphorus biomolecules.

# I. Orthophosphate monoesters

Phospholipid
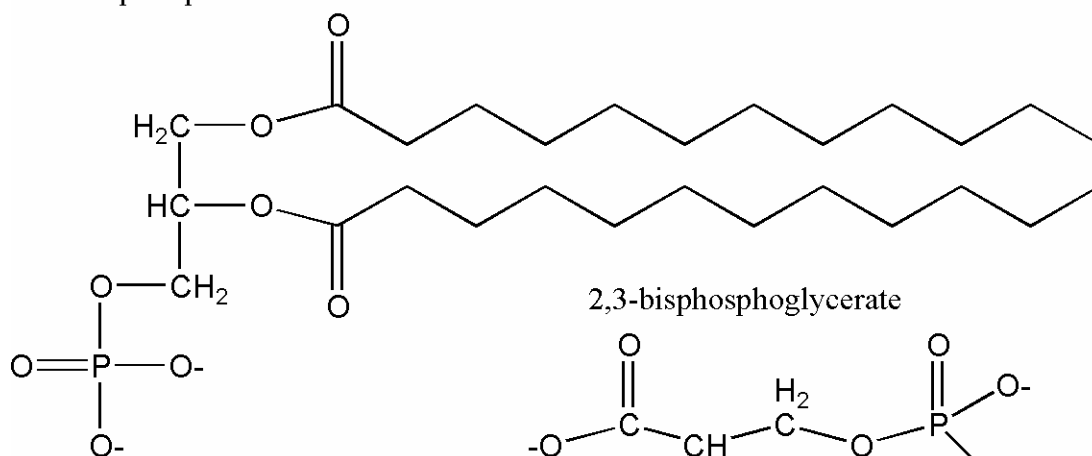


2,3-bisphosphoglycerate
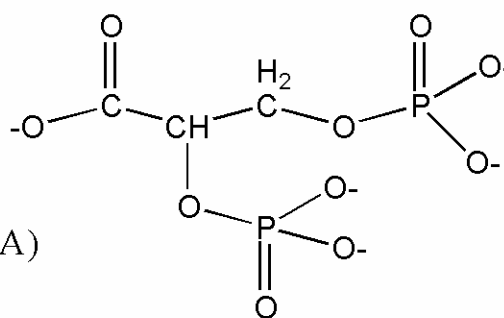
# II. Orthophosphate Diesters (DNA)
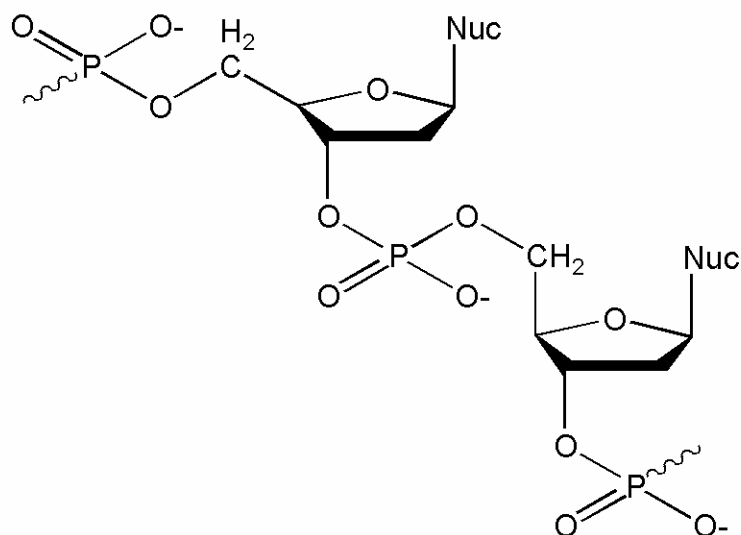


# III. P-C Compounds (aminoethylphosphonate)
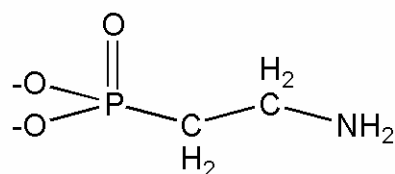
Orthophosphate diesters have two organic groups linked to phosphate through an O atom. Phosphate serves as a "bridge" for these molecules, connecting distinct organic functional groups. Orthophosphate diesters include the informational molecules DNA and RNA (species 2, figure 4). Both RNA and DNA consist of long chains of repeating, alternating 5-carbon sugars and phosphate groups. Other examples of orthophosphate diesters include cyclic nucleotides and some phospholipids. At physiologic pH the orthophosphate group of all orthophosphate diesters is negatively charged.

A final moiety for stable P compounds consist of direct P-C linkages. This linkage is uncommon although some P-C compounds are ubiquitous, like aminoethylphosphonate (species 3, figure 4). Aminoethylphosphonate is the type example of a P-C biomolecule, and has been detected in sea anemones, snail eggs, bacteria, protozoa, bovine nervous tissue, and human heart tissue (McGrath et al. 1997). P-C linkages were first identified by the work of Horiguchi and Kandatsu (1959), though their purpose and extent in biological systems remains unknown at present. The P-C bond in these molecules is very strong and thus these compounds are among the most stable of all P biomolecules.

1.4 Overcoming the "Phosphorus Problem"

A working theory for the origin of life must address the origin of P biomolecules. An origin of life on Earth without P is inconceivable given its omnipresence in life today and the chemical dependence life has on its characteristics. Several researchers have suggested means of overcoming the phosphorus problem, and I provide a review of proposed solutions, followed by a critical analysis. Many prebiotic P experiments do not show how the first P biomolecules came into existence using suitably prebiotic starting conditions. Hence geochemical systems seem incapable of forming P biomolecules, and a recommended alternative to geochemical systems is presented.

There have historically been three approaches to overcoming the "Phosphorus Problem." The three approaches are to employ energetic organic compounds as condensing agents, to use energetic P compounds as phosphorylating agents, and to add energy to reactions in the form of heat, light, or radioactivity to drive them to phosphorylation.

Phosphorylation reactions are simplified as follows:

$$\text{Organic} + \text{P source} + \text{"Energy"} \rightarrow \text{Organic-P} + H_2O \tag{9}$$

The phosphorylation process proceeds through a similar mechanistic pathway for all three types of reactions wherein a reactive P intermediate is formed which in turn phosphorylates the organic molecule, i.e.:

$$\text{P source} + \text{"Energy"} \rightarrow \text{Reactive P} + H_2O \tag{10}$$

or

$$\text{Energetic organic} + \text{P source} \rightarrow \text{Reactive P} + H_2O \tag{11}$$

followed by:

$$\text{Organic} + \text{Reactive P} \rightarrow \text{Organic-P} \tag{12}$$
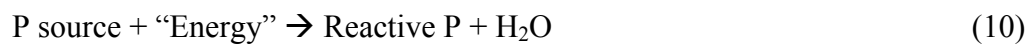
All proposed prebiotic phosphorylation reactions involve the production of water and thus these reactions are inhibited by the presence of water.

Energetic organic compounds react with orthophosphate to form phosphorylated organic intermediates. A review of these reactions is presented in Hulshof and Ponnamperuma (1976), and in table 4. An example is the reaction of cyanate, a high-energy organic compound, with orthophosphate to form carbamyl phosphate:

$$NCO^- + H_2PO_4^- \rightarrow H_2NCOOPO_3^{2-} \tag{13}$$
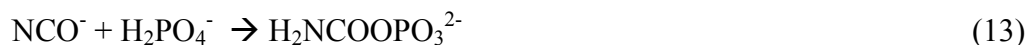
(Keefe and Miller 1995). Carbamyl phosphate may either react with itself to form pyrophosphate:

$$2H_2NCOOPO_3^{2-} + H_2O \rightarrow 2H_2NCOOH + P_2O_7^{4-} \tag{14}$$
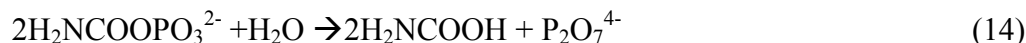
(Miller and Parris 1964) or may react with other organics to phosphorylate them through phosphate transfer:

$$H_2NCOOPO_3^{2-} + \text{Adenosine} \rightarrow AMP + H_2NCOOH \tag{15}$$
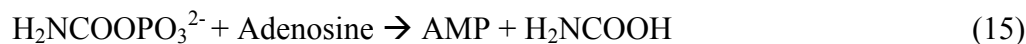
(Yamagata et al. 1979). Reactions (14) and (15) have yields of 26% and 6%, respectively. Is either reaction reasonable in terms of the context of prebiotic chemistry? Cyanate is a plausible prebiotic compound, but orthophosphate would have a low total abundance limited by its geochemistry. Assuming an abundance of orthophosphate of $10^{-6}$ M, the total production of AMP would proceed to a concentration of $10^{-8}$ M, too low for the production of RNA. Additionally, cyanate reacts with amines to form urea

derivatives, and thus chemistry with cyanate would further increase the complexity of the prebiotic chemistry.

Adding external energy to a system consisting of organics and orthophosphate phosphorylates organics through a reactive P intermediate (table 5). These experiments were initially phenomenological, and later work revealed these reactions to proceed through the reactions (10) and (12).

Many proposed prebiotic syntheses used external energy sources to produce reactive P compounds (table 6) which are then used to phosphorylate organics through the reactions of table 7. Examples include the production of polyphosphates from the heating of orthophosphate. This reaction is driven by the loss of water through heating, which pushes the reaction towards products. High energy P compounds like polyphosphates and trimetaphosphate react with organics to produce organophosphates. Phosphate-group transfer from inorganic polyphosphates to organic sugars is a spontaneous process, but is moderately kinetically inhibited. As such, these reactions have low yields.

Even with the assumption that organic compounds (especially nucleotides) were phosphorylated through abiotic processes, the next step is even more difficult. The next step key to the "strong" RNA world in prebiotic chemistry is to take the phosphorylated nucleotides and assemble them into a strand of RNA. In life this is accomplished through activating nucleotides by making triphosphates and discarding a pyrophosphate on reaction:

$$N'TP + N'' \rightarrow N'\text{-}N'' + P_2O_7^{4-} \tag{16}$$

(As a side note, this is an elegant reaction where the products are both much rarer than the reactants. Compare this to the reaction from a diphosphate nucleotide:

$$N'DP + N'' \rightarrow N'\text{-}N'' + HPO_4^{2-} \tag{17}$$

Orthophosphate is released from this reaction. Orthophosphate is abundant in biologic systems, and thus this second reaction would be inhibited from proceeding to completion.) Triphosphate compounds are difficult to produce through prebiotic chemical reaction. Many have sought alternatives to triphosphates that would lead to either the polymerization of RNA or of peptides, and these are summarized in table 8. This group of reactions includes the clay-catalyzed synthesis of RNA using imidazole-phosphate nucleotides (Ferris and Ertem 1993). Imidazole-phosphate nucleotides have been criticized as being non-prebiotic (Shapiro 2000). In general, this argument for prebiotic polymerization suffers from many of the same faults as prebiotic phosphorylation reactions. These faults are detailed below:


1) Many high energy organic compounds used in prebiotic phosphorylations are
    ephemeral, and are not likely to be produced on a large scale on the early Earth.
2) Many of these high energy organic compounds are not specific to orthophosphate.
    Several react with other compounds in their environment, removing them from the
    system.
3) Many of these reactions use unreasonably high concentrations of phosphate to produce
    reactive organophosphate intermediates, typically with no geochemical justification.

4) Related to critique 3) is that several experiments use phosphate minerals like acidic

   phosphates such as $Ca(H_2PO_4)_2$, which are not known to occur on the surface of the

   Earth.  Whitlockite, $Ca_3(PO_4)_2$, is used for some phosphorylation experiments, but it

   is not a very common terrestrial mineral.  Unless the phosphate mineral used is

   apatite, the reaction can't be considered "prebiotic" without a geochemical context.

5) High temperatures induce phosphorylations and production of reactive P compounds,

   but geochemical rationales for these dry, high temperature regions are rare.

6) Energetic phosphate minerals are uncommon. The processes proposed by 5) are thus

   uncommon as well.  There are currently three known polyphosphate minerals:

   Canaphite, $CaNa_2P_2O_7 \cdot 4H_2O$, Wooldridgeite, $CaNa_2Cu_2(P_2O_7)_2$, and Kanonerovite,

   $MnNa_3P_3O_{10} \cdot 12H_2O$ (Peacor $et\ al.$ 1985, Hawthorne $et\ al.$ 1999, Popova $et\ al.$ 2002).

   These minerals are generally associated with pegmatites and may have a total mass of

   100 kg on the surface of the Earth.  However, Yamagata et al. (1991) detected some

   polyphosphates in the vicinity of hydrothermal vents, with concentrations of $\sim 10^{-6}$ M.

   The hydrothermal source of polyphosphates shall be revisited later in this dissertation.

7) Finally, the yields are typically very low, which is especially troubling given that the

   concentrations of both the energetic organic compounds and orthophosphate

   employed in these experiments are much higher than would naturally occur on the

   surface of the Earth.

   A review of many previous experiments is provided in tables 4-8. These tables build

on the review of Keefe and Miller (1995), but include experiments done after their

original tabulation.  These tables serve to show the research and efforts that have been

made to solve this problem, as it is one of the key difficulties to understanding the origin of life.

## 1.4.1 Meteorites as the Source of Phosphorus

Phosphorus is a key element for biology and was likely a key element for the origin of life. The early terrestrial environment was limited by the lack of reactive terrestrial phosphate minerals and was not conducive to prebiotic phosphorylation. However, extraterrestrial material brings in a sizable quantity of reactive P, and this material may have been useful for prebiotic phosphorylation. The next chapter examines the chemical changes that occur to extraterrestrial P minerals when they land on the surface of the Earth.

Table 4. Phosphorylation through energetic organic condensing agents.

| Organic compound | P compound | Reaction conditions | Product | Yield (%) | Reference |
|---|---|---|---|---|---|
| 2-Aziridinecarbonitrile | $H_3PO_4$:$H_2O$ 93:7 $NaH_2PO_4$ (0.02 M) | 80° C | Glycolaldehyde phosphate | 22.5 | Wa90 |
| Ethanethioic esters | | W/apatite | PPi | ~4 | We82 |
| Imidazole | CTP | 90° C | Oligonucleotide | 0.3 | Ib71 |
| Cyanate | Apatite | | PPi | 26 | MP64 |
| Cyanate | Apatite $Ca_3(PO_4)_2$ and | | PPi | 1-2 | BO65 |
| Cyanate | $Na_5P_3O_{10}$ | | Trimetaphosphate | 1 | BO65 |
| Cyanate | Phosphate | Electric discharge | Carbamyl phosphate | 6 | YM82 |
| Cyanate, Adenosine | Phosphate | Electric discharge | AMP | 0.02 | Ya79, Ya81 |
| Carbamyl Phosphate | AMP, ADP | | ADP, ATP | 2-17 | Sa81 |
| Acetate | Carbamyl Phosphate | | Acetyl Phosphate | 30 | Sa83 |
| Ferricyanide | Phosphate | Under visible light | Carbamyl phosphate | 15 | Sa81 |
| Dicyandiamide | Phosphate | | PPi | 0.2-1.8 | St65 |
| Dicyandiamide | ADP + phosphate | With Clay | ATP | 0.5 | St65 |
| Dicyandiamide | Phosphate | | PPi | <0.1 | BO65 |
| Carboiimide | Phosphate | | PPi | <0.1 | BO65 |
| Dithionite | Phosphate | Under $O_2$ | PPi | 0.24 | Ga68 |
| Diacetyl cysteamine and imidazole | Phosphate | | PPi, PPPi | 3-8 | We81 |
| Cyanimide | dTMP | | dTppdT | 58 | SO77 |
| $NH_4HCOO$ | Phosphate | | PPi | 53 | KM96 |
| Thiocyanate and $H_2O_2$ | Phosphate | | PPi | 26 | KM96 |
| Maleic anhydride | Phosphate | | PPi | 5 | KM96 |
| Pantoyl lactone | Phosphate | | PPi | 5 | KM96 |
| Polymerizing HCN | Phosphate | | PPi | 4 | KM96 |
| Imidazole and $CaCl_2$ | Phosphate | | PPi | 4 | KM96 |

Table 4. Cont'd

| Organic compound | P compound | Reaction conditions | Product | Yield (%) | Reference |
|---|---|---|---|---|---|
| Cyanate, Uridine | Phosphate | | UMP | 1 | LO68 |
| Cyanamide, Glucose | Phosphate | pH 2 | Glucose-6-phosphate | 1.5 | St64 |
| Cyanamide, Ribose | Phosphate | | Ribose-1-phosphate | 8 | Ha69, HS70 |
| Carbodiimide, Uridine | Phosphate | | UMP | 3 | LO68 |
| Dicyandiamide, Glucose | Phosphate | pH 2 | Glucose-6-phosphate | 2.4 | St64 |
| Dicyandiamide, Glucose | Phosphate | | Glucose-6-phosphate | 1.9 | St65 |
| Cyanogen, Ribose | Phosphate | | Ribose-1-phosphate | 20 | Ha69, HS70 |
| NCCONH$_2$, Uridine | Phosphate | | UMP | 2 | LO68 |
| Ethylisocyanide, Uridine | Phosphate | | UMP | 1-10 | LO68 |
| Oxiranecarbonitrile | Phosphate | | Glycolaldehyde phosphate | 47 | Pi94 |
| Diiminosuccinonitrile | AMP | | cyclic AMP | 18 | Fe84 |
| Cyanogen bromide | AMP | | cyclic AMP | 18 | Fe84 |
| Diiminosuccinonitrile, Uridine | Phosphate | | UMP | 4 | Fe84 |
| Nucleotide Di-P, cyanate | Ca$_3$(PO$_4$)$_2$ | | NTP | 25 | Ya99 |
| Nucleotide Mono-P, cyanate | Ca$_3$(PO$_4$)$_2$ | | NDP | 19 | Ya99 |
| Acetyl phosphate (0.05 M) | | Fe(II) minerals | PPi | 0.25 | dZ04 |
| Phosphoenolpyruvate (0.05 M) | | Fe(II) minerals | PPi | 0.14 | dZ04 |

For table 4 through table 8: Phosphate typically refers to Na$_2$HPO$_4$ in concentrations of ~0.01 M. PPi is pyrophosphate, and PPPi is triphosphate, Poly-P is polyphosphate, AMP is adenosine monophosphate, UMP is uridine monophosphate, TMP is thymidine monophosphate, NTP is nucleotide triphosphate. BDL is below detection limit.

Table 5. Phosphorylation through addition of energy.

| Organic Compound | P source | Conditions | Compound produced | Yield (%) | References |
|---|---|---|---|---|---|
| Uridine | $Ca(HPO_4)_2$ | 160°C, 2hrs | UMP | 11 | PM65, PC71 |
| Uridine | $H_3PO_4$ | 160°C, 2hrs | UMP | 8.3 | St64, PM65, PC71 |
| Uridine | $NaH_2PO_4 \cdot H_2O$ | 160°C, 2hrs | UMP | 16 | St64, PM65, PC71 |
| Uridine | $Na_2HPO_4 \cdot 7H_2O$ | 160°C, 2hrs | UMP | 1.0 | St64, PM65, PC71 |
| Uridine | $Na_3PO_4 \cdot 12H_2O$ | 160°C, 2hrs | UMP | 0.6 | St64, PM65, PC71 |
| Uridine | $NH_4H_2PO_4$ | 160°C, 2hrs | UMP | 5.9 | St64, PM65, PC71 |
| Uridine | $(NH_4)_2HPO_4$ | 160°C, 2hrs | UMP | 13.4 | St64, PM65, PC71 |
| Uridine | $Ca_3(PO_4)_2$ | 160°C, 2hrs | UMP | 0.1 | St64, PM65, PC71 |
| Uridine | $KH_2PO_4$ | 162°C, 2hrs | UMP | 4.9 | PC71 |
| Uridine | $NaH_2PO_4 \cdot H_2O$ | 126°C, 6hrs | UMP | 5.4 | PC71 |
| Uridine | $Na_2HPO_4 \cdot 7H_2O$ | 126°C, 6hrs | UMP | 1 | PC71 |
| Uridine | $Ca(H_2PO_4)_2$ | 126°C, 6hrs | UMP | 0 | PC71 |
| Uridine | $Ca(H_2PO_4)_2 \cdot H_2O$ | 126°C, 0.1hrs | UMP | 9.7 | PC71 |
| Uridine | $Ca(H_2PO_4)_2 \cdot H_2O$ | 98°C, 2 days | UMP | 29.2 | PC71 |
| Uridine | $Ca(H_2PO_4)_2 \cdot H_2O$ | 98°C, 14 days | UMP | 26.8 | PC71 |
| Urea, Uridine | $Ca_3(PO_4)_2$ | 85°C | UMP | 30-80 | Ha73 |
| Urea, Thymidine | $Na_2HPO_4$ | 65°C | TMP | 25 | Bi72 |
| $(NH_4)_2C_2O_4$, Thymidine | $Ca_3(PO_4)_2$ | 90°C | TMP | 15-30 | Sc75 |
| $(NH_4)_2C_2O_4$, Thymidine | $Ca_3(PO_4)_2$ | 90°C | Poly-P | 1-50 | Sc75 |
| Trehalose | $NaH_2PO_4$ (0.1 M) | 56°C | Trehalose phosphate | 15 | TW93 |

Table 6. Synthesis of high energy phosphorus compounds.

| Organic | P compound | Conditions | P products | Yield (%) | References |
|---|---|---|---|---|---|
| | $H_3PO_4$ | 160°C, 2hrs | PPi, PPPi | 30-50, 1-5 | Ra68 |
| | $NaH_2PO_4 \cdot H_2O$ | 160°C, 2hrs | PPi, PPPi | 32 | PC71 |
| | $Na_2HPO_4 \cdot 7H_2O$ | 160°C, 2hrs | PPi, PPPi | BDL | Ra68 |
| | $Na_3PO_4 \cdot 12H_2O$ | 160°C, 2hrs | PPi, PPPi | BDL | Ra68 |
| | $NH_4H_2PO_4$ | 160°C, 2hrs | PPi, PPPi | 64 | PC71 |
| | $(NH_4)_2HPO_4$ | 160°C, 2hrs | PPi, PPPi | 10-30, 5-10 | Ra68 |
| | $Ca(H_2PO_4)_2 \cdot H_2O$ | 160°C, 2hrs | PPi, PPPi | 30-50, 10-30 | Ra68 |
| | $CaHPO_4$ | 160°C, 2hrs | PPi, PPPi | BDL | Ra68 |
| | $KH_2PO_4$ | 160°C, 2hrs | PPi, PPPi | BDL | Ra68 |
| | $Ca_3(PO_4)_2$ | 160°C, 2hrs | PPi, PPPi | BDL | Ra68 |
| Urea, dThymidine | $NH_4H_2PO_4$ | 100°C, 4 days | Trimetaphosphate | 23 | OO72 |
| | $MgHPO_4$ | 250-550°C | Poly-P | 50 | Sa92 |
| | $NaH_2PO_4$ | 500-600°C | Trimetaphosphate | 100 | VW58 |
| | $NaH_2PO_4$ and $KH_2PO_4$ | 200-600°C | Poly-P | 100 | VW58 |
| Urea | $NH_4H_2PO_4$ | 85-100°C | Poly-P | 60-100 | OO72 |
| | $Ca(H_2PO_4)_2 \cdot H_2O$ | 90°C, 1 week | PPi,PPPi | 2-5, 2-5 | PC71 |
| | $NaH_2PO_4 \cdot H_2O$ | 90°C, 1 week | PPi,PPPi | 2-5, 2-5 | PC71 |
| | $NH_4H_2PO_4$ | 90°C, 1 week | PPi,PPPi | ~1, ~1 | PC71 |
| | $Ca(H_2PO_4)_2 \cdot H2O$ | 65°C, 2 months | PPi | 1 | PC71 |
| | $NaH_2PO_4 \cdot H_2O$ | 65°C, 2 months | PPi | 1 | PC71 |

Table 7. Phosphorylation through high energy phosphorus compounds.

| Organic | P compound | Conditions | Product | Yield (%) | Reference |
|---------|-----------|-----------|---------|-----------|-----------|
| Uridine | $Na_2H_2P_2O_7$ | 126°C, 6hrs | UMP | 29.8 | PC71 |
| Uridine | $Na_5P_3O_{10}$ | 126°C, 6hrs | UMP | 21.1 | PC71 |
| Uridine | $Na_5P_3O_9$ | 126°C, 6hrs | UMP | 12.9 | PC71 |
| Uridine | $Na_{x+2}P_xO_{3x+1}$ (Graham's salt) (1 M) | 126°C, 6hrs | UMP | 28.2 | PC71 |
| Uridine | $Na_5P_3O_{10}$ | 162°C, 0.1hrs | UMP | 15.4 | PC71 |
| Uridine | $Na_5P_3O_9$ | 162°C, 0.1hrs | UMP | 7 | PC71 |
| Adenosine | $Na_4P_2O_7$ (1 M) | Room temp, pH ~8 | | 0 | SP68 |
| Adenosine | $Na_5P_3O_{10}$ (1 M) | Room temp, pH ~8 | AMP | 1.08 | SP68 |
| Adenosine | $Na_{x+2}P_xO_{3x+1}$(Graham's salt) (1 M) | Room temp, pH ~8 | AMP | 0.94 | SP68 |
| Adenosine | $Na_{x+2}P_xO_{3x+1}$(Graham's salt) (1 M) | 100°C, pH ~8 | AMP | 1.52 | SP68 |

Table 8. Activation by phosphorylations.

| Organic | P compound | Conditions | Products | Yields | Reference |
|---|---|---|---|---|---|
| Glyglycine | Trimetaphosphate | | Glyglycine polymers | 2 | YI97 |
| | Phosphoimidazolide ribonucleotides (1.0 M) | | Polynucleotides | 4-65 | Ka97 |
| | Phosphoimidazolide ribonucleotides (1.0 M) | Clay Catalyzed | Polynucleotides | | FE93 |
| | Dimethylaminopyridinium-phosphonucleotides | Clay Catalyzed | Polynucleotides | 74 | PF97 |
| Glycolate | Trimetaphosphate (0.01 M) | Hydrotalcite catalyzed | Glycolate phosphate | 34 | Ko97 |
| | Glycolaldehyde phosphate, 2-glyceraldehyde phosphate | Clay Catalyzed | Pentose-2,4-bisphosphate, ribose-2,4-bisphosphates | 24, 11.5 | Kr99a |
| Nucleosides, urea | $NaH_2PO_4$, (0.02-0.1 M) | Dry heated film | Nucleoside-5-monophosphates | 18 | RZ99 |
| Glycolaldehyde | Trimetaphosphate (0.1M-60 $\mu$M) | $NH_3$, $Mg^{2+}$ | Glycolaldehyde phosphate | 5-76 | Kr99b |
| Oligonucleotides-5 phosphates | Trimetaphosphate (0.04 M) | $Mg^{2+}$ | Oligonucleotides-5 polyphosphates | 37 | GO00 |
| Adenosine | Trimetaphosphate (0.2 M) | $Ni^{2+}$ | cyclic-AMP, ATP | 30 total | Ch02 |
| | nucleoside N-phosphonoaminoacids | | di to tetra Peptides | low | Li05 |

Abbreviations for references used for tables 4-8.
BO65 = Beck and Orgel 1965
Bi72 = Bishop et al. 1972
Ch02 = Cheng et al. 2002
dZ04 = de Zwart et al. (2004)
Fe84 = Ferris et al 1984
Fe93 = Ferris and Ertem 1993
Ga68 = Gabel 1968
GO00 = Gao and Orgel 2000
Ha69 = Halmann et al. 1969
HS70 = Halmann and Schmidt 1970
Ha73 = Handschuh et al 1973
Ib71 = Ibanez et al 1971
Ka97 = Kanavarioti 1997
KM96 = Keefe and Miller 1996
Kr99a = Krishnamurthy et al 1999a
Kr99b = Krishnamurthy et al 1999b
Ko97 = Kolb et al. 1997
Li05 = Lin et al. 2005
LO68 = Lohrmann and Orgel 1968
MP64 = Miller and Parris 1964
OO72 = Osterburg and Orgel 1972
Pi94 = Pitsch et al. 1994
PF97 = Prabahar and Ferris 1997
PM65 = Ponnamperuma and Mack 1965
PC71 = Ponnamperuma and Chang 1971
Ra68 = Rabinowitz 1968
RZ99 = Reiman and Zubay 1999
Sa92 = Sales et al 1992
Sa81 = Saygin 1981
Sa83 = Saygin 1983

Sc75 = Schwartz et al 1975
SP68 = Schwartz and Ponnamperuma 1968
SO77 = Sherwood and Oro 1977
St64 = Steinman et al. 1964
St65 = Steinman et al 1965
TW93 = Tarelli and Wheeler 1993
VW58 = Van Wazer 1958
Wa90 = Wagner et al 1990
We81 = Weber 1981
We82 = Weber 1982
Ya79 = Yamagata et al 1979
Ta81 = Yamagata et al 1981
Ya99 = Yamagata 1999
YI97 = Yamagata and Inomata 1997
YM82 = Yamagata and Mohri 1982

CHAPTER 2


PHOSPHORUS FROM METEORITES


The presence of amino acids in primitive meteorites has led to speculation that

extraterrestrial materials could have seeded early Earth with precursor biomolecules (e.g.,

Chyba and Sagan 1992). Thus, study of the forms of P in early solar system materials

may also provide important insight into compounds available for the prebiotic

phosphorylation. Meteorites delivered a significant portion of the current crustal P

abundance by the end of the late-heavy bombardment (estimated at ~10%, Macia et al.

1997). Based on the mass statistics of meteorite falls and Antarctic finds, approximately

half of the meteoritic mass that impacts the Earth is chondritic material, excluding the

large impactors. Phosphorus is dominantly in phosphate minerals in chondrites (Ramdohr

1963), similar to those in Earth's crust. The balance of meteoritic P occurs in reduced

form as schreibersite, $(Fe,Ni)_3P$, predominantly in iron meteorites (Buchwald 1977) and

reduced primitive meteorites such as the enstatite chondrites. Of the total crustal P, ~5%

was at one time extraterrestrial schreibersite, an amount greater than that in the current

biosphere (Macia et al. 1997). The mass balance of meteoritic P is explored in greater

detail in chapter 4.

To date, experimental studies have not addressed the relevance of schreibersite as

a source of P for the formation of organic P molecules on the early Earth. It has been

speculated that the corrosion of schreibersite could lead to the formation of phosphonic acids (Schwartz 1972, de Graaf et al. 1995), which are present in nanomolar concentrations in the Murchison meteorite (Cooper et al. 1992). Gulick (1955) was the first to suggest that the corrosion of meteoritic P could provide reduced P useful for the origin of life, but no follow up research was performed until now.

This chapter describes an investigation of the corrosion of schreibersite. The process of schreibersite corrosion is addressed through two approaches: An experimental study of synthetic $Fe_3P$ corrosion and a mineralogical study of a corroded schreibersite grain in a meteorite.

## 2.1 An Experimental Approach to Phosphide Corrosion

The following sets of experiments were performed to discern the general behavior of phosphide corrosion:

1) General phosphide corrosion experiments were performed under air and sought to explore the nature of schreibersite corrosion and the effects of corrosion on organic compounds. Inorganic solutions were chosen to explore the effect of salt (both $Na^+$ and divalent cations) on corrosion and P speciation, and of alkaline pH. Simple organic solutions were chosen to explore the effect of organic functional group on solution chemistry.

2) Inert phosphide corrosion experiments repeated some of the general corrosion experiments under an inert atmosphere to determine the effect of air on corrosion speciation and rates.

3) Two phosphate solvation experiments experiments were performed to test the solubility of fluoroapatite, $Ca_5(PO_4)_3F$.

4) Phosphorus compound stability experiments were performed to elucidate the reaction pathway of molecular P transformations in solution. In particular, I designed experiments to test the stability and reactivity of phosphite, hypophosphite, orthophosphate, hypophosphate, and pyrophosphate.

5) General corrosion experiments were modified to employ advanced analytical techniques that determine the specific reaction chemistry of phosphide corrosion.

6) One set of experiments uses the P species determined from the corrosion experiments as reaction compounds for directed synthesis of organic P molecules or of pyrophosphate.  The goal of these second-tier experiments was to replicate some of the prebiotic phosphorylation experiments discussed in chapter 1, using the reactive phosphide powder at room temperature.

2.1.1 Materials and Conditions

The conditions of all corrosion experiments are given in table 9. Solid reactants included phosphate and phosphide compounds, iron metal, and magnetite. Phosphide was introduced as pure $Fe_3P$ powder (-40 mesh, purchased from CERAC, Inc.). High-purity

Table 9. Explorative studies. NMR is nuclear magnetic resonance spectrometry, ICP-MS is inductively coupled plasma-mass spectrometry, XRD is X-ray diffractometry, ES- TOF-HR-MS is negative electron spray time of flight-high resolution-mass spectrometry, ESR is electron spin resonance spectrometry, EMPA is electron microprobe point analysis. Experiments 1-25 were NMR studies of phosphide corrosion, 26-37 were stability experiments, 38-40 were detailed phosphide corrosion studies.

| No. | Method(s) | Solution | Solid (mass in g) | pH |
|-----|-----------|----------|-------------------|-----|
| 1 | [1]NMR Air, ICP-MS, XRD, EMPA | Water | $Fe_3P$ (1.0473 g) | 7 |
| 2 | [1]NMR Air, ICP-MS, XRD. EMPA | $MgCl_2/CaCl_2$ (0.025 M) | $Fe_3P$ (1.4100 g) | 7 |
| 3 | [1]NMR Air, ICP-MS, XRD | $CH_3COONa$ (0.4 M), EtOH (0.4 M) | $Fe_3P$ (1.1347 g) | 6.5 |
| 4 | [1]NMR Air, ICP-MS | $MgCl_2/CaCl_2$ (0.04 M),$CH_3COONa$ (0.2 M), EtOH (0.2 M) | $Fe_3P$ (1.0368 g) | 6.5 |
| 5 | [1]NMR Air | $NaHCO_3$ (0.5 M) | $Fe_3P$ (0.6941 g) | 9.5 |
| 6 | NMR Air | NaCl (0.4 M) | $Fe_3P$ (0.9811 g) | 7 |
| 7 | NMR Air | NaOH (0.1 M) | $Fe_3P$ (0.9883 g) | 13 |
| 8 | NMR Air | NaOH (0.05 M), EDTA (0.025 M) | $Fe_3P$ (1.0686 g) | 13 |
| 9 | NMR Air | $CH_3CN$ (0.4 M) | $Fe_3P$ (1.0765 g) | 7 |
| 10 | NMR Air | EtOH (0.4 M) | $Fe_3P$ (0.8216 g) | 7 |
| 11 | NMR Air | Acetone (0.4 M) | $Fe_3P$ (0.9636 g) | 7 |
| 12 | NMR Air | $CH_3COONa$ (0.4 M) | $Fe_3P$ (0.7378 g) | 6.5 |
| 13 | NMR Air | $CH_3COONa$ (0.4 M) | $Fe_3P$ (2.3102 g) | 6.5 |
| 14 | NMR Air | Pyruvate, $C_3H_3O_3Na$ (0.7 M) | $Fe_3P$ (0.8421 g) | 6 |
| 15 | NMR Air | Acetaldehyde, $CH_3CHO$ (1.2 M) | $Fe_3P$ (0.8212 g) | 7 |
| 16 | NMR Air | $H_2O_2$ (0.6 M) | $Fe_3P$ (1.3313 g) | 7 |
| 17 | NMR Air | $CH_3COONa$ (0.4 M), Apatite (1.0008 g) | $Fe_3P$ (1.0912 g) | 6.5 |
| 18 | NMR Air | Adenosine (0.15 M), Apatite (0.9539 g) | $Fe_3P$ (1.0652 g) | 7 |
| 19 | NMR Air | Adenosine (0.15 M), Apatite (0.9633 g) | $Fe_3P$ (0.9474 g) | 13 |
| 20 | NMR Air | Water | Apatite (2.3624 g) | 7 |
| 21 | NMR Air | NaOH (0.05 M), EDTA (0.025 M) | Apatite (2.2898 g) | 13 |
| 22 | [1]NMR Argon, Gas Analysis | Water | $Fe_3P$ (1.2197 g) | 7 |
| 23 | [1]NMR Argon | $MgCl_2/CaCl_2$ | $Fe_3P$ (1.0325 g) | 7 |
| 24 | [1]NMR Argon | $CH_3COONa$ (0.4 M), EtOH (0.4 M) | $Fe_3P$ (1.1629 g) | 6.5 |
| 25 | [1]NMR Argon | $NaHCO_3$ (0.5 M) | $Fe_3P$ (1.3208 g) | 9.5 |
| 26 | NMR Argon | Glycolaldehyde, $C_2H_4O_2$ (0.4 M) | $Fe_3P$ (0.9848 g) | 7 |

Table 9 cont'd.

| No. | Method(s) | Solution | Solid (mass in g) | pH |
|---|---|---|---|---|
| 27 | [1]NMR Air | $Na_2HPO_3$ (0.01 M) | Fe (0.7158 g) | 7 |
| 28 | [1]NMR Air | $Na_2HPO_3$ (0.01 M) | - | 7 |
| 29 | NMR Air | $Na_2HPO_3$ (0.01 M) | $Fe_3P$ (0.9584 g) | 7 |
| 30 | [1]NMR Air | $Na_2HPO_3$ (0.03 M) | $Fe_3O_4$ (0.5912 g) | 7 |
| 31 | [1]NMR Air | $NaH_2PO_2$ (0.05 M) | Fe (0.6758 g) | 7 |
| 32 | [1]NMR Air | $NaH_2PO_2$ (0.05 M) | - | 7 |
| 33 | NMR Air | $NaH_2PO_2$ (0.08 M), $Na_2HPO_3$ (0.03 M) | - | 7 |
| 34 | NMR Air | $NaH_2PO_2$ (0.08 M), $Na_2HPO_3$ (0.03 M) | $Fe_3O_4$ (0.6500 g) | 7 |
| 35 | NMR Air | $Na_2HPO_3$ (10.0 M) | Fe (1.2749 g) | 13 |
| 36 | NMR Air | $Na_2HPO_4$ (0.5 M) | Fe (~0.5 g) | 7 |
| 37 | NMR Air | $Na_4P_2O_6$ (0.05 M) | Fe (1.0721 g) | 13 |
| 38 | NMR Air | $Na_4P_2O_7$ (0.5 M) | Fe (~0.5 g) | 13 |
| 39 | ES- TOF-HR-MS Air | $CH_3COONH_4$ (0.4 M) | $Fe_3P$ (0.9857 g) | 8 |
| 40 | ESR Air | NaOH (0.1 M), DMPO (0.2 M) | Fe (~1 g) | 13 |
| 41 | ESR Air | DMPO (0.2 M) | $Fe_3P$ (~1 g) | 7 |

[1]Data presented in Pasek and Lauretta (2005). Included here for completeness.

Table 10. Synthesis reactions.

| Reactants | P compounds | Conditions | Goal Product |
|---|---|---|---|
| Pyruvate (0.1 M) | $HPO_3^{2-}$ (0.1 M), $P_2O_7^{4-}$ (0.1 M) | - | Phosphoenolpyruvate |
| Pyruvate (0.1 M) | $HPO_3^{2-}$ (0.1 M), $P_2O_7^{4-}$ (0.1 M) | Fe (~1 g) | Phosphoenolpyruvate |
| Pyruvate (0.1 M) | $HPO_3^{2-}$ (0.1 M), $P_2O_7^{4-}$ (0.1 M), $Na_2HPO_4$ (0.1 M) | - | Phosphoenolpyruvate |
| Pyruvate (0.1 M) | $HPO_3^{2-}$ (0.1 M), $P_2O_7^{4-}$ (0.1 M), $Na_2HPO_4$ (0.1 M) | Fe (~1 g) | Phosphoenolpyruvate |
| Pyruvate (0.1 M) | $HPO_3^{2-}$ (0.07 M), $P_2O_7^{4-}$ (0.5 M), $P_2O_6^{4-}$ (0.1 M) | - | Phosphoenolpyruvate |
| Pyruvate (0.1 M) | $HPO_3^{2-}$ (0.07 M), $P_2O_7^{4-}$ (0.5 M), $P_2O_6^{4-}$ (0.1 M) | $MgCl_2$ (0.02 M), $NH_4Cl$ (0.06 M) | Phosphoenolpyruvate |
| Pyruvate (0.1 M) | $HPO_3^{2-}$ (0.07 M), $P_2O_7^{4-}$ (0.5 M), $P_2O_6^{4-}$ (0.1 M) | $NH_4Cl$ (0.06 M) | Phosphoenolpyruvate |
| Pyruvate (0.1 M) | $HPO_3^{2-}$ (0.07 M), $P_2O_7^{4-}$ (0.5 M), $P_2O_6^{4-}$ (0.1 M) | $MgCl_2$ (0.02 M) | Phosphoenolpyruvate |
| Glycolaldehyde (0.1 M) | $HPO_3^{2-}$ (0.07 M), $P_2O_7^{4-}$ (0.5 M), $P_2O_6^{4-}$ (0.1 M) | - | Glycolaldehyde-phosphate |
| Glycolaldehyde (0.1 M) | $HPO_3^{2-}$ (0.07 M), $P_2O_7^{4-}$ (0.5 M), $P_2O_6^{4-}$ (0.1 M) | $MgCl_2$ (0.02 M), $NH_4Cl$ (0.06 M) | Glycolaldehyde-phosphate |
| Glycolaldehyde (0.1 M) | $HPO_3^{2-}$ (0.07 M), $P_2O_7^{4-}$ (0.5 M), $P_2O_6^{4-}$ (0.1 M) | $NH_4Cl$ (0.05 M) | Glycolaldehyde-phosphate |
| Glycolaldehyde (0.1 M) | $HPO_3^{2-}$ (0.07 M), $P_2O_7^{4-}$ (0.5 M), $P_2O_6^{4-}$ (0.1 M) | $MgCl_2$ (0.02 M) | Glycolaldehyde-phosphate |
| Acetate (0.4 M) | $HPO_3^{2-}$ (0.1 M) | - | Acetyl-phosphate |
| Acetate (0.4 M) | $HPO_3^{2-}$ (0.1 M) | Fe (~1 g) | Acetyl-phosphate |
| Acetate (0.4 M) | $HPO_3^{2-}$ (0.1 M), $P_2O_6^{4-}$ (0.035 M) | - | Acetyl-phosphate |
| Acetate (0.4 M) | $HPO_3^{2-}$ (0.1 M), $P_2O_6^{4-}$ (0.035 M) | Fe (~1 g) | Acetyl-phosphate |
| $H_2O_2$ (0.02 M) | $PO_4^{3-}$ (0.1 M) | w/w/o Fe (~0.4 g) | Pyrophosphate |
| $H_2O_2$ (0.02 M) | $HPO_3^{2-}$ (0.2M) | w/w/o Fe (~0.4 g) | Pyrophosphate |
| $H_2O_2$ (0.02 M) | $P_2O_6^{4-}$ (0.1M) | w/w/o Fe (~0.4 g) | Pyrophosphate |
| $H_2O_2$ (0.02 M) | $PO_4^{3-}$ (0.1 M), $HPO_3^{2-}$ (0.2M) | w/w/o Fe (~0.4 g) | Pyrophosphate |
| $H_2O_2$ (0.02 M) | $PO_4^{3-}$ (0.1 M), $HPO_3^{2-}$ (0.2M) | w/w/o Fe (~0.4 g) | Pyrophosphate |
| $H_2O_2$ (0.02 M) | $HPO_3^{2-}$ (0.2M), $P_2O_6^{4-}$ (0.1M) | w/w/o Fe (~0.4 g) | Pyrophosphate |
| $H_2O_2$ (0.02 M) | $PO_4^{3-}$ (0.1 M), $HPO_3^{2-}$ (0.2M), $P_2O_6^{4-}$ (0.1M) | w/w/o Fe (~0.4 g) | Pyrophosphate |

iron powder (99+%, Alfa Aesar) was used in some of the corrosion experiments. Natural specimens of fluorapatite (Minas do Panasquiera, Fundao, Portugal) and magnetite (Serro, Minas Gerais, Brazil) were used in other experiments. The conditions for all synthesis experiments are given in table 10. Unless stated otherwise, the conditions and reactants used are identical to those of the corrosion experiments.

The solution volume for all experiments was 25 mL. Aqueous solutions were either pure deionized water, purified in house using a Barnstead NANOpure® Diamond Analytical combined reverse osmosis-deionization system, or solution created by adding compounds to the deionized water. Solutions were created by adding salts of Mg- and Ca-chloride (98%, from Alfa Aesar), reagent alcohol (90.5% ethanol, 5% isopropanol, and 4.5% methanol from VWR lab supplies), acetic acid (99.7% from EMD lab supplies), $Na_2EDTA$ (from VWR, 0.1000 M stock solution), $NaHCO_3$ (Arm and Hammer, 100%), adenosine (Avocado Research Chemicals, Ltd, 99+%), glycolaldehyde (MP Biomedicals LLC., 99+%), acetaldehyde (Merck, $>= 99\%$), $H_2O_2$ (30% in water, VWR lab supplies), pyruvate (Alfa Aesar, 98%), acetonitrile (J.T. Baker, 99.8%), 5-5-dimethyl-1-pyrroline-N-oxide (DMPO from Alexis Biochemicals, 100%, stored at -10°C) or a combination of these components. Molecular diagrams for the organic compounds are shown in figure 5. The initial pH was held constant between 6.5 – 8 in most experiments. Acidic solutions were buffered using NaOH (from VWR, 10.0 N stock solution) or $NH_4OH$ (from ADChemco Scientific Inc., 28-30% in water). Half of each solution was isolated from the P mineral and saved for comparison as a blank. Solution chemistry and powder mineralogy were determined before and after reaction.

Figure 5. Organic compounds employed in corrosion experiments.
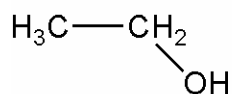
Ethanol                Acetic Acid               Acetone
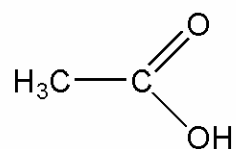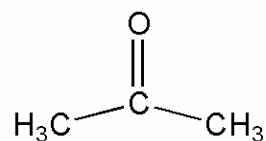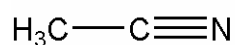
Acetonitrile           Acetaldehyde              Pyruvic Acid
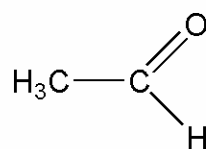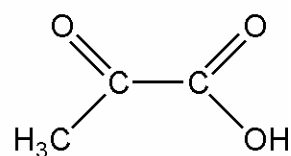
EDTA (Ethylenediaminetetraacetic Acid)
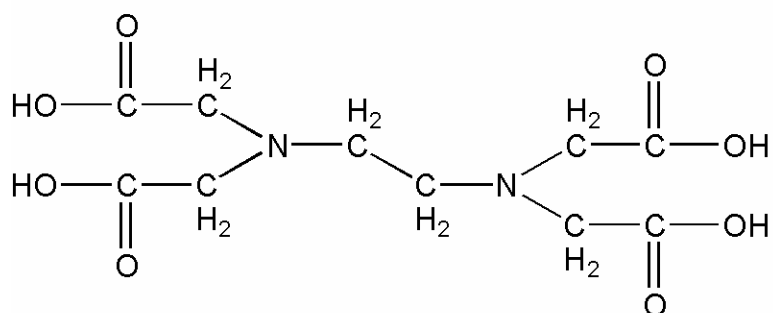
5-5-dimethyl-1-pyrroline-N-oxide
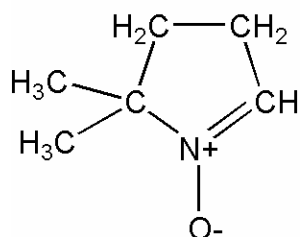
Pure compounds were used as standards for species identification and were prepared at 0.01 M in $D_2O$ and NaOH (pH 13). Standards used include $H_3PO_3$, $H_3PO_4$, $Na_4P_2O_7$, $NaH_2PO_2$, $C_2H_5PO_3H_2$, $CH_3PO_3H_2$, $(CH_3)_3PO_4$, $Ba(PO_3)_2$ and $P_2O_5$ and were acquired from VWR International, and acetylphosphonic acid ($H_2O_3PCH_2COOH$, 98+%) was acquired from Alfa Aesar.  Since hypophosphate is not commercially available, several grams were prepared by the method outlined by Yoza and Ohashi (1965).  The resulting hypophosphate was verified to be pure by $P^{31}$ NMR.  Several of these pure compounds were used during corrosion and synthetic experiments. The temperature in all experiments was held constant at ~20° C and variations in temperature were slight, ±3° C at most. Some experiments were performed under ambient atmospheric conditions, others were performed under high-purity (99.99%) Ar (University of Arizona Laboratory Stores) to remove all dissolved $O_2$ from the water as well as maintain an inert atmosphere prior to introduction of the phosphide to the water. This procedure eliminates the possibility of dissolved atmospheric $O_2$ playing a role in the corrosion of the phosphide.

2.1.2 Experimental Setup

*General phosphide corrosion experiments and synthesis experiments.*  Experiments denoted by "NMR Air" were sealed under air at ambient atmospheric pressure.  No attempt was made to remove $O_2$ from these systems, though performing experiments under atmospheric conditions did not greatly change the resulting solution chemistry, as described later.  All synthesis experiments were performed under air.

*Inert corrosion experiments.* These experiments were performed under an argon atmosphere and repeated the phosphide and deionized water experiment, phosphide and $NaHCO_3$ experiment, phosphide and acetic acid and ethanol experiment, and phosphide and $MgCl_2$ and $CaCl_2$ experiment, in the same concentrations as listed above. I also performed an experiment with glycolaldehyde and phosphide. I did not repeat the $MgCl_2/CaCl_2$/organics experiment under argon as the results with air initially seemed identical to the solution without organics. In each experiment the solution was frozen, vacuumed down, melted, and flushed with argon gas a total of three times. During these cycles, the phosphide powder was prevented from coming in contact with the solution by suspending the powder with a magnet. After the final melting of the solution, removal of the magnet introduced the phosphide powder to the solution.

*Phosphate solvation experiments.* Samples of fluoroapatite were crushed into a fine white powder. One solution consisted of deionized water, the other was an 0.05 M EDTA (ethylenediaminetetraacetic acid) and 0.25 M NaOH solution used in soil sciences (Cade-Menun et al. 2002). These experiments were performed under air.

*P compound stability experiments.* I took a solution of 0.01-10.0 M P compound and placed samples of 25 mL of solution in two round bottomed flasks. One sample was sealed and kept separated, and to another ~0.5-1 g of iron powder was added, though one set of experiments substituted ~0.5 g of crushed magnetite for the iron powder. Samples were analyzed after one day of constant stirring.

After one day of corrosion, the experiments described above were brought to a pH of 13 by addition of NaOH to sharpen NMR peaks and allow for comparison with

previous studies. Samples with Mg and Ca salts precipitated a white powder upon addition of NaOH. The NaHCO$_3$ solutions were left at a pH of 9.5 so as to minimize dilution of these buffered solutions (too much NaOH would need to be added to change the pH to 13). The sample was filtered, the extract concentrated by vacuum and then redissolved in 5 mL of D$_2$O (99.7%, Alfa Aesar).

*Detailed phosphide corrosion experiments.* One experiment replicated the phosphide corrosion in acetic acid under air experiment, but used NH$_4$OH as a buffer instead of NaOH. This allowed analysis by ES- TOF-HR-MS (negative Electron Spray Time Of Flight High Resolution Mass Spectrometry) as CH$_3$COONa formed clusters that swamped the signal and prevented detection of minor P species.

The final experiments described in table 9 were simple corrosion experiments analyzed by Electron Paramagnetic Resonance (EPR) spectrometry. Samples were prepared by removing a small quantity of solution and adding DMPO to the solution for a final concentration of DMPO of about 0.2 M. DMPO was added to each solution since hydroxyl and phosphite radicals are very short-lived (Ozawa and Hanaki 1987) and can not be detected unless specific spin traps are used. No NaOH was added to the phosphide sample.

## 2.1.3 Analytical Methods

The gas phase, solid phase, and liquid phase of these experiments were analyzed by a variety of techniques summarized below.

*Gas phase analysis.* The composition of the gas above the sealed system was monitored using a Stanford Research Systems Quadrupole Mass Spectrometer (SRS-QMS-100) Residual Gas Analyzer to determine gases evolved during corrosion. Masses monitored include 2 ($H_2$), 4 (He), 12 (C), 14 (N, $CH_2$), 16 (O, $CH_4$), 17 (OH), 18 ($H_2O$), 28 ($N_2$, CO), 31 (P), 32 ($O_2$), 40 (Ar), and 44 ($CO_2$). The residual gas analyzed was calibrated by introducing a series of binary mixtures of known composition at different mass ratios of $H_2$-CO, $H_2$-$CO_2$, CO-$CO_2$, as well as ambient air. The gas analyzer removes ~0.4 mbar of gas per second, which was compensated for by a steady stream of Ar gas.

*Solid phase analyses.* X-ray diffraction analyses were performed using a Philips X'Pert Pro MPD powder and thin-film X-ray diffractometer on the experimental powders before and after corrosion at the University of Arizona Molecular Structure Laboratory. Scans were from a 2θ of 10° to 79.98° with continuous spinning and a copper (Kα) X-ray source. Spectra were then compared to available mineral data to match compounds present.

Electron microprobe samples of phosphide powder were mounted in epoxy, polished, and analyzed by an SX50 electron microprobe.  Samples of unreacted powder, and of two dry corrosion experiment powders were analyzed by this method.  The standards used for analysis are summarized in section 2.4 of this chapter.

*Liquid phase analyses.* Each solution was analyzed using ^{31}P NMR on a Varian 300 four-nucleus probe FT-NMR (Fourier Transform-Nuclear Magnetic Resonance) spectrometer at 121.43 MHz and 24.5 ºC. The number of scans ranged from 256 to

35000, depending on the desired signal-to-noise ratio. Spectra were first acquired

decoupled with respect to H, and then fully coupled to determine connectivity.  NMR is a

quick and exact technique that gives great detail into molecular bond structure, but lacks

the sensitivity and quantitative analysis of other methods.  It has a detection limit of ~10-

100 $\mu$M.

The bulk dissolved P content was measured using a ThermoFinnigan ELEMENT2

high-resolution Inductively Coupled Plasma Mass Spectrometer (ICP-MS). Experimental

fluids were diluted by a factor of 300 to reduce the total abundance in solution within the

range of detection. A series of standard solutions were prepared ($KH_2PO_4$ in water) with

concentrations of 10 ppb, 100 ppb, and 1 ppm ($3.2 \times 10^{-7}$ M, $3.2 \times 10^{-6}$ M, $3.2 \times 10^{-5}$ M,

respectively). 1-$\sigma$ deviations using this method are 1.7%. ICP-MS provides an extremely

accurate quantitative analysis of total abundance of elements, but provides no information

on bonding.

After determining bulk aqueous P composition, the abundance of each compound

was determined by integration of the NMR spectrum. NMR integration is quantitative if

the integration is done over a narrow range of frequencies (typically less than 50 ppm),

and if the Nuclear Overhauser Effect (NOE) is eliminated by turning off the proton

decoupler prior to acquisition.  It was later determined that the NOE did not affect

integrations significantly, despite the presence of H-P compounds.

Mass spectrometry was performed using a Waters LCT Premier Time of Flight

High-Resolution Mass Spectrometer (TOF-HR-MS) at the astrochemistry lab at NASA

GSFC.  The solution was directly injected into the mass spectrometer with no separation

and was ionized by electron spray and measured in W mode (double bounce) for increased resolution. The mass range was 50 to 400 m/z, and adenine ($C_5H_5N_5$) was used as the standard mass lock. Fragmentation is rare with this MS and most masses are molecular masses ±1 AMU depending on whether one is detecting positive or negative ions. Negative ions were observed, but the species in solution did not ionize in positive mode. The spectrum was acquired for 3 minutes after which time the spectra were summed and averaged. Mass deviations were <100 ppm for nearly all species, corresponding to a mass resolution of 10,000. TOF-HR-MS gives very precise information on the masses of species formed but does not provide information on the molecular characteristics, and can not distinguish between different structural isomers. Detection limits are 100 nM - 1 μM.

EPR analyses were performed using the University of Arizona chemistry department's continuous wave X-band (9-10 GHz) EPR spectrometer, model ESP-300E manufactured by Bruker. Samples were siphoned into capillary tubes and analyzed with a 1 Gauss modulation and a 20 mW microwave power source. Each spectrum consists of 30 scans from 3290 to 3390 Gauss. EPR is an excellent technique for detecting radical species.

2.2 Results

For experiments 1-26, analyses of blank solutions by NMR revealed no P compounds in solution as a contaminant of water or as a constituent of solutions (figure 6). All P observed by NMR in solution originated from the corroded phosphide.

2.2.1 Corrosion Experiments

In all experiments exposed to air the phosphide powder changed color from gray to a reddish brown. In the experiments isolated from air and flushed under argon, color change was limited to black. The pH of all systems remained relatively unchanged. Besides external appearance, a number of P species were identified in aqueous solution. The abundances of all P species and total abundance of P in each experiment is given in table 11. The ionic species were identified based on comparison to standards and literature values (Yoza et al. 1994).

The bulk P in solution was analyzed by ICP-MS for five experiments. Based on these data, the bulk P in solution was determined from NMR spectra using a relationship between the signal to noise, number of scans, and molarity established by five experiments analyzed by ICP-MS. I use the relationship to determine molarity *[M]* defined by a quadratic curve fit ($R^2 = 0.9939$):

Figure 6. Sample NMR spectrum of blank solution.  Number of scans = 4096.  No P compounds are present in solution.
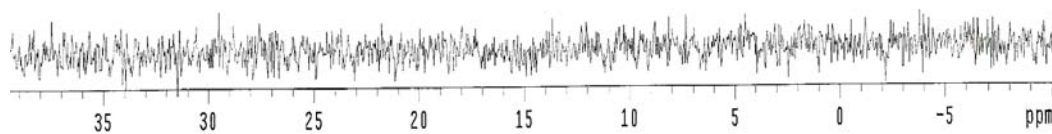
Table 11. Results of corrosion experiments. P compounds given in μM, and in percent for stability experiments. Pi is orthophosphate, P3 is phosphite, P4 is hypophosphate, and PPi is pyrophosphate. "Other" includes a number of varied species with definite identifications listed. Errors are ~1% for ICP-MS, and ~10% for NMR.

| No. | Atmo | Solution | Material Corroded | Bulk P in mM, (method) | Pi μM | P3 μM | P4 μM | PPi μM | Other μM (Identification) |
|---|---|---|---|---|---|---|---|---|---|
| 1 | Air | Water | $Fe_3P$ | 2.30 (ICP-MS) | 430 | 1100 | 360 | 450 | |
| 2 | Air | $MgCl_2/CaCl_2$ | $Fe_3P$ | 1.07 (ICP-MS) | | 1100 | | | |
| 3 | Air | $CH_3COONa$, EtOH | $Fe_3P$ | 9.49 (ICP-MS) | 3000 | 4200 | 1300 | 140 | 1610 (Many) |
| 4 | Air | $MgCl_2/CaCl_2$, $CH_3COONa$, EtOH | $Fe_3P$ | 0.368 (ICP-MS) | | 370 | | | Minor P-O-C ? |
| 5 | Air | $NaHCO_3$ | $Fe_3P$ | 14.7 (NMR) | 6700 | 2700 | 620 | 2900 | 1800 (Diphosphite) |
| 6 | Air | NaCl | $Fe_3P$ | 5.2 (NMR) | 930 | 2500 | 750 | 700 | |
| 7 | Air | NaOH | $Fe_3P$ | 1.1 (NMR) | 530 | 340 | 130 | 72 | |
| 8 | Air | NaOH, EDTA | $Fe_3P$ | 3.8 (NMR) | 1300 | 1600 | 460 | 430 | 26 (P-H compounds) |
| 9 | Air | $CH_3CN$ | $Fe_3P$ | 6.4 (NMR) | 1700 | 3500 | 770 | 470 | |
| 10 | Air | EtOH | $Fe_3P$ | 0.89 (NMR) | 420 | 340 | 91 | 44 | |
| 11 | Air | Acetone | $Fe_3P$ | ND | | | | | Turned to tar |
| 12 | Air | $CH_3COONa$ | $Fe_3P$ | 11.7 (NMR | 5400 | 4000 | 790 | 120 | 1400 (Many) |
| 13 | Air | $CH_3COONa$ | $Fe_3P$ | 7.9 (NMR) | 2700 | 3500 | 980 | 490 | 270 (Many) |
| 14 | Air | Pyruvate | $Fe_3P$ | 0.66 (NMR) | 170 | 240 | 68 | 50 | 140 (Many) |
| 15 | Air | Acetaldehyde | $Fe_3P$ | 0.40 (NMR) | 180 | 120 | 110 | 29 | Trace (Many) |
| 16 | Air | $H_2O_2$ | $Fe_3P$ | 5.3 (NMR) | 2800 | 1600 | 750 | 250 | 35 (Many) |
| 17 | Air | $CH_3COONa$, Apatite | $Fe_3P$ | 4.4 (NMR) | 2000 | 1300 | 650 | 200 | 220 (Many) |
| 18 | Air | Adenosine, Apatite | $Fe_3P$ | ND | | | | | Turned to tar |
| 19 | Air | Adenosine, Apatite, NaOH | $Fe_3P$ | 0.31 (NMR) | 230 | 48 | 25 | 8 | |
| 20 | Air | Water | Apatite | ~0.001 | 1 | | | | |
| 21 | Air | NaOH, EDTA | Apatite | ~1 (NMR) | 1000 | | | | |
| 22 | Argon | Water | $Fe_3P$ | 0.269 (ICP-MS) | 130 | 100 | 18 | 23 | |
| 23 | Argon | $MgCl_2/CaCl_2$ | $Fe_3P$ | 0.27 (NMR) | | 270 | | | |
| 24 | Argon | $CH_3COONa$, EtOH | $Fe_3P$ | 3.1 (NMR) | 940 | 1300 | 340 | 510 | 80 (Many) |
| 25 | Argon | $NaHCO_3$ | $Fe_3P$ | 0.33 (NMR) | 120 | 130 | 22 | 44 | 22 (Diphosphite) |
| 26 | Argon | Glycolaldehyde | $Fe_3P$ | ND | | | | | Turned to tar |

Table 11 cont'd.

| No. | Atmo | Solution | Material Corroded | Bulk P in mM, (method) | Pi % | P3 % | P4 % | PPi % | Other % (Identification) |
|---|---|---|---|---|---|---|---|---|---|
| 27 | Air | $Na_2HPO_3$ | Fe | ND | 46% | 54% | | | |
| 28 | Air | $Na_2HPO_3$ | - | ND | | 100% | | | |
| 29 | Air | $Na_2HPO_3$ | $Fe_3P$ | ND | 15% | 85% | | | |
| 30 | Air | $Na_2HPO_3$ | $Fe_3O_4$ | ND | | All | | | |
| 31 | Air | $NaH_2PO_2$ | Fe | ND | | 25% | | | 75% (hypophosphite) |
| 32 | Air | $NaH_2PO_2$ | - | ND | | 25% | | | 75% (hypophosphite) |
| 33 | Air | $NaH_2PO_2$, $Na_2HPO_3$ | - | ND | | 52% | | | 48% (hypophosphite) |
| 34 | Air | $NaH_2PO_2$, $Na_2HPO_3$ | $Fe_3O_4$ | ND | | 70% | | | 30% (hypophosphite) |
| 35 | Air | $Na_2HPO_3$ | Fe | ND | Too much phosphite (signal swamped) | | | | |
| 36 | Air | $Na_2HPO_4$ | Fe | ND | 100% | | | | |
| 37 | Air | $Na_4P_2O_6$ | Fe | ND | | | 100% | | |
| 38 | Air | $Na_4P_2O_7$ | Fe | ND | | | | 100% | |

ND is not determined

$$[M] = 0.0075 \times \left( \frac{\left( \frac{S}{N} \right)}{\sqrt{Scans}} \right)^2 + 0.0007 \times \left( \frac{\left( \frac{S}{N} \right)}{\sqrt{Scans}} \right) + 0.0001 \qquad (18)$$

where $S$ is the signal, $N$ is the noise, and *Scans* is the number of scans taken (figure 7).

The rationale for this relationship is that the NMR signal to noise ratio is proportional to

the square root of the number of scans, and the abundances are calculated from the signal

to noise ratio or the total area under a peak.  While not as exact as ICP-MS, it is accurate

to ~10% over the range of $10^{-4}$ to $10^{-2}$ M based on the sample spectra acquired.

Table 12 summarizes the coupling constants, peak locations, and other pertinent

NMR data from the experiments detailed below.

*Phosphate Solvation.* Aqueous dissolution of apatite yields orthophosphate

concentrations $<10^{-6}$ M although in extremely basic water with a chelating agent, the

concentration is ~1 mM. These yields are consistent with the known solubility of apatite

and with its solubility reported in the presence of chelating agents (Schwartz 1971).  No

other P species were detected.  The apatite powder remained the same color during both

experiments.

*Phosphide Corrosion in Deionized Water.* Corrosion of $Fe_3P$ in deionized water

proceeds rapidly at 20° C and produces multiple P-bearing compounds (figure 8). The x-

ray diffraction pattern of the corroded powder was consistent with schreibersite, despite

the reddish coloration (which is most likely goethite, based on other experiment results).

EMPA analysis confirmed the powder's identity, and also revealed a small quantity

Figure 7. Relationship between ICP-MS concentration and NMR S/N. The signal to noise ratio is divided by square root of the number of scans. Vertical uncertainties are smaller than the symbols used.
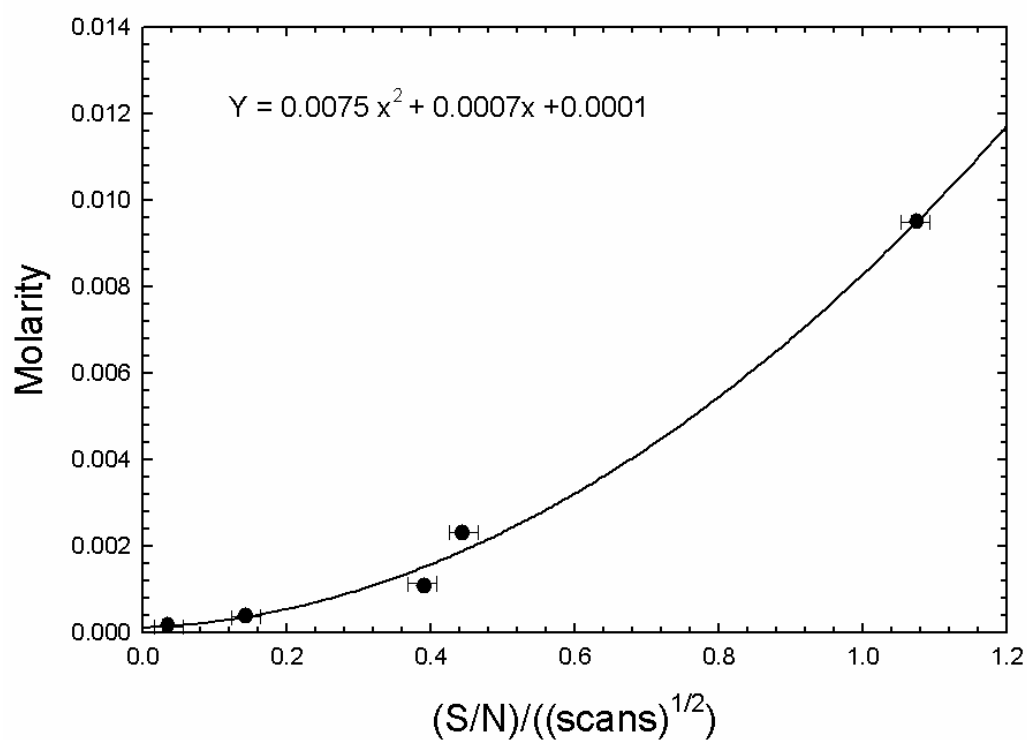
Table 12. NMR peak location data.  pH of 13, unless otherwise noted.

| Compound ID | Peak (ppm) | Coupling constant |
|---|---|---|
| **Deionized water and Saline Experiments** | | |
| Hypophosphate | 14.4264 | |
| Orthophosphate | 6.42304 | |
| Phosphite | 4.17083 | 1 bond P-H (570 Hz) |
| Pyrophosphate | -3.52734 | |
| | | |
| **Acetate Experiment** | | |
| Unknown P compound | 37.7126 | 1 bond P-P (308 Hz), 2 bond P-P (40 Hz) |
| Unknown P compound | 37.3909 | |
| Unknown P compound | 34.8571 | |
| Unknown P compound | 34.5736 | |
| P-H compound* | 26.6125 | 1 bond P-H (449 Hz) |
| P-H compound* | 22.7918 | 1 bond P-H (444 Hz) |
| Methyl Diphosphite | 19.4 | |
| Unknown organic P compound | 17.8 | 2 bond P-H (72 Hz) |
| Acetyl phosphonate | 15.593 | |
| Unknown organic P compound | 12.7775 | |
| Hydroxylmethyl phosphonate | 11.8927 | 2 bond P-H (20 Hz) |
| Unknown organic P compound | 11.3296 | |
| Unknown P compound | 9.31873 | |
| Unknown P compound | 9.19808 | |
| Phosphoglycolate | 3.4 | 3 bond P-H (18 Hz) |
| Unknown P compound | -2.626 | |
| Unknown P compound | -2.827 | |
| Other condensed phosphates | -9.3424 | |
| Other condensed phosphates | -10.7903 | |
| Other condensed phosphates | -17.5871 | |
| Other condensed phosphates | -19.2763 | |
| | | |
| **pH of 9.5 locations (NaHCO$_3$ buffered)** | | |
| Hypophosphate | 14.4666 | |
| Orthophosphate | 4.25127 | |
| Phosphite | 4.1321 | 1 bond P-H (570 Hz) |
| Diphosphite | -3.2695 | 1 bond P-H (650 Hz), 3 bond P-H (20 Hz) |
| Pyrophosphate | -4.27495 | |

*Also in $H_2O_2$ experimental corrosion.

Figure 8. NMR spectrum of phosphide corrosion in de-ionized water.  Phosphorus species are identified.
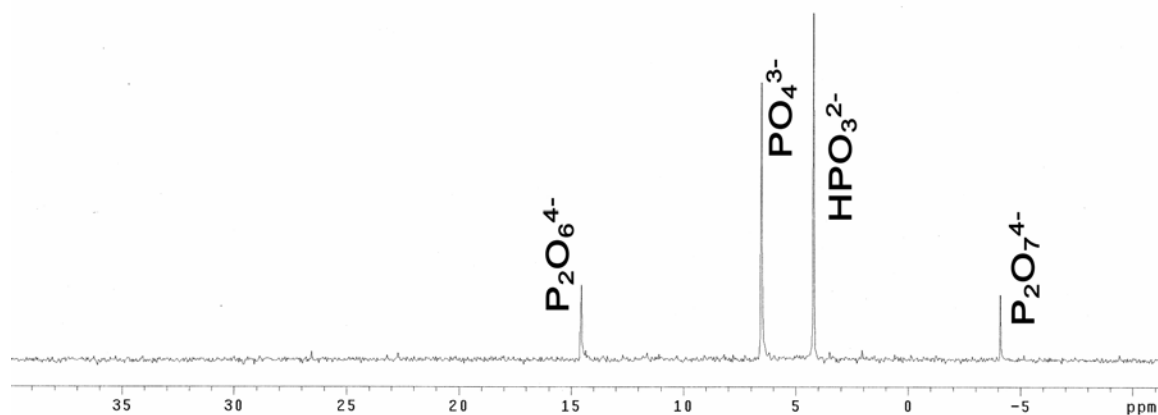
(~5%) of $Fe_2P$. The total P concentration of this solution was $2.30 \pm 0.04$ mM. The most abundant molecules are orthophosphate, phosphite, hypophosphate, and pyrophosphate. The evolution and abundance of multiple gases was monitored during the experiment with deionized water flushed with argon using the SRS-QMS-100. The total abundance of P in this experiment was $\sim 0.269 \pm 0.005$ mM. The only gas that showed any variation upon addition of $Fe_3P$ was $H_2$ (figure 9). The total amount of hydrogen gas evolved during corrosion in deionized water is calculated from the ideal gas law and the pumping rate of the gas analyzer ($\sim 35$ bar of gas removed /day). The volume of the total container was 250 mL, the pressure change of $H_2$ was $\sim 1$ mbar, at a temperature of 293 K, giving a total of $\sim 4 \pm 2 \times 10^{-4}$ moles of $H_2$ gas evolved during one day.

*Phosphide Corrosion in Inorganic Solutions.* Yields of P species from corrosion of synthetic schreibersite in $Mg^{2+}$ and $Ca^{2+}$ chloride salts are significantly different from those in deionized water (total P concentration $1.07 \pm 0.02$ mM). In particular, orthophosphate, hypophosphate, and pyrophosphate are not present at levels above the detection limit. Phosphite, however, is present in significant abundance (100%- see figure 10). Additionally, the resulting corroded powder contains goethite and Ca, Mg, and Fe P-oxides. Mineral identification is incomplete as the XRD library did not have data for Ca and Mg salts of reduced or poly-phosphorus species. The XRD patterns for unreacted $Fe_3P$ and the heavily reacted $MgCl_2/CaCl_2$ with $Fe_3P$ are shown in figure 11, and the peak list is summarized in table 13. Repetition of this experiment in a sealed argon-flushed flask did not change the solution chemistry, only the abundance of phosphite observed ($0.27 \pm 0.03$ mM).

Figure 9. $H_2$ production following addition of $Fe_3P$ to water. There is a baseline of about 2.8 mbar of $H_2$ resulting from the dissociation of water in the SRS-QMS-100 mass spectrometer. The actual increase in $H_2$ pressure is about 1 mbar.
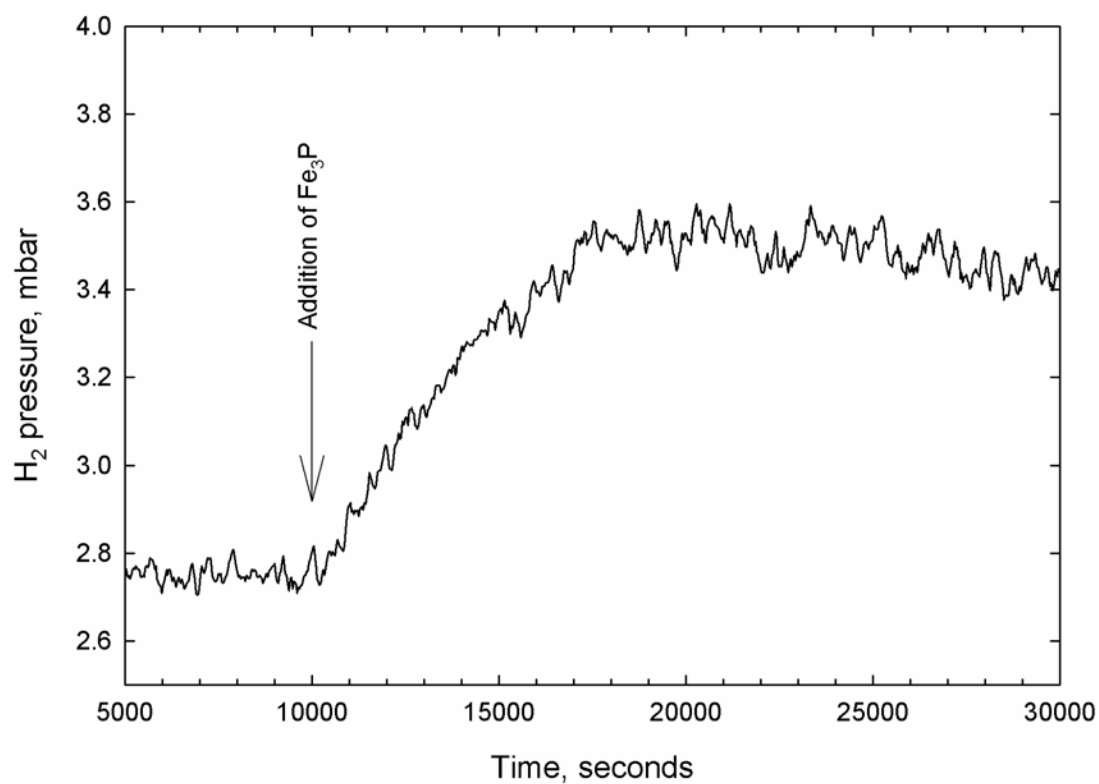
Figure 10. NMR spectrum of phosphide corrosion in $Mg^{2+}$ and $Ca^{2+}$ solution. The single peak is phosphite.
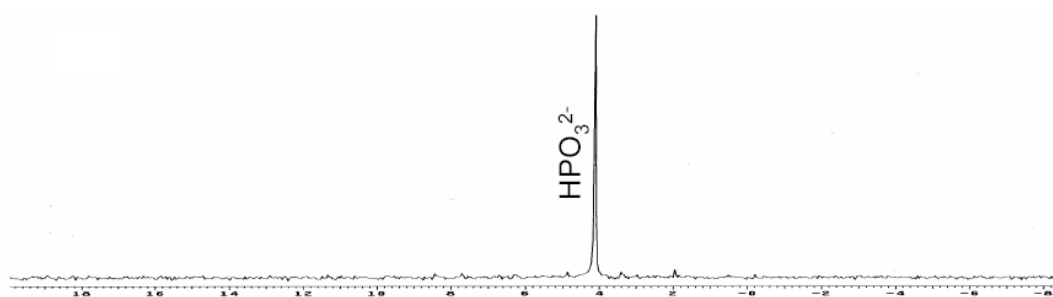
Figure 11.  X-ray diffraction spectra.
A) XRD spectrum of unreacted Fe$_3$P powder.
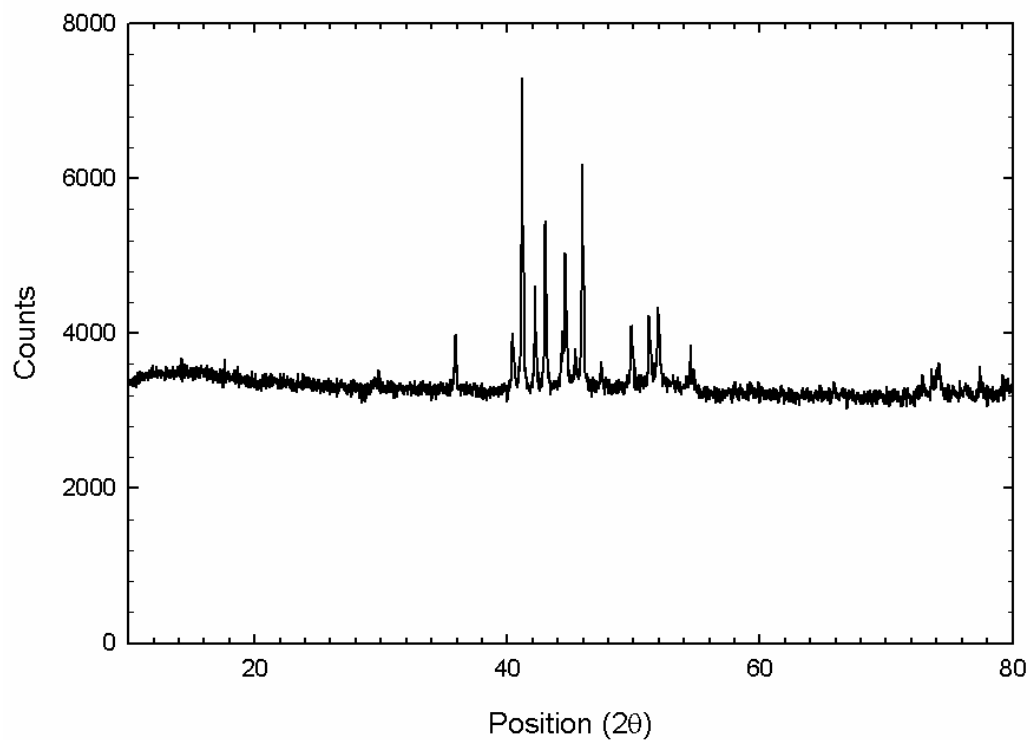


B) XRD spectrum of Fe$_3$P powder reacted with MgCl$_2$/CaCl$_2$.
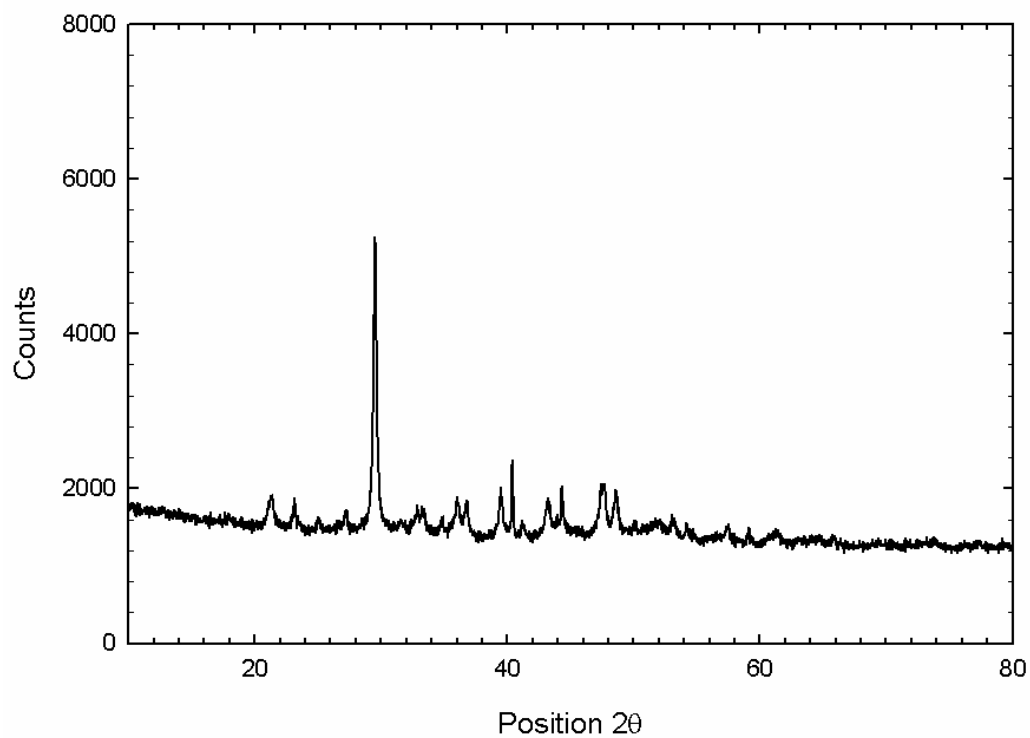
Table 13. XRD data for unreacted $Fe_3P$ powder and Mg and Ca reacted powder. Pos. is $2\theta$ ° position, cts is counts, FWHM is full width at half-maximum, A is angstroms, Sch is schreibersite, Bar is barringerite, Goe is goethite and other Fe-O-H compounds, $Ca-PO_4$ is data consistent with miscellaneous phosphate minerals. Identification is incomplete since reduced P-O species have not been characterized by XRD, and is likely a mixture of many components.

| | | Unreacted Powder | | | |
|---|---|---|---|---|---|
| Pos. [°2Th.] | Height [cts] | FWHM [°2Th.] | d-spacing [Å] | Rel. Int. [%] | ID |
| 29.6169 | 111.98 | 0.8029 | 3.01632 | 2.41 | Sch |
| 35.8880 | 724.59 | 0.0612 | 2.50027 | 15.61 | Sch |
| 40.4263 | 768.25 | 0.1320 | 2.22943 | 16.55 | Sch, Bar |
| 41.1753 | 4640.91 | 0.0931 | 2.19059 | 100.00 | Sch |
| 42.1963 | 1590.77 | 0.0907 | 2.13992 | 34.28 | Sch |
| 43.0145 | 2550.92 | 0.0957 | 2.10109 | 54.97 | Sch |
| 44.3364 | 646.54 | 0.0612 | 2.04147 | 13.93 | Bar |
| 44.5959 | 1621.95 | 0.0612 | 2.03018 | 34.95 | Sch |
| 45.3768 | 402.88 | 0.1224 | 1.99705 | 8.68 | Sch |
| 45.9445 | 2931.15 | 0.0816 | 1.97368 | 63.16 | Sch |
| 47.4633 | 241.77 | 0.2448 | 1.91401 | 5.21 | Bar |
| 49.8266 | 763.52 | 0.0816 | 1.82862 | 16.45 | Sch |
| 51.2359 | 853.94 | 0.0816 | 1.78158 | 18.40 | Sch |
| 51.9481 | 971.77 | 0.0816 | 1.75882 | 20.94 | Sch |
| 54.5359 | 370.62 | 0.2448 | 1.68132 | 7.99 | Sch, Bar |
| 74.1558 | 332.21 | 0.3264 | 1.27766 | 7.16 | Sch |
| 77.4243 | 377.69 | 0.1224 | 1.23167 | 8.14 | Sch |

Table 13 cont'd.

| Pos. [°2Th.] | Height [cts] | FWHM [°2Th.] | d-spacing [Å] | Rel. Int. [%] | ID |
|---|---|---|---|---|---|
| | | **Fe$_3$P+MgCl$_2$/CaCl$_2$** | | | |
| 21.3824 | 377.45 | 0.2007 | 4.15564 | 10.08 | Goe |
| 23.1377 | 325.55 | 0.1338 | 3.84421 | 8.70 | Ca-PO$_4$? |
| 25.0808 | 131.44 | 0.2007 | 3.55061 | 3.51 | Ca-PO$_4$? |
| 27.2137 | 198.07 | 0.2676 | 3.27698 | 5.29 | ? |
| 29.5157 | 3743.83 | 0.1506 | 3.02644 | 100.00 | Ca-PO$_4$? |
| 31.4588 | 524.20 | 0.0279 | 2.84379 | 14.00 | Ca-PO$_4$? |
| 32.9103 | 830.00 | 0.2082 | 2.72162 | 22.17 | Ca-PO$_4$? |
| 33.3605 | 233.30 | 0.2676 | 2.68591 | 6.23 | Goe |
| 34.8336 | 158.01 | 0.2007 | 2.57562 | 4.22 | Goe |
| 36.0304 | 397.14 | 0.2342 | 2.49277 | 10.61 | Goe |
| 36.8399 | 387.54 | 0.2342 | 2.43983 | 10.35 | Goe |
| 39.4981 | 591.38 | 0.2342 | 2.28155 | 15.80 | Ca-PO$_4$? |
| 40.4030 | 997.90 | 0.0612 | 2.23066 | 26.65 | Bar |
| 41.2031 | 144.70 | 0.2676 | 2.19099 | 3.87 | Goe |
| 43.2053 | 402.77 | 0.2342 | 2.09399 | 10.76 | ? |
| 44.3240 | 581.35 | 0.0612 | 2.04201 | 15.53 | Bar |
| 47.3864 | 562.62 | 0.1004 | 1.91852 | 15.03 | Goe; Bar |
| 47.6410 | 1241.70 | 0.4182 | 1.90886 | 33.17 | Goe |
| 48.5929 | 521.52 | 0.2342 | 1.87367 | 13.93 | Ca-PO$_4$? |
| 53.1296 | 152.76 | 0.3346 | 1.72388 | 4.08 | Goe; Bar |
| 54.2482 | 122.04 | 0.2007 | 1.69095 | 3.26 | Goe; Bar |
| 57.4600 | 178.04 | 0.2676 | 1.60384 | 4.76 | Goe; ? |
| 59.1727 | 75.43 | 0.4015 | 1.56144 | 2.01 | Goe |
| 61.3504 | 119.97 | 0.5353 | 1.51114 | 3.20 | Goe; ? |
| 65.8433 | 94.86 | 0.3264 | 1.41732 | 2.53 | Goe; ? |

A basic solution with a pH of ~13 maintained throughout the entire experiment produces results similar to the deionized water experiment. The bulk P abundance is slightly less than the deionized water experiment, at $1.1 \pm 0.1$ mM. Corrosion in a salt solution with only NaCl produced slightly higher concentrations of P compounds compared to deionized water corrosion solutions, at $5.2 \pm 0.5$ mM, but compound species were not significantly different.

The presence of $NaHCO_3$ in solution results in the production of one additional compound, diphosphite (figure 12). This compound was identified by peak coupling constants and by comparison to Yoza et al. (1994), a study of the pH dependence of NMR spectral peaks of various P compounds. The yields in this experiment were among the highest, with total soluble P at $14.7 \pm 1.0 \times 10^{-2}$ mM. The most abundant compound was orthophosphate, followed by pyrophosphate and phosphite, then by diphosphite, and finally by hypophosphate. Total yields are reduced when the reaction is performed under the inert Ar atmosphere ($0.33 \pm 0.03$ mM). However, all five compounds are still detected, albeit at different relative ratios.

The $H_2O_2$ and phosphide solution (figure 13a) is by far the most complex of the inorganic corrosion solutions. The powder was an orange-pink color after corrosion. The P abundance is high, at about $4.9 \pm 0.5$ mM total P. Many of the P species observed in the NMR spectrum are unknown, but likely are peroxy-phosphate compounds. Two large peaks at 26.6125 and 22.7918 ppm have large J-couplings to hydrogen, indicating they are P-H compounds. The results of this experiment are qualitatively similar to the corrosion products of $Fe_3P$ and $CH_3COO^-$ compounds.

Figure 12. NMR spectrum of phosphide corrosion in NaHCO$_3$ solution.
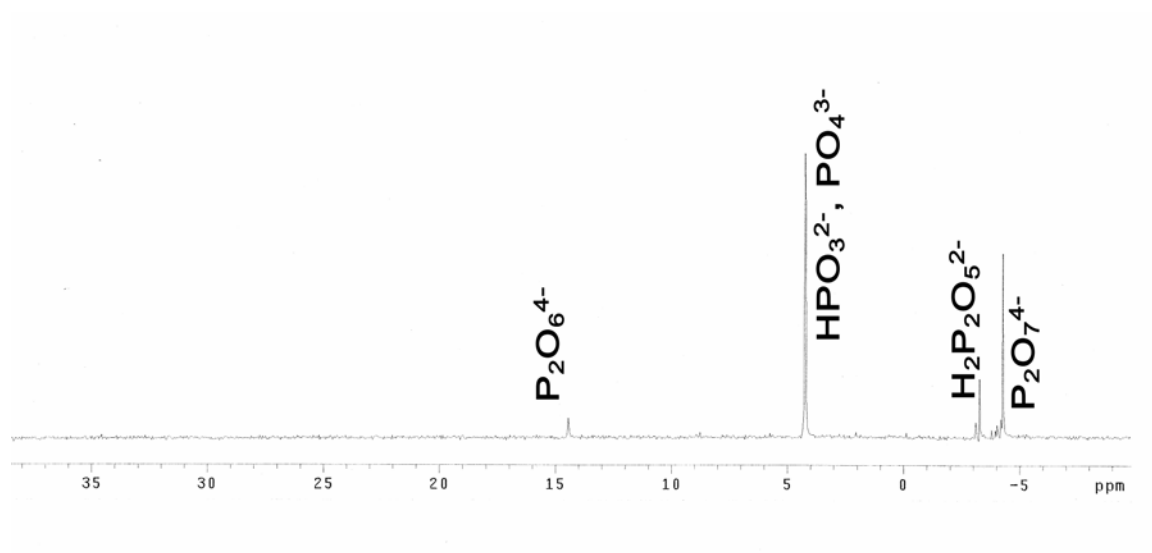
Figure 13. A comparison of NMR spectra.   a) $Fe_3P$ with $H_2O_2$ (0.6 M) and b) $Fe_3P$ with sodium acetate ± ethanol (0.4 M).  The peak heights of both spectra have been increased substantially to allow for comparison between solutions.  Major peaks are otherwise identical to those of figure 7.  Note the organic P compounds present between 15-20 ppm in b).  A spectrum of b) with higher signal to noise is presented in c).



a)      $H_2O_2$      $P_2O_6^{4-}$      $PO_4^{3-}$  $HPO_3^{2-}$      $P_2O_7^{4-}$

b)      NaOAc      org-P  $P_2O_6^{4-}$      $PO_4^{3-}$  $HPO_3^{2-}$      $P_2O_7^{4-}$

c)     NaOAc                                  $P_2O_6^{4-}$       $PO_4^{3-}$  $HPO_3^{2-}$     $P_2O_7^{4-}$
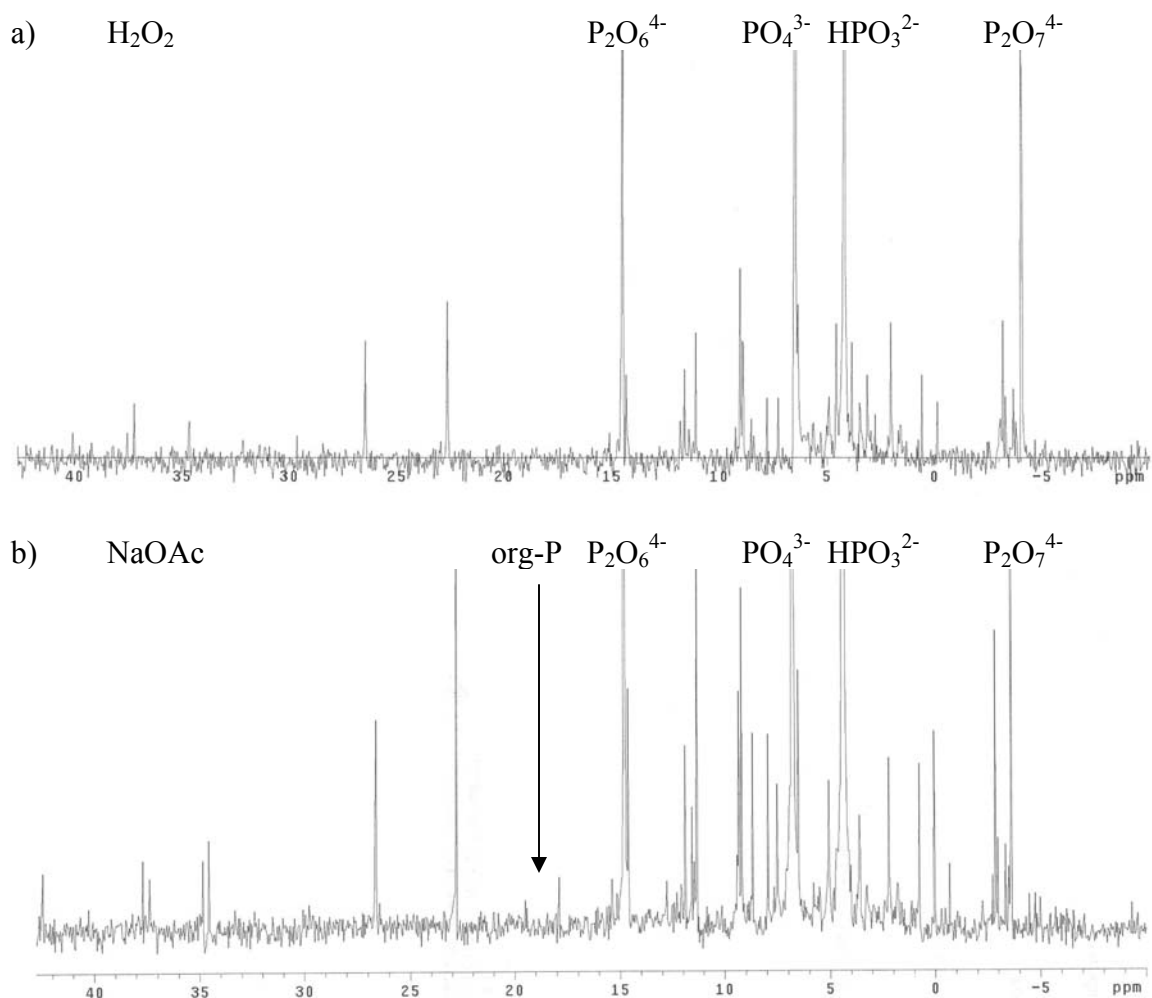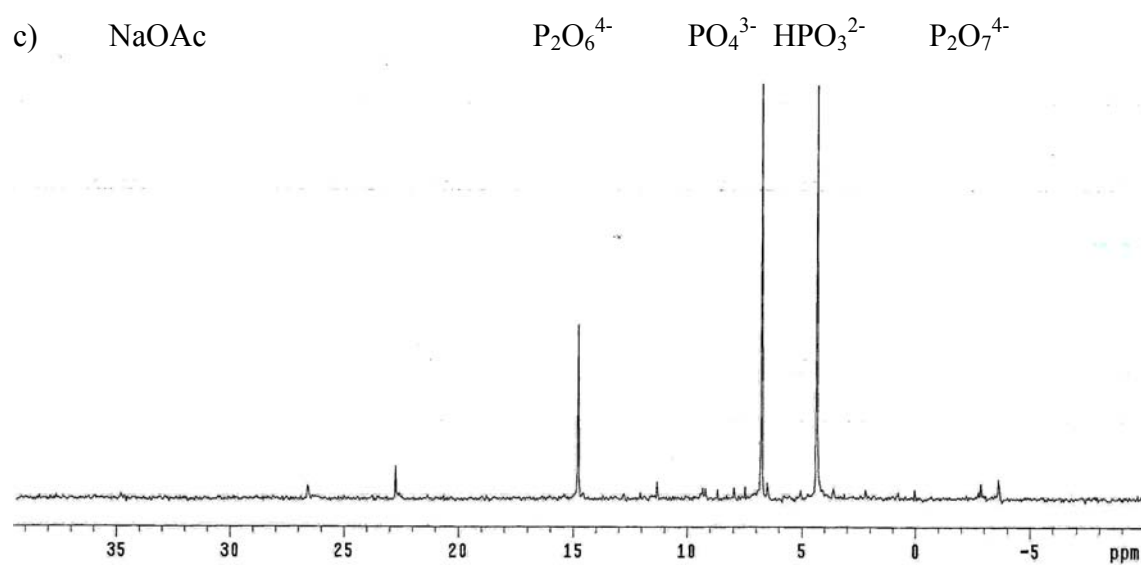
*Phosphide Corrosion in Organic-rich Solutions.* Introduction of acetic acid and ethanol to the solution significantly increases the abundances and variety of compounds formed (figure 13 b & c). As before, the x-ray diffraction pattern of the red corroded powder was consistent with schreibersite. The total P concentration in this sample was $9.49 \pm 0.02$ mM. Many of these compounds are similar to the species observed in the $H_2O_2$ corrosion experiment. Figure 12 shows that these two solutions have similar minor products in addition to similar major products. Identifying each peak is difficult as the suite of compounds produced is immense. One compound, acetyl phosphonate, was positively identified by comparison to a prepared standard. Others were identified through literature comparisons (e.g., Satre et al. 1989, Robitaille et al. 1991, Noguchi et al. 2004). Still other identifications are detailed in the ES- TOF-HR-MS section. The organic P compounds are summarized in section 2.3.

The solution remained dark grey with a slight reddish tint under argon. Organic P compounds are also present in this solution, though at a lower total abundance. The total abundance of P species is substantially less than those performed under air ($3.1 \pm 0.3$ mM), however, the species generated still indicate synthesis of organophosphorus compounds.

The acetate, ethanol, and Mg and Ca salt phosphide corrosion experiment produced mainly phosphite in solution. However, a small quantity of a compound with a peak consistent with an organophosphate was detected (figure 14). Unfortunately, when this solution was analyzed a second time ~2 months later, this peak was no longer

Figure 14. NMR spectrum of phosphide corrosion in saline and organic solution. The minor P species is just to the right of the central phosphite peak.
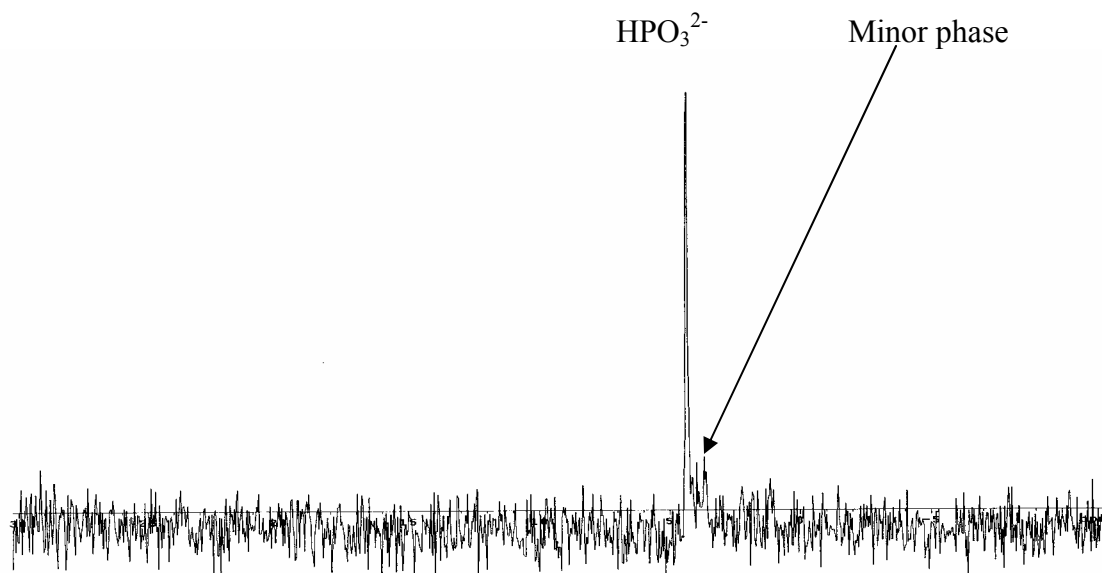
present. This peak was thereby either an artifact of the NMR analysis or was a detection of a short-lived organophosphate.

Phosphide corrosion experiments with single organic compounds in solution show that ethanol and acetonitrile are not phosphorylated in solution. Thus ethanol is inactive in the experiments described above. Acetate is phosphorylated and is the main species affected by the corroding phosphide. Phosphide corrosion in the presence of EDTA produces some compounds similar to those seen in the acetate experiment, notably the H-P compounds. This is not too much of a surprise given the chemical similarity of EDTA and acetate. EDTA is a tetraacetic acid.

Phosphide corrosion in a solution with glycolaldehyde changed color to a dark brown. NMR was impossible with this experiment, as the particulate Fe matter could not be removed from solution. It is proposed that the glycolaldehyde polymerized to form a tarry carbohydrate material rich in particulate Fe. Acetone likewise formed a tarry material from which no data could be obtained. Similarly adenosine formed a tarry material, except in the presence of base, which formed P compounds identical to those found in the deionized water experiments.

The NMR spectra of both acetaldehyde and pyruvate corrosion experiments indicates that these solutions formed species similar to those produced in the acetate experiment, including some organophosphorus compounds. Total yields were lower, 6.6 $\times 10^{-4}$ M for pyruvate and $4.0 \times 10^{-4}$ M for acetaldehyde. These low yields complicated full spectral analysis.

*P Compound Stability Experiments.* The motivation for this set of experiments was to understand the stability and reactivity of P species in the presence of metal. Hypophosphite ($H_2PO_2^-$) is a plausible intermediate between $Fe_3P$ and $HPO_3^{2-}$. It does not appear in any of the above corrosion experiments, but it may serve as a short-lived reactive intermediate. I determined the stability of this compound through monitoring this compound over the course of one day. After one day, ~25% of hypophosphite is converted to phosphite under air, independent of material added to the solution (no material, Fe added, $Fe_3O_4$ added).

Phosphite is more stable over longer periods of time, with no conversion to other P compounds under ambient conditions. Addition of Fe metal to the solution results in a conversion of ~46% of phosphite to orthophosphate in one day (figure 15). Addition of $Fe_3P$ metal to the phosphite solution resulted in a 15% conversion of phosphite to orthophosphate, with no other P compound detected at the 1 mM concentration level, whereas addition of magnetite has no effect and phosphite is unchanged. Hypophosphite added to the solution increases the total abundance of phosphite though no other P species appear. Addition of magnetite to a hypophosphite/phosphite mix significantly increases the amount of phosphite, though this may be a result of adsorption of hypophosphite onto magnetite.

Experiments with orthophosphate, hypophosphate, and pyrophosphate added to Fe metal did not change significantly with time. No additional P compounds were produced, indicating the stability of these three compounds is high compared to

Figure 15.  NMR spectrum of phosphite decomposition.  A) NMR spectrum of a solution of phosphite, and B) NMR spectrum of a solution of phosphite in the presence of Fe metal after one day of metal corrosion.
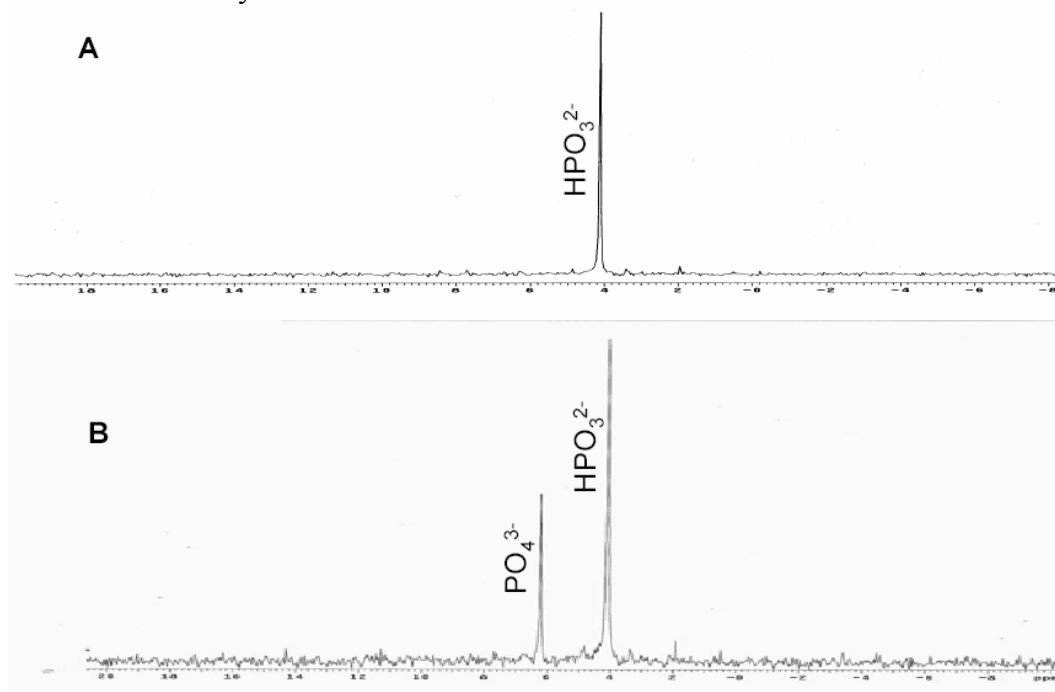
phosphite.  These stabilities are consistent with those observed by other investigators (Van Wazer 1958, Schwartz and Van der Veen 1973).

2.2.2 Synthetic Experiments

The series of synthetic experiments detailed in table 10 were unsuccessful in generating the intended goal product.  Pyruvate is not phosphorylated to any extent by P anions. Minor amounts of phosphate were generated during any experiment using $HPO_3^{2-}$ and Fe, though beyond this, little other changes were observed.  In the experiments with pyruvate and glycolaldehyde with P anions, no organic compound was phosphorylated.  However, in the experiments with $MgCl_2$, $P_2O_6^{4-}$ was the first to bond to Mg, indicating a very low solubility for this compound compared to pyrophosphate and phosphite.  No pyrophosphate was generated from solutions of phosphite, orthophosphate, and hypophosphate with or without iron.

Pyrophosphate must be produced in the corrosion experiments *via* a route that uses compounds other than these species.  The lack of phosphorylation serves as testament to the difficulty of prebiotic phosphorylation, even when using reactive P species.  Nearly all attempts at room temperature phosphorylation with P salts will probably be unsuccessful.

2.2.3 Mass Spectral Experiments

Mass spectral analysis of the $CH_3COONH_4$ and $Fe_3P$ experiment indicates an enormous

variety of P compounds are produced during this corrosion experiment (table 14). All

peaks with a height less than 1000 counts were removed from this list. The mass

spectrum is presented in figure 16. The abundances of the four species $H_2PO_3^-$, $H_2PO_4^-$,

$H_3P_2O_6^-$, and $H_3P_2O_7^-$ are known from NMR experiments. The concentrations of other

species are determined from the relationship between peak height and abundance

established by these four species. The best fits are power law and exponential fits, and

both produce similar results. A linear regression fit was highly inaccurate for a low M/Z.

The three relationships are given here:

Exponential: $\quad [C] = \dfrac{H}{0.1298e^{0.0332M}}$ $\qquad\qquad R^2 = 0.9784$ $\qquad\qquad$ (19)

Power: $\qquad\quad [C] = \dfrac{H}{3 \times 10^{-8}\ M^{4.0727}}$ $\qquad\qquad R^2 = 0.9634$ $\qquad\qquad$ (20)

$[C]$ is the concentration in μM, $H$ is the peak height, and $M$ is the mass in AMU. The

exponential law was chosen due to its predicted low abundance of compounds of mass ~

400 AMU, consistent with NMR results. The power law may also be employed as the

results are not significantly different. The mass spectrum adjusted for abundances is

shown as figure 17.

Nitrogen has been excluded from peak identifications in table 14. $NH_4^+$ is a

relatively inert species acting mostly to preserve charge balance. Despite this, N species

may be present at low total concentrations.

Table 14. Mass spectral peaks of $NH_4OOCCH_3$ and $Fe_3P$ corrosion solution. "Peak" is the location on the MS, "Height" is its height in arbitrary units, "Formula" is the proposed identification, and "Calculated Mass" is the mass for the "Formula". Differences between "Peak" and "Calculated Mass" are all less than 100 ppm.

| Peak | Height | Calculated Mass | Formula |
|---|---|---|---|
| 62.9643 | 1174 | 62.96359 | $PO_2$ |
| 78.9563 | 6611 | 78.95851 | $PO_3$ |
| 80.9709 | 10050 | 80.97416 | $H_2PO_3$ |
| 94.9508 | 844 | 94.95342 | $PO_4$ |
| 96.9619 | 7253 | 96.96907 | $H_2PO_4$ |
| 110.9894 | 1003 | 110.9847 | $HOCH2PO3H$ |
| 112.9593 | 2046 | 112.9640 | $H_2PO_5$ |
| 124.9642 | 905 | 124.964 | $H_2PCO_5$ |
| 126.9275 | 6752 | 126.9350 | $HP_2O_4$ |
| 138.9777 | 1137 | 138.9796 | $HOOCCH_2PO_3H$ |
| 140.9343 | 1347 | | ? |
| 142.9206 | 9997 | 142.9299 | $HP_2O_5$ |
| 144.9364 | 22280 | 144.9456 | $H_3P_2O_5$ |
| 145.0669 | 1250 | | ? |
| 147.0538 | 1289 | | ? |
| 153.0081 | 1012 | 152.9953 | $HOOCCH_2CH_2PO_3H$ |
| 154.9842 | 1246 | 154.9746 | $HOOCCH_2OPO_3H$ |
| 157.9327 | 1911 | | ? |
| 158.9191 | 8388 | 158.9248 | $HP_2O_6$ |
| 160.9313 | 40680 | 160.9405 | $H_3P_2O_6$ |
| 162.9478 | 21870 | 162.9561 | $H_5P_2O_6$ |
| 165.0138 | 1064 | | ? |
| 172.0862 | 1223 | | ? |
| 173.0665 | 1006 | | ? |
| 174.9456 | 1756 | 174.9561 | $H_2O_3PCH_2PO_3H$ |
| 175.9416 | 4976 | 175.9514 | $H_2P_2O_7$ |
| 176.9252 | 36440 | 176.9354 | $H_3P_2O_7$ |
| 178.9419 | 13800 | 178.9511 | $H_5P_2O_7$ |
| 182.9121 | 2212 | 182.9248 | $HP_2O_6C_2$ |
| 184.9285 | 13550 | 184.9405 | $H_3P_2O_6C_2$ |
| 186.1041 | 6157 | | ? |
| 187.0904 | 2139 | | ? |
| 190.9515 | 1540 | 190.9511 | $H_2O_3POCH_2PO_3H$ |
| 192.9243 | 2524 | 192.9303 | $H_3P_2O_8$ |
| 194.9360 | 5770 | 194.9460 | $H_5P_2O_8$ |
| 197.0462 | 1071 | | ? |
| 198.9058 | 1191 | | ? |
| 200.1067 | 1279 | | ? |
| 200.9222 | 5524 | 200.9354 | $H_3P_2O_7C_2$ |
| 201.0917 | 1023 | | ? |

Table 14 cont'd.

| Peak | Height | Calculated Mass | Formula |
|---|---|---|---|
| 202.9360 | 1165 | 202.9511 | $HOOCCH_2P_2O_5H_2$ |
| 206.8978 | 1094 | 206.9013 | $H_2P_3O_7$ |
| 208.9235 | 2091 | 208.917 | $H_4P_3O_7$ |
| 210.9329 | 1872 | 210.9326 | $H_6P_3O_7$ |
| 214.1263 | 1300 | | ? |
| 216.9207 | 2007 | | ? |
| 220.1369 | 1207 | | ? |
| 222.8975 | 2783 | 222.8963 | $H_2P_3O_8$ |
| 224.8996 | 4761 | 224.9119 | $H_4P_3O_8$ |
| 226.9170 | 7991 | 226.9276 | $H_6P_3O_8$ |
| 233.1452 | 2097 | | ? |
| 236.9143 | 2135 | 236.9119 | Cyclic P compound |
| 237.8994 | 2115 | 237.8833 | $HP_3O_9$ |
| 238.9032 | 2186 | 238.8912 | $H_2P_3O_9$ |
| 239.9091 | 1398 | 239.8990 | $H_3P_3O_9$ |
| 240.8961 | 6756 | 240.9068 | $H_4P_3O_9$ |
| 242.9097 | 13890 | 242.9225 | $H_6P_3O_9$ |
| 244.9249 | 5865 | 244.9381 | $H_8P_3O_9$ |
| 246.8863 | 1535 | | ? |
| 248.8972 | 5339 | 248.9119 | $H_4P_3O_8C_2$ |
| 252.9153 | 1148 | 252.9068 | $H_4P_3O_9C$ |
| 255.9049 | 2177 | | ND |
| 256.8907 | 7427 | 256.9017 | $H_4P_3O_{10}$ |
| 258.9053 | 2366 | 258.9174 | $H_6P_3O_{10}$ |
| 260.9204 | 16430 | | ND |
| 262.8810 | 4902 | | ND |
| 264.8907 | 2121 | | ND |
| 266.9066 | 8209 | 266.9225 | $HOOCCH_2P_3O_7H_3$ |
| 270.8820 | 15540 | | ND |
| 272.9115 | 1192 | | ND |
| 273.9169 | 1367 | | ND |
| 274.1706 | 1785 | | ND |
| 274.8996 | 1098 | | ND |
| 276.9117 | 7406 | | ND |
| 278.8790 | 2681 | | ND |
| 280.8849 | 1295 | | ND |
| 282.8997 | 6482 | | ND |
| 284.9198 | 10090 | | ND |
| 286.8790 | 1623 | 286.8512 | $H_3P_4O_{10}$ |
| 288.8898 | 1505 | 288.8833 | $H_5P_4O_{10}$ |
| 290.8864 | 3385 | 290.8990 | $H_7P_4O_{10}$ |
| 292.9100 | 4627 | | ND |
| 293.1621 | 1611 | | ND |
| 296.8793 | 1460 | | ND |

Table 14 cont'd

| Peak | Height | Calculated Mass | Formula |
|------|--------|-----------------|---------|
| 298.8954 | 2583 | | ND |
| 300.9140 | 4202 | 300.9197 | Cyclic P compound |
| 302.8689 | 1457 | | ND |
| 304.8820 | 1078 | | ND |
| 306.8799 | 2447 | | ND |
| 308.8932 | 7864 | | ND |
| 312.8693 | 3295 | | ND |
| 314.8924 | 2336 | | ND |
| 318.8809 | 1917 | | ND |
| 319.8762 | 1189 | | ND |
| 320.8755 | 1197 | | ND |
| 321.8882 | 2321 | | ND |
| 322.8735 | 1907 | | ND |
| 324.8871 | 11590 | | ND |
| 326.8943 | 5612 | | ND |
| 328.8600 | 2478 | | ND |
| 330.8749 | 3799 | 330.8939 | Acetyl-4P |
| 334.8852 | 9902 | | ND |
| 336.8714 | 2728 | 336.8681 | $H_5P_4O_{13}$ |
| 337.8842 | 1913 | | ND |
| 338.1791 | 2396 | | ND |
| 338.8684 | 2548 | | ND |
| 339.8973 | 8048 | | ND |
| 340.8820 | 1672 | | ND |
| 342.8908 | 7469 | | ND |
| 344.8550 | 2687 | | ND |
| 346.8689 | 4942 | | ND |
| 348.8838 | 13860 | | ND |
| 350.8759 | 13540 | | ND |
| 352.8655 | 1860 | 352.8547 | $H_6P_5O_{12}$ |
| 353.8757 | 2051 | | ND |
| 354.8595 | 1538 | | ND |
| 356.8753 | 3554 | | ND |
| 358.8812 | 4371 | | ND |
| 360.8503 | 1665 | | ND |
| 361.8782 | 3713 | | ND |
| 362.8625 | 1556 | | ND |
| 364.8777 | 12160 | | ND |
| 366.8668 | 11340 | | ND |
| 368.8554 | 1566 | | ND |
| 370.8645 | 1992 | | ND |
| 372.8694 | 4181 | | ND |
| 374.1539 | 2609 | | ND |
| 376.8528 | 1444 | | ND |

Table 14 cont'd.

| Peak | Height | Calculated Mass | Formula |
|---|---|---|---|
| 377.8614 | 1743 | | ND |
| 378.8568 | 1056 | | ND |
| 380.8720 | 6196 | | ND |
| 382.8634 | 5733 | | ND |
| 384.8493 | 1086 | | ND |
| 386.8518 | 1909 | | ND |
| 388.8633 | 3699 | | ND |
| 392.8456 | 2646 | | ND |
| 394.8488 | 1582 | 394.8653 | Acetyl-5P |
| 396.8641 | 4062 | | ND |

ND = Not determined, ? = is not understood

Figure 16. Mass spectrum of $NH_4OOCCH_3$ and $Fe_3P$ corrosion solution.
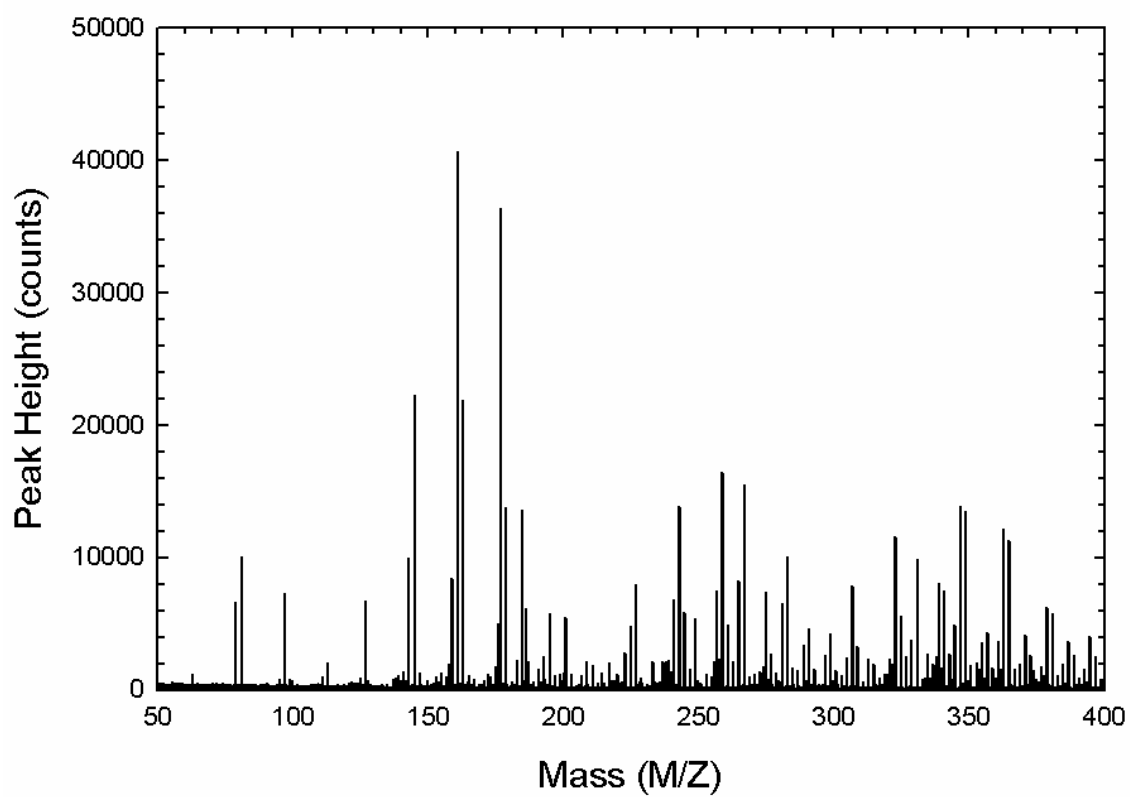
Figure 17.  Mass spectrum adjusted for abundances.  Abundances were determined from
the exponential law (17). A) Absolute scale, B) logarithmic scale.

A)



B)
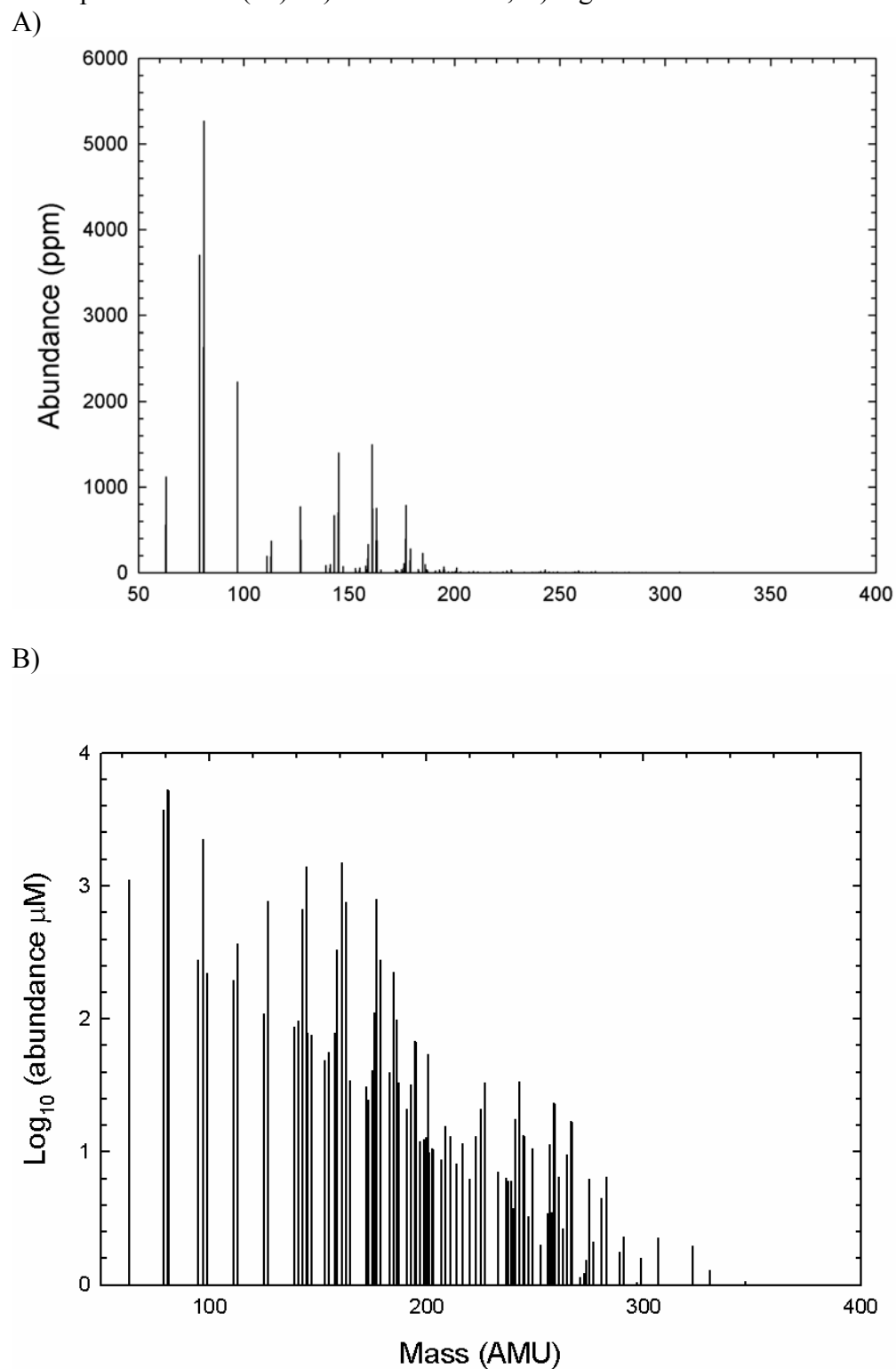
Some the mass peaks are consistent with series of H-P-O compounds. For instance, the mass peak at 208.9235 ($H_4P_3O_7$) has two mass peaks ± ~2.015 AMU, corresponding to the addition or subtraction of two H atoms to this peak, giving formulae of $H_2P_3O_7$ and $H_6P_3O_7$. These compounds correspond to P compounds with three coordinate atoms as opposed to the usual four, or to a P=P double bond, both of which are highly unusual. The origin of these compounds is unknown, but may result from the structural rearrangement of radicals in the solution phase (discussed in the next chapter).

Many of the mass peaks are consistent with H-P-O, C-H-O, and H-P-O-C compounds. Some information on the nature of the solution is determined from the deviation from an integer mass. Compounds rich in P and O tend to have a negative deviation from an integer mass due to the atomic masses of these two elements, which are both less than 31 and 16, respectively. Conversely, compounds consisting of C and H tend to have positive deviations from an integer mass (C has an integer mass, and H is above 1 AMU). The molecules in solution form two trends (figure 18). Organic P compounds typically lie between these two trends, and the masses of some of these compounds are consistent with identifications by NMR, including acetyl phosphonate, methyl diphosphite, hydroxylmethyl phosphonate, and phosphoglycolate.

Several P species are complex, multiple-P compounds that are not detected in NMR spectra. The general formulae for these species ranges from $H_{n+1}P_nO_{n+2}^-$ to $H_{n+1}P_nO_{4n}^-$. When the mass spectra is compared to these idealized species (figure 19), the general trend is that most lie in the area defined by these compounds. Many of the peaks have mass isomers, so the identifications listed in table 14 are not necessarily unique.

Figure 18. Mass differences (in AMU) from the integer mass. Compounds that have been identified as organic P compounds are hollow circles. These compounds tend to be intermediate of the two trends. The area of the circles is larger than the error for this graph.
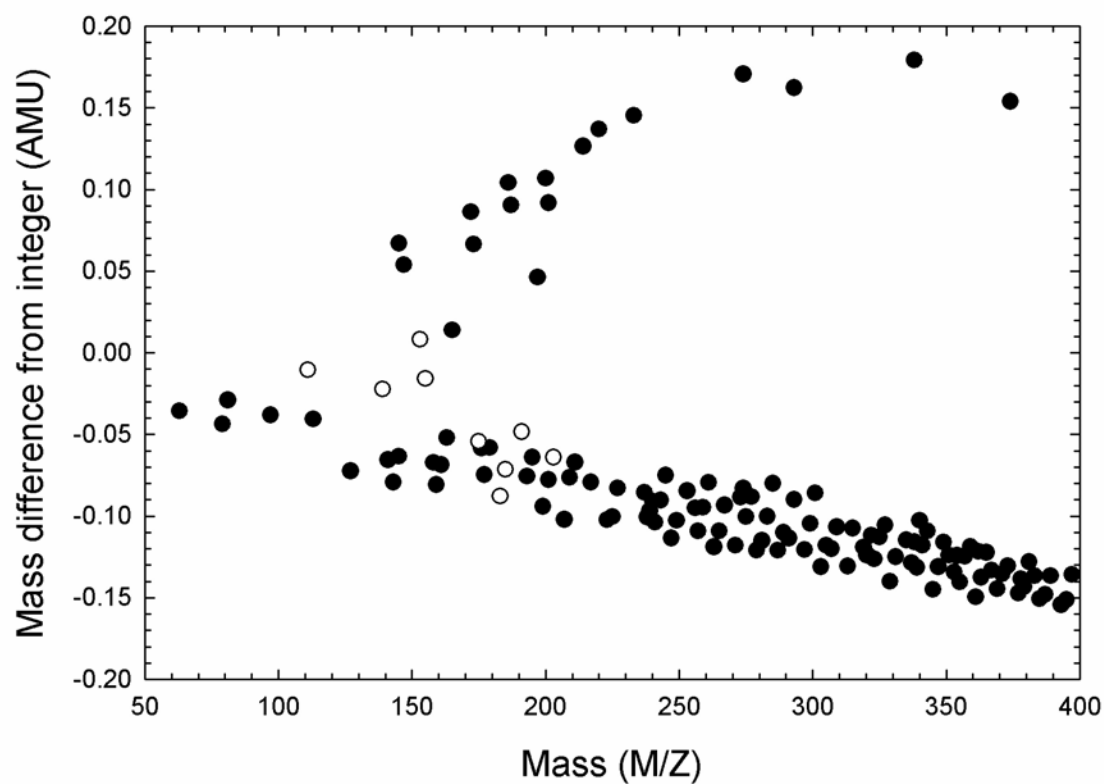
Figure 19. Deviations from simple P-O-H compounds. P-O-H compounds are simple with no P-P double bonds and four coordination state. The idealized P-O-H type compounds are black circles, and the empty circles are the data points.
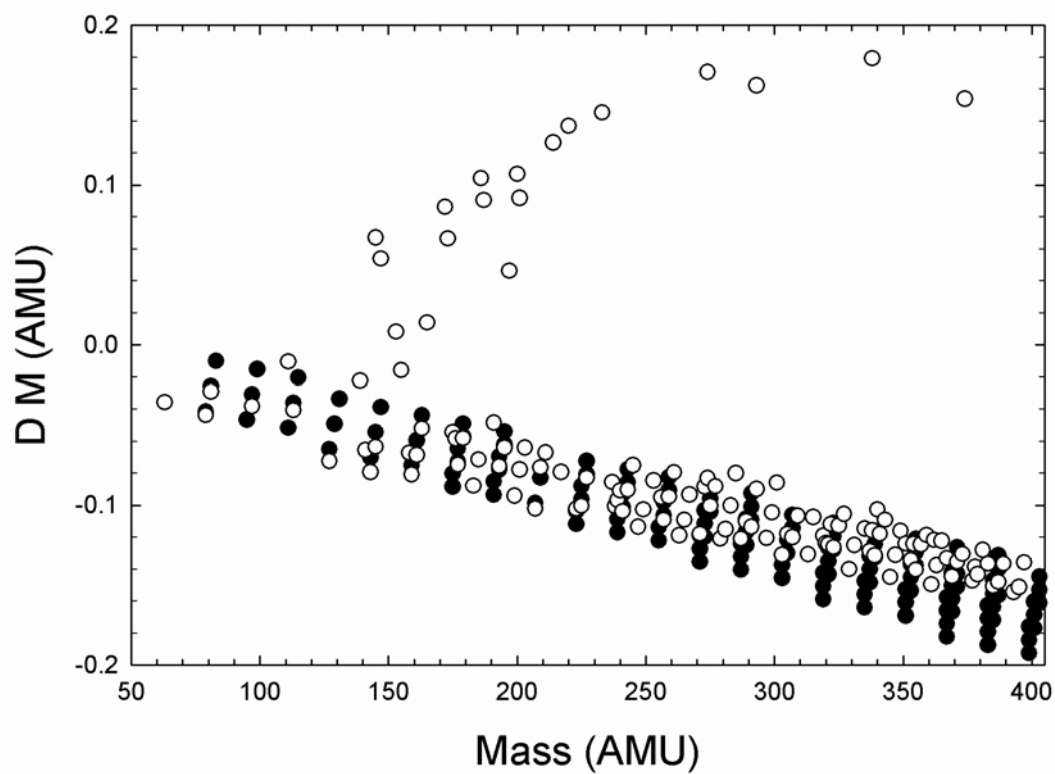
Some species appear to lie above the line, and these likely include small amounts of -

$CH_2$- groups replacing O bridges.  This is especially true of the high mass species.


2.2.4 Electron Paramagnetic Resonance Spectrometry Experiments


Samples of Fe and $Fe_3P$ were corroded in deionized water to determine the nature and

abundance of radicals in solution.  Figure 20 shows the EPR spectra from 5,5-Dimethyl-

1-pyrroline-N-oxide (DMPO) and water (background), DMPO and Fe in basic solution,

and DMPO and $Fe_3P$ in neutral deionized water.  No peaks are observed in the

background spectrum, indicating that the diradical $O_2$ from air is not trapped as a radical

species to any significant observable extent.  The peaks shown in figures 20b and 20c

confirm the presence of radical species in solution.

The EPR spectrum of DMPO and Fe (figure 20b) in basic solution corresponds

well to literature spectra of the radical DMPOOH (Sankarapandi and Zweier 1999).  The

EPR spectrum of DMPO and $Fe_3P$ (figure 20c) corresponds to a mixture of DMPOOH

and DMPOX radicals in a 5:3 ratio (Ozawa and Hanaki 1989).  DMPOX radicals are

formed from the interaction of $^{\cdot}PO_3^{2-}$ radicals with DMPO.  The rationale for these

identifications is discussed below.

Figure 20.  EPR spectra of solutions.  Note the change in scale.

a) Water and DMPO
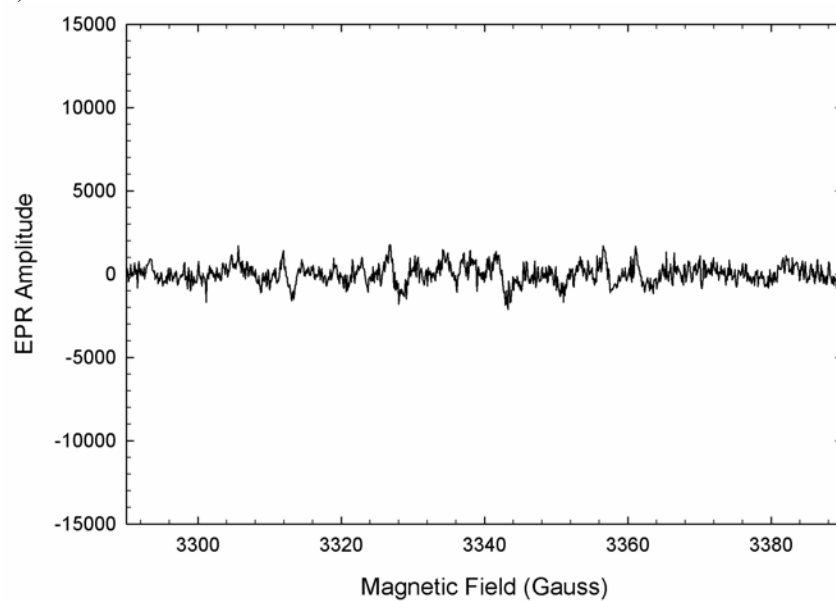


b) Basic solution (pH 13), Fe metal, and DMPO
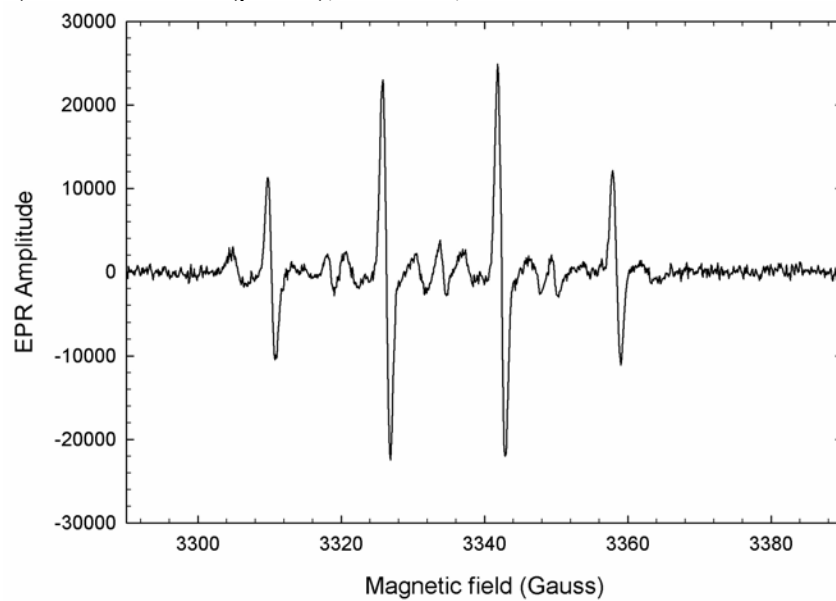
Figure 20 cont'd.
c) Water, phosphide powder, and DMPO
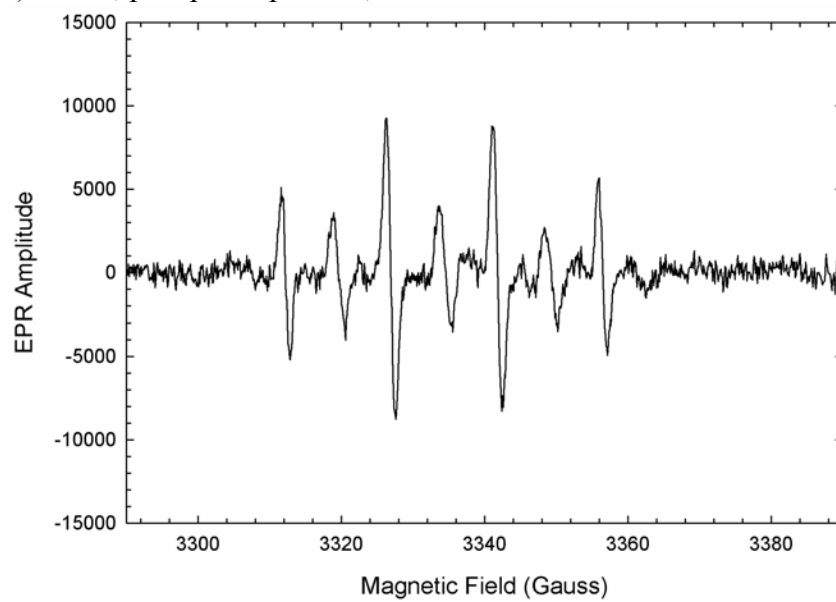
The radicals $^{\cdot}$OH and $^{\cdot}$PO$_3{}^{2-}$ are both short-lived species that are difficult to observe in solution by EPR and thus spin traps (molecules that form long-lived radicals) are used to detect these species.  The spin trap DMPO was employed for these analyses (pictured below).



DMPO      + $^{\cdot}$Nu      →      DMPO-Nu                (21)
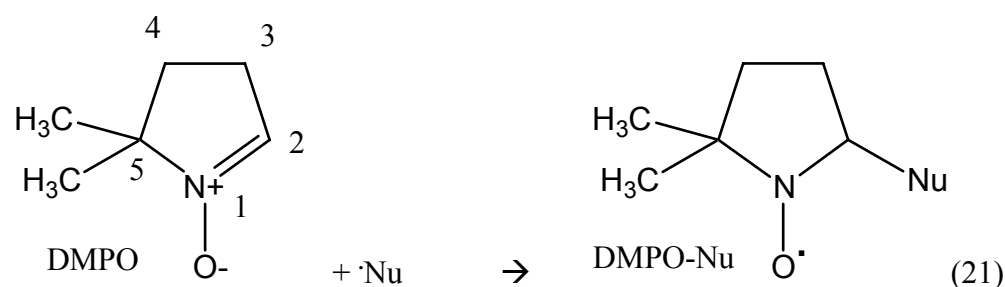
This molecule reacts with nucleophilic radicals ($^{\cdot}$Nu) to produce a long-lived nitroxyl radical, DMPO-Nu (reaction shown above).  EPR details local chemistry based on splitting patterns from nearby nuclei.  In the case of DMPO-Nu, the oxygen radical is one bond away from a nitrogen atom (with a nuclear spin of +1).  As a result, the peak from the free electron is split into three equal peaks (figure 21a).  These three peaks are each split into doublets due to the hydrogen (+1/2 spin) at position 2, adjacent to the nucleophile, which overlap to form a 1-2-2-1 quadruplet (figure 21b).  The nucleophile is $^{\cdot}$OH in these experiments, giving DMPOOH.

Figure 21. Schematic EPR spectra of DMPO and related radicals. The axes are identical to figure 20.
a) Splitting due to N atom
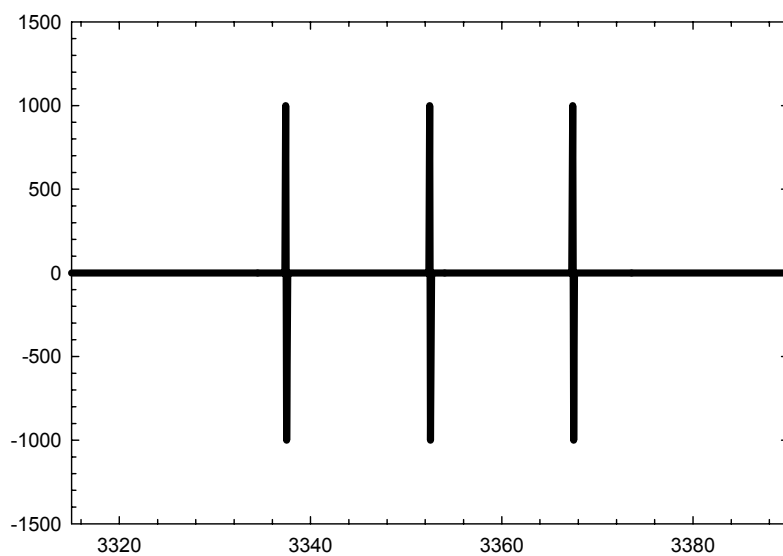


b) Spectrum of DMPOOH radical
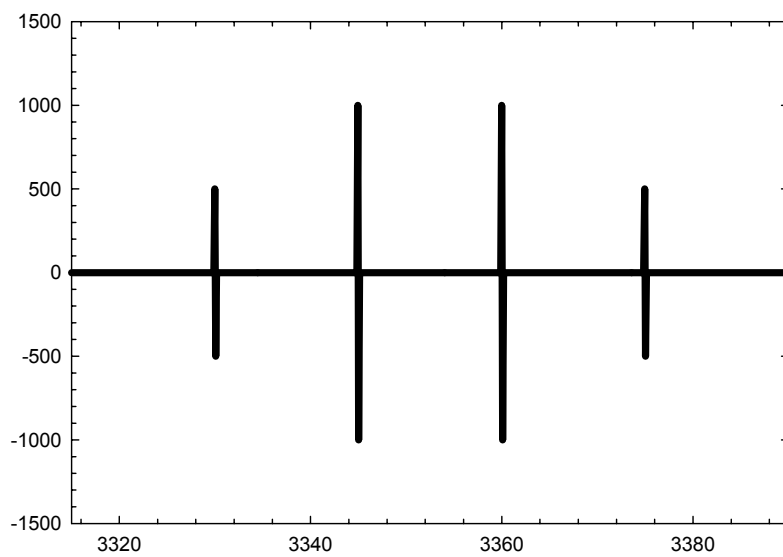
Figure 21 cont'd.
c) Spectrum of DMPOX radical
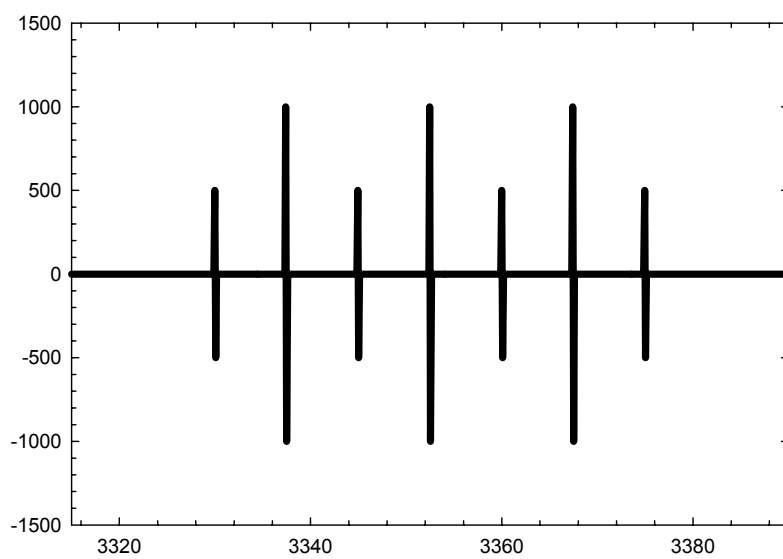


d) Spectrum of DMPOOH and DMPOX radicals in a 2.75 : 1 mixture ratio.
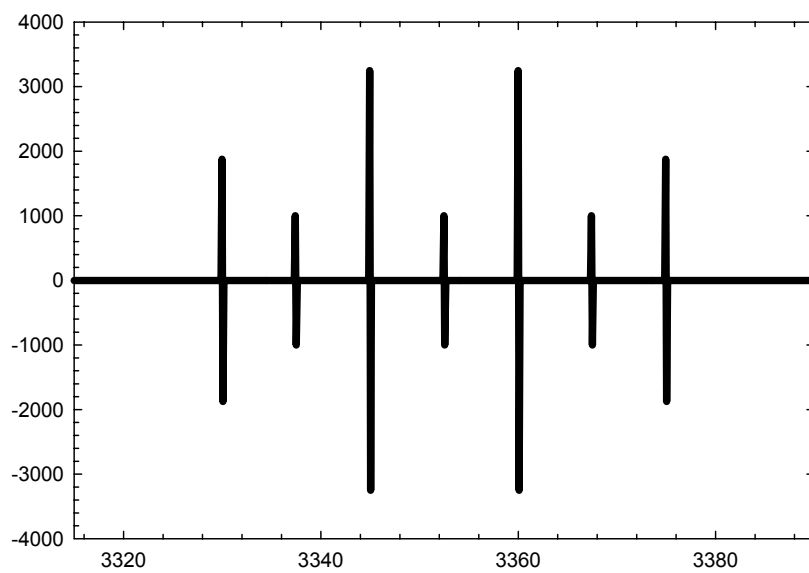
An alternate reaction occurs with phosphite radicals and DMPO. Phosphite radicals are strong oxidizing agents and will oxidize DMPO by the following reaction



$$DMPO + Oxidant \rightarrow DMPOX \qquad (22)$$
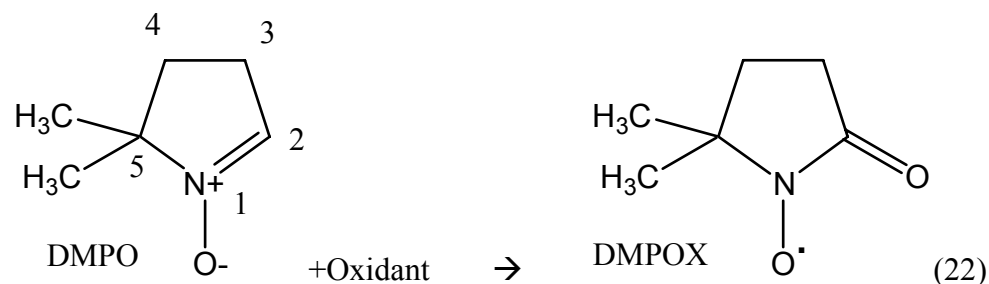
to form a DMPOX radical. The spectrum of this molecule is a septet, resulting from each peak of the triplet from the nitrogen being split into triplets by the two hydrogens at position 3. The septet has a 1-2-1-2-1-2-1 pattern (figure 21c).

Figure 20c is actually a combination of DMPOOH and DMPOX, and the four minor peaks from DMPOX spectra coincidentally overlap the four peaks from DMPOOH (figure 21d). This spectrum was made by multiplying spectrum 21b by a factor of 2.75, and adding spectrum 20c. The peak heights for this combination spectrum are 15 : 8 : 26 : 8 : 26 : 8 : 15, which provides a quantitative match to the seven peaks of figure 19c. Thus the ratio of DMPOOH to DMPOX is 5:3, and assuming roughly equal reaction rates with DMPO, the ratio of $\cdot OH$ to $\cdot PO_3^{2-}$ is also 5:3.

2.3 Summary of Solution Chemistry

The solubility of apatite in these experiments is consistent with the known solubility of apatite. The yield of orthophosphate was maximized ($10^{-3}$ M) by introduction of chelating organics and base. The solubility in the absence of added compounds is

minimal. This deficiency is consistent with the well-known "Phosphorus Problem" of the origin of life.

The total yields of dissolved P compounds relative to the amount of phosphide material employed in corrosion range from 0.1% to 10%. The two major factors affecting yield are solution chemistry and atmosphere composition where solution chemistry appears to have a larger effect.

The corrosion of synthetic schreibersite in deionized water yields a $10^3$-fold increase in the concentration of P compared to apatite, and a $10^2$-fold increase in the absence of all oxidizing gases, which substantially slows down the reaction by decreasing the corrosion rate of metal. The P compound release rate is approximately equal to 1 mM per day, and given a suitably large volume of water, the phosphide would corrode to completion. Phosphorus compounds are most abundant in the solutions with organic molecules or with sodium bicarbonate. This is likely due to two effects: the ability of acetate and carbonate to form compounds with iron, which stabilizes the dissolution of iron(II) and enables the further release of P to the solution, and the presence of $Na^+$ (as sodium bicarbonate or sodium acetate) in the system, which encourages corrosion of the metal phosphide.

$Mg^{2+}$ and $Ca^{2+}$ phosphorus salts both precipitated in saline solutions, decreasing the total P abundance in solution compared to the P abundance in deionized water. Hypophosphate is the least soluble of the four major P salts and is the first to precipitate a solid. The low abundances of most P-bearing ions in the saline solutions are best explained by the precipitation of $Ca^{2+}$ and $Mg^{2+}$ salts:

$$3 \text{ Ca}^{2+} + 2 \text{ PO}_4{}^{3-} \rightarrow \text{Ca}_3(\text{PO}_4)_2 \qquad\qquad (23)$$

$$2 \text{ Ca}^{2+} + \text{P}_2\text{O}_6{}^{4-} \rightarrow \text{Ca}_2\text{P}_2\text{O}_6 \qquad\qquad (24)$$

$$2 \text{ Ca}^{2+} + \text{P}_2\text{O}_7{}^{4-} \rightarrow \text{Ca}_2\text{P}_2\text{O}_7 \qquad\qquad (25)$$
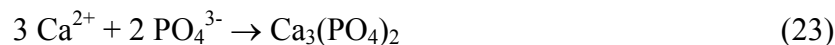
which is consistent with XRD spectra. Phosphonate salts are significantly more soluble than the other, more oxidized P salts, due to the increased capacity for hydrogen bonding.

Mass spectral data confirms that solution chemistry is very complex, though many species have a low abundance. EPR data suggests that at least two radicals are formed in solution during the corrosion of the phosphide. Both data sets are addressed in the next chapter.

Experiments performed under argon have consistently lower yields than those experiments performed under air, indicating that metal corrosion rates determine the production of soluble P species. Metal corrosion is slowest in water free of dissolved $O_2$, but even in the absence of $O_2$, P in iron phosphide is reactive enough to strip away oxygen from water (releasing $H_2$) and form P species of oxidation state +3 to +5. This agrees with the thermodynamic data available for the species in the system (Gulick 1955). Although the relative abundances of P compounds may change with the removal of oxygen, the same species are formed, which indicates that production of P species is dependent mainly on solution chemistry. The compounds formed by corrosion are not in the most stable thermodynamic form but are instead a mixed-valence mixture of P-O-H compounds. The plausible reaction pathway is discussed in the following chapter, in which the reactivity towards organic compounds is detailed as well.

2.3.1 Organic Phosphorus Compounds Formed

Phosphide corrosion in an acetate solution produced several unidentified P species and

many organic P compounds.  Other organic solutions produced similar species, albeit at

lower total abundances.  Organic compounds lacking a C=O double bond did not produce

any unusual speciation products and were otherwise similar to corrosion in deionized

water.  Some organic corrosion experiments produced tar and could not be analyzed

consistently with other experimental products.   The $H_2O_2$ corrosion solution produced

results qualitatively similar to the acetate corrosion solution.

The organic P compounds produced broadly fall into three categories (figure 22):

acetyl-P compounds (I), methyl-P compounds (II), and cyclic P compounds.  One

additional compound detected that does not fall in any of these groups is

phosphonoformate:

$$\text{HO}-\underset{\underset{\text{OH}}{|}}{\overset{\overset{\text{O}}{\|}}{\text{P}}}-\overset{\overset{\text{O}}{\|}}{\text{C}}-\text{OH}$$
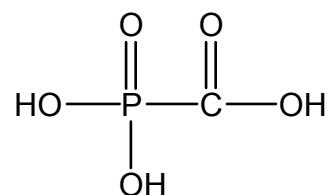
The masses and total abundances are listed in table 15.  Comparison to NMR

literature spectra confirms the presence of methyl diphosphite, acetyl phosphonate, and

hydroxylmethyl phosphonate.  Phosphoglycolate may also be present, and this peak may

be visible in the acetate/ethanol and $Mg^{2+}$ and $Ca^{2+}$ solution.  Organophosphates are more

soluble in solution than phosphate minerals (e.g., Boerio-Goates et al. 2001), and the

Figure 22. Structures of organic P compounds produced.

I. Acetyl-P compounds

$= C_2O_2H_3$

Acetyl phosphonate

Phosphoglycolate

Hypophosphatoacetate

Tri-P-acetate

Quad-P-acetate

Penta-P-Acetate

Etc.

II. Methyl-P Compounds

Hydroxylmethyl phosphonate

Methyl diphosphite
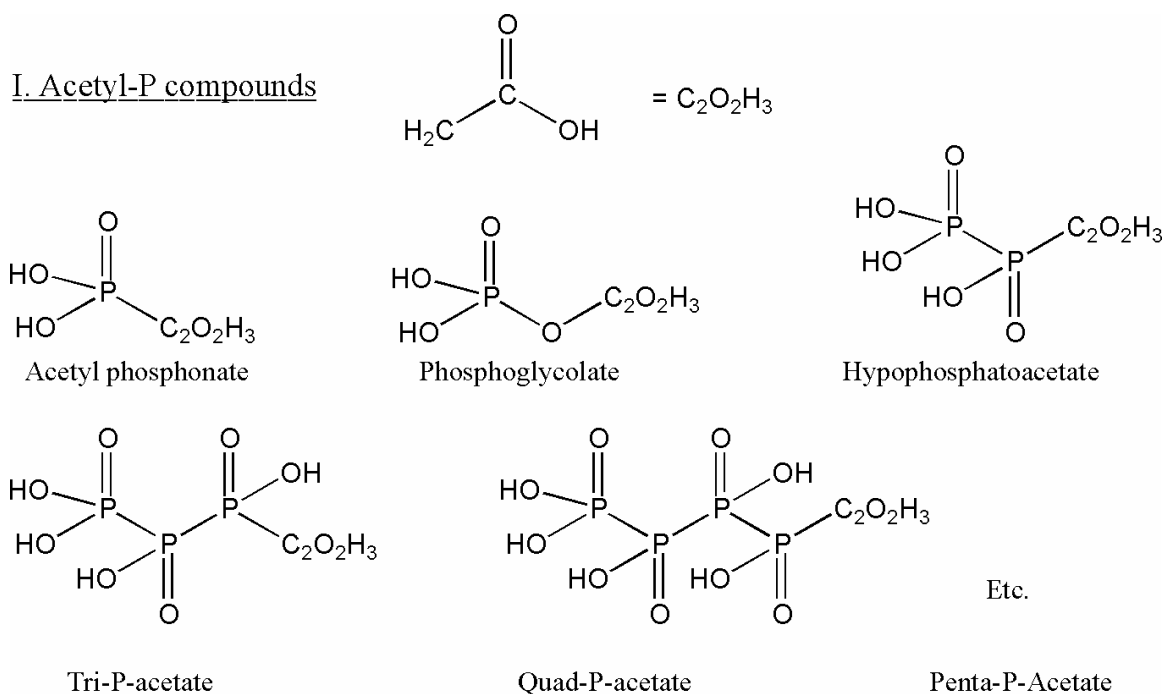
Phosphonomethylphosphate
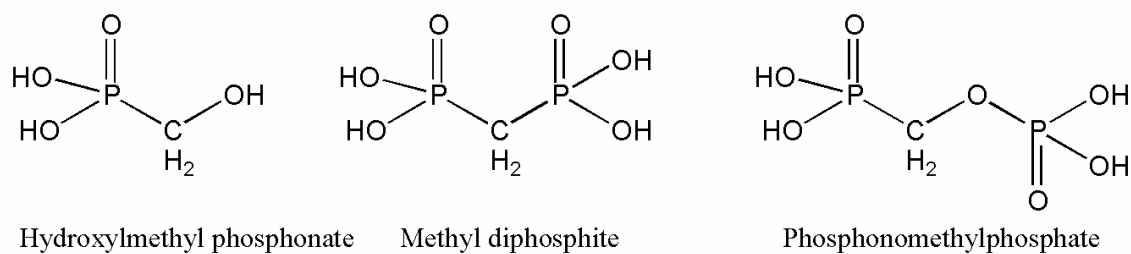
III. Cyclic P Compound: Possible isomers

a)

b)

c)
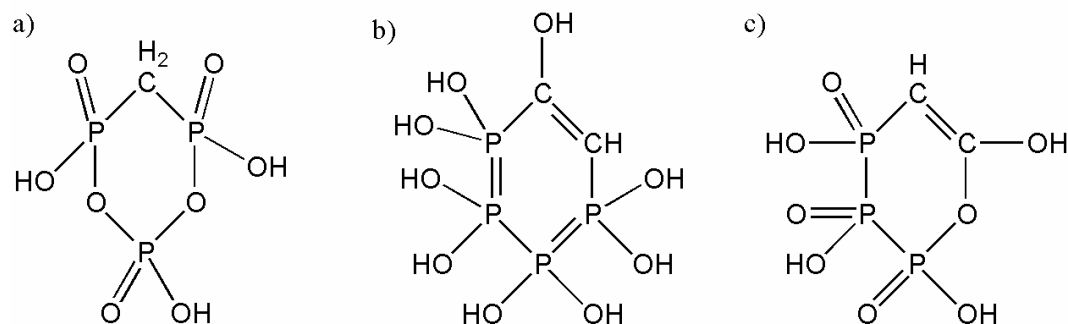
Table 15.  Organic P compounds produced in the $NH_4OOCCH_3$ and $Fe_3P$ experiment

| Mass Peak | Compound | Name | Abundance (µM) | NMR? |
|---|---|---|---|---|
| 110.9894 | $H_4PO_4C$ | Hydroxylmethyl phosphonate | 150 | Y |
| 124.9642 | $H_2PO_5C$ | Phosphonoformic acid | 90 | ? |
| 138.9777 | $H_4PO_5C_2$ | Acetyl phosphonate | 70 | Y |
| 154.9842 | $H_4PO_6C_2$ | Phosphoglycolate | 50 | ? |
| 174.9456 | $H_5P_2O_6C$ | Methyl diphosphite | 40 | Y |
| 190.9515 | $H_5P_2O_7C$ | Phosphonomethylphosphate | 25 | N |
| 202.936 | $H_5P_2O_7C_2$ | Hypophosphatoacetate | 16 | N |
| 236.9143 | $H_4P_3O_8C$ | IIIa | 15 | N |
| 248.8972 | $H_4P_3O_8C_2$ | IIIc | 30 | N |
| 266.9066 | $H_6P_3O_9C_2$ | Tri-P-acetate | 35 | N |
| 300.914 | $H_9P_4O_9C_2$ | IIIb | 10 | N |
| 330.8749 | $H_7P_4O_{11}C_2$ | Quad-P-acetate | 7 | N |
| 394.8488 | $H_8P_5O_{13}C_2$ | Penta-P-acetate | 1 | N |

small peak may have been indicative of an ephemeral organophosphate compound like phosphoglycolate.

Ring compounds may be formed at small concentrations (species III). Pasek and Lauretta (2005) state that a ring compound like:
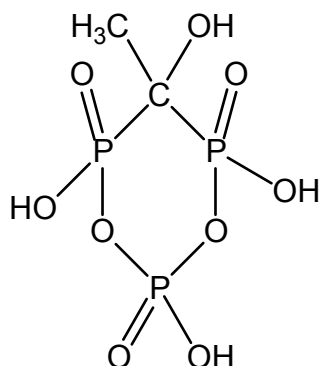


may be present in solution based on NMR peak locations. However, the two NMR peaks upon which this identification was based at ~9.2 ppm and ~ -2.7 ppm are also present in analyses of the experiment with $H_2O_2$, which had no organic compounds in solution (figure 13a). This compound is likely not present at concentrations detectable by NMR. TOF-HR-MS data suggest this compound may be present, however, its mass is identical to the tri-P acetate compound, and the two can not be distinguished by this method.

The linkages formed are primarily C-P linkages, however, some P-O-C linkages may also have been produced during the corrosion reaction. If so, then this study is among the first to produce detectable organophosphate compounds at room temperature using simple starting conditions. The total organic P concentration is ~500 μM, and the total concentration of P-O-C compounds is ~100 μM, giving yields of ~4% and ~1%, respectively.

2.4 Understanding the Corrosion of Schreibersite

2.4.1 Meteoritic Phosphorus Compounds


The CM chondrite meteorite Murchison is the gold standard of meteorite organics.

Murchison fell in 1969 near Murchison, Australia over an area of ~12.5 km$^2$ (Grady 2000

and refs therein). Analysis of this meteorite revealed several organic compounds, and

~20% of the total carbon in the meteorite was soluble. Quick collection of this meteorite

diminished the possibility of contamination by terrestrial organisms, in addition to the

identification of several non-biotic organic compounds (Cronin *et al.* 1988).

Murchison has been pervasively altered by water through its history. The

resultant mineralogy of this meteorite is rich in clay minerals, hydrated sulfide minerals

like tochilinite (Mackinnon and Zolensky 1984), and magnetite. This process has also

been implicated in the synthesis of the Murchison organic compounds (Shock and Shulte

1990), although this hypothesis has been disputed (Wright and Gilbert 1990).

Of primary interest to this work are the phosphonic acids, an unusual class of

meteorite organics first detected by Cooper *et al.* (1992). Phosphonic acids have low

total abundances, ~20 nmol/g of Murchison (compared to 600 nmol/g of amino acids).

This represents a total of ~0.2% of all P available in the meteorite. These compounds

represent a mystery in meteorite organic chemistry as they are unfamiliar on the surface

of the Earth. The phosphonic acids consist of a suite of organic compounds with direct

C-P linkages, and range from methyl- to butyl- phosphonic acid, MPA and BPA

respectively:
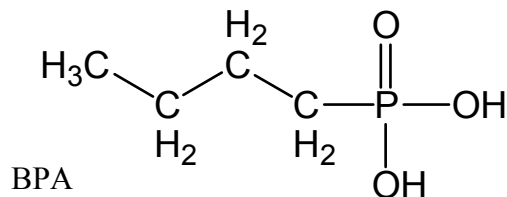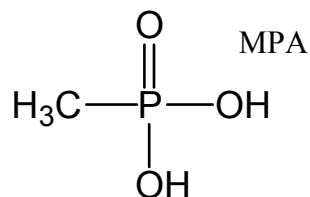
The origin of these compounds is unclear. Cooper et al. (1992) and Macia (2005) suggest an origin from C-P radical molecules in the interstellar medium followed by hydrolysis to form phosphonic acids. In this hypothesis, the C-P linkages are formed pre-accretion.

De Graaf et al. (1995, 1997) pose an alternate hypothesis that the C-P linkages were formed post-accretion through the interaction of phosphite radicals with organic radicals produced by UV light. In this experimental model, $HPO_3^{2-}$ and formaldehyde were mixed under UV light to form hydroxymethyl phosphonic acid. Their reaction pathway is similar to the reactions described by Cadogan (1967), which provides a simple means of obtaining phosphonic acids by means of a radical aliphatic carbon interacting with phosphorous acid:

$$RCH=CH_2 + H_3PO_3 \rightarrow RCH_2CH_2PO_3H_2 \tag{26}$$
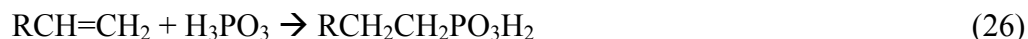
These models state the origin of the phosphite is from schreibersite corrosion, though this process was never investigated.

No P-O-C linkages have ever been detected in the organic fraction of meteorites. Partially soluble phosphate has been detected (Cooper et al. 1992, Pasek et al. 2004), but this material is inorganic orthophosphate salts. If formed, P-O-C linkages would likely decay to C-O-H and orthophosphate over the few billion years the compounds have been sitting in the meteorite. The C-P bond of the phosphonic acids is comparatively much

stronger as it is less susceptible to hydrolysis, and thereby could exist for billions of years.

2.4.2 Importance of Determining Corrosion Pathway

Organophosphorus compounds are synthesized by the corrosion experiments described in prior sections.  These compounds are typically P-C organophosphorus compounds, though some P-O-C bonds are also present.  The presence of P-C linkages is consistent with the organic inventory of the meteorite Murchison and suggests that P-C linkages may have been present on the surface of the early Earth.  However, the presence of P-O-C linkages in our solutions is especially intriguing given the prevalence of orthophosphate esters in biology (see chapter 1).

It is necessary to understand the process of schreibersite corrosion and the subsequent solution chemistry to detail the relevance of this system to prebiotic or early biotic systems.  Important sets of questions to ask are: 1) Is schreibersite corrosion even a physical process?  What happens to meteoritic schreibersite as it corrodes?  These questions are addressed in the next chapter.  2) Why are the major products of schreibersite corrosion a mixture of +3, +4, and +5 inorganic P salts? How are the organic P compounds produced and at what yields?  What is the relevant phosphorylating agent in these systems?  Answers to these questions shall be presented in chapter 4.

CHAPTER 3


SCHREIBERSITE CORROSION IN SITU


Schreibersite is an abundant trace constituent of many meteorites. This section describes an analytical investigation of the corrosion of schreibersite in a weathered meteorite. This study helps constrain the corrosion of schreibersite as a natural process and informs the previously described experiments. It should be noted that the systems described in the previous section are not equivalent to the likely environment of the corroded schreibersite of this portion of the study. Several key differences are worth noting:


- The water to rock ratio in the experiments was approximately 25:1, mass per mass. The meteorite described here was collected from the desert of northwest Africa and the likely water to rock ratio was much lower than the experimental ratio, though this is hard to tell without constraints from terrestrial age data.

- The experimental systems were much simpler than the corroded meteorite. No additional minerals were employed in corrosion studies, whereas meteorite mineral corrosion involves many species.

- Nickel makes up ~12% by weight of the schreibersite in the meteorite. The experimental phosphide powder had no Ni.

- The terrestrial age of the meteorite may be several thousand years. The experimental timescales ranged from days to weeks.

Despite these differences, study of meteorite weathering provides information on corrosion as a physical process. The data set presented here demonstrates that schreibersite corrosion is a very real, physical phenomenon that occurs over relatively short geologic timescales. Also, the mineralogy resulting from the corrosion of schreibersite is consistent with the experiments described in the previous sections of this chapter, within the range of error associated with the analytical techniques employed to study this corrosion product.

3.1 Background

The corrosion of schreibersite is a terrestrial phenomenon and has received little attention from the meteoritics community. This is likely due to the fact that most corrosion is not an extraterrestrial phenomenon, but is one that is limited to the surface of the Earth.

Ivanov *et al.* (1993) investigated the aqueous alteration of schreibersite in the meteorite Kaidun to determine the alteration history of the Kaidun parent body. Kaidun is an unusual meteorite breccia which fell in 1980 with a variety of lithologies, including reduced enstatite chondrite clasts, oxidized carbonaceous chondrite clasts, and brecciated material (Ivanov 1989). Based on the spatial and chemical features of the corroded lithologies studied, Ivanov et al. (1993) discerned several alteration events must have occurred on the parent body of this meteorite.

Some P-S sulfides have also been attributed to the aqueous alteration of schreibersite (Devouard and Buseck 1997). These sulfide grains are most abundant in the CM chondrite class, and are in chondrules, chondrule rims, PCP (poorly or partially characterized phases), and the matrix. The exact mineralogy of these grains is unclear at present, but they may be a mixture of distinct phases. Their occurrence in PCPs and the matrix indicates that they may be aqueous alteration products of schreibersite.

The schreibersite corrosion analyzed here is in an aubrite meteorite. Aubrites are presumed to be differentiated enstatite chondrites as these two groups share mineralogical and chemical similarities like silicate and sulfide mineralogy, and oxygen isotopes. Enstatite chondrites and aubrites were presumably formed under reducing conditions (Chapter 5), and all P should be in phosphide minerals under these conditions. Once introduced to the surface of the Earth, reduced meteorites weather in the highly oxidizing terrestrial conditions.

The meteorite SWL080 is an aubrite from northwest Africa. This meteorite is awaiting designation but has not been formally classified (no NWA number) and SWL080 is not an official designation for this meteorite. Sulfate minerals, carbonates, rust, and other phases indicate that this meteorite has experienced significant weathering on the surface of the Earth. Presumably this weathering occurred after the meteorite landed on the Earth, based on the relatively high abundances of alkali elements which have been introduced from the terrestrial setting.

3.2 Visual Characteristics of Corroded Schreibersite Grain

SWL080 has been weathered by aqueous fluids. At one time, SWL080 had a large 1-1.5 mm schreibersite grain which has since altered to an unusual iron-calcium-phosphorus-hydroxide mineral assemblage. Under plane-polarized light the phosphide corrosion area is stained red with iron (III) oxides which also make up the majority of material surrounding the phosphide corrosion area. Schreibersite is still present in the corrosion area as severely corroded grains ranging in size from 50 to 200 μm. The corrosion acts in an unusual pattern, eating away cubic pieces of individual schreibersite grains (figure 23). Schreibersite is a tetrahedral mineral and water may act along imperfections of the c axis, resulting in the square patterns visible in the backscattered electron (BSE) images.

A BSE microprobe image of the thin section is shown in figure 24. Four main minerals are distinguished in this section. The brightest spots in this image are schreibersite grains. The darkest portions are silicates. Surrounding the schreibersite grains are two distinct phases. The lighter phase consists mostly of iron oxyhydroxides (Fe-Ni-O-H material), whereas the darker phase is the corroded phosphide material, or a Fe-Ca-P-O-H mixture. The Fe-Ca-P-O-H phase has a higher average atomic number than the silicates, and hence is lighter than the silicates. Likewise, the Fe-Ni-O-H material has an even higher average atomic number, and is brighter still.

Figure 23.  BSE images of corroded schreibersite grains.  A) The scale bar is in the bottom left corner.  Note the cubic corrosion pattern.



20 um   BSE1    15 kV  20 nA
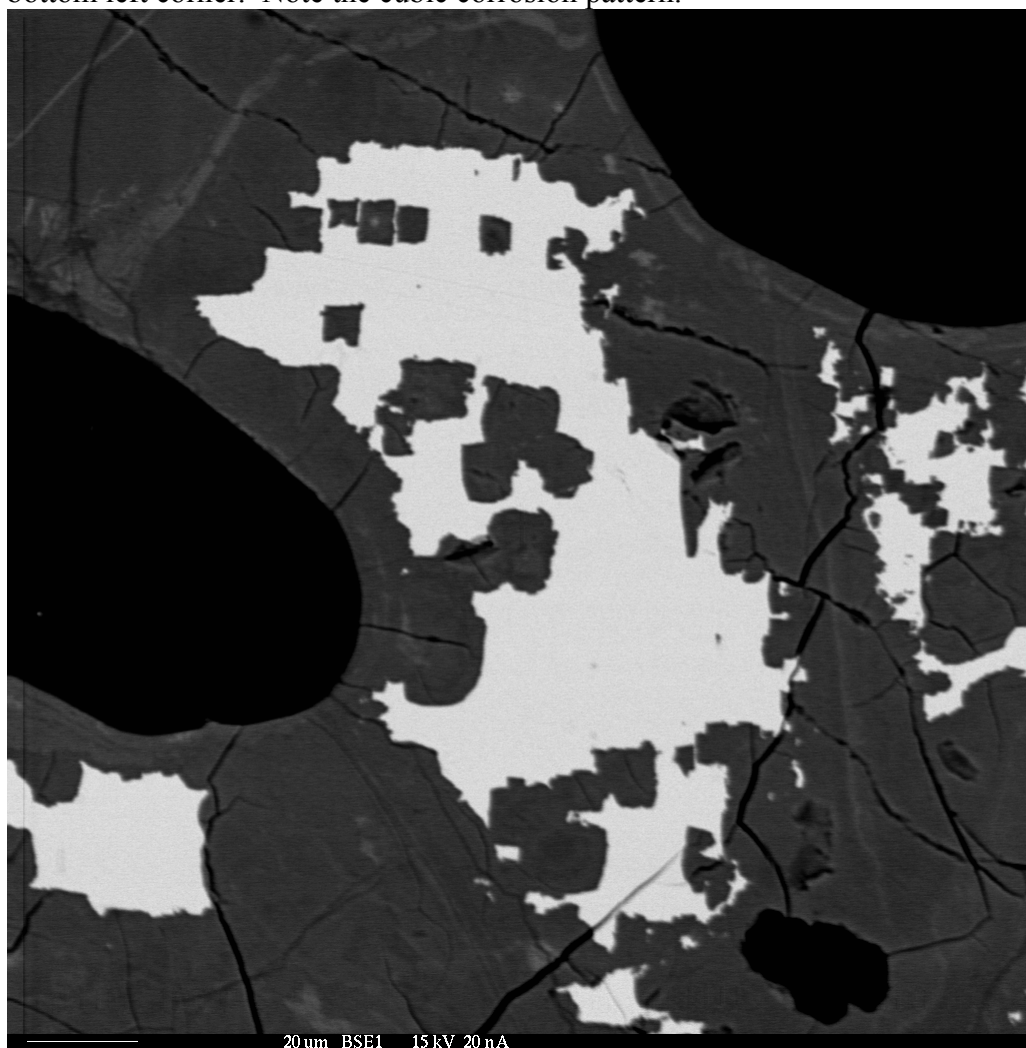
Figure 23 B).  A second example of unusual corrosion pattern.  Note the change in scale.
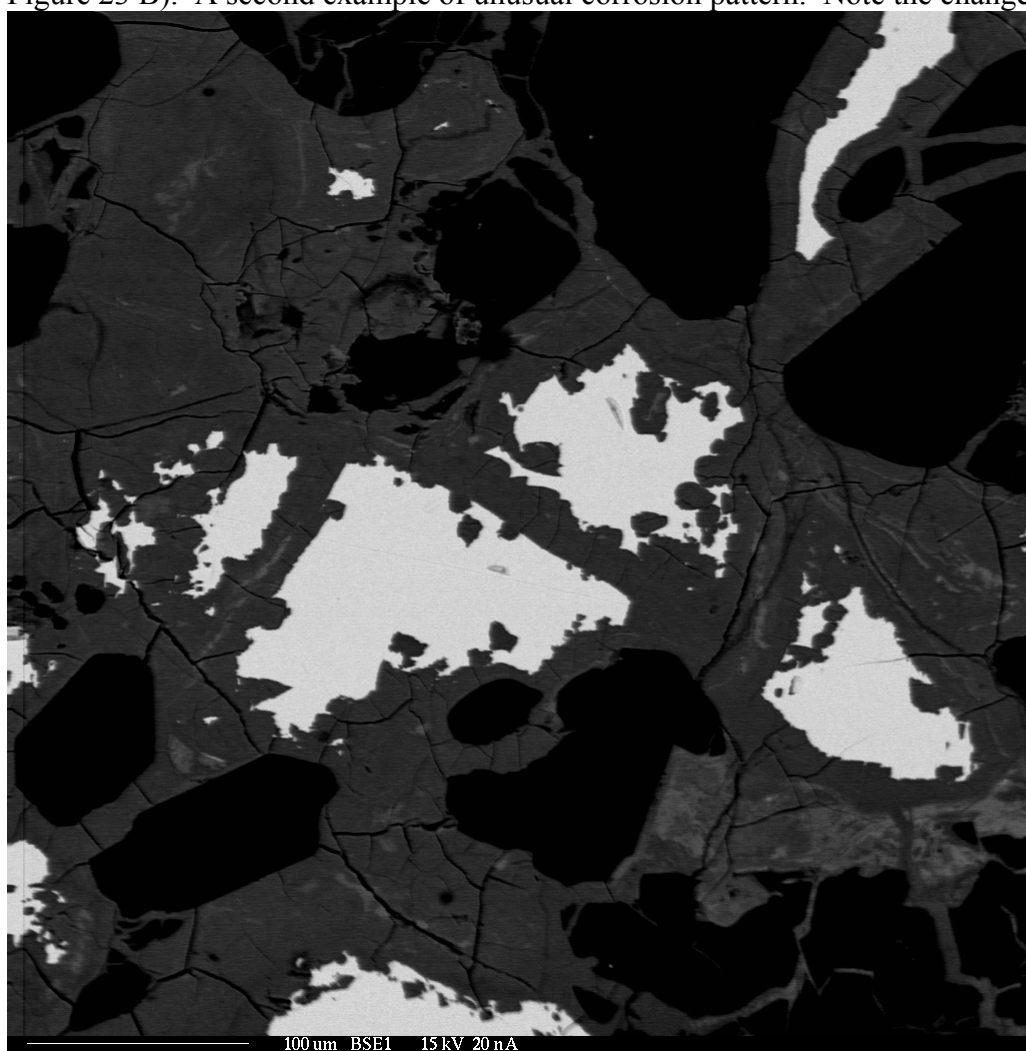
Figure 24.  Full BSE map of SWL080 discussed in section 2.4.  A 500 mm scalebar is at the bottom of this figure.  The mineralogy from darkest to lightest is silicates → Fe-Ca-P-O-H corrosion product → rust → schreibersite (Sch).
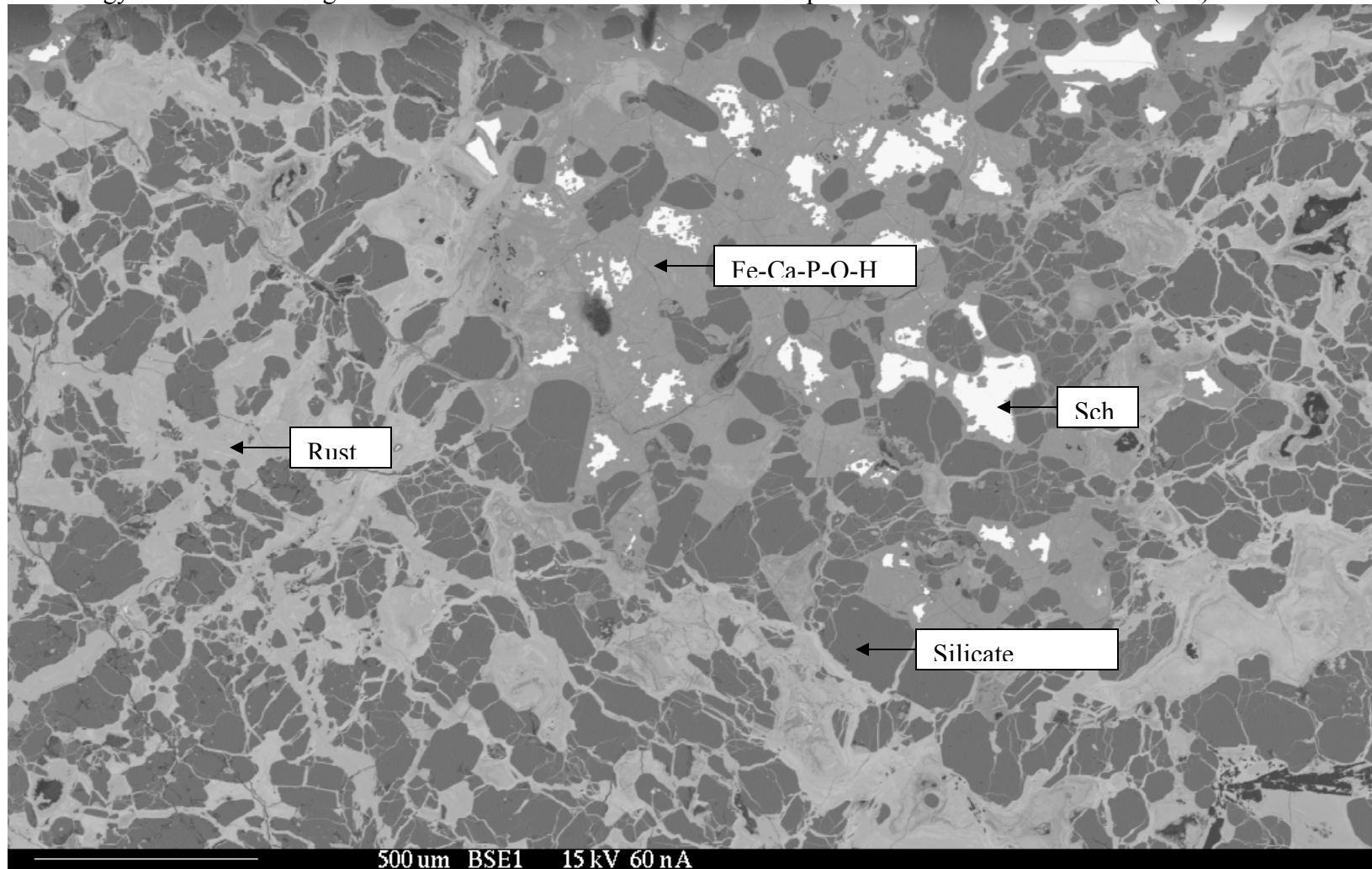
The material surrounding the phosphide corrosion area is mostly silicate material and iron oxide rust. Many of the enstatite grains are separated by cracks filled with corroded phosphide material or rust.

## 3.3 Chemical Characteristics of Corroded Schreibersite Grain

### 3.3.1. Method

Elemental abundances were determined through electron microprobe point analysis using the standards shown in table 16. Twelve analyses of schreibersite were taken, and there were a total of 56 analyses of the oxide corrosion area.

### 3.3.2 Results

A color coded map is shown as figure 25. This map is a composite of three elemental maps, color-coded red for P, green for Ni, and blue for Ca. Ca-P-oxides are purple, and schreibersite is orange. Other green areas are iron oxide material. Red material is mostly Fe-P-oxides. The iron elemental map had poor contrast, which is why Ni was used instead. The blue vein on the left side of the image is a calcite-filled crack. Potassium and Ca correlate well with P, suggesting that the alteration process hinged on the introduction of minor amounts of Ca and K to the material.

Table 15.  Standards used for metal point analysis.

| Element | Standard |
|---|---|
| **Metals** | |
| Si | Si |
| P | InP |
| S | $CuFeS_2$ |
| Cr | Cr |
| Mn | Mn II |
| Fe | $CuFeS_2$ |
| Ti | Ti |
| Ni | Ni |
| Co | Co |
| | |
| **Oxides** | |
| Si | $CaMgSi_2O_6$ |
| O | $Fe_2O_3$ |
| P | $Ca_5(PO)_3OH$ |
| K | $KAlSi_3O_8$ (orthoclase) |
| Ca | $CaMgSi_2O_6$ |
| Fe | $Fe_2SiO_4$ |
| Ni | Nidi |

Figure 25. Color coded map of schreibersite corrosion in SWL 080.



500 um   Ni     15 kV 60 nA
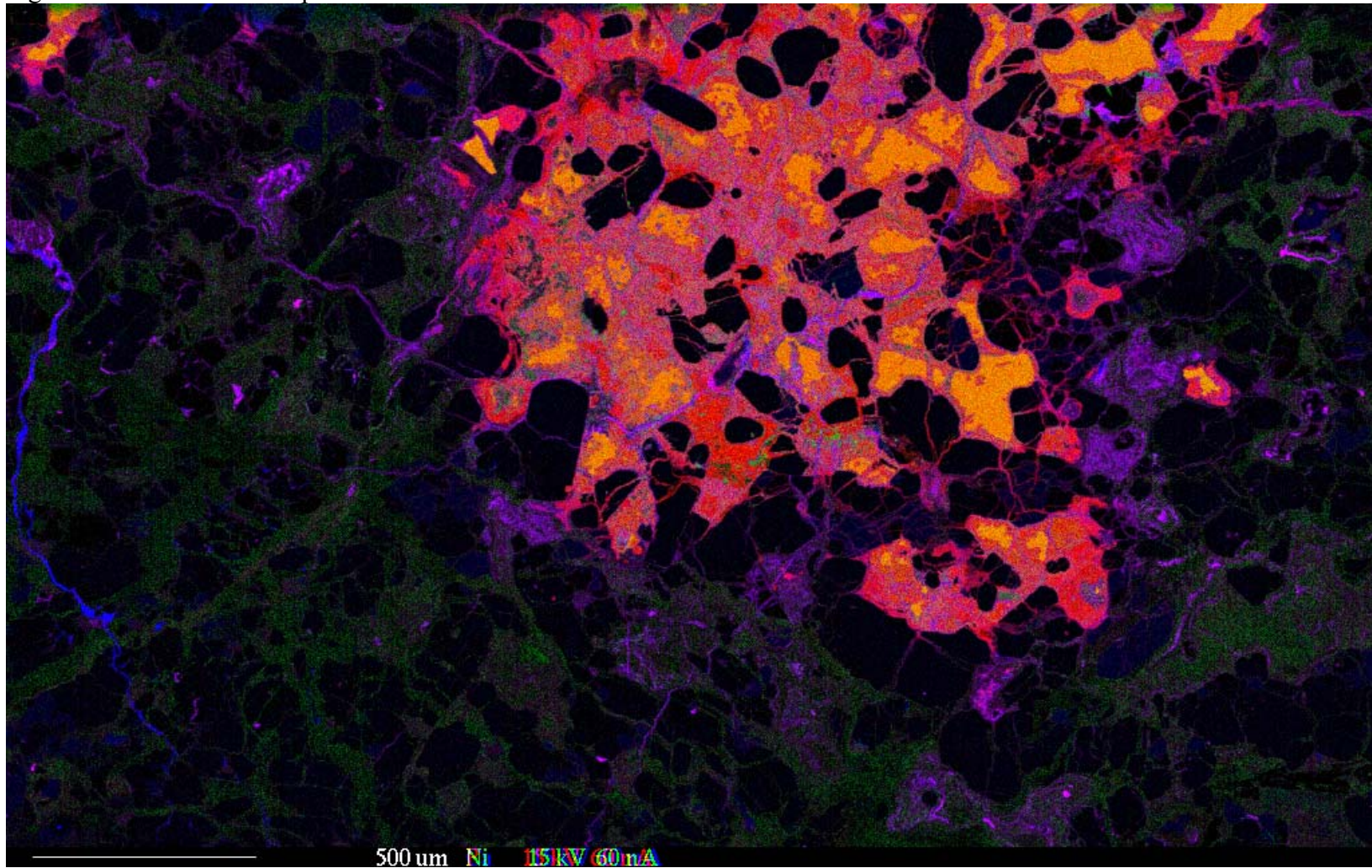
Point analyses of the uncorroded schreibersite are summarized in table 17. The schreibersite is fairly uniform in composition for these 12 analyses, and the average schreibersite composition is

$$(Fe_{2.549\pm0.022}Ni_{0.43\pm0.03}Co_{0.004\pm0.001})(P_{1.000\pm0.009}S_{0.006\pm0.003}Si_{0.008\pm0.002})$$
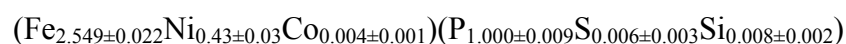
with a $1\sigma$ deviation. The composition of the schreibersite in SWL080 is comparable to the average for schreibersite in enstatite meteorites.

Point analyses of the corroded phosphide material are summarized in table 18. These 56 points were taken throughout the corroded material and show much greater heterogeneity and variation with location in the sample. Most points have low totals, indicating a significant fraction of light elements in the material (likely mostly H with minor C).

3.4 Discussion

Geochemical trends are displayed in figure 26, which shows elements pairs with the least scatter and strongest correlative relationships. Correlations are presented in table 19. The elements with the strongest correlations are P-O, Fe-O, Fe-P, and Fe-Ca. The lack of correlation is due to the porous nature of the material and multiple phases.

Table 17.  EMPA data for schreibersite grains.  Values given in weight %.  The overall average is given on the previous page.

|  | Si | P | S | Cr | Mn | Fe | Ti | Ni | Co | Total |
|---|---|---|---|---|---|---|---|---|---|---|
| #1 | 0.08 | 15.212 | 0.083 | 0 | 0 | 70.089 | 0 | 14.554 | 0.16 | 100.178 |
| #2 | 0.154 | 15.133 | 0.092 | 0.007 | 0.001 | 69.516 | 0 | 11.99 | 0.114 | 97.007 |
| #3 | 0.103 | 15.434 | 0.084 | 0.002 | 0 | 70.85 | 0.025 | 12.288 | 0.138 | 98.924 |
| #4 | 0.107 | 15.512 | 0.052 | 0.017 | 0 | 69.63 | 0 | 12.983 | 0.091 | 98.392 |
| #5 | 0.099 | 15.192 | 0.048 | 0.001 | 0 | 69.908 | 0 | 12.695 | 0.156 | 98.099 |
| #6 | 0.107 | 15.365 | 0.093 | 0 | 0 | 70.397 | 0.015 | 13.545 | 0.086 | 99.608 |
| #7 | 0.093 | 15.214 | 0.053 | 0.008 | 0 | 70.139 | 0 | 13.914 | 0.102 | 99.523 |
| #9 | 0.099 | 15.312 | 0.089 | 0 | 0 | 70.832 | 0 | 11.921 | 0.041 | 98.294 |
| #10 | 0.102 | 15.125 | 0.099 | 0 | 0.013 | 70.586 | 0.023 | 12.173 | 0.201 | 98.322 |
| #11 | 0.109 | 15.339 | 0.11 | 0 | 0 | 70.525 | 0 | 12.134 | 0.165 | 98.382 |
| #12 | 0.102 | 15.421 | 0.079 | 0.029 | 0.019 | 70.822 | 0.008 | 12.084 | 0.154 | 98.718 |
| #13 | 0.082 | 15.462 | 0.075 | 0 | 0 | 71.137 | 0 | 12.196 | 0.122 | 99.074 |

Table 18. EMPA of oxide material surrounding corroded schreibersite. Values given in weight %. The average for the total is 95.9 wt. %.

|     | Na | Si | O | P | K | Ca | Fe | Ni | Total |
|-----|------|--------|--------|--------|-------|--------|--------|-------|---------|
| #1  | 0.075 | 0.388 | 45.505 | 12.857 | 0.702 | 5.77 | 27.209 | 4.826 | 97.332 |
| #2  | 0.04 | 1.413 | 42.21 | 11.375 | 0.38 | 7.194 | 28.895 | 2.701 | 94.208 |
| #3  | 0.034 | 0.262 | 43.795 | 12.619 | 0.56 | 5.382 | 28.59 | 5.575 | 96.817 |
| #4  | 0.068 | 0.402 | 38.831 | 3.343 | 0.086 | 3.495 | 44.902 | 3.169 | 94.296 |
| #5  | 0.088 | 0.631 | 42.16 | 9.082 | 0.193 | 11.629 | 28.348 | 5.93 | 98.061 |
| #6  | 0.095 | 0.091 | 38.233 | 6.175 | 0.882 | 0.419 | 41.81 | 5.141 | 92.846 |
| #7  | 0.747 | 0.525 | 43.334 | 11.758 | 0.074 | 19.21 | 20.391 | 0.677 | 96.716 |
| #8  | 0.184 | 0.166 | 45.603 | 12.401 | 0.178 | 17.188 | 23.949 | 1.142 | 100.811 |
| #9  | 0.078 | 0.136 | 45.419 | 13.852 | 0.544 | 9.752 | 26.535 | 0.864 | 97.18 |
| #10 | 0.035 | 2.056 | 37.535 | 2.731 | 0.025 | 3.869 | 48.206 | 1.123 | 95.58 |
| #12 | 0.566 | 3.198 | 43.106 | 11.548 | 1.697 | 6.258 | 29.757 | 0.873 | 97.003 |
| #13 | 0.108 | 1.308 | 45.127 | 13.825 | 0.61 | 10.168 | 24.021 | 1.3 | 96.467 |
| #14 | 0.113 | 0.632 | 44.457 | 11.819 | 0.18 | 17.699 | 23.546 | 0.862 | 99.308 |
| #15 | 0.005 | 0.716 | 36.304 | 0.572 | 0.003 | 0.656 | 55.369 | 1.629 | 95.254 |
| #16 | 0.019 | 1.003 | 32.485 | 0.826 | 0.015 | 1.302 | 58.17 | 2.541 | 96.361 |
| #17 | 0.138 | 0.166 | 42.932 | 13.597 | 0.616 | 9.526 | 27.339 | 0.667 | 94.981 |
| #18 | 0.131 | 0.42 | 42.896 | 13.153 | 1.331 | 3.16 | 28.614 | 5.483 | 95.188 |
| #19 | 0.176 | 0.199 | 46.885 | 15.041 | 1.474 | 1.507 | 30.208 | 2.775 | 98.265 |
| #20 | 0.15 | 0.155 | 46.395 | 14.442 | 1.451 | 0.403 | 30.963 | 2.956 | 96.915 |
| #21 | 0.14 | 0 | 43.731 | 12.846 | 0.723 | 4.914 | 28.53 | 4.109 | 94.993 |
| #22 | 0.155 | 0.192 | 44.871 | 13.943 | 1.141 | 4.004 | 29.327 | 2.136 | 95.769 |
| #23 | 0.075 | 2.112 | 44.667 | 12.968 | 0.521 | 21.472 | 13.383 | 1.078 | 96.276 |
| #24 | 0.135 | 0.133 | 43.76 | 14.401 | 0.954 | 5.066 | 28.872 | 1.433 | 94.754 |
| #25 | 0.112 | 0.283 | 43.655 | 12.802 | 0.47 | 6.123 | 26.4 | 5.427 | 95.272 |
| #26 | 0.099 | 0.088 | 47.56 | 13.276 | 1.561 | 6.068 | 31.778 | 4.475 | 104.905 |
| #27 | 0.13 | 0.832 | 41.69 | 9.467 | 0.124 | 5.485 | 31.535 | 6.556 | 95.819 |
| #28 | 0.127 | 0.31 | 41.639 | 12.692 | 0.473 | 5.788 | 28.356 | 3.804 | 93.189 |
| #29 | 0.078 | 0.208 | 43.366 | 13.493 | 1.174 | 3.414 | 30.03 | 2.898 | 94.661 |
| #30 | 0.094 | 0.396 | 43.586 | 13.216 | 0.391 | 7.769 | 28.893 | 2.083 | 96.428 |
| #31 | 0.138 | 0.112 | 43.901 | 13.957 | 0.978 | 5.39 | 29.595 | 1.918 | 95.989 |
| #32 | 0.103 | 0.333 | 44.679 | 13.084 | 0.417 | 7.222 | 27.958 | 3.094 | 96.89 |
| #33 | 0.055 | 12.029 | 44.047 | 6.458 | 0.885 | 13.059 | 17.233 | 2.376 | 96.142 |
| #34 | 0.099 | 0.096 | 43.159 | 13.441 | 1.609 | 0.212 | 31.837 | 3.483 | 93.936 |
| #35 | 0.049 | 3.151 | 40.568 | 8.073 | 0.205 | 12.986 | 27.026 | 3.22 | 95.278 |
| #36 | 0.074 | 0.103 | 43.08 | 13.061 | 1.137 | 2.401 | 31.738 | 3.633 | 95.227 |
| #37 | 0.035 | 0.306 | 42.333 | 12.897 | 0.866 | 2.518 | 32.788 | 1.764 | 93.507 |
| #38 | 0.131 | 0.178 | 42.706 | 14.576 | 1.274 | 0.654 | 33.438 | 1.171 | 94.128 |
| #39 | 0.041 | 5.018 | 40.694 | 6.424 | 0.176 | 11.545 | 26.436 | 5.818 | 96.152 |
| #40 | 0.195 | 0.059 | 44.274 | 13.11 | 2.226 | 0.754 | 32.811 | 3.213 | 96.642 |
| #41 | 0.131 | 3.309 | 43.283 | 10.535 | 0.809 | 9.239 | 26.333 | 3.659 | 97.298 |
| #42 | 0.176 | 0.055 | 43.034 | 13.335 | 1.944 | 0.159 | 31.392 | 4.75 | 94.845 |
| #43 | 0.099 | 0.081 | 45.659 | 13.832 | 1.601 | 0.332 | 32.515 | 4.66 | 98.779 |
| #44 | 0.426 | 0.069 | 43.542 | 12.574 | 1.454 | 2.279 | 31.788 | 3.231 | 95.363 |

Table 18 cont'd.

|     | Na    | Si    | O      | P      | K     | Ca    | Fe     | Ni    | Total  |
|-----|-------|-------|--------|--------|-------|-------|--------|-------|--------|
| #45 | 0.781 | 0.125 | 45.235 | 14.987 | 1.956 | 0.784 | 31.396 | 1.657 | 96.921 |
| #46 | 0.255 | 0.511 | 47.363 | 13.358 | 1.159 | 3.318 | 30.664 | 2.4   | 99.028 |
| #47 | 0.098 | 0.067 | 42.367 | 13.663 | 1.619 | 0.202 | 31.772 | 3.754 | 93.542 |
| #48 | 0.13  | 0.479 | 43.656 | 12.12  | 0.457 | 6.292 | 27.893 | 4.942 | 95.969 |
| #49 | 0.226 | 0.364 | 41.251 | 12.174 | 0.06  | 4.136 | 30.763 | 3.279 | 92.253 |
| #50 | 0.079 | 0.082 | 43.698 | 12.814 | 2.159 | 0.905 | 28.815 | 4.422 | 92.974 |
| #51 | 0.264 | 0.025 | 45.621 | 12.997 | 1.524 | 4.873 | 27.669 | 1.206 | 94.179 |
| #52 | 0.142 | 0.984 | 42.65  | 11.58  | 1.183 | 7.245 | 29.342 | 3.301 | 96.427 |
| #53 | 0.037 | 0.161 | 43.187 | 13.068 | 1.13  | 4.152 | 30.271 | 3.467 | 95.473 |
| #54 | 0.076 | 0.043 | 44.752 | 14.922 | 1.735 | 3.663 | 30.252 | 0.718 | 96.161 |
| #55 | 0.044 | 0.322 | 39.553 | 12.174 | 0.257 | 3.777 | 33.498 | 2.95  | 92.575 |
| #56 | 0.057 | 0     | 44.273 | 13.315 | 1.823 | 1.779 | 31.269 | 3.676 | 96.192 |
| #57 | 0.003 | 0.181 | 43.846 | 13.525 | 0.731 | 7.77  | 24.862 | 4.658 | 95.576 |

Figure 26. Geochemical trends of schreibersite corrosion area.  All values are wt %.
a) Fe vs. Ca                                b) Fe vs. O
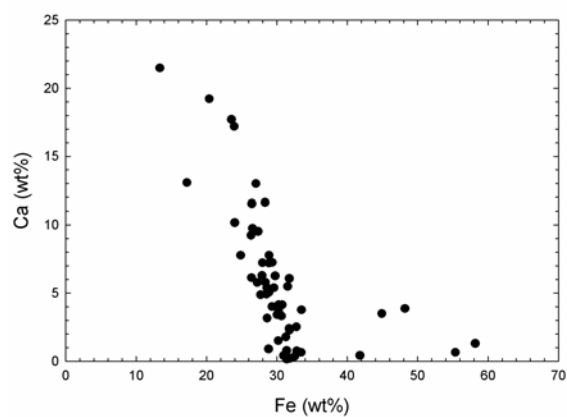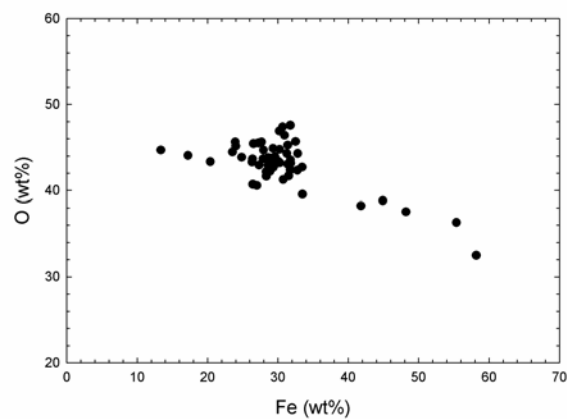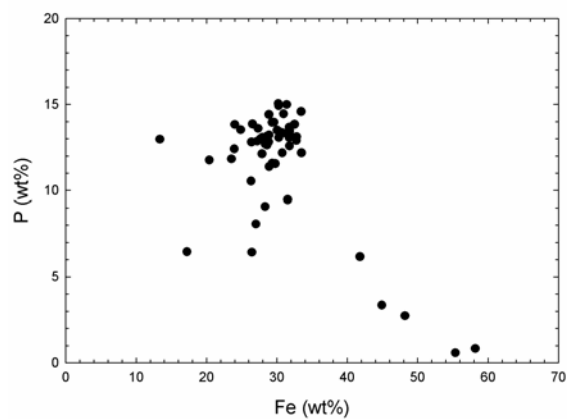


c) Fe vs. P                                d) Fe vs. Total
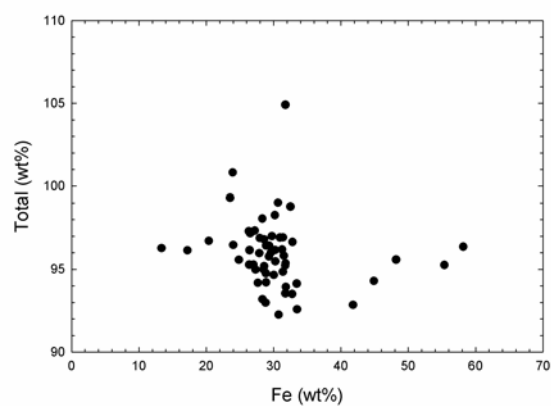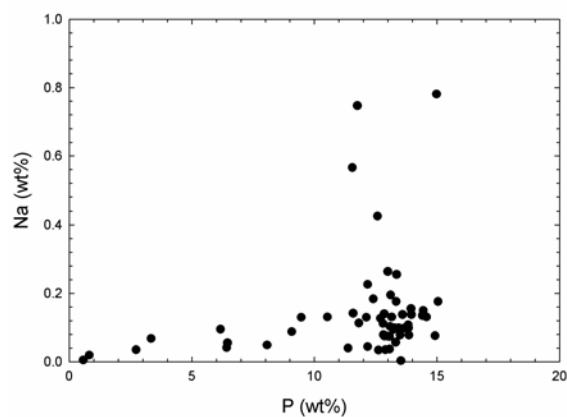


e) P vs. Na                                f) P vs. O
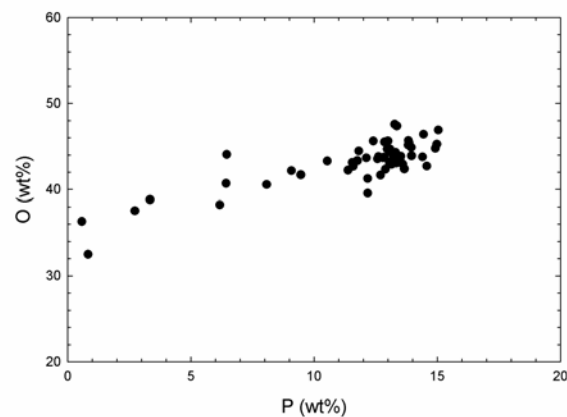
Figure 26. Cont'd.

g) Ca vs. K
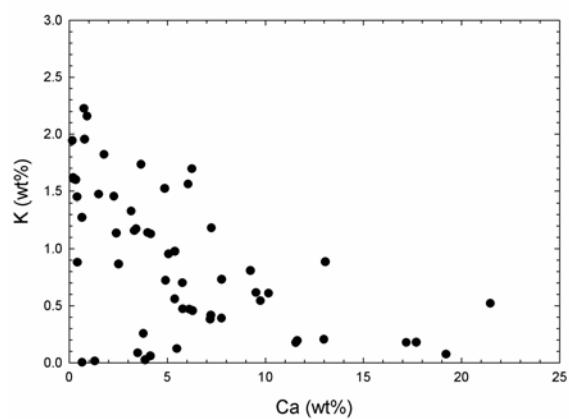
h) Ca vs. P
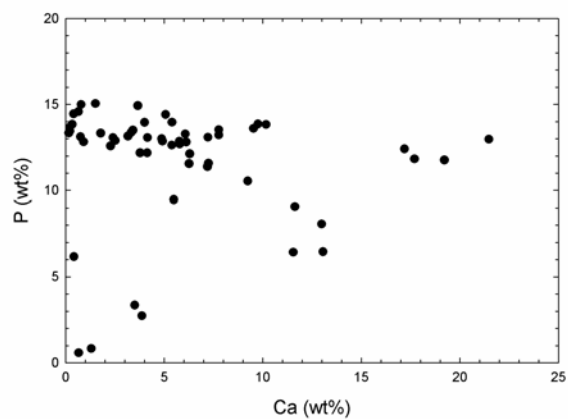


i) Ca vs. O
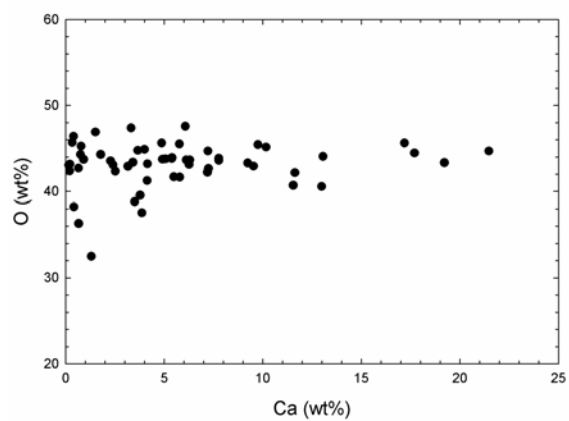
j) Total vs. O
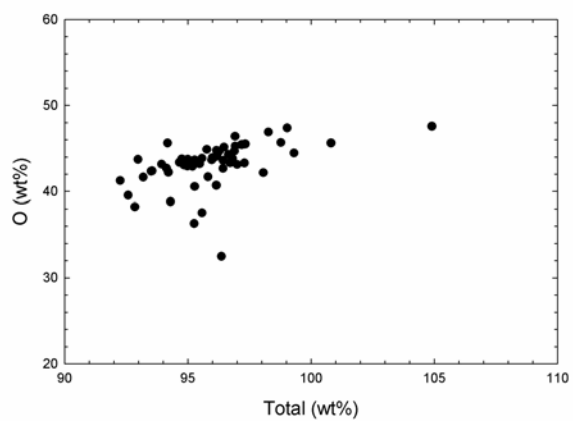
Table 19. Linear regressions of schreibersite corrosion material data. The coefficients are for the equation: Y = AX + B.

|  | A | B | $R^2$ |
|---|---|---|---|
| **Fe-Ca** | -0.4241 | 18.669 | 0.3841 |
| **Fe-P** | -0.2956 | 20.719 | 0.4072 |
| **Fe-O** | -0.2614 | 51.068 | 0.5201 |
| **Fe-Tot** | -0.0498 | 97.464 | 0.0302 |
| **P-Na** | 5.4549 | 10.944 | 0.06 |
| **Ca-O** | 0.0847 | 42.622 | 0.0256 |
| **Ca-P** | -0.0303 | 11.892 | 0.002 |
| **Ca-K** | -0.067 | 1.2769 | 0.2879 |
| **Tot-O** | 0.6033 | -14.774 | 0.2271 |
| **P-O** | 0.6438 | 35.567 | 0.6771 |

3.4.1 Fe, Ni, P Depletion

The elemental abundances of Fe, Ni, and P in the corroded material are normalized by the respective abundances of these elements in the average schreibersite grain (defined above). In equation form, this relationship is defined as $Q$:

$$Q = \frac{[At\% \; Element_{corroded \; material}]}{[At\% \; Element_{Schreibersite}]} \tag{27}$$

with data points from Fe oxides removed (see figure 27). Fe oxides are defined as compounds with less than 7 wt. % P. These relationships demonstrate that the loss of Fe and Ni from the starting schreibersite is much greater than the loss of P in the corroded material. The $Q$s for P, Fe, and Ni are 0.43 0.21, and 0.13 respectively. The $Q$s for Fe and P have minimal scatter and indicate relative homogeneity for these two elements. Ni has significantly more scatter, indicating more mobility during alteration or weathering.

There are two possible causes for the depletion of these elements from schreibersite. First, these depletions may represent mixing of Fe, P, and Ni with other elements (like oxygen), resulting in a net dilution in terms of weight percent. Alternatively, these elements may have been mobilized by water and the depletion indicates that they have moved through the matrix. A combination of both these causes is the most likely explanation. The differing values for $Q$ for P and Fe indicate that mixing alone is not the cause, and the spatial cohesion of the corrosion area indicates that mobilization alone likewise is not the cause. The spatial cohesion for P suggests that P was not highly mobilized and this is in agreement with its relatively insoluble chemical nature. If P was

Figure 27.  P, Fe, and Ni depletion of oxides. Depletions are set relative to the standard schreibersite grain.
a) Phosphorus.
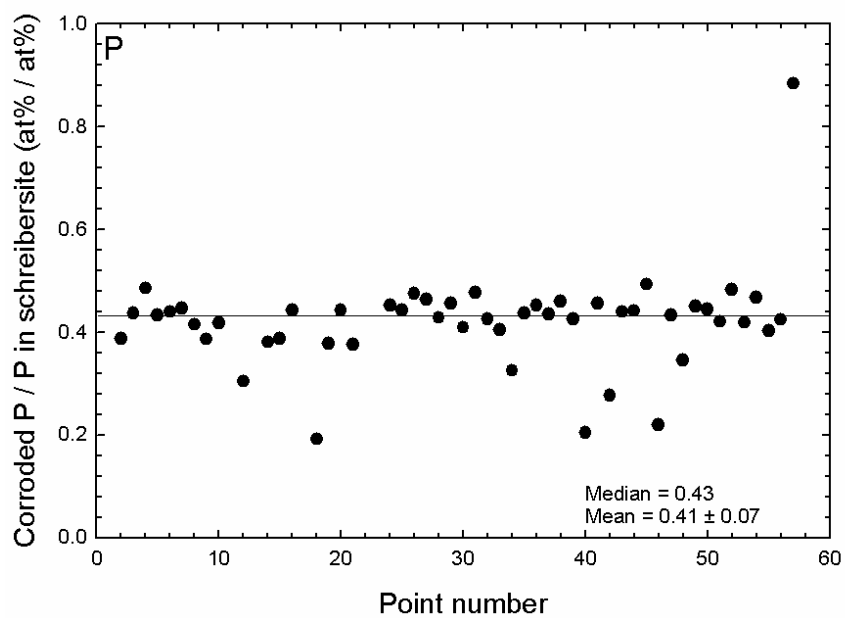


b) Iron.
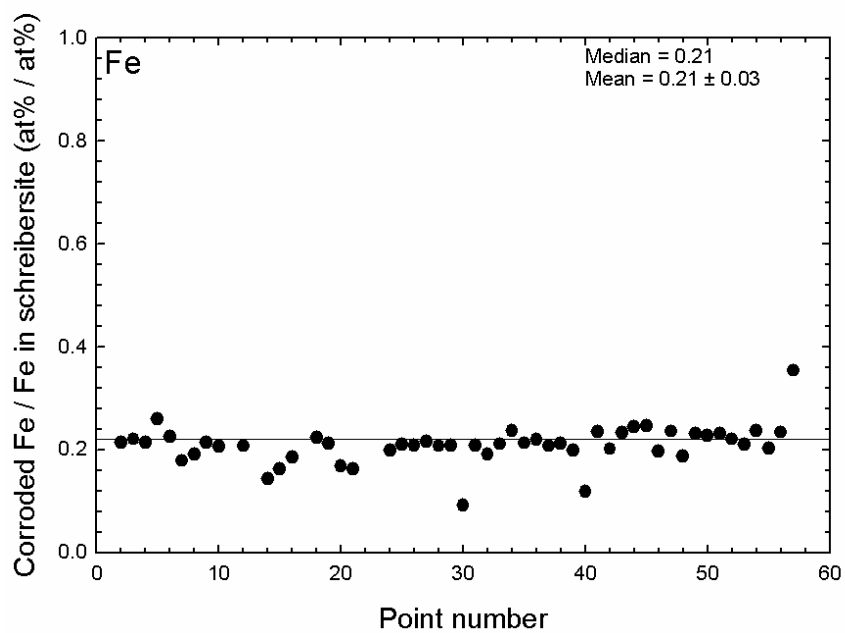
Figure 27 cont'd
c) Nickel.
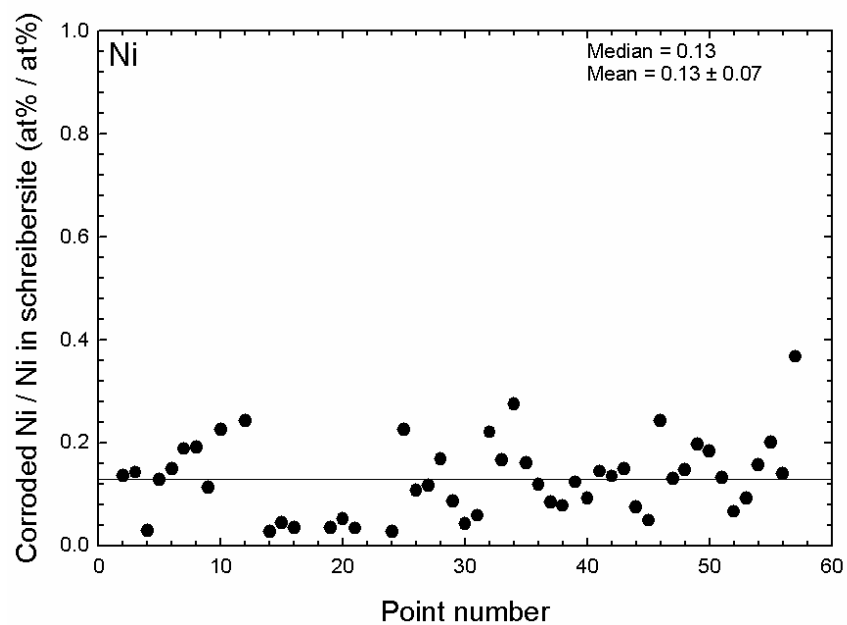
not mobilized, then Fe was mobilized to a significant extent in order to conserve mass.

The net chemical reaction is likely:

$$Fe_{2.5}Ni_{0.5}P + H_2O \rightarrow Fe_2PO_{9.5}H_? + (Fe,Ni)OOH_? \qquad (28)$$

where every unit of Fe-P oxide formed also forms an equivalent unit of Fe oxyhydroxide.

This reaction also provides an explanation for the prevalence of Fe-Ni-O-H compounds

outside of the P rich corrosion area. P did not mobilize and remained close to the source

schreibersite as it corroded, but Fe oxidized and spread throughout this section of the

meteorite. This schreibersite-P rich corrosion- Fe oxyhydroxide mineralogy is observed

in some locations (figure 28). Fe oxyhydroxide rarely appears to touch uncorroded

schreibersite.

It is apparent from simple stoichiometric calculations that schreibersite corroded

to form two phases, an Fe-Ca-P-O-H phase and a Fe-Ni-O-H phase. This transition

would be accompanied by a 2-3 fold increase in volume. Given the proximity of the

schreibersite to the silicate grains, this provides a rationale behind the apparent cracking

of the meteorite by the P rich oxide and Fe oxyhydroxide phases.


3.4.2 Ca, K, O and Light Element Addition


Both elements K and Ca are concentrated in the phosphide corrosion area (figure 29).

The spatial relationship of these elements to the P corrosion area indicates that they were

likely introduced during terrestrial alteration and are not native to the meteorite.

Figure 28. Spatial relationship of schreibersite, corrosion product, and rust. Schreibersite surrounded by a P-rich corrosion area, in turn surrounded by a P-poor corrosion area. A 20 μm scale bar is at the bottom left of the image. Sch is schreibersite, P-rust is the Fe-Ca-P-O-H corrosion product, and rust is an Fe-Ni-O-H material.
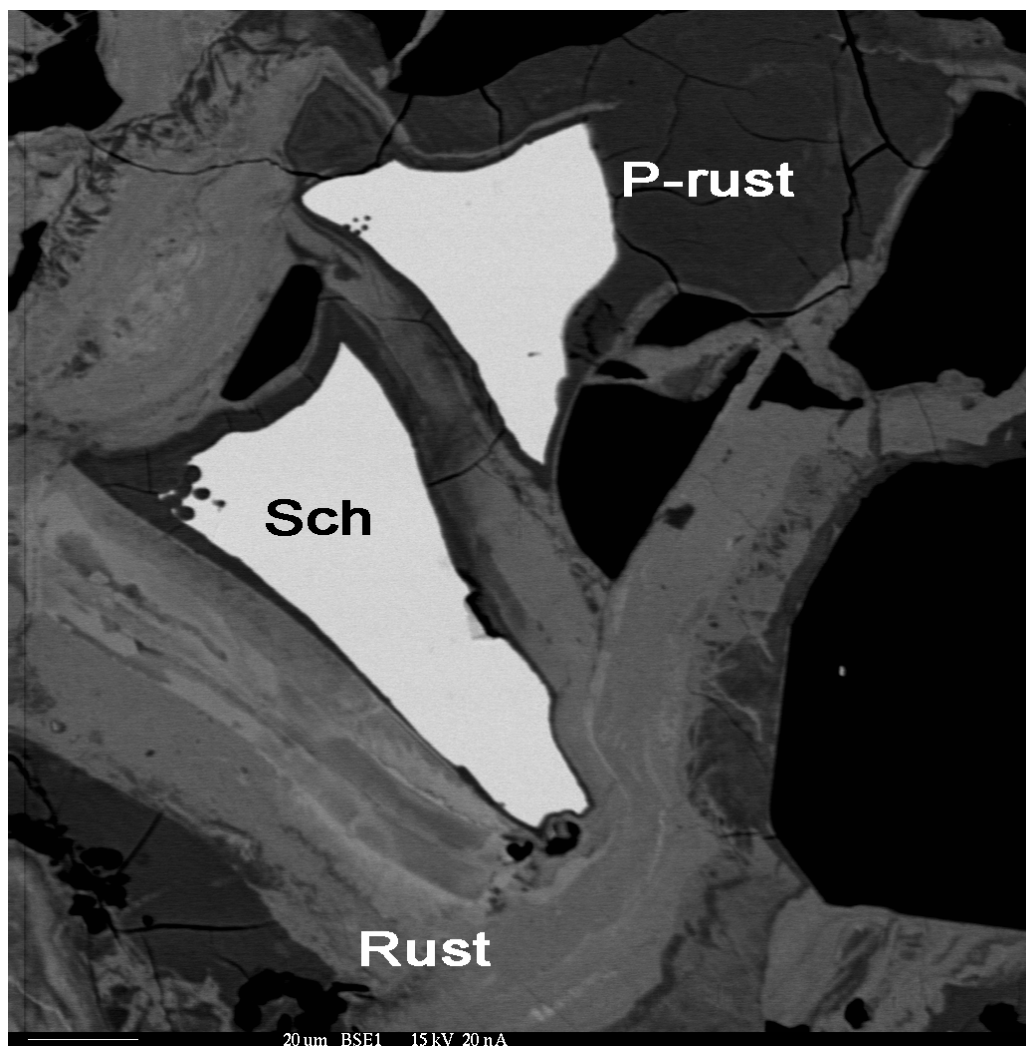
Figure 29.  Map of K abundance.  The brightness is proportional to abundance.  Scale bar at bottom left.  The maximum K wt% in the bright areas is ~1-2 wt. %.



500 um   K      15 kV 60 nA
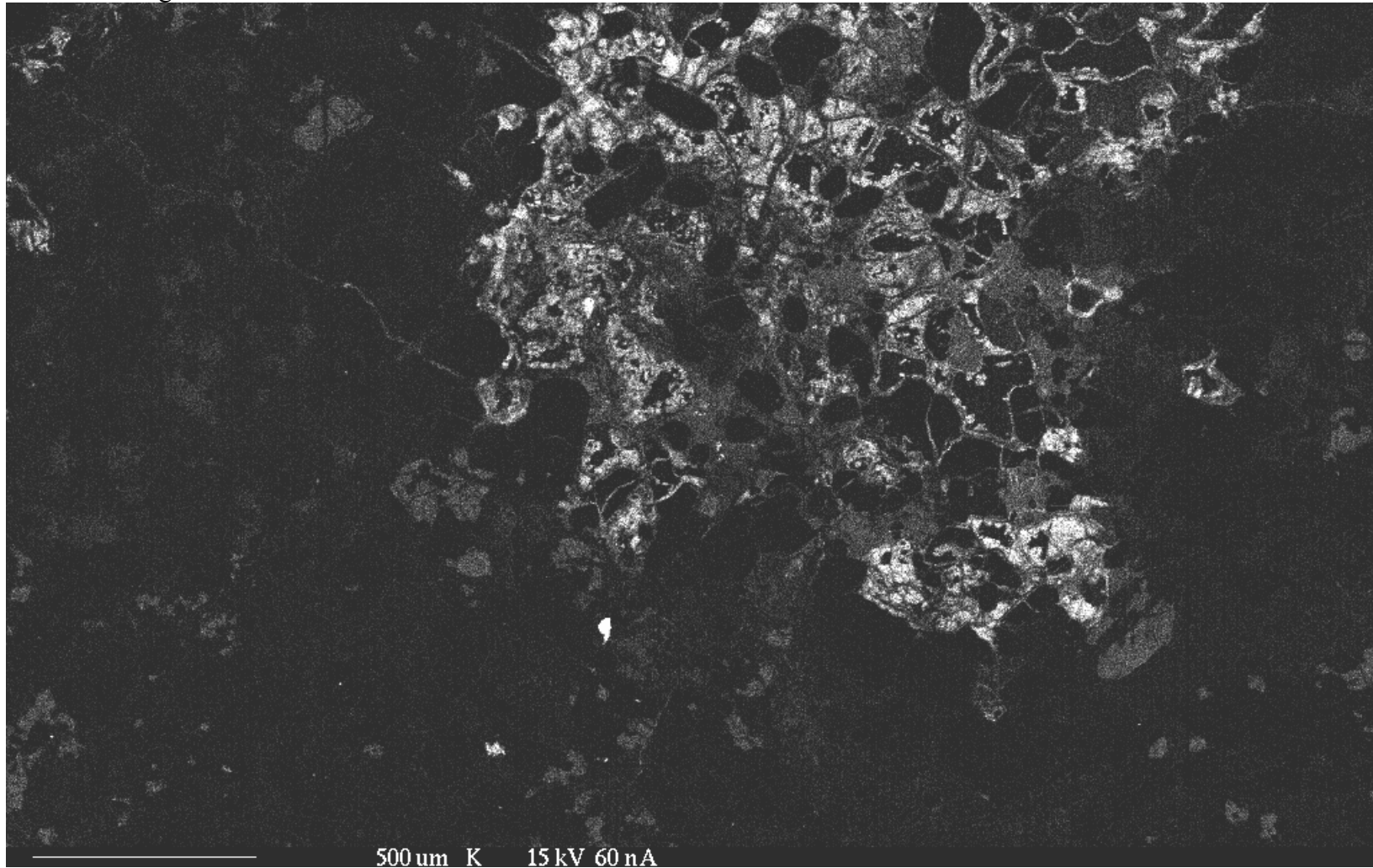
The abundance of oxygen in the corroded schreibersite material is fairly constant relative to the abundance of P. The median ratio of O to P in atom % to atom % is 6.40 O atoms per P atom, and the mean ratio is 6.57 O atoms per P atom (excluding low P points). For Fe-Ni-O-H (low total P) data points, the O to Fe ratio ranges from 2 to 5. These data correspond to formulae ranging from FeOOH to $Fe(OH)_3 \cdot 2H_2O$, based on charge balance with hydrogen.

The average total abundances are lower than 100% and indicate the contribution of a light element like H or C. The average ratio of H atoms per Fe atom may range from as low as 1:1 to as high as 7:1, which is consistent with the range of total abundances. The great variation between totals in the schreibersite corrosion area indicates a significant heterogeneity in the characteristics of the corrosion product.

The amount of light elements must increase with the increase of P in the corrosion product. When the O and P molar abundances are normalized by the sum $1.5 \times N_{Fe} + N_{Ni} + N_{Ca}$ where $N$ is the number of moles of a given element, then there is a linear relationship between O and P (figure 30). The factor of 1.5 multiplies the number of moles of iron by the charge on ferric iron and thus references P and O abundances to the total cationic element charge. The Na, Si, and K charge contribution is minimal relative to these three elements. The slope of this relationship implies that, relative to the abundance of 2+ cations, every P atom is balanced by 3.3 O atoms. The charge balance of this relationship requires the addition of light elements with the increase of P. Otherwise, the charge on P would have to be +6.6, which can only occur in plasma.

Figure 30. Relationship between moles of O and moles of P.  Values have been normalized to the molar abundances of Fe × 1.5, Ca, and Ni.
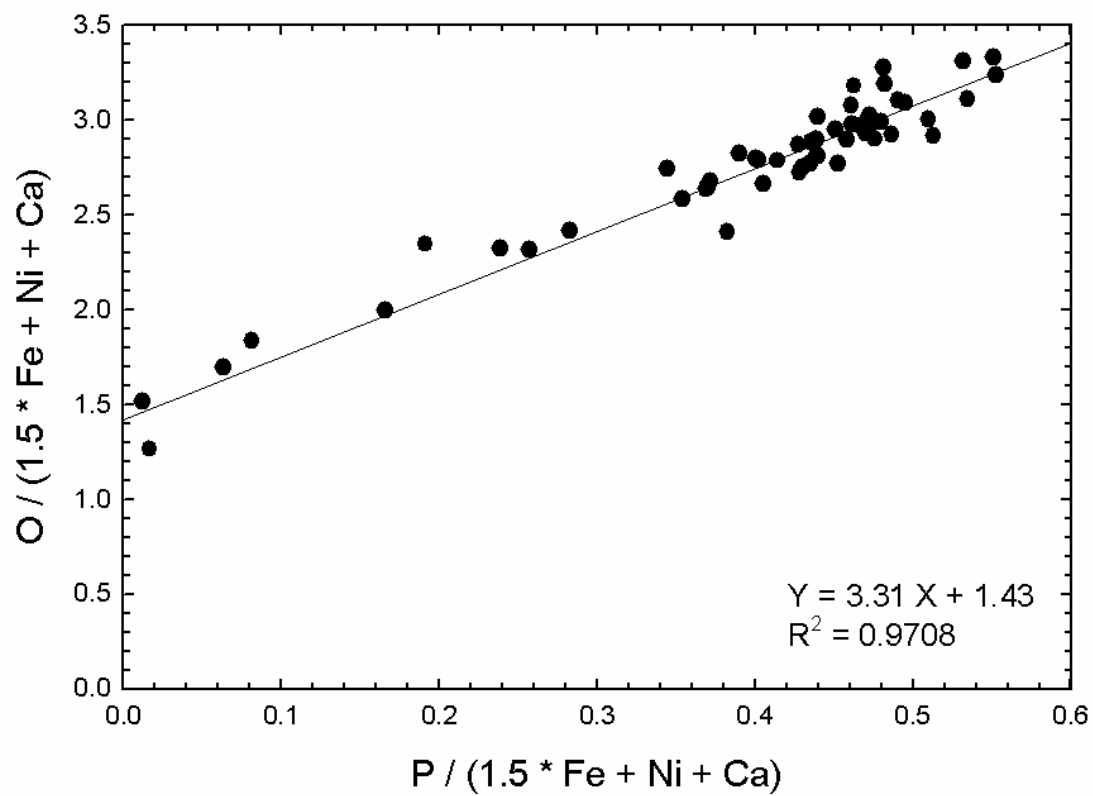
3.4.3 Oxidation State of P

The results from our experiments with synthetic $Fe_3P$ powder and water indicate that the corrosion of schreibersite produces a mixed valence solution of P salts with oxidation states ranging from +3 to +5 for P. How does this compare to the calculated valence state of the corrosion product in this meteorite?

The valence of P in the schreibersite corrosion is strongly dependent on the amount of light element constituents. The possible mineral formulae range from $Fe,Ca(HPO_3)OH$ to $Fe,Ca(PO_4)OH$ with indeterminate coefficients for Fe, Ca, O, and H. It is impossible to determine the exact valence state of P in the corrosion area due to the large errors with the oxygen wt. %, the total wt. %, and the lack of a clear determination of the light element composition. For instance, distinguishing between the two members $Fe,Ca(HPO_3)(OH)_2$ and $Fe,Ca(PO_4)OH$ can not be done. However, some possibilities to aid in the identification of the valence state of P may still be discussed.

Could the schreibersite corrosion area be representative of an apatite-iron oxyhydroxide mixture? If so, then the Ca:P ratio should be independent of the amount of Fe, O and H present in the sample. Figure 31 demonstrates the Ca to P ratio for the data set. Two sets of minerals are shown: pure apatite, $Ca_5(PO_4)_3(X)$, and Ca-reduced P compounds, $Ca[HPO_3, (P_2O_6)_{1/2}, (P_2O_7)_{1/2}]$. The data set is not consistent with a pure apatite-Fe oxyhydroxide as very few points approach the 5:3 Ca:P apatite line. This data set is also not consistent with a pure end-member reduced/condensed P and Ca phase as

147

Figure 31.  Ca: P in the corrosion area.  Also added are the apatite Ca : P ratio, and the reduced Ca : P ratio.
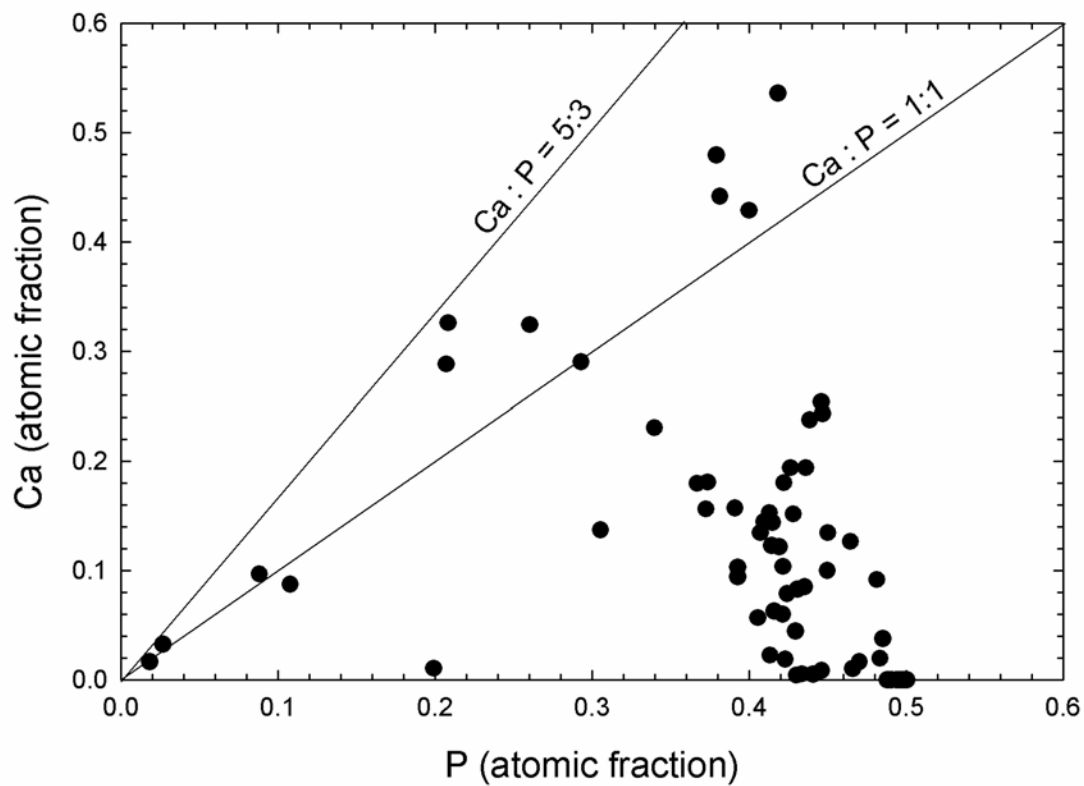
many points lie above the 1:1 Ca:P line. Many analyses show very low Ca and

respectively higher Fe, indicating the presence of significant Fe-P oxides.

If we assume a systematic error and state that there are 3 H atoms per Fe atom,

consistent with the charge balance described above, then the average oxidation state of P

is 4.56, indicating that the corrosion product is indeed slightly reduced.

An alternate means of obtaining a "typical" formula weight is to use the

correlations of table 19. If we assume that there are two phases: an FeOH phase and a

CaPOH phase, then we can calculate what the CaPOH phase would be in the absence of

all Fe. The y intercept for the relationships established between Fe-P, Fe-O, Fe-Ca, and

Fe-Total determines a formula of $CaP_{1.43}O_{6.83}H_{5.35}$, assuming all the difference between

the total and 100% is due to H atoms. The charge of P in this mineral would again be

4.56.

Finally, the slope of figure 30 implies that every P atom is balanced by 3.3 O

atoms. This ratio is most consistent with a mixture of reduced P species like $HPO_3^{2-}$,

$P_2O_6^{4-}$, $P_2O_7^{4-}$, and $PO_4^{3-}$. The O to P ratios of the corrosion experiments described

earlier this chapter approach this value.


3.5 Future Work and Conclusions


A grain of schreibersite in the aubrite SWL080 has clearly corroded to form a mixture of

iron oxides and iron-calcium phospho-oxides. The stoichiometry of this corrosion

product clearly indicates that the material is heterogeneous and is not just a mixture of

calcium phosphate and iron oxyhydroxide.  Microprobe analyses of this product are not

inconsistent with a reduced valence state for P, similar to the oxidation states indicated by

the corrosion experiments described earlier in this dissertation.  More work is necessary

with this material, and better technological approaches for calculating the amounts of

light elements (H and C) are necessary to determine the exact nature of this corrosion

product.  This research is intended to be presented as a set of data available for future

research.

The difficulty of determining the oxidation state of P limits our ability to compare

this sample to the experimental results.  Other techniques may yield superior results,

including micro-Raman spectroscopy and XRD analysis of the thin section.  Micro-

Raman spectroscopy may detail the nature of the P bonds in the section, after comparison

to standard compounds.  XRD would require preparation of standard iron-P sample

which may be difficult given the heterogeneity of the corrosion region in the section.

Future work may entail exploration of both of these methods for analysis.

CHAPTER 4


REACTION PATHWAY



Schreibersite corrodes to form inorganic P salts and organophosphorus compounds.

Understanding the reaction pathway is critical to an evaluation of the prebiotic input of

schreibersite to the origin of life, and to the origin of the P-C molecules in the organic

inventory of meteorites.  The term "reaction pathway" is used in this section as the

alternate term, "reaction mechanism," implies a rigorous knowledge of the kinetics for

each reaction step, precise transfer of electrons, and the experimental and controlled

chemical analyses demonstrating these facets of a pathway.  Given the nature and

complexity of the corroding schreibersite system (consider the number of species in table

14, for instance), that sort of knowledge is not possible.  Regardless, the reaction pathway

described in this section is consistent with NMR experiments, MS experiments, EPR

experiments, and general arguments from stoichiometry.  It provides a rationale for the

origin and diversity of P species in experimental solutions.


4.1 Proposed Reaction Pathway


The reaction pathway described by Pasek and Lauretta (2005) was accurate for the

experiments considered.  Further work informed the current proposal for the reaction

pathway which involves the generation, propagation, and termination of phosphate, phosphite, hydrogen, hydroxyl, and acetate radicals. This reaction pathway provides a pathway to the P salts and to phosphorylated organic compounds.

Pasek and Lauretta (2005) described a reaction pathway using oxidation/reduction reactions to produce the diversity of P compounds present in solution:

$$Fe_3P + 7\ H_2O \rightarrow Fe_3O_4 + H_3PO_3 + 5\tfrac{1}{2}\ H_2\,(g) \qquad (29)$$

$$H_3PO_3 + H_2O \rightarrow H_3PO_4 + H_2\,(g) \qquad (30)$$

$$2\ H_3PO_3 \rightarrow H_4P_2O_6 + H_2(g) \qquad (31)$$

$$H_4P_2O_6 + H_2O \rightarrow H_4P_2O_7 + H_2(g) \qquad (32)$$

$$H_4P_2O_7 + H_2O \rightarrow 2\ H_3PO_4 \qquad (33)$$
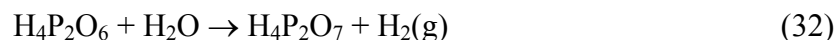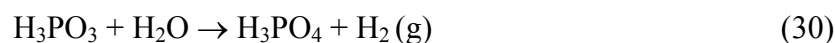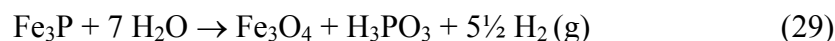
This proposed reaction pathway was investigated in the series of experiments detailed in the results sections on P compound stability and synthetic experiments, but did not produce the products predicted. Furthermore, orthophosphate ($PO_4^{3-}$), hypophosphate ($P_2O_6^{4-}$), and pyrophosphate ($P_2O_7^{4-}$) are stable and unreactive over the timescales and reaction conditions studied in the experiments described in chapter 2. Phosphite and iron react to form orthophosphate and $Fe^{2+}$, but this reaction alone is not an oxidation/reduction reaction since no species is reduced. Hypophosphite ($H_2PO_2^{-}$) is reactive, but is never detected in a corrosion solution. Additionally, the stoichiometric ratios of the various P species is roughly constant, which would not be expected if one species turned to another through reaction with water or other P salts.

Phosphide corrosion proceeds through a radical chemistry pathway. Electron paramagnetic resonance spectroscopy proves the existence of radicals in solution as this

method detects only unpaired electrons.  A brief discussion of aqueous radical chemistry follows to provide a background for the later presentation of the reaction pathway.

4.1.1 Introduction to Radical Chemistry

Free radical chemistry is a "younger" branch of chemistry, having originated in the experiments of Gomberg in 1900.  Modern industry uses significant quantities of radical inducers in the production of polymers, and progress has been made recently in the environmental chemistry applications of radicals and radical inducers.  Radical chemical reactions have three steps: initiation, propagation, and termination.

*Initiation.* Free radicals result from the homolytic dissociation of a bond, i.e. the splitting of a bond resulting in the retention of one of the electrons of the bond by both species:

$$AB \rightarrow {}^{\cdot}A + {}^{\cdot}B \tag{34}$$

with unpaired electrons denoted by a bullet.  Radicals may be formed by irradiation with UV light, X-rays, or $\gamma$-rays, high temperatures, and even the specifics of chemistry. Some species spontaneously become radicals if the radical is sufficiently stable.

*Propagation.* Electrons can be transferred from a free radical species to a non-radical species or vice versa, resulting in a new radical species:

$$A^{\cdot} + C \rightarrow C^{\cdot} + A \tag{35}$$

This radical reaction is known as a propagation reaction.

*Termination.* Most radicals are extremely energetic, and the termination of two radical species by their combination:

$$\cdot C + \cdot B \rightarrow CB \tag{36}$$

is almost always thermodynamically favorable and most radical termination reactions will overcome energetic barriers that block non-radical reaction pathways. However, due to the reactivity of radical reactions, the chemistry resulting from these reactions is less selective than non-radical reactions. A careful balance between total production and yield must be considered for radical reactions in chemical synthesis.

Several common reaction processes have recently been identified as proceeding through a radical reaction pathway. Nearly all reactions that occur with air as $O_2$ are radical reactions, as $O_2$ is a diradical species. The drying of paint, the oxidation of fat, and several biochemical reactions have recently been recognized as radical reactions, such as reactions with vitamin C, DNA repair, and reactions with enzymes such as ribonucleotide reductase and malonyl-CoA mutase (Parsons 2000, Nelson and Cox 2005).

A few P reactions relevant to phosphide corrosion have conditions characteristic of radical reactions, but the reaction pathways have never been determined and these reactions have never been analyzed by EPR to specifically identify radical intermediates. Schwartz and Van der Veen (1973) describe a reaction that generates hypophosphate from phosphite in the presence of UV light:

$$2HPO_3^{2-} \rightarrow P_2O_6^{4-} + H_2\,(g) \tag{37}$$

UV light breaks the P-H bond and aids in dimerization of phosphite to form

hypophosphate. Reactions proceeding by UV light are typically synonymous with radical

pathways. The addition of $BrO^-$ to a solution of hypophosphate generates pyrophosphate

(Blaser and Halpern 1933):

$$H_4P_2O_6 + H_2O \rightarrow H_4P_2O_7 + H_2\,(g) \tag{38}$$

Reactions with bromine as a reactant are also frequently radical type reactions (e.g.,

Hegedus et al. 2000). Finally the synthesis of hypophosphate proceeds by the addition of

hydrogen peroxide to red phosphorus powder (Yoza and Ohashi 1965):

$$P(red) + H_2O_2 \rightarrow H_4P_2O_6 \tag{39}$$

Reactions with peroxides are also usually indicative of a radical mechanism. Thus

historical P reactions that synthesize the molecules resulting from schreibersite corrosion

seem to proceed *via* a radical pathway, though a detailed investigation by EPR would be

necessary for positive identification.


4.1.2 Generation of Radicals


Except for the most reducing fluids (Eh < -0.1 V at pH = 7), orthophosphate is the stable

form of P in water. Phosphorus in schreibersite exists as oxidation state 0. Thus, the

driving force during corrosion of phosphide is oxidation of P from 0 to +5. The reaction

between water and $Fe_3P$ produces phosphite radicals, and several equivalents of $H_2$ gas:

$$3Fe_3P + 12H_3O^+ + 2H_2O \rightarrow 5H^{\cdot} + 5^{\cdot}OH + 3^{\cdot}PO_3^{2-} + 15H_2 + 9Fe^{2+} \tag{40}$$

Both P and Fe are oxidized in this net reaction. The oxidation state of P changes from 0 to nominally +4 and Fe from 0 to +2. Three radical species are formed: $H\cdot$, $\cdot OH$, and $\cdot PO_3^{2-}$. The production of significant quantities of $H_2$ gas occurs as the $Fe_3P$ corrodes and is consistent with the observed release of $H_2$ (figure 9). The net amount of $H_2$ expected from this reaction from a total P yield of 2.3 mM is $2.87 \times 10^{-4}$ moles. This is comparable to the net $H_2$ release of $\sim 4 \times 10^{-4}$ moles, within the range of error of the calculated pumping rate. The ratio of phosphite to hydroxyl radicals is derived from the EPR spectrum, and may be off by a factor of 2 or so, depending on the nature of the chemical reactions that form DMPOOH and DMPOX. Hydrogen radicals are hypothesized based on the production of $H_2$ and phosphite.

Two distinct lines of evidence lead to the radical reaction pathway: the stoichiometric ratios of P species in the solution-dependent chemistry seen by NMR data, and the ES- TOF-HR-MS data for polyphosphorus species.

4.1.2.1 Stoichiometric Ratios of Phosphorus Compounds

All phosphide corrosion solutions without $Mg^{2+}$ and $Ca^{2+}$ have at least four P species: orthophosphate, pyrophosphate, hypophosphate, and phosphite. The production of three of these P species is readily explained by radical termination reactions, for instance, phosphite is produced through the reaction of a phosphite radical with a hydrogen radical:

$$\cdot PO_3^{2-} + H\cdot \rightarrow HPO_3^{2-} \tag{41}$$

All termination reactions from the initial radical mixture are summarized in a radical matrix (table 20). The $H_2$ evolved during corrosion is a radical termination of 2H atoms.

The production of orthophosphate, hypophosphate, and phosphite is predicted from the initial radical termination products of schreibersite corrosion. Radical reaction pathways rapidly approach steady state, with constant ratios of products. Ratios of these species are constant provided solution chemistry does not greatly affect the relative production rates of the P molecules. Orthophosphate is the stable form of P in most environments, and hypophosphate (Schwartz and van der Veen 1973) is kinetically stable, so these species are not affected by hydrolysis reactions. Their production is interrelated and the ratio of these species is expressed as a mathematical relation:

$$\frac{[P_2O_6^{4-}]}{[PO_4^{3-}]+[HPO_3^{2-}]} = K \tag{42}.$$

$K$ is $0.15 \pm 0.05$ for all experiments without Mg and Ca, a total of 17 experiments ($1\sigma$, table 21). Though the denominator of this relationship may seem contrived, radical reactions and solution chemistry affect the abundance ratios of phosphite and orthophosphate (see experiments 26 & 28 and discussion below), and thus this ratio is constant only for the sum of the abundances of these two species. The relative constancy of this relationship is most consistent with a radical reaction pathway. The rationale for this relative constancy is as follows: consider the radicals formed through reaction 40. The bulk constituent of most solutions is water, and water is the main active agent in corrosion of the phosphide powder. Thus the relative abundances of the radicals produced during phosphide corrosion can be assumed to be roughly constant.

Table 20. Radical termination matrix. Non-radical species are formed through the termination of two radical species. The three radicals H·, ·OH, and ·$PO_3^{2-}$ can terminate in nine different ways, three of which are redundant.

|                 | **H·**          | **·OH**         | **·$PO_3^{2-}$**   |
|-----------------|-----------------|-----------------|--------------------|
| **H·**          | $H_2$           | $H_2O$          | $HPO_3^{2-}$       |
| **·OH**         | $H_2O$          | $H_2O_2$        | $HPO_4^{2-}$       |
| **·$PO_3^{2-}$**| $HPO_3^{2-}$    | $HPO_4^{2-}$    | $P_2O_6^{4-}$      |

Table 21.  K values for experiments.  Experiments that turned to tar or with Mg/Ca are not listed.

| No. | K |
|-----|-------|
| 1 | 0.235 |
| 3 | 0.181 |
| 5 | 0.066 |
| 6 | 0.149 |
| 7 | 0.159 |
| 8 | 0.148 |
| 9 | 0.119 |
| 11 | 0.084 |
| 12 | 0.158 |
| 13 | 0.166 |
| 14 | 0.250 |
| 15 | 0.170 |
| 16 | 0.197 |
| 18 | 0.090 |
| 21 | 0.078 |
| 23 | 0.152 |
| 24 | 0.088 |

The termination of these radicals produces P products at a constant ratio since the abundances is mainly determined by stoichiometry of the radicals. However, both $HPO_3^{2-}$ and $HOPO_3^{2-}$ can be oxidized or otherwise lost to form new radicals- phosphite and orthophosphate may be interchanged through a few reactions (see reaction 48 and section 4.3.2.1). The relative constancy of $K$ is surprising, given the error associated with the NMR integration and variation in solution chemistry. Solution chemistry may affect $K$ by promoting some radicals at the expense of others (i.e., an oxidizing environment vs. a reduced environment). It can be assumed that phosphite radicals will always be less abundant than OH and H radicals since Fe generates radicals and Fe is three times more abundant than P in the phosphide, so the $K$ should always be much less than 1.

Pyrophosphate is a ubiquitous product of all corrosion experiments, but its abundance is the most variable of the four main P species. Pyrophosphate is not predicted as a product resulting from radical termination step, given the radicals described in reaction 40. There are two possible reaction pathways that may lead to pyrophosphate: condensation, and a second-generation radical termination step. Both are evaluated below.

A condensation reaction produces pyrophosphate through loss of water:

$$2HPO_4^{2-} \rightarrow P_2O_7^{4-} + H_2O \qquad (43)$$

This reaction is non-spontaneous under normal reaction conditions (+19.2 kJ/mol), though it has been extensively produced in previous experiments using heat (see chapter 1), but never at room temperature. Heat drives the experiment by removing water,

pushing equilibrium to the products. Potentially, the surface of schreibersite grains could become extremely "dry" by the removal of water to produce radicals:

$$Fe(in\ Fe_3P) + 2H_2O \rightarrow 2H^{\cdot} + 2OH^- + Fe^{2+} \tag{44}$$
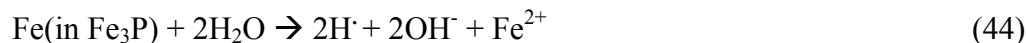
thus driving the production of pyrophosphate. If true, then other diphosphorus compounds should be formed, including diphosphite and isohypophosphate:

Diphosphite production: $\qquad 2H_2PO_3^- \rightarrow H_2P_2O_5^{2-} + H_2O \qquad$ (45)

Isohypophosphate production: $\qquad H_2PO_3^- + HPO_4^{2-} \rightarrow HP_2O_6 + H_2O \quad$ (46)

Diphosphite is detected in the sodium bicarbonate solutions and possibly in acetate experiments. Isohypophosphate has never definitively been detected. Phosphorous acid ($H_3PO_3$) is very acidic, with a $pK_a$ for its second H of about 4. The solution pH must be very low for the condensation to proceed. This is not a problem for phosphoric acid as the $pK_a$ for the third H is about 13 and allows for condensation. Given that diphosphite is formed in sodium bicarbonate solutions (pH of about 9.5), the condensation pathway for diphosphite does not seem reasonable for some experiments.

Alternatively, the synthesis of pyrophosphate may proceed via a radical pathway. Pyrophosphate could be formed through the reaction:

$$^{\cdot}PO_3^{2-} + ^{\cdot}OPO_3^{2-} \rightarrow P_2O_7^{4-} \tag{47}$$

This necessitates a source of phosphate ($^{\cdot}OPO_3^{2-}$) radicals. Phosphate radicals could be formed through orthophosphate interacting with a phosphite radical via a radical propagation reaction:

$$HOPO_3^{2-} + ^{\cdot}PO_3^{2-} \rightarrow ^{\cdot}OPO_3^{2-} + HPO_3^{2-} \tag{48}$$

$$^{\cdot}PO_3^{2-} + ^{\cdot}OPO_3^{2-} \rightarrow P_2O_7^{4-} \tag{47}$$
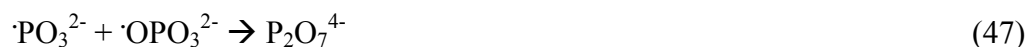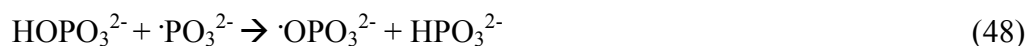
This reaction is countered by the oxidation of phosphite to phosphate (section 4.3.2.1).

The proposed pathways for pyrophosphate does not explain the solution-dependent occurrence of diphosphite. Diphosphite and other P compounds may owe their presence to reaction of hydrogen peroxide with the phosphide powder, as they appear only in solutions where $H_2O_2$ is indirectly detected, though this is unclear.

Hydrogen peroxide is a predicted product from radical termination of two hydroxyl radicals. Peroxide forms hydroxyl radicals in the presence of ferrous iron:

$$Fe^{2+} + HOOH \rightarrow Fe(OH)^{2+} + \cdot OH \tag{49}$$

This is the Fenton reaction (Walling 1976). In most of the inorganic corrosion experiments, this reaction removes all $H_2O_2$, generating ferric iron and hydroxyl radicals. The net result is that all hydrogen peroxide is rapidly removed from the system and thus prevented from affecting P chemistry. However, in solutions with significant chelating molecules like acetate and EDTA, the $Fe^{2+}$ forms Fe organic complexes:

$$Fe^{2+} + 2CH_3COO^- \rightarrow Fe(OOCCH_3)_2 \tag{50}$$
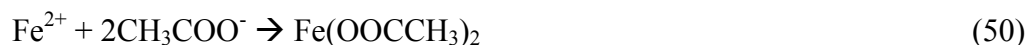
allowing $H_2O_2$ to build up and react with the powder and dissolved P species. Thus the addition of excess $H_2O_2$ in water to $Fe_3P$ produced species similar to the addition of $CH_3COONa$ (figure 13). Other solutions with chelating agents (like EDTA, pyruvate, and bicarbonate) also have diverse P speciation products.

4.1.2.2 Mass Spectral Discussion of Phosphorus Speciation

The mass spectra shown in figure 16 and table 14 demonstrate that there is a huge

diversity of P compounds in solution when acetate is added to iron phosphide. Among

these compounds are peroxyphosphate ($H_2PO_5^-$) and peroxypyrophosphate ($H_3P_2O_8^-$).

Both compounds are consistent with the buildup of $H_2O_2$ resulting from the loss of

reactive $Fe^{2+}$:

$$H_2O_2 + Fe^{3+} \rightarrow {}^\cdot OOH + H^+ + Fe^{2+} \tag{51}$$

$$ {}^\cdot PO_3^{2-} + {}^\cdot OOH \rightarrow HOOPO_3^{2-} \tag{52}$$

Peroxypyrophosphates are consistent with the presence of phosphate radicals:

$$2\ {}^\cdot OPO_3^{2-} \rightarrow O_3POOPO_3^{4-} \tag{53}$$

Among the diverse chemistry of the P compounds in solution, some appear to be

organophosphorus compounds; these are discussed in the next section. The majority are

multi-P oxides. How could these compounds form?

Radical reactions lack specificity, and radical reactions frequently produce

unusual minor products. These minor products are formed from propagation /

terminations steps. As an example, consider the reaction of hypophosphate with a radical

inducer (like $^\cdot PO_3^{2-}$):

$$P_2O_6H_3^- + {}^\cdot PO_3^{2-} \rightarrow {}^\cdot P_2O_5H_3^- + PO_4^{3-} \tag{54}$$

$$ {}^\cdot P_2O_5H_3^- + {}^\cdot PO_3^{2-} + H^+ \rightarrow H_4P_3O_8^- \tag{55}$$

This tri-P compound is detected in the MS data. This process can repeat several times to

form species like $H_5P_4O_{10}^-$, $H_6P_5O_{12}^-$, and so on. These reactions occur less and less

frequently as the products become rarer and rarer, consistent with MS abundances (figure 17).

The MS data also demonstrates the presence of unusual P compounds with too many or too few H atoms. The example given earlier was for $H_4P_3O_7$, which also showed peaks corresponding to compounds with formulae of $H_2P_3O_7$, and $H_6P_3O_7$. The MS is likely detecting a radical species which rearranges and steals H atoms from or loses H atoms to water before entering the MS. $H_4P_3O_7$ and its rearrangement are shown in figure 32. Rearrangement also explains the presence of peaks corresponding to $PO_3^-$ (rearrangement of $^.PO_3H^-$ radical), $PO_2^-$ (rearrangement of $^.PHO_2^-$) radical, and $PO_4^-$ (rearrangement of $^.OPO_3H^-$ radical).


4.1.3 The Inorganic $Fe_3P$ Corrosion Reaction Pathway


The reaction pathway for the inorganic corrosion of $Fe_3P$ consists of a series of radical initiation, propagation, and termination steps. The species formed are consistent with NMR, EPR, and MS data. Figure 33 summarizes the reaction pathway.

Inorganic P chemistry provides an overview of how the P species commonly observed are formed. Organic P compounds are investigated next as these species hold greater relevance to the origin of the P biomolecules.

Figure 32. Radical rearrangement leading to ± 2H compounds from MS data.
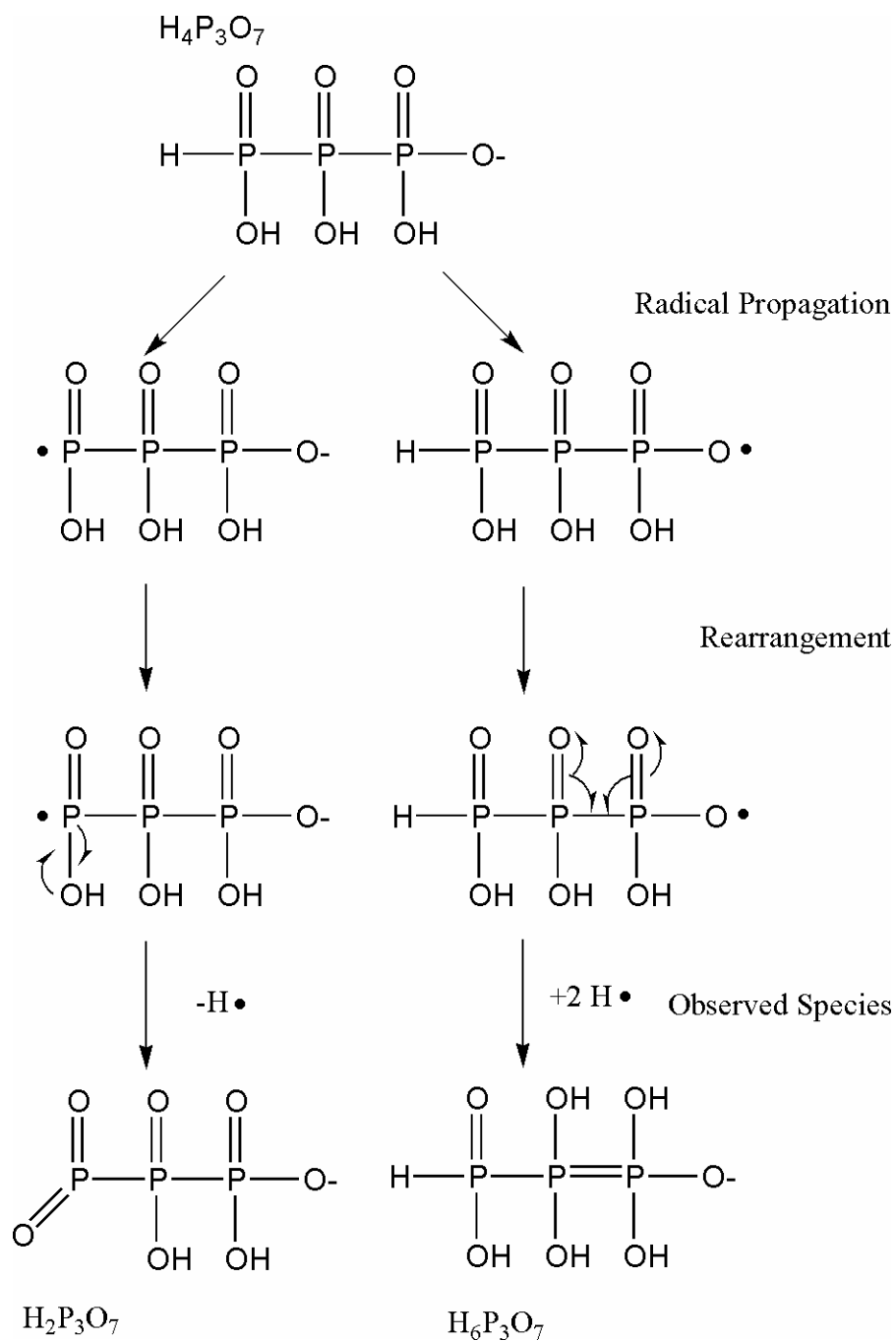
Figure 33. Inorganic corrosion pathway.
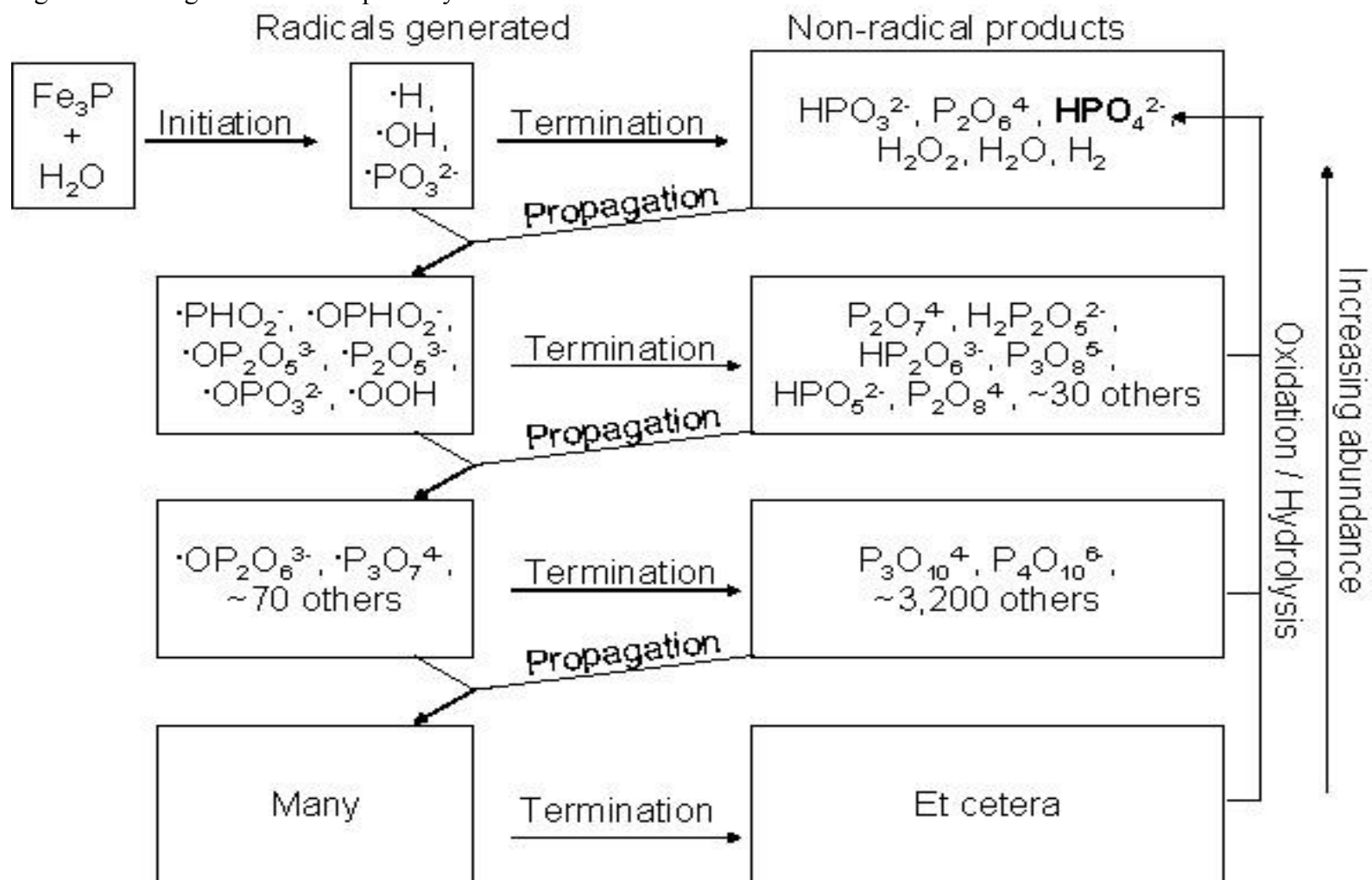
4.1.3.1 Predictions of Corrosion Pathway

Phosphorus compounds produced through these reaction pathways are complex, and there are many ways to produce several key species. Consider the formation of orthophosphate. Orthophosphate may be synthesized directly through termination of radicals generated during the initiation step:

$$\cdot OH + \cdot PO_3^{2-} \rightarrow HOPO_3^{2-} \tag{56}$$

or through termination of radicals generated through propagation steps:

$$\cdot H + \cdot OPO_3^{2-} \rightarrow HOPO_3^{2-} \tag{57}$$

or through hydrolysis of energetic P species:

$$P_2O_7^{4-} + H_2O \rightarrow 2HOPO_3^{2-} \tag{58}$$

or through oxidation of reduced P species:

$$HPO_3^{2-} + H_2O \rightarrow HOPO_3^{2-} + H_2 \tag{59}$$

Orthophosphate may also be removed by radical propagation steps:

$$HOPO_3^{2-} + \cdot PO_3^{2-} \rightarrow \cdot OPO_3^{2-} + HPO_3^{2-} \tag{60}$$
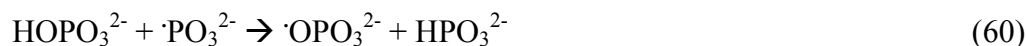
or through condensation reactions:

$$2HOPO_3^{2-} \rightarrow P_2O_7^{4-} + H_2O \tag{61}$$

These six reactions could allow a calculation of the steady state abundance of orthophosphate:

$$\frac{d[HOPO_3^{2-}]}{dt} = \begin{bmatrix} k_1[\cdot OH][\cdot PO_3^{2-}] + k_2[\cdot H][\cdot OPO_3^{2-}] + k_3[H_2O][P_2O_7^{4-}] + \\ k_4[H_2O][HPO_3^{2-}] - k_5[\cdot PO_3^{2-}][HOPO_3^{2-}] - k_6[HOPO_3^{2-}]^2 \end{bmatrix} \tag{62}$$

where $k$ is the rate constant of a given reaction. The individual $k$ values for these reactions are unknown, though $k_3$, $k_4$, and $k_6$ can all be assumed to be smaller than the other three $k$ values. The total set of reactions would necessarily involve many other reaction pathways. Making quantitative predictions from this reaction pathway is very difficult considering the number of unknowns. However, general characteristics of radical reaction pathways include the following: 1) radical termination reactions are preferred compared to radical propagation reactions, and 2) radical reaction rates are inversely proportional to the masses of the reactants.

Radical termination reactions are energetically preferred to radical propagation reactions. This implies that radicals react faster with other radicals than with non-radical species. As a result, compounds that are formed first through radical termination reactions should be more abundant than compounds formed through propagation/termination reactions. This is reflected in the abundances determined by NMR and TOF-HR-MS. The P species formed directly through radical termination reactions ($HPO_3^{2-}$, $HOPO_3^{2-}$, $P_2O_6^{4-}$) are more abundant than the P species formed through a radical propagation reaction followed by a radical termination reaction (e.g., $P_2O_7^{4-}$, $H_2P_2O_5^{2-}$, $HOOPO_3^{2-}$, $P_2O_8^{4-}$). These species are in turn more common than the corresponding tertiary products, those products formed from radicals propagated from the second group of P species followed by termination reactions.

The mass of reactants also determines the reaction rate for a given reaction, as the mass determines the kinetic energy of a compound which in turn determines the

frequency of collisions.  As an example, consider the radical termination reactions from table 20 below:

$$H^\cdot + {}^\cdot PO_3{}^{2-} \rightarrow HPO_3{}^{2-} \tag{63}$$

$$^\cdot OH + {}^\cdot PO_3{}^{2-} \rightarrow HOPO_3{}^{2-} \tag{64}$$

$$2\ ^\cdot PO_3{}^{2-} \rightarrow P_2O_6{}^{4-} \tag{65}$$
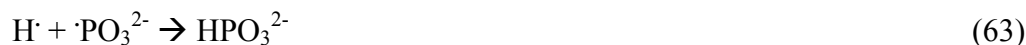
If the reaction rates were dependent only on stoichiometry, then the proportions of products should be dependent only on the stoichiometry described by reaction (40), or 5:5:3.  The value $K$ should be equal to 3/13 or 0.23.  The actual average $K$ is about half of this value, which may be due to a difference in reaction rates due to mass differences. This mass dependence is reflected in the NMR data and the TOF-HR-MS data (see figure 17).

The P products are most likely produced through radical termination reactions. They may be removed through oxidation, hydrolysis, or radical propagation reactions. Radical reactions are faster than oxidation or hydrolysis reactions due to the vast difference in energy between the reaction intermediates and products for radical reactions.  Thus the suite of P species is the most complex as the phosphide starts to corrode.  The system reaches steady state and the abundances of P species are closely related to the amount of total phosphide that has corroded.

This steady state system ends after all the phosphide has corroded as the corrosion is the source of radicals for the system.  With time the system will start to oxidize to form orthophosphate.  The system has four (six if carbon is present) types of energetic bonds as corrosion products: H-P bonds like phosphite, P-P bonds like hypophosphate, P-O-P

bonds like pyrophosphate, P-O-O bonds like peroxyphosphate, C-P bonds like

acetylphosphonate, and C-O-P bonds like phosphatoacetate.  Of these, the H-P and the P-

O-O bonds will be the first to be broken, as the H-P bond is the weakest of these bonds

and is broken through the oxidation of metal, and metal catalyzes the breakage of the P-

O-O bond.  These compounds will be removed on the order of days to months.  The C-O-

P and P-O-P bonds will break next, as hydrolysis breaks these bonds on the order of

months to years.  The C-P and the P-P bonds are among the strongest bonds present, and

may not be broken except on geologic timescales.  The final products predicted from the

long timescale of corrosion are orthophosphate with some C-P and P-P compounds.


4.2 Proposed Organic Phosphorus Reaction Pathway


Acetate is phosphorylated in solution to form a series of P-C and P-O-C linkages.  The

total yields for organic P compounds are low, ~3.6% of the total dissolved P are organic

P compounds.  This low yield is consistent with the low abundance of acetate, which has

a mole fraction of ~0.7 % in the solution. Only acetate, pyruvate, and possibly EDTA and

acetaldehyde appear to react with the corroding phosphide powder to produce organic P

compounds.  Ethanol and acetonitrile were not phosphorylated to any significant extent.

Other organic compounds were turned to tar in corroding solutions, including adenosine,

glycolaldehyde, and acetone.

4.2.1 Generation of Organic Radicals

Why is acetate phosphorylated in solution?  Why are ethanol and acetonitrile not

phosphorylated?  Why do carboxylic acid or carbonyl functional groups encourage the

phosphorylation of these organics?

The differences between the structure of these organics is key to their reactivity in

solution with the phosphide powder.  The important differences between the organics are

1) whether the organic can tautomerize, and 2) whether the organic is an ionic species

under normal conditions.

Tautomerization is a chemical transformation that increases the stability of a

molecule and is shown in figure 34.  Acetate, EDTA, pyruvate, glycolaldehyde, acetone,

and acetaldehyde are capable of a keto-enol tautomerization transformation whereas

neither ethanol nor acetonitrile tautomerize.  Keto-enol tautomerization increases the

acidity of protons on $\alpha$ carbons next to carbonyl groups.

As an example, consider the role of tautomerization in the formation of an acetate

radical.  Acetate radicals are formed through the interaction of acetate with either $\cdot OH$ or

$\cdot PO_3^{2-:}$

$$H_3C\!-\!C{\overset{\displaystyle O}{\diagdown}}_{O^-} + \cdot OH, \cdot PO_3^{2-} \rightarrow \quad \cdot H_2C\!-\!C{\overset{\displaystyle O}{\diagdown}}_{O^-} + H_2O, HPO_3^{2-} \quad (66)$$
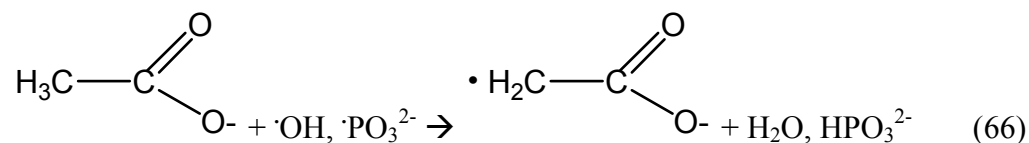
 Both compounds are oxidizing enough to remove the slightly acidic proton on the methyl

group.  The acetate radical is stabilized by tautomerization to the enol form:

Figure 34.  Tautomerization of organic species in solution.

$$\bullet H_2C - C \underset{O^-}{\overset{O}{\vert\vert}} \quad \longleftrightarrow \quad H_2C = C \underset{O^-}{\overset{O\bullet}{\vert}} \qquad (67)$$
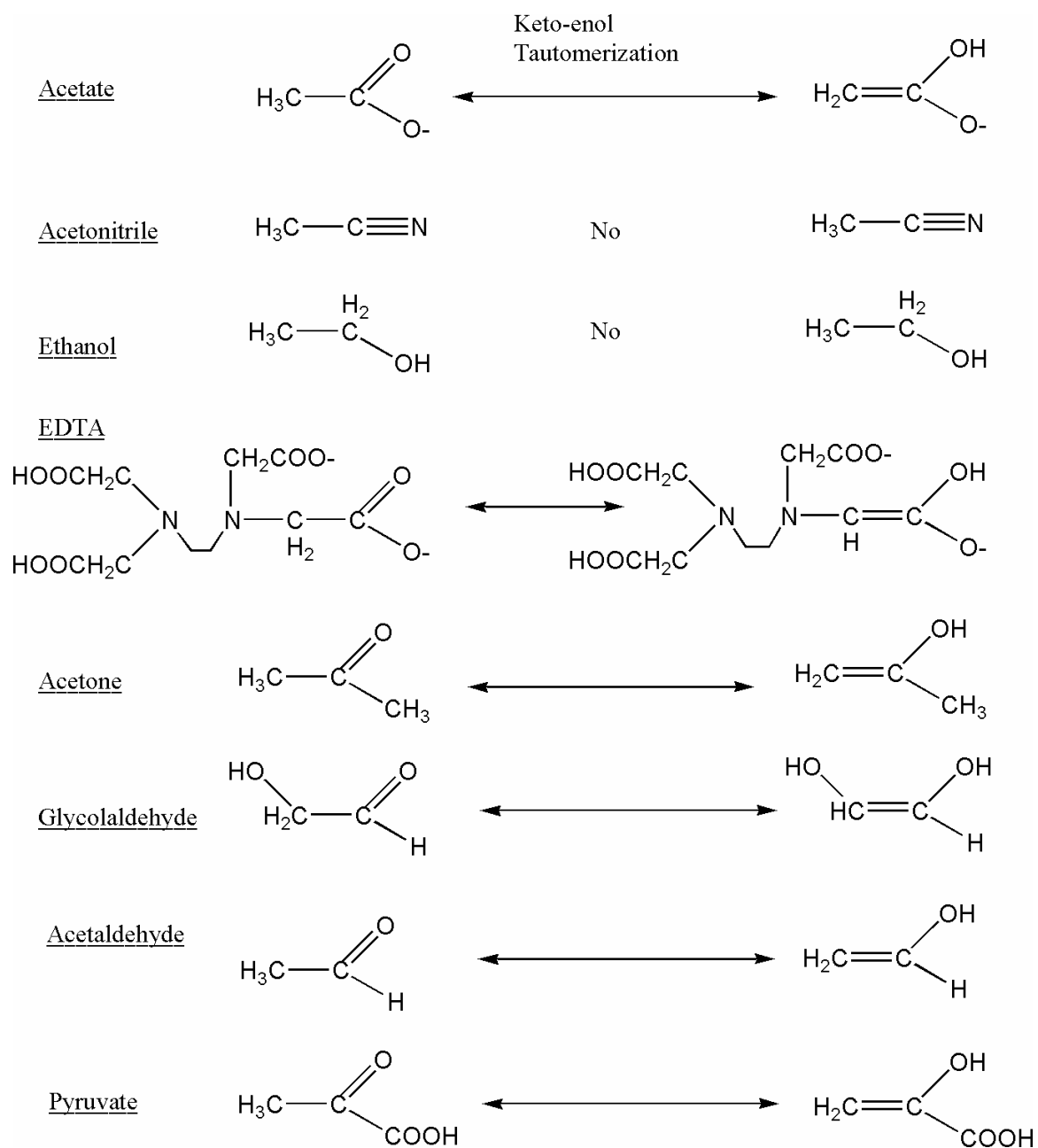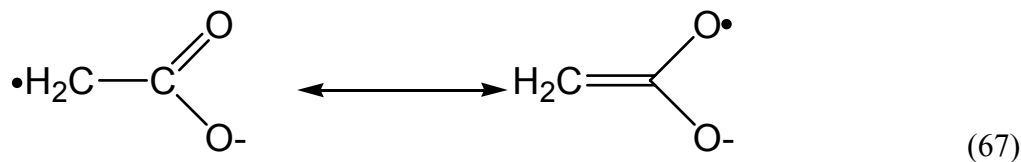
and thus persists for a long enough time to react with other radicals in solution.
Acetonitrile and ethanol do not tautomerize and do not form long-lived radical species.

Charged functional groups serve to stabilize reactive iron metal and ferrous and ferric iron through chelation, and limiting iron's ability to degrade organic compounds. Charged functional groups repel each other and limit polymerization. For instance, the formation of a glycolaldehyde radical occurs through a process analogous to the formation of an acetate radical:

$$HO - H_2C - C \overset{O}{\underset{H}{\diagdown}} \quad \rightarrow \quad HO - HC - C \overset{O}{\underset{H}{\diagdown}} \qquad (68)$$
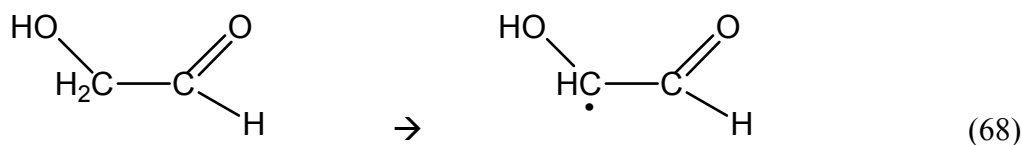
However, the acetate radical is charged and repels other acetate radicals, whereas the glycolaldehyde radical does not repel other glycolaldehyde radicals. This leads to a series of termination and propagation radical reactions which eventually lead to a polymerized product. Additionally, metal cations like $Fe^{2+}$ and $Fe^{3+}$ serve as catalysts for aldol reactions, which results in polymerization of these uncharged compounds.

$$2 \; HO - H_2C - C \overset{O}{\underset{H}{\diagdown}} \quad \rightarrow \quad H_2C - \underset{OH}{\overset{OH}{\underset{\vert}{CH}}} - \underset{OH}{\overset{}{\underset{\vert}{CH}}} - CH \overset{O}{\vert\vert} \quad \rightarrow etc. \rightarrow Tar \; (69)$$
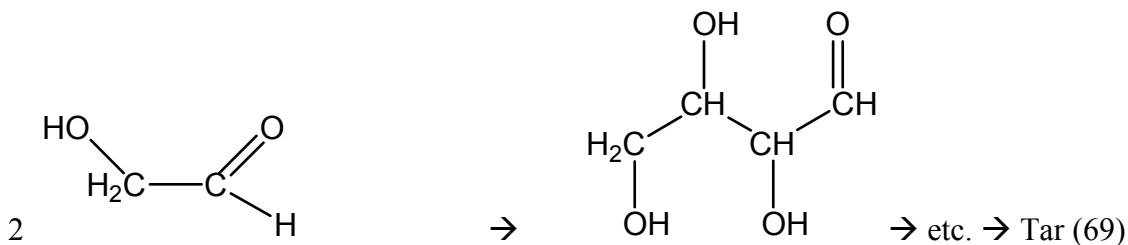
These reactions demonstrate the benefits to having an anionic group capable of limiting the reactivity of iron cations.

The propagation of acetate radicals forms two distinct radicals: $\cdot CH_2COO^-$, and $CH_3COO\cdot$. The radical $CH_3COO\cdot$ is unstable and rapidly decarboxylates:

$$CH_3COO\cdot \rightarrow \cdot CH_3 + CO_2 \tag{70}$$

though $CO_2$ may also form a radical. The $\cdot CH_2COO^-$ radical is comparatively stable (Wang et al. 2001). EDTA would be expected to form similar radicals, losing an H from the methyl bridge. The concentration of EDTA (0.025 M) used in these experiments was much lower than the concentration of acetate (0.4 M), so organic P compounds were comparatively much more difficult to detect in those solutions.

4.2.2 Reaction Pathway

The organic P compounds are broadly grouped into three sets: the P-acetyl compounds, the P-$CH_2$ compounds, and the cyclic P compounds. The most abundant species are the ones with the lowest molecular weight, consistent with relative abundances of radical species and reaction rates dependent on mass.

The organic P compounds in the acetate experiment are synthesized through radical termination reactions between the inorganic radicals resulting from corrosion described in the section 4.1 and the acetate radical described above. The organic P products formed include acetyl phosphonate, phosphoglycolate, acetyl hypophosphate,

and even acetyl tri-P, 4-P, and 5-P type compounds. The reaction pathway for these compounds is the relatively simple radical termination reaction series (figure 35).

The acetyl-P species also undergo radical propagation reactions to form new C-P radicals. Several of these radicals are unstable and spontaneously decay by decarboxylation. For instance, the acetyl phosphonate radical will decarboxylate:

$$O_3PCH_2COO^{3-} + {}^{\cdot}OH \rightarrow O_3PCH_2COO^{\cdot\,2-} + OH^{-} \rightarrow \quad O_3PCH_2^{\cdot\,2-} + HCO_3^{-} \quad (71)$$
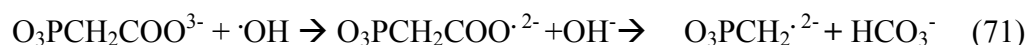
(e.g., Wang et al. 2001). These reactions introduce a whole new set of radicals into solution, which are also capable of reacting with other radicals via termination reactions to form a new group of organic P compounds (figure 36). Higher-order P compounds with P-CH$_2$-P linkages are likely abundant at higher mass, given the deviation from P-O-P linkages (figure 19). Alternatively, the $CO_2$ can retain the free radical and react with a phosphite radical to form phosphonoformate:

$$O_3PCH_2COO^{\cdot\,2-} \rightarrow O_3PCH_2^{-} + {}^{\cdot}CO_2^{-} \rightarrow {}^{\cdot}CO_2^{-} + {}^{\cdot}PO_3^{2-} \rightarrow O_2CPO_3^{3-} \quad (72)$$
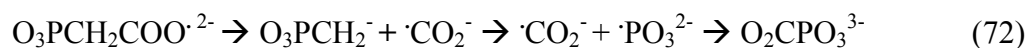
The organic P compounds may also spontaneously form cyclic compounds due to the energetic favorability of these isomers. Most of the cyclic P compounds could form through spontaneous dehydration reactions although some may be formed through radical propagation reactions (figure 37). These reactions are a bit more nebulous and the exact pathway is less understood.

Figure 35.  Formation of acetyl-P compounds.
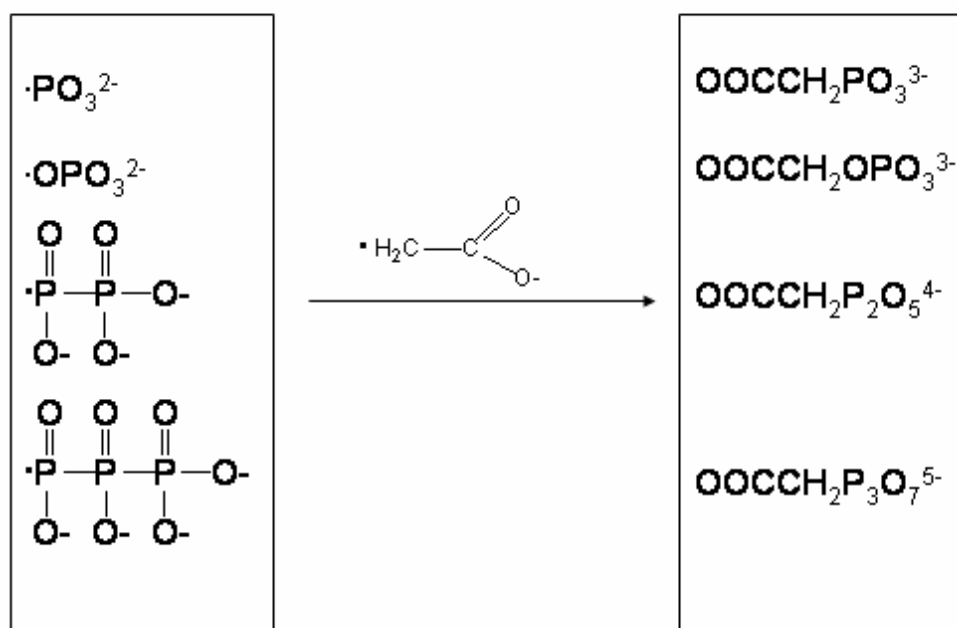
Figure 36. Formation of $CH_2$-P compounds.

$$\cdot OH$$
$$\cdot PO_3{}^{2-}$$
$$\cdot OPO_3{}^{2-}$$

$\xrightarrow{\cdot CH_2PO_3{}^{2-}}$

$$HOCH_2PO_3{}^{2-}$$
$$O_3PCH_2PO_3{}^{4-}$$
$$O_3PCH_2OPO_3{}^{4-}$$
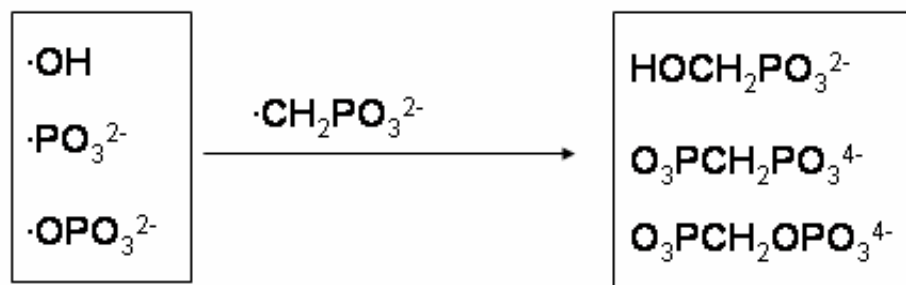
Figure 37.  Production of cyclic organic P compounds.
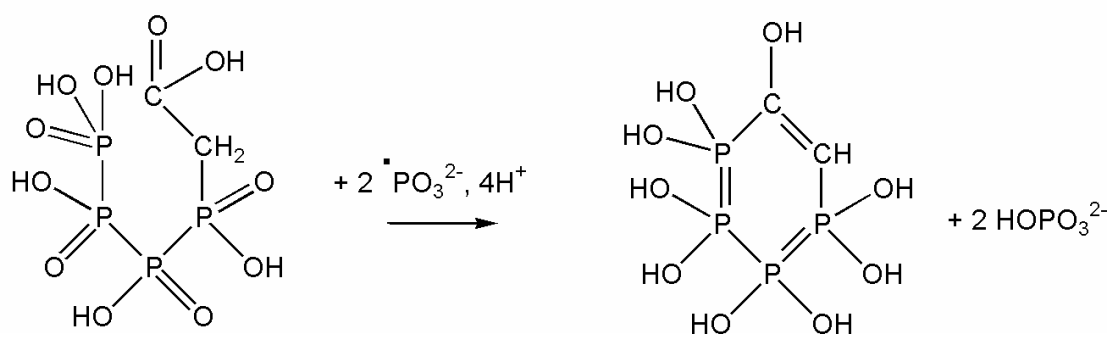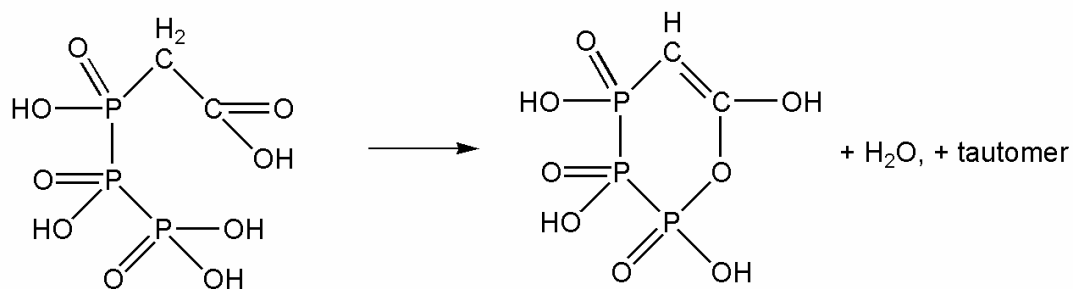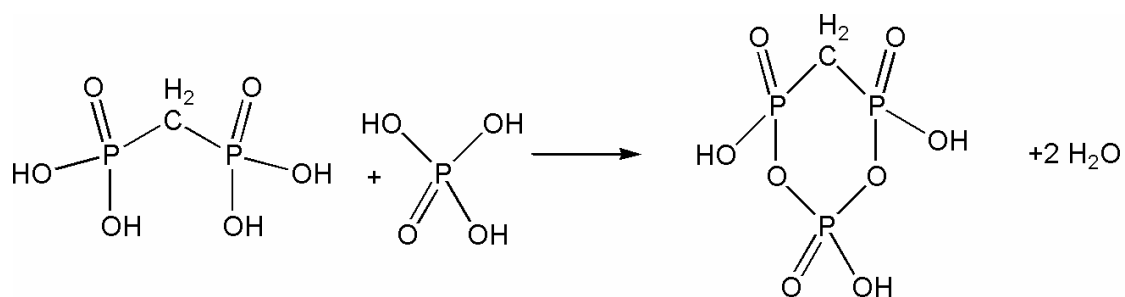
4.2.3 Other Organic Compounds

Several complex organic compounds are also formed during the corrosion experiments. These compounds are much more difficult to identify, but consist of the high mass component of the species shown in figure 18. These compounds have an excess of H atoms and/or C atoms, and a corresponding deficiency of P or O atoms, as determined by the heightened overall mass for these species.

It is impossible to get a clear ID on most of these MS peaks. These compounds appear to be heavily oxidized, and the typical identification has a C:H ratio of about 1:1 . (Identifications were made using the program, "Molecular Weight Calculator" [Munroe 2004] ). This ratio is consistent with polyaromatic species. No polyaromatic species were used in solution, so the exact origin of these organic compounds is unclear. These compounds may result from the interaction of oxidizing radicals with organic constituents. For instance, the general reaction:

$$C_nH_{2n+2} + 2 \cdot OH \rightarrow C_nH_{2n} + 2H_2O \rightarrow repeat \rightarrow C_nH_n \qquad (73)$$

is consistent with the oxidizing nature of hydroxyl radicals.

This oxidation of organic molecules has implications for a variety of other fields, including other meteoritical studies. The generation of $\cdot$OH radicals from corroding iron metal suggests reaction pathways involving iron metal should be reconsidered in light of radical chemistry.

4.3 General Implications of Corroding Metal

Iron metal alloy is a common component of many meteorites. Iron metal occurs as two

minerals: kamacite, the low (<6%) Ni member, and taenite, with >6% Ni. Recent

research suggests that the phase taenite may actually be an ultrafine mixture of high Ni-

Fe tetrataenite and kamacite (Yang *et al*. 1996). Several of these minerals are very small-

μm to nm in size. Like many meteoritic minerals, these metal alloys are

thermodynamically unstable on the surface of the Earth. Metal corrosion is observed in

the many weathering stages of chondritic meteorites (e.g. Wlotzka 1993).

Iron metal corrosion is an oxidation-reduction type reaction forming magnetite

with the process summarized as:

$$3Fe + 4H_2O \rightarrow Fe_3O_4 + 4H_2 \text{ (g)} \tag{74}$$

Electrons are transferred from an iron atom to the hydrogen atoms of water. This net

reaction releases $H_2$ gas from the corrosion of iron metal.

It is notable here that industry has studied the corrosion of metal in depth.

However, this study focuses on the effect of metal corrosion on the corrosive aqueous

system, which is frequently neglected in industrial studies.

Figure 20b demonstrates that ˙OH radicals are produced during the corrosion of

iron metal. What is the origin of these hydroxyl radicals? Hydroxyl radicals are strong

oxidizing agents capable of a number of chemical reactions. The generation of these

radicals has consequences in environmental and meteoritical sciences. Understanding

their formation is a key to understanding how metal reacts with water, air, organics and

other compounds.  I propose two pathways for the formation of hydroxyl radicals:

reaction with oxygen in air, and reaction with acidic protons in solution.

4.3.1 The Reaction with Air

The generation of radicals by interaction of Fe metal with air must be considered since

the solutions examined by EPR were not performed under argon.  $\cdot$OH radicals may be

produced through reaction of $O_2$ gas with the iron metal:

$$Fe + O_2 \rightarrow Fe^{2+} + O_2^{2-} \tag{75}$$

$$O_2^{2-} + 2H^+ \rightarrow H_2O_2 \tag{76}$$

$$Fe^{2+} + H_2O_2 \rightarrow Fe(OH)^{2+} + \cdot OH \tag{49}$$

This reaction pathway indubitably explains some of the $\cdot$OH radicals in solution,

but likely is not the sole source of these compounds.  Hydrogen gas is evolved during the

corrosion of iron metal and this is not consistent with this reaction pathway being the sole

reaction pathway.  Also, phosphide corrosion experiments performed under argon

produce results similar to those performed under air, albeit with lower concentrations.

Were this mechanism acting on a large scale, then orthophosphate would be the dominant

P product (through the $\cdot PO_3^{2-} + \cdot OH$ termination reaction).  Furthermore experiments in

environmental chemistry suggest that organic pollutants are both reduced and oxidized by

reaction with iron metal and solution, instead of solely oxidized.  These point to another

active mechanism, instead of a sole reaction with air.

4.3.2 The Reaction with Acidic Protons

Fe metal could react with acidic protons in solution to generate radicals which in turn

react with water to form hydroxyl radicals. This reaction occurs as follows:

$$Fe + 2H^+ \rightarrow Fe^{2+} + 2H^{\cdot} \tag{77}$$

H atom radicals are not detectable by EPR or by the methods used. These radical

hydrogen atoms subsequently react with either other radical hydrogen atoms to form

hydrogen gas:

$$2H^{\cdot} \rightarrow H_2(g) \tag{78}$$

or react with water to form a hydroxyl radical:

$$H^{\cdot} + H_2O \rightarrow H_2(g) + {}^{\cdot}OH. \tag{79}$$

Both these reactions are summarized in the radical matrix for phosphide corrosion shown

earlier (table 20). It is through this mechanism that the stoichiometry described in (74) is

retained. The amount of hydrogen generated by the system remains proportional to the

electrons transferred from iron to hydrogen. However, the electrons generated by this

system are continuously transferred to other species in the system unless the process is

terminated by reaction with another radical. The hydroxyl radical reacts with either a

hydrogen radical to reform water:

$$H^{\cdot} + {}^{\cdot}OH \rightarrow H_2O \tag{80}$$

or with other hydroxyl radicals to form hydrogen peroxide:

$$2{}^{\cdot}OH \rightarrow H_2O_2. \tag{81}$$

The above reactions terminate the radical propagation and generate end products. This reaction pathway is consistent with the release of $H_2$ gas from the corrosion of iron, and is also consistent with the overall reductive capacity of iron metal, by which Fe donates H atoms to a variety of compounds in solution, and with the phosphide corrosion experiments.

Iron corrosion oxidizes phosphite in solution (see experiments 27 & 29 in chapter 2). The corrosion of iron has been employed in the process of using zero valent iron for environmental cleanup. Iron metal corrosion may also have implications for the phosphide corrosion experiments, and for the alteration of meteoritic organics. These three points are discussed next.

4.3.2.1 Phosphite Oxidation

Phosphite ($HPO_3^{2-}$) is oxidized to orthophosphate ($PO_4^{3-}$) in the presence of corroding metal. Both P and Fe are oxidized during this process, which implies that either $O_2$ gas or $H^+$ in solution is reduced. The agent that oxidizes phosphite is the $\cdot$OH radical. This radical removes the H from the H-P bond of phosphite leaving a phosphite radical $\cdot PO_3^{2-}$. The phosphite radical reacts with excess $\cdot$OH radicals to form orthophosphate.

Hypophosphate could be formed through termination of two phosphite radicals, however, the total abundance of phosphite in these systems is 0.01 M, corresponding to a mole fraction of 0.00018. The probability of a phosphite radical interacting with itself is equal to the mole fraction of phosphite. Thus, the expected abundance of hypophosphate

in solution is calculated at $2 \times 10^{-6}$ M, is too low for adequate detection by NMR. Experiment 35 was designed to overcome this difficulty by increasing the molarity of phosphite to 10 M, which should produce ~1.5 M hypophosphate. However, analytical difficulties prevented accurate determination of the composition of the solution.

4.3.2.2 Environmental Chemistry

Recent developments in the field of environmental chemistry have demonstrated that "zero valent iron," i.e. iron metal powder, is useful in the removal of chlorinated organics like PCBs from groundwater. The literature is burgeoning with descriptions involving dechlorination of organic compounds with fine iron powder, and one of the first descriptions of the degradative power of iron metal emplaced in soil was provided by Sweeny (1981), nine years after patenting the process. Gillham and O'Hannesin (1994) describe the effect of iron in solution on a number of chlorinated compounds, including the effect of iron metal surface area. Reactivity increases with surface area exposed- i.e. a smaller mean particle size typically result in faster rates. Degradation half lives are on the order of hours for nearly all chlorinated compounds. $H_2$ gas is evolved during their experiment, but the authors are unclear on the exact mechanism.

Despite the reductive capability of zero valent iron, iron metal is also capable of oxidizing organics in the presence of oxygenated water (Joo *et al.* 2004, 2005) which is difficult to reconcile with a solo redox reaction. The mechanism by which zero valent iron reduces organics is unclear, but this work suggests that the corrosion of iron metal

produces radical species and that these radicals are capable of oxidizing organics in solution.

4.3.2.3 Phosphide Corrosion: Air vs. Argon

In the reactions described earlier, $K$ is constant independent of the atmosphere above the experiments. This result is unusual considering that $O_2$ is a strong oxidant and also a diradical species ($\cdot$O-O$\cdot$), and should interfere with the chemistry of the solutions. However, $O_2$ only seems to serve as a catalyst for the corrosion of $Fe_3P$, increasing the net release of P into solution, but not affecting specific chemistry. This appears to be due to the reduction of $O_2$ by iron. In the inert reaction, hydrogen is reduced:

$$Fe\ (in\ Fe_3P) + 2H_2O \rightarrow Fe^{2+} + 2H^{\cdot} + 2OH^{-} \tag{82}$$

consistent with the reaction pathway described as interaction with acidic protons. Again, H atoms can in turn react with water to form hydroxyl radicals.

$$H^{\cdot} + H_2O \rightarrow H_2 + {}^{\cdot}OH \tag{83}$$

In systems with air, $O_2$ is reduced by iron, is protonated, and then reacts with iron II and III:

$$Fe\ (in\ Fe_3P) + O_2(aq) \rightarrow Fe^{2+} + O_2{}^{2-} \tag{84}$$

$$O_2{}^{2-} + 2H^{+} \rightarrow H_2O_2 \tag{85}$$

$$H_2O_2 + Fe^{2+} \rightarrow FeOH^{2+} + {}^{\cdot}OH \tag{49}$$

The end radical in this set of reactions is mainly $^{\cdot}$OH. The presence of $H_2$ gas suggests that this pathway is not the only one operating, and is probably secondary to the primary

reaction pathway with acidic protons.  Ferric iron is predicted in experiments done under air, consistent with the physical observations and XRD data.

Thus, the atmospheric composition above a phosphide corrosion reaction has surprisingly little effect on types of P products formed from corrosion solutions.

4.3.2.4 Alteration of Meteoritic Organics

Hydroxyl and hydrogen radicals react with organic compounds to oxidize C-O linkages.  For instance, hydroquinone is used as a radical detector as it oxidizes completely to quinone through interaction of two radicals:



(86)
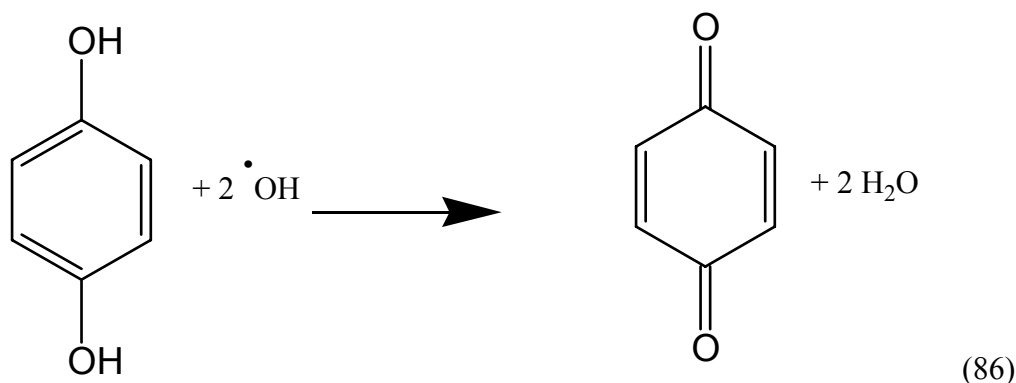
(Howard 1972).  Simple aldehydes may be oxidized to carboxylic acids:



(87)
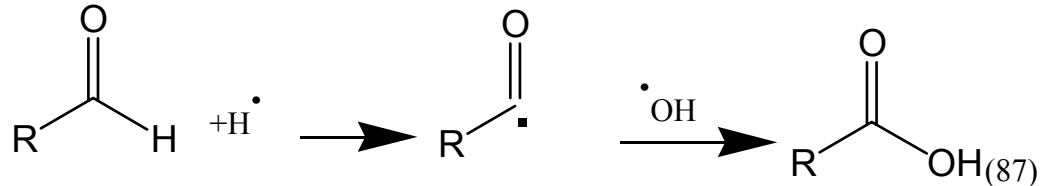
(Walling and Padwa 1963).  Complete oxidation turns the carboxylic acids to carbonates:

$$R\text{-}COOH + \cdot OH \rightarrow R\cdot + H_2CO_3 \qquad (88)$$

Aliphatic carbons lose hydrogen to become more aromatic:

$$R-\underset{\underset{H_2}{\overset{}{\mid}}}{\overset{\overset{H_2}{\overset{}{\mid}}}{C}}-R' \quad \xrightarrow{\cdot OH} \quad R-\underset{\underset{H}{\overset{}{\mid}}}{\overset{\overset{H}{\overset{}{\mid}}}{C}}=\underset{}{C}-R'$$

(89).
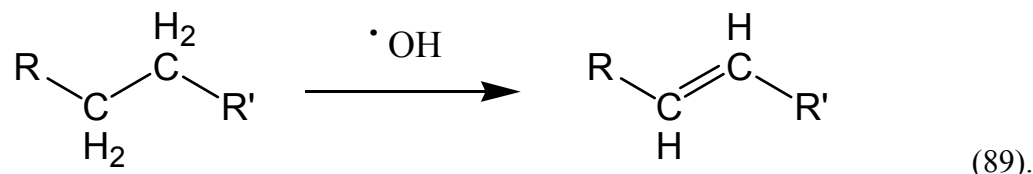
The net effect of radicals on simple organics is a progressive oxidation: alcohols become carbonyls (86), carbonyls become carboxylic acids (87), and carboxylic acids become carbonates and alkyl radicals (88). Aliphatic hydrocarbons are oxidized to aromatic species or alkenes (89). The net result would be more carboxylic acids than alcohols, and carbonyls will be in between for a mixture of organics. Carbonates are the result of complete oxidation of organics from reaction (89), and carbonates are the most abundant product of complete oxidation by Fenton reaction processes. The organic inventory of the meteorite Murchison matches progressive oxidation by OH radicals (table 22).

Cody and Alexander (2005) describe the general chemical characteristics of the insoluble organic matter of several meteorites. Solid state NMR analyses of CR chondrites, CI chondrites, CM chondrites, and the Tagish Lake chondrite reveal a progressive oxidation of the insoluble organic matter in the matrix of these chondrites. The oxidation is mainly evident in the oxidation of aliphatic hydrocarbons to aromatic/alkene hydrocarbons. The authors attribute this progressive oxidation to the extent of aqueous alteration that each meteorite class has experienced. The CR chondrites are the least aqueously altered, and Tagish Lake is among the most altered. The authors propose that hydrogen peroxide is the initial oxidant for the organic matter, which reacts via the Fenton reaction (49) to form hydroxyl radicals. Thus hydroxyl radicals are the actual energetic oxidant which acts in the ways described in reactions (86)-(89) above. Cody and Alexander (2005) attribute the production of peroxide to the

Table 22.  Organic inventory of Murchison.  Organic carbon data from Cronin *et al*. (1988).  Carbonate data from Brearley et al. (2000)

| Class | Weight, ppm |
| --- | --- |
| Alcohols | 11 |
| Aldehydes and ketones | 27 |
| Carboxylic acids | 330 |
| Carbonate | ~4000 |

UV irradiation of low temperature ices. I would alter their proposal to state that hydroxyl radicals are the natural result of the corrosion of iron metal present in the meteorites. Indeed, the least oxidized meteorites, the CRs, have the most unaltered metal, and the CIs, CMs, and Tagish Lake all have virtually no metal in their matrices, consistent with this hypothesis. The reactions that took place on the parent bodies of these meteorites would have been akin to the zero-valent iron groundwater remediation treatment currently employed in environmental cleanup.

4.4 Summary

Phosphide corrodes in water to form three major species- hydroxyl, hydrogen, and phosphite radicals. The termination of these three radicals produces the orthophosphate, phosphite, and hypophosphate species. Secondary radical propagation reactions produce pyrophosphate and minor P species. Interactions of these radicals with organic radicals in turn forms organophosphorus compounds, with P-C and P-O-C linkages.

The dominant process acting during the corrosion of Fe in phosphide is interaction with acidic protons to form H$^{\cdot}$ and $^{\cdot}$OH radicals. The iron in iron phosphide is capable of removing $O_2$ from solution to produce $^{\cdot}$OH radicals which neutralizes the effect of air. The solution chemistry of phosphide corrosion experiments suggests that the atmosphere plays a minor role in the types of P species formed.

The corrosion of phosphide material is presented as a plausible means of generating organic P compounds and of generating reactive P compounds. The

meteoritic mass flux of schreibersite to the surface of the Earth is determined in the next chapter. This determination demonstrates the prebiotic relevance of schreibersite to the surface of the early Earth.

CHAPTER 5

THE FLUX OF METEORITIC P, C, AND Ir TO THE EARTH

Meteorites have shaped our understanding of organic compounds and the natural processes through which they are formed.  Much of our understanding of extraterrestrial organic compounds comes from meteorites.  Meteorites provided a partial verification of early prebiotic chemistry, showing that organics can be formed through abiotic processes.  With growing evidence for a late-heavy bombardment period 4-3.8 billion years ago, meteorites and comets may have been an important source of organic carbon and of reactive P.  Life may have originated shortly after the late-heavy bombardment, when concentrations of organic compounds and reactive P were high enough to "kick life into gear".  This work quantifies the sources of reactive extraterrestrial P and C- large impactors, meteorites and interplanetary dust particles- and argues for crater-lakes as a plausible environment for the origin of life.

5.1 Types of Extraterrestrial Material

Extraterrestrial matter of all sizes falls to the Earth and is broadly divisible into three groups by size. The most massive impactors are infrequent catastrophic colliders and include comets and large asteroids. Meteorites are more common and strike the Earth several thousand times per year, and our understanding of the nature of this material is the best out of all extraterrestrial material. Interplanetary dust particles (IDPs) are small, extraterrestrial material, with masses less than 1 mg.

It is important to note that while these three classes are distinct, they form a continuum. The most massive meteorites result from large impactors, and much of the IDP material is similar to meteorite and cometary material. Any calculation of mass flux will include some duplicate counting.

Understanding the nature of P and C compounds in these classes of extraterrestrial matter in turn informs our understanding of the nature of early Earth chemistry.

5.1.1 Large Impactors

Large impactors are the least studied group. They fall too infrequently to accurately study their nature and chemistry. Large impactors strike with catastrophic amounts of energy, and have been implicated in several mass extinction events. There are two broad types of impactors: asteroidal impactors (rocky bodies), and cometary impactors (volatile-rich bodies). Asteroidal impactors are considered to be roughly equal in

composition to meteorites (discussed below).  Cometary impactors are rich in volatiles

and hence organic compounds.  The complete suite of organics detected in comets is

available in Bockelee-Morvan et al. (2004).  Organic compounds make up ~10-20% of

the mass of a comet.  There have been no positive detections of P compounds in comets,

and this lack of volatility indicates that P is probably in a mineral phase (i.e.,

orthophosphate) in comets, in contrast to a volatile phase like $PH_3$.  Phosphorus in

cometary material is assumed to be similar to carbonaceous chondritic material for the

calculations that follow.

5.1.2 Meteorites

The mineralogy of meteorites is key to understanding the nature of C and P compounds

that fall to the Earth.  Some minerals are reactive on the surface of the Earth, like

carbides and phosphides, whereas some are inert, like carbonates and phosphates.

Organic C and P compounds of potential biologic utility have also been detected in

meteorites. These overviews of meteoritic mineral assemblages were taken from Cronin

et al. (1988), Brearley and Jones (1998), and from Mittlefehldt et al. (1998), and from

references therein.

5.1.2.1. Inorganic Carbon

There are two forms of carbon in meteorites: inorganic carbon and organic carbon. Inorganic carbon consists of carbonate minerals (principally calcite), carbides like cohenite ($Fe_3C$), and SiC, and of pure carbon phases like graphite and diamond. Carbonate minerals are common matrix minerals in carbonaceous chondrites, especially the CM, CR, and CI chondrites. These meteorites have experienced aqueous alteration resulting in matrix carbonates. Cohenite is rarer in chondritic meteorites, appearing in CV chondrites and in a few other unusual mineral assemblages. It is comparatively much more abundant in reduced meteorites and in iron meteorites. Graphite, diamond, silicon carbide and related carbides like TiC and ZrC are primarily constituents of presolar grain material, a very small but ubiquitous component of many meteorites.

Of these inorganic C phases, only cohenite could be argued to have any prebiotic importance (e.g., Oparin 1938). Cohenite has historically been proposed to be the source of petroleum (Mendeleyev 1891) and recent experiments suggest hydrocarbons are produced by the corrosion of this mineral (Oró 2002). Carbonates are the inert, stable carbon phase on the surface of the Earth, and are thus unlikely to form useful carbon compounds. Graphite, SiC, and diamond are all capable of being oxidized on the surface of the Earth, but the kinetics are slow for these reactions and imply limited reactivity.

5.1.2.2 Organic Carbon

Organic carbon molecules have a significant C-H bond component, and organics are a significant phase in carbonaceous chondrites, with ~75% of all meteoritic carbon in this form.  Carbon has a total abundance of ~1-4 weight percent of CM, CI, and CR chondrites.  The carbon in these meteorites consists of two groups, an insoluble macromolecular (IOM) fraction, and a soluble fraction.  The ratio of the two ranges from 70% IOM to 30% soluble in Murchison to 99% IOM to ~1% soluble in Tagish Lake.

The insoluble organic matter in meteorites varies in characteristics across meteorite classes.  Cody et al. (2002) studied the IOM of Murchison by solid state NMR, and Cody and Alexander (2005) detailed a larger set of meteorites.  The material is highly heterogeneous, but is a mixture of aliphatic (C as $sp^3$) and aromatic carbon (C as $sp^2$).  The exact origin of the insoluble organic matter is unclear at present.

The soluble carbon phase includes carboxylic acids, alcohols and polyols, amino acids, and simple aromatic species.  Table 23 summarizes the abundances of soluble organic species in two carbonaceous chondrites, Murchison and Tagish Lake.  Murchison is rich in soluble organic matter, whereas Tagish Lake is not.   Many of these species are used in modern biology, fueling speculation on the importance of meteorites to the origin and evolution of life on the earth.

Table 23.  Soluble meteorite organics.

| Compound type | Tagish ppm | Murchison ppm |
|---|---|---|
| Aliphatic hydrocarbons | 5 | >35 |
| Aromatic hydrocarbons | 1 | 15-28 |
| Polar hydrocarbons | nd | <120 |
| Carboxylic acids | 40 | >300 |
| Amino acids | <.1 | 60 |
| Hydroxy acids | bd | 15 |
| Dicarboxylic acid | 17.5 | >30 |
| Dicarboximides | 5.5 | >50 |
| Pyridine carboxylic acid | 7.5 | >7 |
| Sulfonic acids | >20 | 67 |
| Phosphonic acids | nd | 2 |
| N-heterocycles | nd | 7 |
| Amines | <.1 | 13 |
| Amides | <.1 | nd |
| Polyols | nd | 30 |
| Alcohols | nd | 11 |
| Aldehydes and ketones | nd | 27 |

nd is not determined.  Data from Pizarello 2006, Cronin et al. 1988.

5.1.2.3 Phosphorus

Phosphorus is typically in two distinct valence states in meteorites: +5 in phosphate minerals, and 0 as an alloy in phosphide minerals. Meteoritic phosphate minerals include phosphates like apatite, whitlockite, and monazite, and some unusual phosphate minerals, some of which are formed from schreibersite oxidation. Carbonaceous chondrites, ordinary chondrites, and differentiated silicate meteorites have phosphate minerals, whereas iron meteorites, enstatite chondrites and aubrites have phosphide minerals.

Phosphorus in ordinary chondrites is in both phosphates and metallic alloys (Goreva and Lauretta 2004). A majority is assumed to be in phosphate minerals for the calculations that follow. P phases like organophosphorus species are part of the soluble organic phase (Cooper et al. 1992) and phosphorus-sulfides (Nazarov et al. 1998) are in the matrix of CM chondrites. Neither P compound holds a significant fraction of the total P of a meteorite. The majority of P in carbonaceous chondrites is in orthophosphate minerals (Pasek et al. 2004), and P has an abundance of ~1000 ppm for chondrites.

Other unusual P rich phases in meteorites include phosphoran olivine and P-rich chondrule mesostases. Phosphoran olivine is a component of several main group pallasites. Phosphoran olivine is olivine, $(Mg,Fe)_2SiO_4$, with up to 2 weight % P as an oxide substituting for silicate (Buseck 1977). The oxidation state of P in this phase is +5, and its reactivity is likely similar to phosphate minerals. P-rich chondrule mesostases are P-rich zones in the interior of chondrules. This material has between 1-2 weight % P, probably as an oxide (Jones 1990), and is likely relatively inert compared to schreibersite.

Schreibersite is the most common meteoritic phosphide mineral, though there are a few others which are summarized in table 24. All have the potential to alter in water to form biologically useful P compounds, as per chapter 2.

The majority of P in iron meteorites is in schreibersite, whereas the majority of P is in phosphate minerals in carbonaceous and ordinary chondrites. Some phosphate minerals are in iron meteorites, as examined by Olsen et al. (1999). There are several occurrences of phosphate minerals in IIIAB iron meteorites, including sarcopside and graftonite, $(Fe,Mn)_3(PO_4)_2$; Johnsomervilleite, $Na_2Ca(Fe,Mn)_7(PO_4)_6$; Galileiite, $Na_2(Fe,Mn)_8(PO_4)_6$; Buchwaldite, $NaCaPO_4$; and others. Most of these phosphates are rare grains in troilite nodules. Of the 127 meteorites examined by Olsen et al (1999), these minerals were rare occurrences in 12 meteorites, and majority of P-bearing material is schreibersite in the IIIAB class. Phosphate minerals are more common in the IVB iron meteorites, but these meteorites are relatively rare and do not affect calculations significantly.

For the calculations that follow, all P in iron meteorites is assumed to be in schreibersite, and 1% of all P in ordinary and chondritic meteorites is assumed to be reactive or soluble. This is an acknowledged source of error, but deviations from this assumption are small and assumed to cancel out: phosphates from iron meteorites are countered by phosphides in stony meteorites.

Table 24.  Meteoritic phosphide minerals.  The first reference for these minerals is also listed.  Schreibersite has been known since the first iron meteorites were cut, and was first described by Berzelius (Norton 2002).

| Mineral Name | Formula | First Found in | Ref, if applicable |
| --- | --- | --- | --- |
| Schreibersite | $(Fe,Ni)_3P$ | Irons | |
| Perryite | $(Ni,Fe)_8(Si,P)_3$ | Enstatite chondrite | Reed (1968) |
| Barringerite | $(Fe,Ni)_2P$ (hexagonal) | Pallasite | Buseck (1969) |
| P-S sulfides | S,P | Murchison | Nazarov et al. (1998) |
| Nickelphosphide | $(Ni,Fe)_3P$ | Irons | Britvin et al (1999) |
| Florenskyite | $Fe(Ti,Ni)P$ | Kaidun | Ivanov et al. (2000) |
| Allabogdanite | $(Fe,Ni)_2P$ (orthorhombic) | Iron | Britvin et al (2002) |
| Melliniite | $(Ni,Fe)_4P$ | Acapulcoite | Moggi-Cecchi et al. (2005) |

5.1.3 IDPs

The majority of material that reaches the surface of the Earth is delivered as interplanetary dust particles (IDPs- Love and Brownlee 1993). IDPs are more difficult to collect than meteorites due to their small mass, but it is apparent that IDPs do not mimic meteorite trends in terms of abundances, as carbonaceous IDPs make up ~55% of the total IDP flux. Carbonaceous IDPs are varied: some are similar to the anhydrous carbonaceous chondrites, and others are similar to the aqueously altered carbonaceous chondrites. Metallic and sulfide IDPs are ~33% of the total IDP flux, with the remainder of the flux composed of silicate and aluminum IDPs (Reitmeijer 1998 and refs. therein). Metallic and sulfide IDPs are highly oxidized, with pentlandite as the dominant sulfide and with iron typically in magnetite.

5.1.3.1 Carbon

Carbonaceous IDPs have 2-3× the amount of carbon as carbonaceous meteorites. The chemistry of IDP carbon is unclear, and the best inferences must be taken from the carbonaceous chondrites, of which there is significantly more material to sample. The carbon in carbonaceous IDPs appears similar to the insoluble organic matter of some meteorites, and cohenite is a rare constituent of some IDPs.

5.1.3.2 Phosphorus

The abundance of P in carbonaceous IDPs ranges from 0.1% to 0.7% (Thomas et al.

1993). Phosphorus chemistry in IDPs is even less well characterized than carbon, and

there have only been two reports of P mineralogy in IDPs- one in a phosphate mineral

(Zolensky and Lindstrom 1992), the other in a phosphide mineral (Rietmeijer 1989). I

make the assumption that carbonaceous IDP material is similar to carbonaceous

chondrites, and that the phosphides make up ~1% of the total P. Sulfide IDPs are highly

oxidized and all P is assumed to be in phosphates.

5.2 Overview of Late Heavy Bombardment

Age dating of lunar samples suggests that the flux of large bodies was at one time much

higher than it is at present, a time known as "heavy bombardment." There are two views

on the heavy bombardment: one is that the lunar record records the gradual drop in

impactors from ~4.4 Ga to ~3.6 Ga, the other is that there was an intense late-heavy

bombardment period (4.0-3.8 Ga) that followed a relatively quiescent pre-bombardment

period (figure 38). Neither hypothesis has garnered incontrovertible proof, although the

cataclysmic late heavy bombardment has been the subject of considerable recent research

by both geochemists and dynamicists.

The existence of a late heavy bombardment period is justified mainly by the lunar

record and lunar age dates (e.g., Ryder 2003) and the fact that all Mare basins sampled

Figure 38.  Schematic diagram of gradual vs. late heavy bombardment.
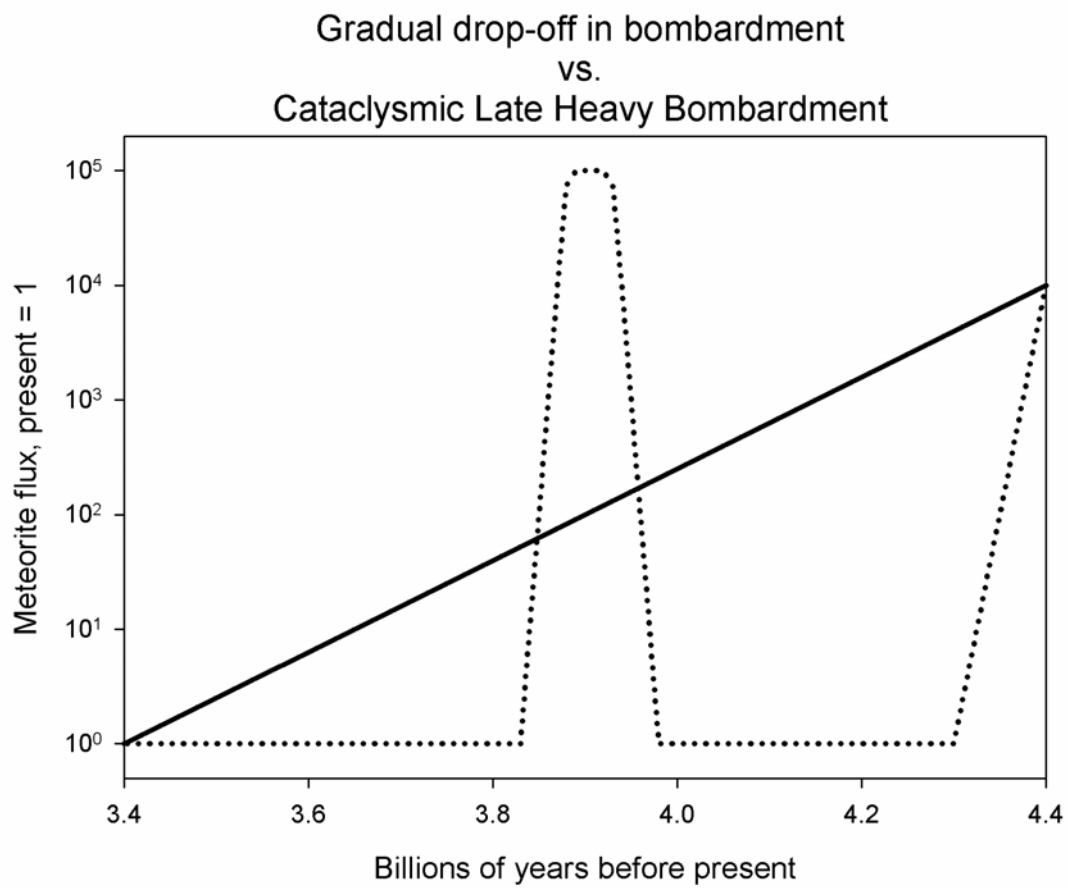
are younger than 4.0 Ga.  Additional evidence is from HED meteorite age dates (Bogard

and Garrison 2003) and ordinary chondrite age dates (Swindle et al. 2006).  Age dating of

lunar meteorites suggests that the moon records several distinct impacts, including a large

number around 3.9 Ga, and none prior to this date (Cohen et al. 2000, 2005).

Geochemical evidence for the catastrophic bombardment includes tungsten isotopes

(Schoenberg et al. 2002), iridium concentrations and shocked zircon (Koeberl et al.

2000), all from ancient terrestrial rocks.

The evidence against a late heavy bombardment period is outlined in Hartmann

(2003).  Hartmann (2003) argues that the lunar record does not record a late-heavy

bombardment period based on age-dates of Lunar Highland material and the

comparatively small aerial expanse of the Apollo missions.  Cr isotopes do not indicate

the presence of significant meteoritic material in the Isua Supracrustal Belt (Frei and

Rosing 2005), and most platinum group element abundances from Isua likewise do not

support a cataclysmic bombardment (Koeberl et al. 2000).

The discussion on gradual vs. cataclysmic bombardment is critical to any analysis

of past meteorite fluxes.  If the meteoritic flux was a gradual drop-off, then the maximum

flux was at most $10^4$ times the current flux.  This higher flux would have operated on a

much longer timescale than any cataclysmic bombardment.  In contrast, the late heavy

bombardment reaches a higher peak flux (~$10^5$ times the present flux) for a short period

of time, about 100 million years.

It is unknown exactly what sort of material was delivered during this period, but

based on siderophile trace element analysis of lunar melts (Kring and Cohen 2002), the

continental crust (Schmidt et al. 2005) and old terrestrial rocks (Schoenberg et al. 2002),

the majority of the material originated in the asteroid belt. Whether or not the meteorite

composition flux was the same in the past as it is today is unclear. I will assume that the

flux of meteorites today is similar to the flux of meteorites in the past for the purpose of

these calculations. Meibom and Clark (1999) argue that ordinary chondrites are

unimportant on the cosmic scale and that our collection is influenced by temporal effects.

Given that the likely time of the lunar cataclysm was $3.9 \pm 0.1$ Ga, asteroidal bodies

would have differentiated and cooled by this time (e.g. Cook et al. 2004), so a metal :

silicate flux ratio similar to the current flux is not unreasonable.


5.3 Methods


The current flux of P and C compounds was determined for these three classes of

extraterrestrial materials using a variety of methods. These fluxes were then placed in the

historical context of the late heavy bombardment to estimate mass fluxes for the period of

time right before the first evidence of life (~3.5 Ga, from the Apex chert). The values

used for P and C abundance calculations, and reasonable maxima and minima are

presented in table 25. For these calculations I assume that the heavy bombardment took

place as a spike, rather than a gradual decrease.

For each estimate of mass flux described below, P and C delivery are estimated

by the simple equation

$$F = M_x \times X_E \times k \tag{90}$$

Table 25.  Values used for calculations, and reasonable maxima and minima.

| | Reasonable average | Minima | Maxima |
|---|---|---|---|
| **Chondrites** | | | |
| Weight percent carbon (CC) | 2.2 (CM%) | 0.44 (CO%) | 3.45 (CI%) |
| Percent soluble carbon (CC) | 10% | 1% (Tagish Lake) | 30% (Murchison) |
| Carbon in OC (ppm) | 2500 (L) | 2100 (H) | 3100 (LL) |
| Phosphorus weight CC,OC (ppm) | 1,000 | | |
| Reactive phosphorus CC,OC (ppm) | 10 | | |
| Iridium concentration, CC (ppm) | 0.5 | | |
| Iridium concentration, OC (ppm) | 0.60 | | |
| | | | |
| **Iron Meteorites** | | | |
| Weight percent phosphorus | 0.52% | 0.04 (IVA) | 2 (IIG) |
| Carbon in carbide weight (ppm) | 100 | 1 ppm (graphite) | 2000 (max Irons) |
| Average Iridium (ppm) | 5 | | |
| | | | |
| **Large Impactors[1]** | | | |
| Percent iron | 60% | 5% | 80% |
| Percent cometary/CC | 20% | 10% | 50% |
| | | | |
| **IDPs** | | | |
| Mass flux of IDPs (kg) | $3 \times 10^7$ | | |
| Percent carbonaceous | 55% | | |
| Mass of carbon in carbonaceous (wt. %) | 8% | 6% | 10% |
| Mass of P in IDPs (wt. %) | 0.3% | 0.1% | 0.7% |
| Percent P as phosphide | 1% (like CC) | 0% (hydrous IDPs) | 10% (highest of OC) |

[1]Large impactor averages are from the recent terrestrial cratering record.  Cometary impactors are assumed to be 50% of the non-metallic impactor material.  The associated minimum assumes that the recent craters with associated iron meteorites have been found due to the associated iron meteorites, resulting in bias.   The maximum of 80% assumes that associated meteoritic material for some craters has not been found yet, or that the metallic impactor was composed of a more friable iron meteorite.

CC is carbonaceous chondrites, OC is ordinary chondrites.

Chondritic abundances of C, P and Ir are from Lodders and Fegley (1997).

where $F$ is the flux, $M_x$ is the yearly mass flux of a given extraterrestrial material group,

$X_E$ is the fraction of the element of interest, and $k$ is a factor determining "useful"

varieties of the element (i.e., soluble carbon fraction, percent P as phosphide).

5.3.1 Large Impactor Flux Calculations

For the purpose of these calculations, the mass of a large impactor is $\geq 5,000$ kg. The

mass of a large impactor is determined from the diameter of the crater it forms on impact

with the surface of the Earth. The crater diameter is related to the energy of an impactor,

which is in turn related to its mass and velocity. The velocity of impactors is assumed to

be constant (correct to a factor of ~2) and thereby the crater diameter is dependent only

on mass, which allows for a direct conversion of crater size to impactor size. The crater

diameter is related to the impactor diameter by a factor of 20:1 (French 1998) for

ordinary chondrite material, and a factor of 25:1 for iron meteorites. The mass is

determined from the impactor diameter by assuming a perfect sphere and multiplying by

3500 kg/m$^3$ for an ordinary chondrite, or 7000 kg/m$^3$ for an iron meteorite. The number

of impactors of a given mass was calculated from the impactor frequency of French

(1998). The most recent craters known are summarized by age, location, size, and

associated meteorite fragments in table 26.

    The mass flux of large impactors per year is given as:

$$Flux = \frac{1}{time} \sum M \times F \qquad\qquad (91)$$

Table 26.  All known recent (<1 Ma) craters and associated meteorites

| Name | Location | Diameter (km) | Age (kA) | Meteorite |
|---|---|---|---|---|
| Barringer | Arizona, U.S.A. | 1.186 | 49±3 | Iron |
| Boxhole | Northern Territory, Australia | 0.17 | 54±1.5 | Iron |
| Campo Del Cielo | Argentina | 0.05 | <4 | Iron |
| Dalgaranga | Western Australia, Australia | 0.024 | ~270 | Mes |
| Haviland | Kansas, U.S.A. | 0.015 | <1000 | Pal |
| Henbury | Northern Territory, Australia | 0.157 | 4.2±1.9 | Iron |
| Ilumetsä | Estonia | 0.08 | >2 | ? |
| Kaalijärv | Estonia | 0.11 | 4±1 | Iron |
| Lonar | India | 1.83 | 52±6 | ? |
| Macha | Russia | 0.3 | <7 | ? |
| Monturaqui | Chile | 0.46 | <1000 | Iron |
| Morasko | Poland | 0.1 | <10 | Iron |
| Odessa | Texas, U.S.A. | 0.168 | <50 | Iron |
| Rio Cuarto | Argentina | 4.5 | <100 | ? |
| Sikhote Alin | Russia | 0.027 | 0.059 | Iron |
| Sobolev | Russia | 0.053 | <1 | ? |
| Tenoumer | Mauritania | 1.9 | 21.4±9.7 | ? |
| Tswaing | South Africa | 1.13 | 220±52 | ? |
| Veevers | Western Australia | 0.08 | <1000 | Iron |
| Wabar | Saudi Arabia | 0.116 | 0.14 | Iron |
| Wolfe Creek | Western Australia | 0.875 | <300 | Iron |
| Zhamanshin | Kazakhstan | 14 | 900±100 | ? |

Data from Paillou et al. (2004).  Mes = Mesosiderite, Pal = Pallasite.  "?" under meteorite denotes no meteorites is known to be associated with the crater.  These craters may be associated with stony or cometary impactors which have completely vaporized on impact.

where *time* is the time interval of interest (1,000 years), $M$ is the mass of an impactor, and $F$ is the frequency with which impactors of mass $M$ impact the Earth.

5.3.2 Meteorite Flux Calculations

Meteorite mass flux calculations are dependent on the data set used. There are three collections upon which to build such a data set: global meteorite finds, global meteorite falls, and Antarctic finds. Global meteorite finds have a significant human bias where the untrained frequently collect most unusual rocks, resulting in the over-collection of meteorites with no terrestrial counterparts. However, this data set is by far the most global data set available and provides significant information on meteorite subgroup classification (especially of iron meteorites). Much of the human bias is eliminated by examining only meteorites observed to fall, and since falls are recorded globally, no regional bias would be expected. However, only larger, cohesive falls are recovered, so small masses are usually ignored, which indubitably results in some bias. Finally, Antarctic studies are the most systematic and have recovered an enormous variety of meteoritic material. Meteorites of all sizes and types are collected and catalogued. However, this collection is regional in scope and may not adequately recognized paired meteorites, much less strewn fields, many of which have been processed by geomorphologic systems acting on the ice. I use data from all three collections to describe the nature of the meteoritic material that has fallen to Earth in this study. Table 27 summarizes collection data sets.

Table 27. Meteorite collection data, accurate to 2002.  Carbonaceous meteorites are considered a subset of stony meteorites.

| Collection (>0.02 kg) | Antarctic finds | Global finds* | Falls |
|---|---|---|---|
| Number | 5,663 | 5,106 | 941 |
| Mass (kg) | 3,381 | 516,616 | 49,616 |
| Average mass | 0.6 | 101.2 | 52.7 |
| | | | |
| % mass stone | 84.1 | 8.1 | 49.7 |
| % mass carbonaceous | 1.7 | 0.1 | 5.3 |
| % mass iron | 15.9 | 91.9 | 50.3 |
| | | | |
| % number stone | 99.3 | 87.4 | 95.9 |
| % number carbonaceous | 2.0 | 2.1 | 4.1 |
| % number iron | 0.7 | 12.6 | 4.1 |

*The global find data set includes many Saharan meteorites.  There is a movement towards systematic collecting of Saharan meteorites.

Estimates of the current meteorite flux likewise vary and are model-dependent. Most

meteorites that fall are not recovered, and our collection is not representative of the actual

meteorite flux. The flux of meteorites with a mass >20g is estimated to be 159 per million

km$^2$ per year, with an error range of a factor of two. This fall rate is consistent

with camera observations (Bland et al. 1996).  The global flux of meteorites is ~80,000

falls per year.

I analyzed the composition vs. mass vs. number relationship using the MetBase

Meteorite Data Retrieval Software (2003). This data set provides frequency and mass

data for both falls and finds (including Antarctic finds) and is current through 2002.  Fall

and Antarctic meteorite data were divided into classifications of ordinary chondrites,

carbonaceous chondrites, achondrites, and iron meteorites.  Each class was then divided

by mass into mass bins starting from 10,000 kg total mass, and dividing by either factors

of 2.5 or by factors of 6.25.  Linear relationships were determined from the number of

meteorites in each mass bin.  Fall meteorite statistics were discontinued after 2.5 kg, as

the collection decreases significantly after this mass due to the difficulty in recovering 1

kg masses after observing a meteor.

The total year mass flux for each class of meteorites is estimated from the log-log

relationship:

$$\text{Log } N = A * \text{Log } M + B \tag{77}$$

where $N$ is the number of meteorites of a mass $M$, and $A$ is the slope of the line

determined from the log-log relationships established by fall and Antarctic find collection

relationships.  The value $A$ is set as the average of the slopes from fall and Antarctic

collections. $B$ is the y intercept, and is determined from the addition of a constant factor to the $B$ determined from Antarctic and fall collections. Of the total yearly flux of ~80,000 meteorites per year, about 70,000 would be ordinary chondrites. In order to match the $B$ value of this hypothetical yearly flux, a factor of 0.2 must be added to the fall $B$ value, and this factor is added to all $B$ values to determine the yearly flux. $B$ is the largest source of error in these calculations.

Expression (91) is equivalent to:

$$10^{(-B/A)} * N^{(1/A)} = M \text{ or } N = M^A * 10^B \tag{92}$$

Integration from 1 meteorite (probability of 1 occurrence) to $N_{tot}$ gives the total mass flux:

$$\int_1^{Ntot} MdN = M_{tot} \tag{93}$$

where $N_{tot}$ is the total yearly flux of meteorites for a given class of meteorite. $N_{tot}$ is set equal to the fraction of material of a specific class times the total flux per year. This is equivalent to the number abundance of a given class. The total mass for one year equals:

$$M_{tot} = \frac{10^{-B/A}}{\frac{1}{A}+1} \times (N_{Tot}^{\frac{1}{A}+1} - 1) \tag{94}$$

and allows for determination of the total mass flux of each meteorite group. These estimates are naturally underestimates due to the nature of our mass-binning process, and the actual total mass may be up to a factor of 2 larger. Nonetheless, this approximation is a good order of magnitude estimate.

Iron meteorites are heterogeneous and describing the bulk composition of this class is akin to describing the bulk composition of all granite rocks. Iron meteorites contain macroscopic phosphide minerals that can significantly influence P flux estimates depending on whether the mineral grain is included or not. Even with this experimental difficulty, the concentration of P in iron meteorites varies by ~2 orders of magnitude across classification type. To illustrate these difficulties, consider two studies of weight percent P in iron meteorites. Doan and Goldstein (1969) estimated ~1% by weight P on average from point count analyses of several iron meteorites, whereas Moore (1971) estimate 0.2 wt. %. Here I use the abundances of Willis (1980) to calculate the mass of P in iron meteorites. Phosphorus is most abundant in the IIAB, IID, IIIAB and the newly classified IIG groups of iron meteorites (>0.6 weight %), and least abundant in the IAB, IIE, IVA, and IVB groups of iron meteorites (<0.2 weight %). The average weight percent of phosphorus in iron meteorites is calculated as

$$P = \frac{\sum (X_{PClass} \times N_{Class})}{N_{Total}} \tag{95}$$

where $X_{PClass}$ is the weight percent of phosphorus in an iron meteorite of "class", $N_{Class}$ is the number of iron meteorites in that class, and $N_{Total}$ is the total number of iron meteorites (table 28). Using table 28 I arrive at a value for P of 0.52 weight percent. This calculation is repeated later for C and Ir.

Table 28. Average abundances of P, C, and Ir in iron meteorites.  The concentration of carbon in iron meteorites is poorly constrained.  Moore et al. (1969) suggests an average of ~140 ppm across iron meteorite classes.  The concentration of iridium in iron meteorites is well constrained and is one of the elements used to classify iron meteorites.

| Class | Number | P wt. % | C wt. % | Ir ppm | N Falls | N Finds | N Antarctic |
|---|---|---|---|---|---|---|---|
| IAB | 117 | 0.21 | | 2.7 | 6 | 100 | 11 |
| IC | 11 | 0.43 | | 0.38 | | 11 | |
| IIAB | 78 | 1 | 0.2 | 10 | 6 | 69 | 3 |
| IIC | 8 | 0.53 | | 6.4 | | 8 | |
| IID | 17 | 0.98 | | 9.9 | 2 | 15 | |
| IIE | 15 | 0 | | 4.1 | 1 | 14 | |
| IIF | 5 | 0.26 | | 6.2 | 1 | 4 | |
| IIG | 5 | 2 | | 0.15 | | 5 | |
| IIIAB | 224 | 0.7 | 0.014 | 4.1 | 11 | 206 | 7 |
| IIICD | 31 | 0.21 | | 2.70 | | 30 | 1 |
| IIIE | 13 | 0.56 | | 4.10 | | 13 | |
| IIIF | 9 | 0.22 | | 3.2 | | 9 | |
| Iron unknown* | 4 | 0.5 | | 6 | | 1 | 3 |
| Iron ungrouped* | 116 | 0.5 | | 6 | 8 | 94 | 14 |
| IVA | 61 | 0.1 | 0.02 | 1.9 | 4 | 56 | 1 |
| IVB | 12 | 0.2 | 0.004 | 22.00 | | 12 | |

Data from Mitthlefeldt et al. (1998) and from Willis (1980)

*The concentration of phosphorus in "iron unknown" (those meteorites with incomplete classification) and the concentration of phosphorus in "iron ungrouped" (meteorites with less than 5 related members) are taken as the average (0.5 wt. %) of all classes.

5.3.3. IDP Flux

The mass flux of IDP material was calculated by Love and Brownlee (1993) to be $3 \times 10^7$ kg/year. The fraction of reactive P in IDP material is assumed to be roughly equal to the average fraction in carbonaceous chondrites with ~1% of all P is soluble or reactive. Carbonaceous chondrites vary significantly with regards to the fraction of P in phosphide minerals, so this value is an educated guess.

5.4 Results

The calculated mass flux for all bodies is shown in table 29. The associated flux of C and P, and reactive C and P compounds is shown in table 30.

5.4.1 Large Impactors Flux and Composition

Large impactors contribute a significant fraction of the yearly mass flux of extraterrestrial material. The mass vs. number flux is shown in figure 39. Large impactors are inherently stochastic events. In any given year, the Earth could be struck by the 1,000,000 year body. The mass of the 1 million year impactor is $6.7 \times 10^9$ kg and corresponds to the total mass of an object that on average strikes the Earth once every million years. Thus the amount of material delivered per year by 1 million year impactors is ~6,700 kg. Calculating the average yearly flux is difficult, and depends on

Table 29. Total mass flux per year of extraterrestrial material, sorted by class.

| Class | Mass of flux (kg) |
|---|---|
| Large impactors | 120,000  (1,000 year average) |
| Iron | 70,000 |
| Not iron | 50,000 |
| 1 year event | 5,000 |
| $10^6$ year event | $6.67 \times 10^9$ |
| | |
| Meteorites | |
| CC | 1,100 |
| OC | 24,000 |
| Iron | 22,000 |
| Achon | 6,700 |
| | |
| IDPs | $3 \times 10^7$ |

CC is carbonaceous chondrites, OC is ordinary chondrites, Iron is iron meteorites, and Achon is achondritic meteorites

Table 30. Biogenic element mass flux per year

| Class | C flux (kg) | P Flux (kg) | Reactive C flux (kg) | Reactive P Flux (kg) |
|---|---|---|---|---|
| **Large impactors** | | | | |
| Iron | 7 | 364 | 7 | 364 |
| Not iron | 550 | 50 | 55 | 0.5 |
| 1 year event iron | 0.5 | 26 | 0.5 | 26 |
| 1 year event not iron | 55 | 5 | 5.5 | 0.05 |
| $10^6$ year event iron | 500,000 | $2.6 \times 10^7$ | 500,000 | $2.6 \times 10^7$ |
| $10^6$ year event not iron | $5.5 \times 10^7$ | $5 \times 10^6$ | $5.5 \times 10^6$ | 50,000 |
| | | | | |
| **Meteorites** | | | | |
| Iron | 2.2 | 114 | 2.2 | 114 |
| CC | 24.2 | 1.1 | 2.42 | 0.011 |
| OC | 60 | 24 | ~0 | 0.24 |
| | | | | |
| **IDPs** | $1.32 \times 10^6$ | 90,000 | 132,000 | 900 |

Figure 39. Large impactor mass vs. number relationship.



$$Log_{10}(N) = -0.9797\,Log_{10}(M) + 9.6245$$

$$R^2 = 0.992$$

Axis labels: $Log_{10}$ (Number/Ma) (vertical), $Log_{10}$ (M) kg (horizontal)
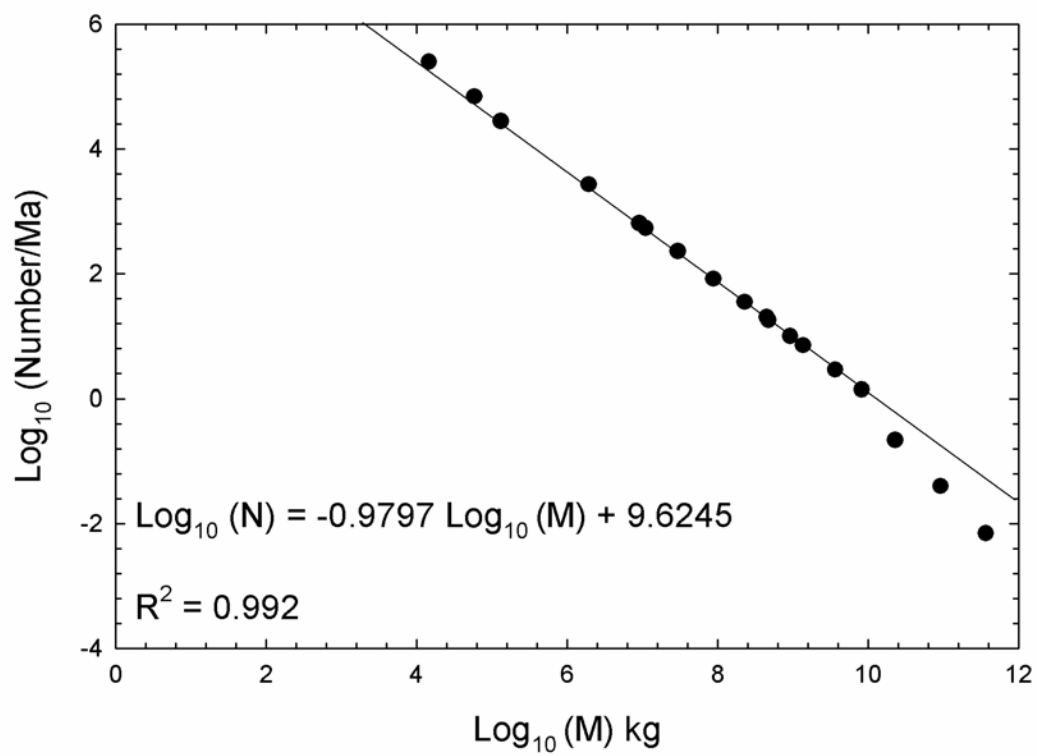
the number of years considered.  The more years that are considered, the larger the net flux since random large events have a proportionately higher chance of occurring.  The yearly flux expressed in table 29 is actually the yearly flux for a 1,000 year period.  The yearly flux for a 1,000,000 year would be larger than this value.

Large impactors deliver a significant amount of reactive P and C to the Earth. Reactive P is supplied by iron meteorite impactors in the form of schreibersite, and reactive C is supplied by cometary or carbonaceous impactors.  Some of this material survives to reach the surface, some does not.  Survival of material is discussed in the discussion section.

The majority of large impactors in the last million years have been iron meteorites (~60%), based on the presence of significant iron meteorite material in locations near to these impact craters.  Large impactors are mostly metallic material.  This trend is reflected in meteorite fall statistics: the slope of the iron meteorite mass line implies a bias towards more massive meteorites, relative to all other types of meteorites.  .

5.4.2 Meteorite Flux and Composition

Several trends are notable in table 27.  The mass of the collections span several orders of magnitude.  Antarctic meteorites are the least massive collection, and have the lowest average meteorite mass at about 0.6 kg.  Iron meteorites make up 0.7% of the total meteorites, and about 16% of the mass.  Compare this to global meteorite finds, where the average mass is ~100 kg, and iron meteorites make up 12.6% of the total number of

meteorites and 91.9% of the mass!  The fall collection of meteorite is intermediate of these two values, with an average mass of about 50 kg, of which 4.1% are iron meteorites, with 50.3% of the mass.  Is this data reasonable- do iron meteorites make up a progressively larger portion of both the mass and number as the average size of meteorites increases?  Or is it just merely that more farmers dig up large rocks and happen to notice when they are made of metal, i.e. a sociologic effect?

Figure 40 provides the Log N vs Log M relationships for ordinary chondrites, iron meteorites, carbonaceous chondrites, and achondrites.  The slopes and intercepts of these lines, $R^2$ values, and the bin sizes used for each line are in table 31.  The slopes of these lines are consistent between fall and Antarctic collections, indicating minimal sampling bias for the two collections.

Note that the previous study (Pasek and Lauretta 2005) provided linear regressions for all meteorites.  The slope of the "all meteorite line" was -0.74, roughly consistent with the Halliday et al. (1989) slope of -0.69.  Here the meteorites are separated according to class with the effect of significantly changing the slope of the log mass vs. log number relationships.  This method is similar to the method used by Halliday et al. (1989), except that the data is completely binned in this study.  Like Halliday et al. (1989), these data show a distinct bend in the curve; Halliday et al. (1989) attribute this to fragmentation differences between size.

Figure 40.  Log mass-log number relationships between A) ordinary chondrites, B) carbonaceous chondrites, C) achondrites, and D) iron meteorites.
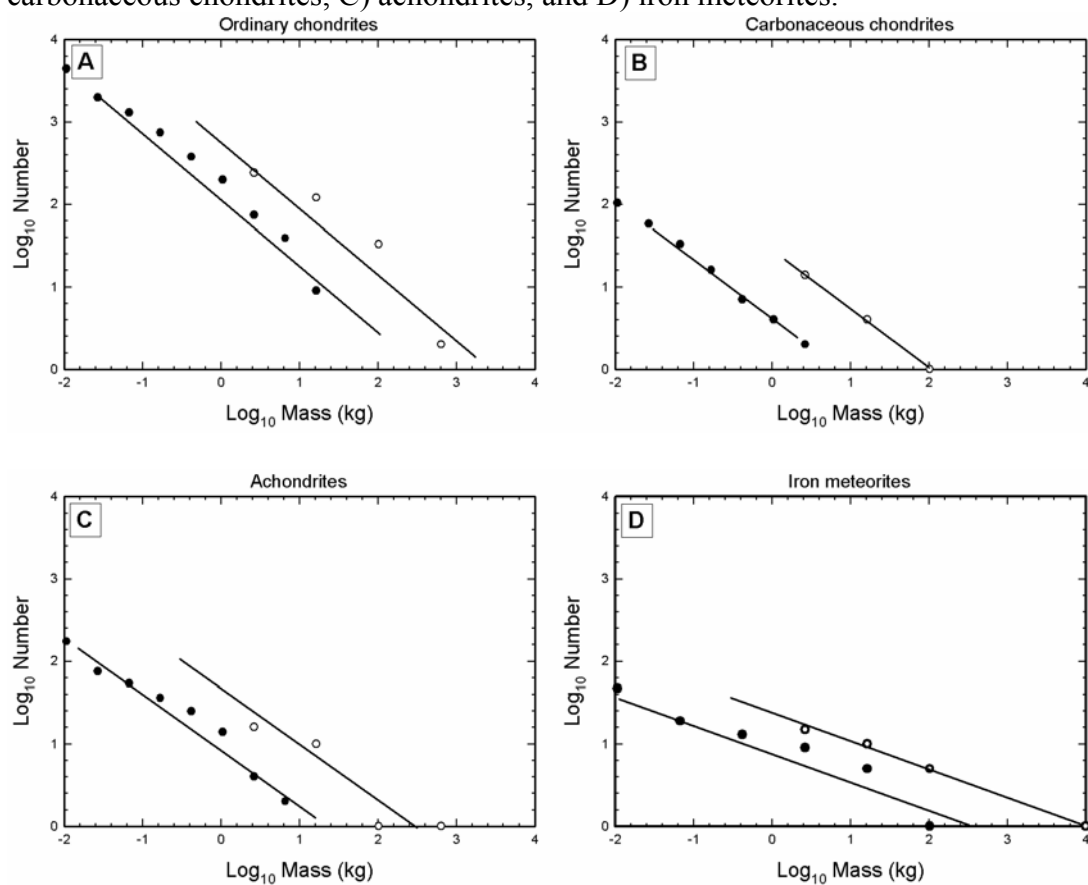
Table 31.  Linear regression fits for various meteorite classes.  The relationship between mass and number is equal to $Log_{10}N = A\ Log_{10}\ M + B$.

| | A | B | $R^2$ | Bin Size |
|---|---|---|---|---|
| **Falls** | | | | |
| Ordinary chondrites | -0.8549 | 2.9485 | 0.9142 | 6.25 |
| Carbonaceous chondrites | -0.7200 | 1.4572 | 0.9991 | 6.25 |
| Achondrites | -0.5795 | 1.4854 | 0.861 | 6.25 |
| Iron meteorites | -0.3361 | 1.3610 | 0.9942 | 6.25 |
| | | | | |
| **Antarctic Finds** | | | | |
| Ordinary chondrites | -0.7931 | 2.1682 | 0.9787 | 2.5 |
| Carbonaceous chondrites | -0.7298 | 0.6214 | 0.9973 | 2.5 |
| Achondrites | -0.6539 | 0.9796 | 0.9606 | 2.5 |
| Iron meteorites | -0.3683 | 0.9606 | 0.9271 | 6.25 |
| | | | | |
| **Global Finds** | | | | |
| Ordinary chondrites | -0.6153 | 2.4523 | 0.8818 | 2.5 |
| Carbonaceous chondrites | -0.4655 | 0.8946 | 0.8446 | 2.5 |
| Achondrites | -0.3121 | 1.2573 | 0.7895 | 2.5 |
| Iron meteorites | -0.0602 | 1.4412 | 0.0454 | 2.5 |

Of the biogenic elements P and C, iron meteorites provide a significant amount of reduced P to the Earth, whereas meteorites as a whole deliver very little reactive C to the Earth.

## 5.4.3 IDP C and P Fluxes

IDPs deliver a lot of material to the surface of the Earth, more than anything else during the average year. IDPs deliver a lot of soluble C to the Earth. IDPs also deliver a significant amount of reactive P. Most of this material is distributed evenly across the surface of the Earth.

## 5.4.4 Late Heavy Bombardment

The late heavy bombardment period provided a huge increase in the flux of material that reached the Earth. Table 32 provides an estimate of the peak fluxes during this period. The peak flux of material is assumed to reach $10^5$ times the present flux. For large impactors, this would mean an increase during that time period of a factor of $10^5$ in the total flux. Additionally, the frequency of impactors may change- impactors that currently fall once every million years may fall every 100 or even every 10 years, resulting in a huge increase of localized reactive P in some localities.

Table 32. Fluxes during the late heavy bombardment.

| Class | C flux (kg) | P Flux (kg) | Reactive C flux (kg) | Reactive P Flux (kg) |
|---|---|---|---|---|
| **Large impactors** | | | | |
| Iron | $7 \times 10^5$ | $3.64 \times 10^7$ | $7 \times 10^5$ | $3.64 \times 10^7$ |
| Not iron | $5.5 \times 10^7$ | $5 \times 10^6$ | $5.5 \times 10^6$ | $5 \times 10^4$ |
| 1 year event iron | $5 \times 10^4$ | $2.6 \times 10^6$ | $5 \times 10^4$ | $2.6 \times 10^6$ |
| 1 year event not iron | $5.5 \times 10^6$ | $5 \times 10^5$ | $5.5 \times 10^5$ | 5,000 |
| $10^6$ year event iron | $5 \times 10^{10}$ | $2.6 \times 10^{12}$ | $5 \times 10^9$ | $2.6 \times 10^{12}$ |
| $10^6$ year event not iron | $5.5 \times 10^{12}$ | $5 \times 10^{11}$ | $5.5 \times 10^{11}$ | $5 \times 10^9$ |
| | | | | |
| **Meteorites** | | | | |
| Iron | $2 \times 10^6$ | $10^8$ | $2 \times 10^6$ | $10^8$ |
| CC | $6 \times 10^5$ | $3 \times 10^4$ | $6 \times 10^4$ | 300 |
| OC | $9 \times 10^6$ | $4 \times 10^6$ | ~0 | $4 \times 10^4$ |
| | | | | |
| **IDPs** | $1.32 \times 10^{11}$ | $9 \times 10^9$ | $1.32 \times 10^{10}$ | $9 \times 10^7$ |

The IDP mass flux is likewise multiplied by a factor of $10^5$ which assumes essentially identical conditions as present. The review by Chyba and Sagan (1992) showed that the best current estimate suggests a relatively constant flux of IDP material for the past several million years, and perhaps into the whole of the Earth's history.

Estimating the meteorite flux during the late heavy bombardment is more difficult as the mass vs. number relationships indicate that increasing the flux will drastically increase the mass. If the intercept is increased by a factor of 10 (one log unit), then the total mass flux increases significantly. However, there appears to be a cut-off for the maximum impactors. The largest chondritic meteorite is ~4,000 kg (Jilin), and the largest iron meteorite is 60,000 kg (Hoba). If these masses are assumed to be the maximum that penetrate the atmosphere to land on the surface, then these values serve as a cut-off for the flux calculations. This is not necessarily reasonable for large iron impactors, as some fraction (~5%) of the material melts on impact and is incorporated with the terrestrial impact material. This facet is considered later in the discussion as part of the large impactors. Assuming this mass cutoff is reasonable, the mass flux of iron meteorites was $2 \times 10^{10}$ kg, of ordinary chondrites was $4 \times 10^9$, and of carbonaceous chondrites was $3 \times 10^7$ kg during the late heavy bombardment.

5.4.5. Mass Flux of Ir

As a sanity check on these calculations, the flux of iridium from extraterrestrial sources

is shown as table 33.  Equation (6) is altered to calculate Ir, and the fluxes from large

impactors, meteorites and IDPs is summed.  The amount per year from IDPs, large

impactors, and meteorites is approximately 16 kg.  For the last 4 Ga of the Earth's history

$10^{14}$ kg of Ir would be deposited from extraterrestrial sources, including the late heavy

bombardment.  The majority of this comes from IDPs, followed closely by large,

infrequent impactors.  The amount of Ir in the Earth's crust is approximately $2 \times 10^{13}$ kg.

The extraterrestrial flux calculated value is a factor of $5 \times$ higher, though much of this

could be erased through subduction, as Ir is more compatible in mantle material than in

crustal material.  The total predicted flux of Ir is about 2% of the total Ir content of the

bulk silicate Earth (Kargel and Lewis 1993).  Thus the flux calculations are reasonable,

though perhaps a bit high.

5.5 Discussion

5.5.1 Extraterrestrial Fluxes

The fall and Antarctic find collections show significant agreement between slopes,

whereas global finds do not show agreement.  The agreement between fall and Antarctic

find collections suggests that these collections sample from the same material, and that as

the Antarctic collection continues to grow, it will eventually match the fall collection by

Table 33. Mass flux of Ir. Large impactors are averaged for 60% iron and 40% stone impactors. Total flux is calculated using the profile of figure 36.

| Body | Ir (kg) / year | Ir, LHB (kg) / year | Total flux, 4 Ga (kg) |
|---|---|---|---|
| Large impactors | 0.375 | 37500 | $2 \times 10^{12}$ |
| 1 year event | 0.016 | 1600 | $1 \times 10^{11}$ |
| $10^6$ year event | 21440 | $2.14 \times 10^6$ | $5 \times 10^{13}$ |
| | | | |
| Meteorites | | | |
| OC | 0.0144 | 2100 | $1 \times 10^{11}$ |
| CC | 0.0006 | 13 | $7 \times 10^8$ |
| Iron | 0.11 | 90000 | $5 \times 10^{12}$ |
| | | | |
| IDP | 15 | $1.5 \times 10^6$ | $9 \times 10^{13}$ |
| | | | |
| Total Flux for Earth | | | $10^{14}$ |

increasing the y-intercept. The fact that all slopes are greater than negative one indicates

that the most massive meteorites are the main mass input. The total mass of iron

meteorites is especially influenced by the most massive meteorites. Thus the effect of

increased iron meteorite mass percent for the fall collection (and probably for the global

find collection) is a real effect, and not just a collection bias. Iron meteorites are heavier

than other meteorites.

Iron meteorites are approximately 4% of the total number of meteorites of both

falls and finds. However, they constitute a large portion of the mass of meteorite

collections. Iron meteorites make up ~88% of the total meteoritic mass of finds, due in

large part to distinctiveness of iron meteorites relative to other terrestrial rocks, enabling

collection by untrained individuals. Fall statistics factor out both of these observational

biases, and iron meteorites are ~50% of the total mass of meteorites observed to fall.

Note here that there is a significant distinction between fall number statistics and fall

mass statistics. It is not sufficient to say that the mass flux of meteorites is equivalent to

the fall flux of meteorites. While it is true that most meteorites are chondritic, most of the

meteoritic mass is not. Iron meteorites are usually larger than chondritic meteorites and

also survive atmospheric entry better. Hence a significant portion of meteoritic mass

coming in contact with the surface of the Earth is differentiated asteroidal core material.

Note that if the iron meteorite Sikhote-Alin (fell 1947) is excluded from these

calculations, then the iron meteorite mass fraction is significantly less. However, the

exclusion of Sikhote-Alin can not be justified unless rationale is provided to demonstrate

that large falls like Sikhote-Alin are rarer than would be assumed from the ~100 years of fall observation data.

5.5.1.1 Slopes

Ordinary chondrites have a slope of about -0.82, indicating bias towards heavier material, i.e. more massive chondrites provide more of the net mass flux.  Carbonaceous chondrites are similar with a slope of -0.72.  Iron meteorites show a slope of -0.345, which implies that massive meteorites are more common for irons than they are for ordinary chondrites, because the iron meteorite slope is less negative than the ordinary chondrite slope. The mass vs. number lines of these two classes intercept and iron meteorites become the dominant meteorite type (figure 41).  The dominance of large, heavy masses of metal in the global find collection is not wholly a sociologic effect, but is a result of the actual mass vs. number distribution of the various meteorite classes.  Note that there are much less visible trends in the global data (figure 42).  The deviation of the global find data from the global fall and Antarctic data is likely combination of a sociologic effect and the difference in deterioration rates between small and large bodies.

The slopes of the log N vs. log M relationships shown in figures 37 and 38 demonstrate significant variations.  For the large impactor line, the slope is approximately -1, which indicates that the most massive impactors contribute as much mass as the least massive impactors.  Large impactors fall much less frequently than small impactors, and

Figure 41. Idealized yearly flux. The x-axis is set to the yearly flux, and Antarctic and fall meteorites are also shown.
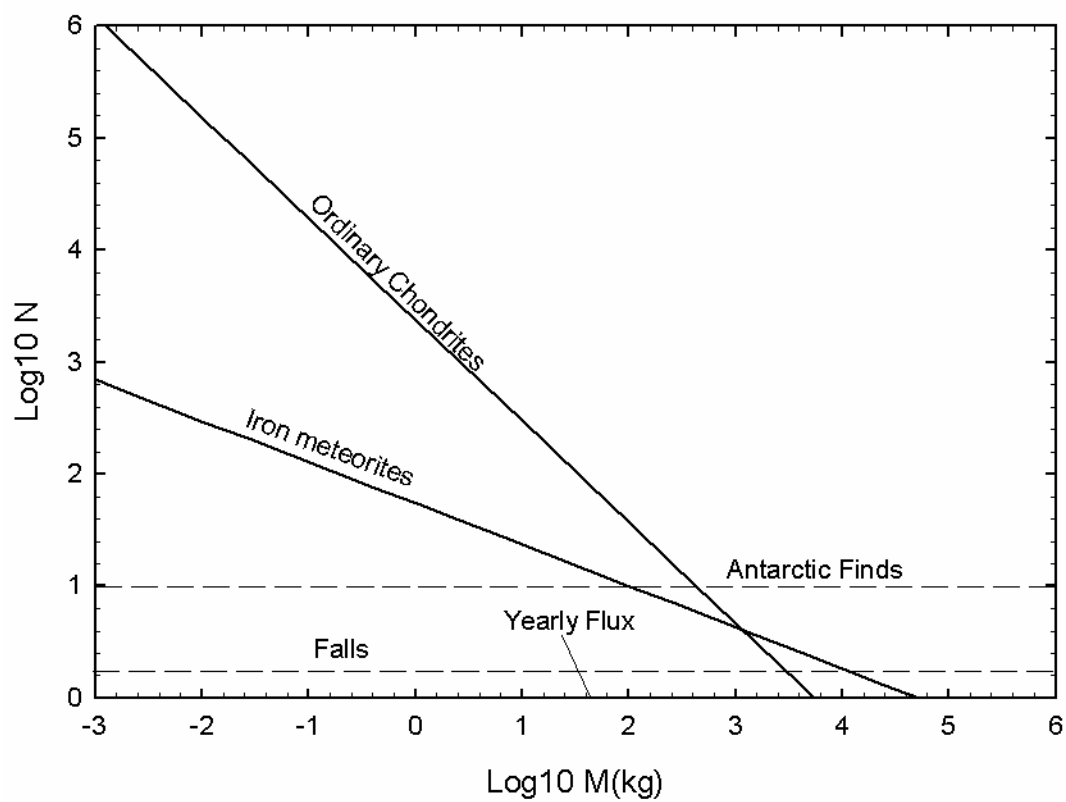
Figure 42. Global find meteorite log-log plot.
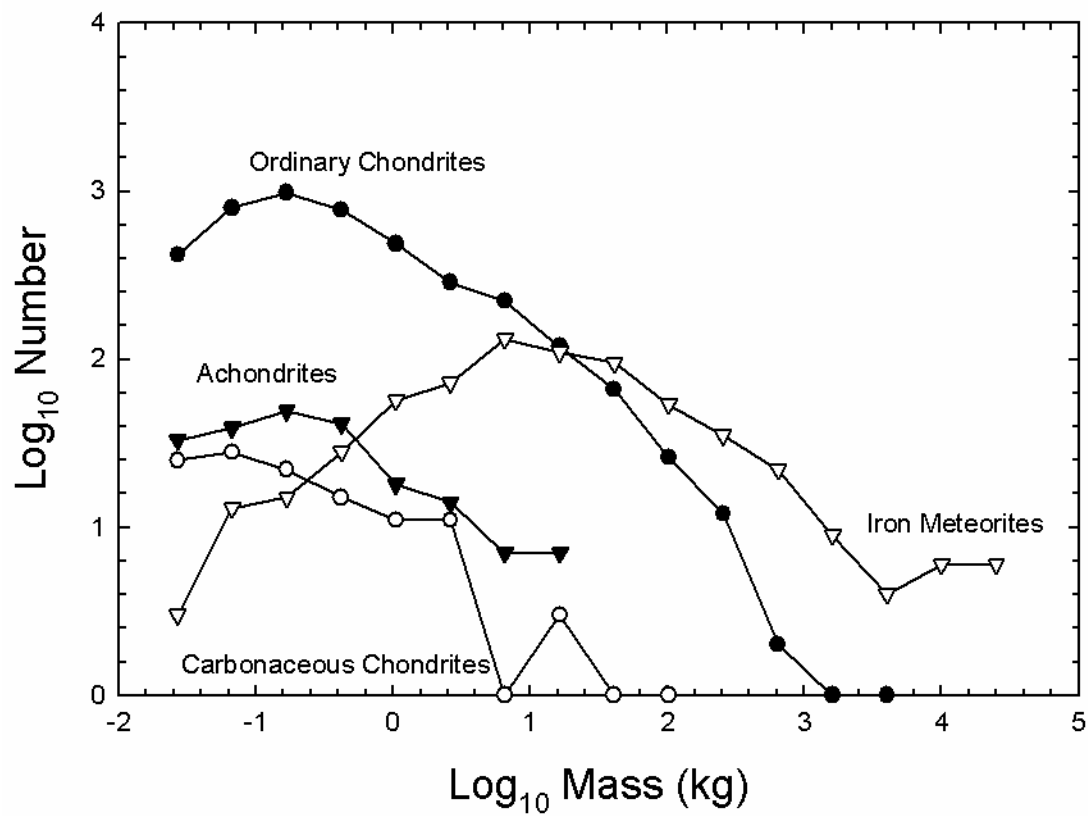
thus the net mass flux from these large falls per year is equivalent to the small mass flux per year. What is the reason for this difference in slope?

5.5.1.2 Amount that Reaches the Surface

The large impactor flux describes the total flux of mass that comes in during a large impact, and includes mass that is vaporized on impact. All of this mass delivers kinetic energy, and is thus part of the size vs. mass relationship for the craters described above. The meteorite mass vs. number relations are for the actual material that reaches the surface and can be collected.

Approximately 99% of carbonaceous chondrite material, 90% of stony material (Alexeev 2003), and 50% of iron material is vaporized / ablated before colliding with the surface of the Earth. Some of this material becomes IDP material, some is vaporized and condenses later. Some forms molten droplets, like the metallic shale around Meteor Crater, AZ, and the total mass of this material is estimated to be about 5% of the total initial impactor mass.

The amount of material lost is dependent on the strength of the object, the surface area of the object, and the mass/energy of the object. Stronger material tends to survive atmospheric entry, as evidenced by the smaller mass loss of iron meteorites. Material with a large surface area to volume ratio is ablated faster than more compact material. Large masses must lose more energy on impact with the Earth and hence more material

must be vaporized.  An accurate calculation of a combination of these factors could

rectify the two curves.

5.5.2 Biogenic Elements

IDP material brings in more reactive P and C than any other extraterrestrial material.

However, it is important to note that all of this mass is dispersed throughout the surface

of the Earth, so the flux of 132,000 kg of soluble C material actually becomes 0.3 g per

$km^2$, and P is actually 2 mg per $km^2$!  Meteorites and large impactors deliver much more

P and C to a much smaller region.

5.5.2.1 Example: Sikhote Alin

Consider the fall of the meteorite Sikhote Alin.  Sikhote-Alin fell in Novolpoltavka,

Russia in 1947.  It is a typical IIAB iron meteorite, and is the largest recovered meteorite

fall.  Approximately 23,000 kg of material fell in an area of ~0.66 $km^2$, pockmarking the

land with craters (Grady 2000 and references therein).  A fall of the size of Sikhote-Alin

happens once every 20 years or so.  The P abundance in this meteorite is ~0.42 weight

percent (Buchwald 1975 and refs. therein), on the lower end of iron meteorite P

abundances.  This meteorite provided a phosphide concentration of ~150 kg of P per $km^2$,

which is large compared to the IDP phosphorus in phosphide contribution of $2x10^{-6}$

kg/year/km$^2$. Thus the Sikhote-Alin fall contributed about 85 million years worth of background IDP reactive P to this locality.

A large, one million year, iron impactor would form a crater with a diameter of about 5 km, with an area of 16 km$^2$. Assuming ~5% of the P survives entry, this would amount to ~100,000 kg of reactive P per km$^2$. Such huge enrichments would have been moderately commonplace during the late heavy bombardment period, and one might expect several of these craters to form every 1,000 years.

## 5.5.2.2 Example: Murchison

Murchison, a carbonaceous CM chondrite, is one of the most organic-rich meteorites. Hundreds of organic compounds have been identified in extracts from this meteorite. Murchison fell in 1969 in Murchison, Victoria, Australia over an area of ~12.5 km$^2$ with a total recovered mass of 100 kg (Grady 2000 and refs therein). The total concentration of soluble organics is ~0.5-1 kg, giving a total organic concentration from this meteorite fall of 0.05 kg/km$^2$. Comparatively the IDP contribution is ~3 × 10$^{-4}$ kg/year/km$^2$. Murchison contributed an equivalent of ~200 years worth of organic compounds from IDPs from this fall. On average, carbonaceous chondrites contribute less than this, since Murchison is among the most soluble-carbon rich of all meteorites.

A large, one million year, cometary impactor would deliver ~30,000 kg of C per km$^2$, assuming a very generous survival of carbon compounds of 1%. Cometary impactors would probably not survive nearly as well as 1%, given the paucity of

carbonaceous meteorite material on the Earth. Most soluble carbon compounds would be volatilized or combusted during impact. A more likely estimate would probably be ~30-300 kg per $km^2$, nearly matching the IDP contribution rate during late heavy bombardment. Regardless, large cometary impactors are a proposed source of amino acids (Pierazzo and Chyba 1999) and may be a more significant source of some amino acids than the Miller-Urey (1953) process on the early Earth.

5.5.3 Consequences of Atmospheric Entry

The atmosphere affects organic compounds the most during the fall of a meteor. Carbon material that falls and is heated in an $O_2$ atmosphere loses most of its hydrogen and become less saturated, and causes organics to graphitize. Interplanetary dust particles with a mass greater than $10^{-5}$ g may be heated sufficiently to destroy most organics, especially amino acids, although some simple volatile organics, like glycine, can survive by sublimation and condensation (Glavin and Bada 2001).

Phosphorus in phosphides in the interior of an impactor will remain relatively unaffected if delivered to the surface of the Earth. Schreibersite is a relatively refractory mineral and would not be affected greatly by temperatures under 1000 K. Schreibersite on the surface of a meteor burns in a 1 bar $O_2$ atmosphere to form primarily PO (3000-5000 K), and $PO_2$ (1500-3000 K) gases, based on thermodynamic calculations of equilibrium.

5.6 Implications for the Origin of Life

Iron meteorites and large impactors deliver a significant quantity of reduced, reactive P to the surface of the Earth.  Much of this mass is concentrated in the impact crater, resulting in a huge local surplus of P.  Meteorites and large impactors are a comparatively poorer source of C to the surface of the Earth.  IDP material is a much larger, albeit dispersed, source of C for the Earth's surface.

5.6.1 Biomass Delivery

The present day biomass is $2\times10^{15}$ kg (Whittaker 1970).  During the late heavy bombardment, a biomass would have fallen to the Earth every few hundred thousand years.  This number differs from the value of 10 million years of Whittet (1997) mainly due to the assumption of a late heavy bombardment period versus the gradual drop off used by Whittet (1997) and Chyba and Sagan (1992).  Is this concentration enough to "jump-start" the origin of life?

5.6.2 The Importance of Crater Lakes

The following discussion is a speculative model of a crater.  It serves to emphasize the plausibility of an enrichment mechanism of organics and P due to the impact of a large body.

Biochemical synthesis of specific compounds typically takes place at concentrations of ~$10^{-4}$ M at the lowest (e.g., Nelson and Cox 2005). One would expect fluxes of organics and P in the global ocean during the late heavy bombardment to be $10^{-9}$ and $10^{-10}$ M per year, respectively (assuming present day ocean mass). At steady state, the concentration of these species would be:

$$[X] = \frac{F_{Year} \times t_{1/2}}{\ln 2} \tag{82}$$

where $F_{Year}$ is the flux of material $X$ per year, and $t_{1/2}$ is the chemical decay half life of the material. Assuming a fairly long half life of ~$10^4$ years, then the steady state concentration of these species may be as high as $10^{-5}$ M and $10^{-6}$ M. With more reasonable half lives of ~100 years, these numbers decrease significantly. However, what if local concentration mechanisms were at work?

Iron meteorites impact to form craters and greatly increase the local concentration of P (see Sikhote-Alin example above). What would happen if a large (1 million year) iron meteorite were to fall to the Earth, forming a crater? The formation of this crater was followed by accumulation of water, resulting in a small lake at the center of the crater. The drainage basin of the lake would equal the size of the crater. Assuming the crater-lake would be ~$1/10^{th}$ the total area of the crater, then the volume of this lake would be ~3,000,000 $m^3$, assuming a 2 m average depth for the lake. The reactive P concentration in this lake would be ~20 M. This is a maximum: the steady state concentration of P depended on the concentration of divalent alkaline earth elements like Ca and Mg, the corrosion rate of the meteorite, and the type of iron meteorite that fell. A

more reasonable estimate would be ~0.01 M, based on the corrosion experiments described in chapter 2.

During the late heavy bombardment, a flux of ~25 kg of soluble carbon material fell to the Earth per $km^2$ per year from IDPs alone, in addition to a similar or larger amount from endogenous synthesis. If the hypothetical crater lake described above has a corresponding drainage basin (as it would be the local low elevation point), then the soluble carbon concentration would be $10^{-6}$ M per $km^2$ of the drainage basin. The crater would be 10× the size of the lake, thus the organic concentration would be at least $10^{-5}$ M per year, excluding endogenous production. Assuming a chemical decay half life of ~100 years, then the total concentration of soluble organics would reach 0.001 M. Locally, this may be enough to kick life into gear.

In the hypothetical crater-lake above, one might expect to find a concentration of amino acids of 0.0001 M, carboxylic acids of 0.004 M, 0.00001 M of pyridine carboxylic acids, and 0.00001 M of N-heterocyclic compounds, and polyols at about 0.000004 M using the relative abundances from Cronin et al. (1988) and Cooper (2002). Carboxylic acids are used in construction of cellular membranes as lipids or in metabolism. Amino acids are used for the construction of proteins, N-heterocyclic compounds are used for replication, catalysis, and metabolism, and polyols (sugars) are used for structure, metabolism, and replication. Whether or not these concentrations would be enough will need to be explored by prebiotic chemists. Concentrations of $10^{-3}$ to $10^{-5}$ M are typical for the process of glycolysis, implying that these concentrations would still perform some chemistry (Nelson and Cox 2005 and refs therein). Phosphorus is central to all of these

functions (see chapter 1) and this environment may have provided the precursor

molecules necessary for life.

A crater-lake might also have the potential to stabilize these organics and

encourage polymerization. Borate minerals might be concentrated in the crater-lake

depending on the target/source rock mineralogy. Borate minerals stabilize ribose

(Ricardo et al. 2004), critical for the RNA-world. The crater-lake would have an excess

of P and a lot of iron, but the excess P as orthophosphate has the potential to remove $Ca^{2+}$

and $Mg^{2+}$ from water by precipitation of orthophosphate minerals. Keeping the

concentration of these ions low is beneficial as these ions may have been deleterious for

the organization of membranes and RNA synthesis (e.g., Monnard et al. 2002). A crater

lake would be a sufficiently low volume to allow for drying cycles which would have the

benefit of enabling polymerization by dehydration. Finally, iron metal may have served

as a food source for the early organisms. Even today, some microorganisms are able to

subsist on a diet of meteoritic iron (Gonzalez-Toril et al. 2005).

To summarize, a crater lake would be an advantageous location for the origin of

life for the following reasons: 1) high levels of reactive P if the crater formed through

impact of an metal body, 2) the drainage basin would accumulate organic compounds to

concentrations of $\sim 10^{-3}$ M or higher, depending on endogenous synthesis, 3) removal of

deleterious Ca and Mg, accumulation of borate stabilizing ribose, 4) potential for

polymerization through drying cycles, 5) a potential food source consisting of iron metal.

Naturally, many obstacles would have to be overcome, including the negative effects on

the surface of solar radiation and the fate of the microbes after the iron had completely

rusted away through oxidation.  Nevertheless, this speculative inquiry shows some benefits.

5.7 Comparison to Previous Calculations

*Extraterrestrial Flux Calculations*: The similarity between the slopes of the fall collection and the Antarctic find collection indicates that the mass vs. number relationships are sampling material whose major difference is the average size.  With the continuous collecting of meteorites from Antarctica, the Antarctic collection mass vs. number relations will approach the global fall mass vs. number relations.  This result is consistent with the calculations of Harvey and Cassidy (1989), Cassidy and Harvey (1991), Huss (1991), and Ikeda and Kimura (1992).  Similarly, the calculated mass vs. number slopes for meteorites ranges from -0.75 to -0.85 (Halliday et al. 1989, Harvey and Cassidy 1989, Cassidy and Harvey 1991, Huss 1991, and Ikeda and Kimura 1992), consistent with the ordinary chondrite slope calculations presented in table 31.

Iron meteorites are predicted to dominate the high mass fraction of meteorites. Previous approximations of total mass flux by meteorite type (Cassidy and Harvey 1991, Huss 1991) frequently omit large impactors like Sikhote-Alin, resulting in an overestimate of ordinary chondritic material flux.  However, estimates large impactor estimates (e.g., Bland and Artemieva 2003) support the dominance of metallic material for large masses.

*Element delivery*: This study quantified the flux of reactive C, P, and total Ir to the surface of the Earth. No previous study has rigorously quantified the flux of P to the surface of the Earth. This study agrees with prior studies (e.g. Anders 1989, Chyba and Sagan 1992) that carbonaceous meteorites were not a significant source of soluble carbon to the surface of the Earth. However, this study disagrees with the flux estimates of Kyte and Wasson (1986). Kyte and Wasson (1986) estimate the total flux of extraterrestrial material per year as $8 \times 10^7$ kg, whereas Love and Brownlee (1993) suggest a flux closer to $3 \times 10^7$ kg per year. The source of this discrepancy is an oversimplification made by Kyte and Wasson. Kyte and Wasson (1986) assume all the material that falls to the Earth is chondritic (0.6 ppm Ir), and neglect metallic material. Calculations with an Ir-enriched fraction (i.e., extraterrestrial metal) remove this discrepancy and bring the total flux closer to the Love and Brownlee (1993) calculated flux.

5.8 Conclusions

The mass flux of meteorites is highly dependent on composition. Despite the large number of ordinary chondrites falling to the Earth per year today, much of the mass of the material actually consists of differentiated core material, which produces spectacular large falls which may single-handedly deliver huge quantities of material to the Earth's surface. Most of the large impactors that collide with the Earth are iron meteorite material.

Interplanetary dust particles provide the vast majority of extraterrestrial carbon to the surface of the Earth. If the late heavy bombardment took place and if this event is scalable to IDPs, then a huge amount of carbon was delivered during this period of intense bombardment. Much of this material may have been soluble carbon species. Likewise, large impactors and iron meteorites delivered a significant quantity of reduced, reactive P to the surface of the early Earth. Locally, iron meteorites may have provided boosts of several million years (compared to steady state IDP fall) worth of P to single locations.

Were a lake to have formed in a crater caused by the fall of a large iron meteorite, the situations may have been ideal for the origin of life. The crater-lake would have provided a source of P, and exogenous and endogenous carbon species would have drained to the center of the lake, perhaps enabling the synthesis of precursor biomolecules including phosphorylated compounds.

CHAPTER 6

SULFUR CHEMISTRY WITH TIME-VARYING OXYGEN ABUNDANCE DURING
SOLAR SYSTEM FORMATION

6.1 Introduction

Sulfur is a biogenic element that has been implicated in several origins of life processes

(e.g., Wachterhauser 1988; Cody 2004). Sulfides are an abundant constituent of

meteoritic material, and understanding the cosmochemical behavior of sulfur is critical to

an evaluation of the influence of meteorites to the origin of life. The work discussed

below is reproduced from Pasek *et al.* (2005).

The importance of water as a condensable and chemically active species in

protoplanetary disks has long been emphasized in planetary literature. The time-varying

location at which water is saturated in a formal thermodynamic sense—"the snow line"

—can be considered the dividing line not only between the inner and outer solar system

but also between the solar nebula of the meteoriticist and that of the planetary astronomer

(Lunine *et al.* 2000). Understanding the coupling between rocky and icy solids has been

difficult for several reasons. Primitive meteorites do not contain water ice or other more

volatile species. Our knowledge of the presence of meteoritic water is limited to the

identification of mineralogic changes in primitive meteorites due to aqueous alteration

from water resulting from the melting of icy material on a meteorite's parent body. In

addition, astronomical observations of comets have not simultaneously tracked

abundances of both silicates and ices. Here we attempt to bridge some of these gaps by

investigating the influence of diffusive water vapor redistribution to the snow line in the early solar system on the major-element chemistry of the inner solar nebula.

This work has important implications for the composition of planetary bodies on both sides of the snow line. The Galileo probe measurements of elemental abundances in Jupiter include sulfur as well as noble gases, carbon, nitrogen, and oxygen, which, unfortunately, is drastically affected by meteorology (Atreya *et al.* 2003). These elemental abundances constrain the mechanisms by which Jupiter acquired its inventory of heavy elements ($Z > 2$), which are well above solar abundance inside all the giant planets. To understand how these abundances relate to the composition of planetesimals that fed Jupiter requires considering processes in both the inner and outer solar system and considering the interaction between dynamics and chemistry. Indeed, as we show in the present paper, oxygen (water) and sulfur-bearing compounds cannot be considered apart from each other, because the chemistry of sulfur and hence the abundance of its principal volatile molecular form, hydrogen sulfide, is greatly affected by the oxygen abundance. Furthermore, observations of circumstellar disks suggest that sulfur is depleted in the gas phase relative to cosmic abundance. That is, $H_2S$ is not the only or even the primary sulfur-bearing species in these disks. These observations suggest that refractory phases contain much of the sulfur in these environments (Dutrey *et al.* 1997).

The present paper quantifies, in more detail than previous work, the chemistry of sulfur-bearing phases in a solar-abundance protoplanetary disk model. However, it goes a step further by examining the sulfur chemistry under various oxygen fugacities in the inner solar nebula (within 5 AU), which result from the time-variable water vapor

abundance inward of a cold-trapping condensation front in the disk (Morfill and Volk 1984). Water is moved from sunward of the snowline out to the condensation front as a result of diffusion driven primarily by radial concentration gradients. Using a simple model of nebular dynamics, we show how the oxygen-dependent chemistry and laboratory based reaction kinetics can explain a depletion of hydrogen sulfide in the disk. Such a depletion may in turn be reflected in the elemental abundance pattern constrained in Jupiter by the Galileo Probe.

Section 6.2 of the paper describes the nebular model we use to determine the temperature and pressure with respect to time, while section 6.3 details the chemical equilibrium codes used. In section 6.4 we consider the coupled effects of the sulfur chemistry, the reaction kinetics, and the changing oxygen abundance due to nebular water transport and condensation on the abundances of the primary sulfur-bearing species. The results are relevant to meteorites, circumstellar disks, and the elemental abundances in Jupiter, as discussed in the final section.

6.2 Nebular Model

To properly evaluate the changing chemistry in the disk, we need a time-dependent model of the solar nebula which gives us the pressure and temperature at each radius as a function of time. In this paper, we use the two-dimensional steady state disk solutions of Huré (2000) as they have been applied by Hersant *et al.* (2001). Other models of the solar nebula produce qualitatively similar results (Cassen 2001). These axisymmetric

disk solutions use an $\alpha$ viscosity (see e.g. Shakura and Sunyaev 1973) and they include

the effects of turbulent pressure, convection, and self-gravity. To use these steady state

solutions, we must know the accretion rate onto the Sun as a function of time. In these

calculations, the accretion rate onto the Sun is described by a power law (see Makalkin

and Dorofeyeva 1991)

$$\dot{M}(t) = \dot{M}_0 \, (1 + t/\tau)^{-s} \tag{96}$$

In this equation, $t$ is the time after the Sun is almost completely formed.  Hence, this

equation describes the quiescent period of the nebula in which the nebula cools as time

passes and the accretion rate onto the Sun continuously drops.  $\dot{M}_0$ is the accretion rate at

$t = 0$ and $\tau$ is the accretion timescale,

$$\tau = \frac{R_{D0}^2}{3 v_{D0}} \tag{97}$$

where $R_{D0}$ is the initial outer radius of the disk and $v_{D0}$ is the turbulent viscosity at $R_{D0}$ at

$t = 0$. As in Drouart *et al.* (1999), we use $s = 1.5$ for the power law exponent. This power

law decay of the accretion rate is consistent with observations of T Tauri stars (see

Hartmann *et al.* 1998).

Note that while the disk solutions of Huré (2000) are infinite in extent, these disks

must be finite so they are cut off at $R_{D0}$ at $t = 0$. As time passes, the disk expands due to

the redistribution of angular momentum in the viscous disk so the outer radius of the disk

increases with time.

In this scenario, $\dot{M}_0$, $R_{D0}$, and $\alpha$ are all variable parameters.  We follow the work

of Hersant *et al.* (2001) which constrains these parameters using four criteria. First, the

total disk mass must be large enough to form all the planets but $\leq 0.3$ M$_\odot$ so that the disk

is not gravitationally unstable (Shu *et al.* 1990). Second, angular momentum must have

been transported outward to where Neptune would form in $2.5 \times 10^5$ years so that icy and

rocky grains could decouple from the gas and ultimately form the core of Neptune. Third,

the temperatures inside $3AU$ must be $\geq 1000$K at early times in the nebula evolution in

order to explain the crystalline silicate distributions in meteorites and comets (see

Bockelée-Morvan *et al.* 2002). Lastly, the nebula model must yield deuterium

enrichments in the planets and meteorites consistent with observations. Hersant *et al.*

(2001) find that there exists a range of acceptable disk solutions which satisfy these

criteria. Specifically, they conclude that $0.006 \leq \alpha \leq 0.04$, $12.8AU \leq R_{D0} \leq 39AU$ and 2.2

$\times 10^{-6}$ M$_\odot$/year $\leq \dot{M}_0 \leq 1 \times 10^{-5}$ M$_\odot$/year.

From these acceptable models, they define a "nominal" model which has $\dot{M}_0 = 5$

$\times 10^{-6}$ M$_\odot$/year, the dimensionless parameter $\alpha = 0.009$ and $R_{D0} = 17AU$. This model

yields an initial disk mass of 0.24 M$_\odot$. In this paper, we focus our chemical calculations

on this "nominal" model. The pressures and temperatures needed as input to our chemical

equilibrium codes (see section 6.3) are the midplane pressures and temperatures in this

"nominal" time-dependent two-dimensional disk model. In figure 43, we plot the

midplane temperature in this nominal model versus radius for four different times. While

focusing on the nominal model, we also investigated the sulfur chemistry using other

models which satisfied their four criteria. Specifically, we also used the "warm" and

"cold" models defined in table 2 of Hersant *et al.* (2001). These models are, on average,

warmer (or colder) than the nominal model throughout the disk at a fixed time. The

Figure 43. Graph showing the time dependence of temperature versus radial distance in the "nominal" solar nebula model from Hersant *et al.* (2001). The dashed and dotted curves represent the time zero distribution in their "warm" and "cold" models for comparison.
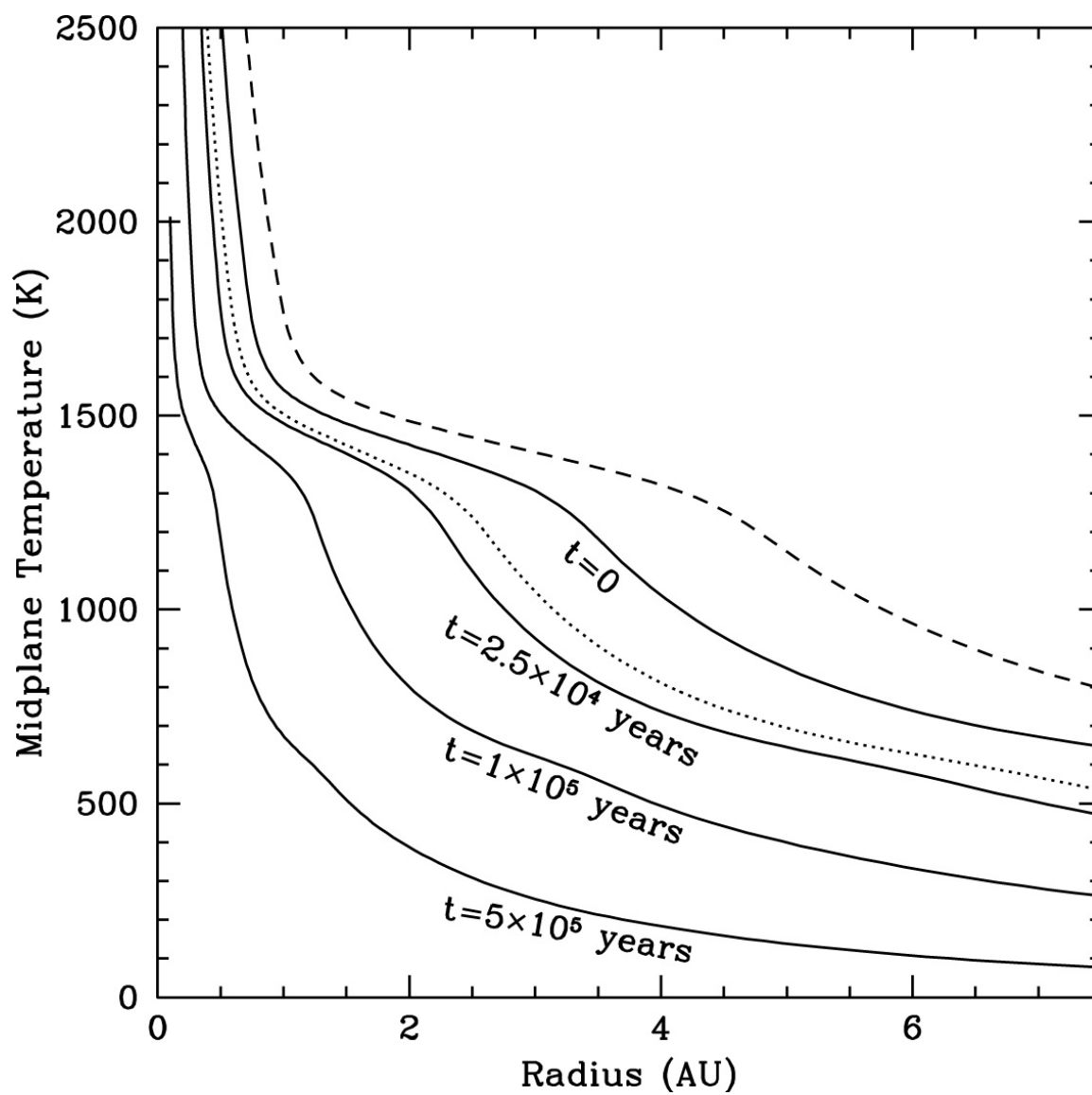
difference between the warm, cold and nominal models is illustrated in figure 43 for time
zero. Additional plots of the structure of these nebulae can be found in Hersant *et al.*
(2001).

6.3  Description of Chemical Equilibrium Codes

We used two different chemical equilibrium codes to determine the abundances of sulfur
species in the solar nebula.  For both codes we use a pressure-temperature profile defined
from the nebular model described in section 6.2.  The use of two distinct chemical
equilibrium codes with slightly different thermodynamic databases provides an internal
check on the results. We now describe each of the codes in detail.

We use a modified version of the SOLGASMIX code (Bessman 1977) which is
described in Sharp & Huebner (1990 & 1993) and Burrows & Sharp (1999).  The original
version of SOLGASMIX was obtained from the Los Alamos National Laboratory in the
mid 1980s.  It was written for a maximum of ten chemical elements and a limited number
(less than about 50) of different chemical species.  In addition to gaseous species, it has
the capability of handling condensed phases and solutions and it was originally intended
for chemical engineering calculations.  The abundances of all the gaseous and condensed
phase species were calculated by minimizing the total Gibbs free energy of the system.
However, the maximum number of species the code could handle was far too small for
realistic astrophysical calculations.  Among a considerable number of enhancements
made to the code over a period of time, the limit of the maximum number of elements

was increased to 40 and the total number of species was increased to 1000.  For

calculations described here, as in Burrows and Sharp (1999), we use only gas phase and

solid species with no solid solutions.

SOLGASMIX uses the White *et al.* (1958) algorithm in which the total

dimensionless Gibbs free energy of the system is minimized using the method of

Langrange undetermined multipliers (Eriksson and Rosé 1973).  The calculations are

subject to the constraint that the total number of atoms of each element is conserved. The

activity of a gas phase species is its partial pressures in atmospheres, and the activity of a

condensate is unity (for calculations and the method of approach, see Sharp and Huebner

1990).

The chemical database for this code has been updated for this work to account for

previous errors and to include critical sulfur and oxygen species and compounds that

become important at increased C/O ratios. Specifically, we include updated data for

gaseous PH, $PH_3$, PN and solid $Mg_3(PO_4)_2$ from Lodders (1999). This corrects for errors

in the JANAF tables (Chase 1982 and 1998). We also correct for an error in the JANAF

table for gaseous HS using data from Barin (1995).  We include the following sulfur

species which were not previously in the database: gaseous $Al_2S$ and $AlS_2$ (Gurvich *et al.*

1994), solid $FeCr_2S_4$ (Petaev *et al.* 1986), solid $CaSO_4$ and $(NH_4)_2SO_4$ (Barin 1995), solid

and gaseous TiS (Barin 1995) and solid CrS (Barin 1995). We also include data from

Barin (1995) for the solids Cr, CrN, $Cr_2N$, $Cr_2O_3$, $TiO_2$, $Ti_2O_3$, $Ti_3O_5$, $Ti_4O_7$, $Fe_3C$, $Al_2O_3$,

CaO, $CaAl_2Si_2O_8$, $CaAl_4O_7$, $CaAl_2O_4$, $CaTiO_3$, $Ca_4Ti_3O_{10}$, $Ca_3Ti_3O_7$, $FeSiO_3$, $MgTiO_3$,

$Mg_2TiO_4$, $MgTi_2O_5$, $MnSiO_3$, $Mn_2SiO_4$, $FeCr_2O_4$, and for the gas phase species CaH,

$TiO$, $CrO$, $CrO_2$ and $CrO_3$. Some of these species were already in the database but were updated for consistency. Additionally, we have included solid $Fe_3P$ from Knacke *et al.* (1991) and solid $CaAl_{12}O_{19}$ from Hallstedt (1990). Lastly, we have included gaseous CrH from Burrows (private communication), gaseous FeH based on spectroscopic data in Dulick *et al.* (2003), gaseous TiH from Bernath (private communication) and gaseous MgH based on spectroscopic data in Weck *et al.* (2003). As no thermodynamic data were readily available for these four metal hydrides, the thermodynamic data are calculated from the dissociation potentials and partition functions, which are in turn calculated from asymptotic formulae for the vibrational and rotational constants of each electronic state (Kassel 1933a&b).

We also performed calculations using the equilibrium module in the HSC Chemistry (v5.1) software package (Outokumpu Research Oy, Finland). This code uses the GIBBS energy minimization equilibrium solver (White *et al.*, 1958). For the purposes of these calculations, all solutions were assumed to be ideal (i.e., $\gamma = 1$). The thermodynamic database provided with this code is frequently updated. Most of the species considered in the SOLGASMIX chemical code were also considered in the HSC5 code, although with a few notable distinctions. Ar gas and Mn- and Co-bearing species were omitted from the calculations, as their inclusion resulted in instability with the code, mainly due to limitations in the code on the number of total elements allowed for calculation. Fortunately, these elements are in low enough abundance that their exclusion does not affect sulfur chemistry. However, fluorine-bearing gases and condensates were included, unlike in the SOLGASMIX code. The thermodynamic data for the species

shown in tables 35 and 36 are available in the thermodynamic database of the code, with the exception of $Fe_3P$, the data for which are found in Zaitsev *et al.* (1995) and $Fe_3C$, the data for which are in Barin (1995).

The elemental abundances from Grevesse & Sauval (1998) were used in these calculations, with several exceptions.  Corrections to Grevesse & Sauval's (1998) values for oxygen and carbon come from Prieto *et al.* (2001 & 2002).  Table 34 lists the standard solar elemental abundances used in the calculations. Tables 35 and 36 list the chemical species used in each code.

All the calculations described in this paper have been performed using both codes. In all cases, the results from both codes are similar.  To illustrate the similarity of the codes, we present the condensation sequence at a pressure of $1 \times 10^{-6}$ bars (table 37) with solar abundances using both codes and also compare the results to Yoneda and Grossman (1995).  In particular, the species $Al_2O_3$, $Mg_2SiO_4$, Fe, $MgSiO_3$, FeS, and the feldspars ($NaAlSi_3O_8$, and $KAlSi_3O_8$) are all in relative agreement.  Most of the differences between the two codes are due to solid solution assumptions.  The condensation sequence generated by the HSC code at $10^{-5}$ bar (figure 44) is in agreement with prior calculations (Wood and Hashimoto 1993). The graphical results we present in figure 46 are those obtained using the SOLGASMIX code.

Table 34. Solar abundances used, taken from Grevesse and Sauval (1998) and Prieto *et al.* (2001, 2002). The values are normalized to 1 mole total.

| Element | Abundance |
|---------|-----------|
| H | $9.10 \times 10^{-1}$ |
| He | $8.89 \times 10^{-2}$ |
| O | $4.46 \times 10^{-4}$ |
| C | $2.23 \times 10^{-4}$ |
| Ne | $1.09 \times 10^{-4}$ |
| N | $7.57 \times 10^{-5}$ |
| Mg | $3.46 \times 10^{-5}$ |
| Si | $3.30 \times 10^{-5}$ |
| Fe | $2.88 \times 10^{-5}$ |
| S | $1.44 \times 10^{-5}$ |
| Al | $2.81 \times 10^{-6}$ |
| Ar | $2.29 \times 10^{-6}$ |
| Ca | $2.04 \times 10^{-6}$ |
| Na | $1.90 \times 10^{-6}$ |
| Ni | $1.62 \times 10^{-6}$ |
| Cr | $4.46 \times 10^{-7}$ |
| P | $3.30 \times 10^{-7}$ |
| Mn | $3.08 \times 10^{-7}$ |
| Cl | $1.73 \times 10^{-7}$ |
| K | $1.23 \times 10^{-7}$ |
| Ti | $7.93 \times 10^{-8}$ |
| Co | $7.40 \times 10^{-8}$ |
| F | $2.75 \times 10^{-8}$ |

Table 35. Gaseous species used- first column is SOLGASMIX code, second is HSC5.

| | | | | | |
|---|---|---|---|---|---|
| Al | Al | $CrO_3$ | $H_2$ | NaCN | PN |
| $Al_2O$ | $Al_2O$ | Fe | $H_2O$ | NaH | PO |
| $Al_2S$ | $Al_2S$ | FeH | $H_2S$ | NaO | PS |
| AlH | AlH | FeO | $H_2SO_4$ | NaOH | S |
| AlO | AlO | FeS | HCl | Ne | $S_2$ |
| $AlO_2$ | $AlO_2$ | H | HCN | Ni | $S_2O$ |
| AlOH | AlOH | $H_2$ | HCO | $Ni(CO)_4$ | SN |
| AlS | AlS | $H_2O$ | HF | NiCl | SO |
| $AlS_2$ | $AlS_2$ | $H_2SO_4$ | HNO | $NiCl_2$ | $SO_2$ |
| Ar | C | $H_2S$ | HOCl | NiH | Si |
| C | $C_2H_2$ | HCl | HS | NiO | SiC |
| $C_2H_2$ | $C_2H_4$ | HCN | He | NiS | SiH |
| $C_2H_4$ | $C_2H_6$ | HCNO | K | O | $SiH_2$ |
| $C_2H_4O$ | $C_3H_8$ | HCO | KCl | $O_2$ | $SiH_3$ |
| $C_4N_2$ | $C_4N_2$ | HNO | KCN | OH | $SiH_4$ |
| $CCl_2$ | $CCl_2$ | HOCl | KH | P | SiN |
| CH | CH | HS | KOH | $P_4O_6$ | SiO |
| $CH_2$ | $CH_2$ | He | Mg | PH | SiS |
| $CH_2O$ | $CH_2O$ | K | MgH | $PH_2$ | Ti |
| $CH_3$ | $CH_3$ | $K_2SO_4$ | MgS | $PH_3$ | TiCl |
| $CH_4$ | $CH_4$ | KCl | $N_2$ | PN | $TiCl_2$ |
| CN | CN | KCN | $N_2H_2$ | PO | TiN |
| CO | CO | KH | $N_2O$ | PS | TiO |
| $CO_2$ | $CO_2$ | KOH | NH | S | $TiO_2$ |
| COS | COS | Mg | $NH_2$ | $S_2$ | TiS |
| CP | CP | MgH | $NH_3$ | $S_2O$ | |
| CS | CS | MgS | NO | SN | |
| $CS_2$ | $CS_2$ | MnH | $NO_2$ | SO | |
| Ca | Ca | MnO | Na | $SO_2$ | |
| CaH | CaH | MnS | NaCl | Si | |
| CaOH | CaOH | N | NaCN | SiC | |
| CaS | CaS | $N_2$ | NaH | SiH | |
| Cl | Cl | $N_2H_2$ | NaO | SiO | |
| $Cl_2$ | $Cl_2$ | $N_2O$ | NaOH | SiS | |
| ClO | ClO | NCO | Ne | Ti | |
| Co | Cr | NH | Ni | $TiC_2$ | |
| CoCl | CrH | $NH_2$ | NiS | $TiC_4$ | |
| $CoCl_2$ | CrN | $NH_3$ | $O_2$ | TiCl | |
| $CoCl_3$ | CrO | NO | OH | $TiCl_2$ | |
| Cr | $CrO_2$ | $NO_2$ | P | TiH | |
| $CrC_2$ | $CrO_3$ | Na | $P_2$ | TiN | |
| CrH | F | $Na_2Cl_2$ | $P_4O_6$ | TiO | |
| CrN | $F_2$ | $Na_2O_2H_2$ | PH | $TiO_2$ | |
| CrO | Fe | $Na_2SO_4$ | $PH_2$ | TiS | |
| $CrO_2$ | H | NaCl | $PH_3$ | | |

Table 36. Solid species used- first column is SOLGASMIX code, second is HSC5.

| | | | |
|---|---|---|---|
| $Al_2O_3$ | $Al_2O_3$ | $K_2SO_4$ | $Mg_2SiO_4$ |
| $Al_2SiO_5$ | $Al_2S_3$ | $KAlSi_3O_8$ | $MgAl_2O_4$ |
| $Al_6Si_2O_{13}$ | AlN | KCl | MgS |
| AlN | C | $Mg_2SiO_4$ | $MgSiO_3$ |
| C | $Ca_2Al_2SiO_7$ | $Mg_2TiO_4$ | $(NH_4)_2S$ |
| $Ca_2Al_2SiO_7$ | $Ca_2MgSi_2O_7$ | $Mg_3(PO_4)_2$ | $Na_2S$ |
| $Ca_2MgSi_2O_7$ | $Ca_3(PO_4)_2$ | $MgAl_2O_4$ | $Na_2SiO_3$ |
| $Ca_3(PO_4)_2$ | $Ca_4Ti_3O_{10}$ | MgS | $NaAlSi_3O_8$ |
| $Ca_3Ti_2O_7$ | $Ca_5(PO_4)_3F$ | $MgSiO_3$ | NaCl |
| $Ca_4Ti_3O_{10}$ | $Ca_5(PO_4)_3OH$ | $MgSO_4$ | Ni |
| $CaAl_{12}O_{19}$ | $CaAl_{12}O_{19}$ | $MgTi_2O_5$ | NiS |
| $CaAl_2O_4$ | $CaAl_2O_4$ | $MgTiO_3$ | P |
| $CaAl_2Si_2O_8$ | $CaAl_2Si_2O_8$ | Mn | $Si_2N_2O$ |
| $CaAl_4O_7$ | $CaAl_2SiO_6$ | $Mn_2SiO_4$ | SiC |
| $CaMgSi_2O_6$ | $CaAl_4O_7$ | MnO | SiS |
| CaO | $CaFe(SiO_3)_2$ | $MnSiO_3$ | $SiS_2$ |
| CaS | $CaMgSi_2O_6$ | $Na_2S$ | Ti |
| $CaSiO_3$ | CaS | $Na_2SiO_3$ | $Ti_4O_7$ |
| $CaSO_4$ | $CaSiO_3$ | $Na_2SO_4$ | TiC |
| $CaTiO_3$ | $CaTiO_3$ | $NaAlSi_3O_8$ | TiN |
| Co | Cr | NaCl | |
| $Co_3O_4$ | $Cr_2FeO_4$ | $(NH_4)_2SO_4$ | |
| $CoCl_2$ | $Cr_2O_3$ | Ni | |
| CoO | CrN | $Ni_3S_2$ | |
| $CoSO_4$ | $CrO_2$ | $Ni_3S_4$ | |
| Cr | CrS | $NiCl_2$ | |
| $Cr_2N$ | Fe | $NiCr_2O_4$ | |
| $Cr_2O_3$ | $Fe_3C$ | NiS | |
| CrN | $Fe_{0.947}O$ | $NiS_2$ | |
| $CrO_2$ | $Fe_2O_3$ | $P_4O_{10}$ | |
| CrS | $Fe_2SiO_4$ | $Si_3N_4$ | |
| Fe | $Fe_3O_4$ | SiC | |
| $Fe_2(SO_4)_3$ | $Fe_3P$ | Ti | |
| $Fe_2SiO_4$ | $Fe_3Si$ | $Ti_2O_3$ | |
| $Fe_3C$ | FeS | $Ti_3O_5$ | |
| $Fe_3O_4$ | $FeS_2$ | $Ti_4O_7$ | |
| $Fe_3P$ | FeSi | TiC | |
| $FeCr_2O_4$ | $FeSi_2$ | $TiCl_2$ | |
| $FeCr_2S_4$ | $FeSiO_3$ | TiN | |
| FeO | $FeTiO_3$ | TiO | |
| FeS | $H_2O$ | $TiO_2$ | |
| $FeSiO_3$ | $K_2S$ | | |
| $FeSO_4$ | $KAlSi_3O_8$ | | |
| $K_2S$ | KCl | | |

Table 37. Comparison between condensation temperatures at $10^{-6}$ bars and solar abundances from SOLGASMIX (first column), and HSC5 (fourth column) and Ebel and Grossman 2000 (fifth column). Ebel and Grossman did not extend their calculations below 1000 K, and included only more abundant oxide and silicate species.

| Temperature (K) | Compound | | Temperature (K) | E&G 2000 |
|---|---|---|---|---|
| 1542 | $Al_2O_3$ | Appears | 1535 | 1570 |
| 1484 | $Al_2O_3$ | Disappears | 1501 | 1470 |
| 1230 | $Mg_2SiO_4$ | Appears | 1228 | 1240 |
| 1201 | Fe | Appears | 1201 | 1210 |
| 1179 | $MgSiO_3$ | Appears | 1208 | 1190 |
| 1117 | $Cr_2O_3$ | Appears | 1091 | 1091 |
| 1114 | $Fe_3P$ | Appears | 1153 | |
| 889 | $Cr_2O_3$ | Disappears | 866 | |
| 889 | $FeCr_2O_4$ | Appears | 866 | |
| 815 | $KAlSi_3O_8$ | Appears | 805 | |
| 810 | $NaAlSi_3O_8$ | Appears | 832 | |
| 691 | FeS | Appears | 689 | |
| 632 | $Ca_3P_2O_8$ | Appears | 723 | |
| 632 | $Fe_3P$ | Disappears | 723 | |

Figure 44. Equilibium condensation sequence for a system at $10^{-5}$ bar and solar abundance. Legends follow Wood and Hashimoto (1993).
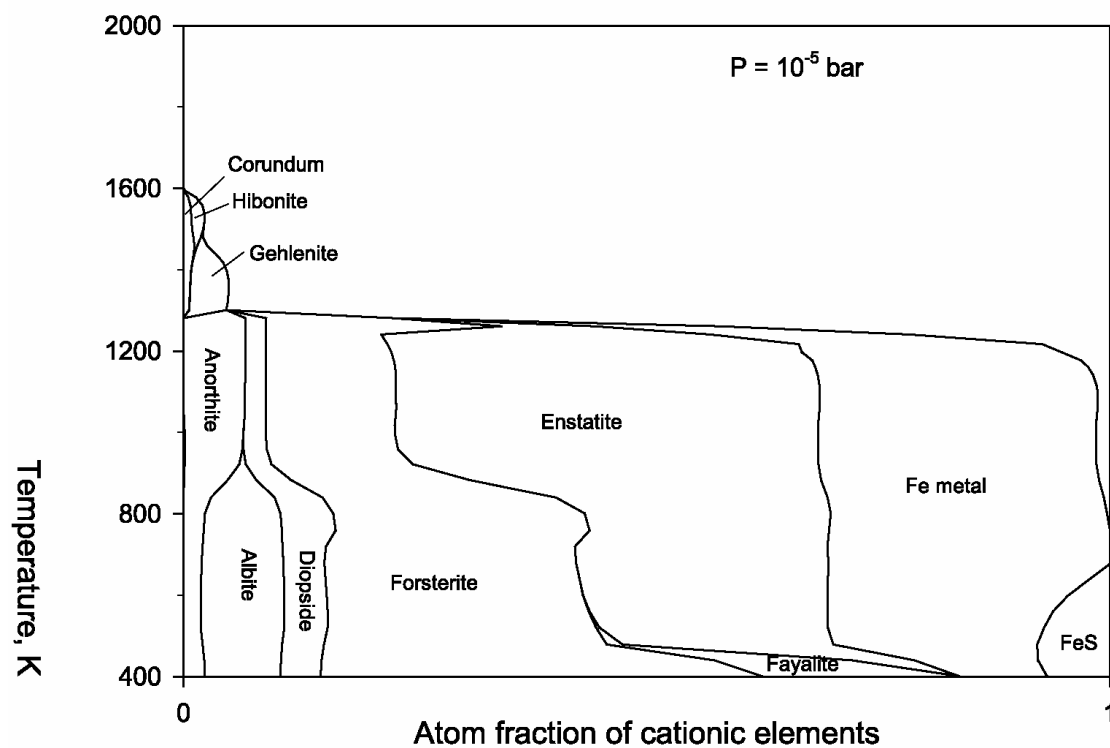
6.4. Sulfur Chemistry Results

6.4.1  Chemical Equilibrium Calculations

We use the time-dependent disk model and the equilibrium codes described in section 6.3 to determine the locations of condensation fronts in the solar nebula.  A set of calculations was performed to determine equilibrium chemistry at the beginning of the quiescent stage of nebular evolution (time zero), when the inner regions of the disk were quite hot.  We restricted our calculation to regions for which T < 2500K, where ionization effects are negligible.  At time zero, this temperature occurs at a distance of 1 AU.  The condensation fronts migrate inward as time passes and the disk cools (figure 45). Troilite and $H_2S$ are the major sulfur-bearing solid and gas species, respectively, and HS, SiS, S, PS, $S_2$, and AlS are additional minor gas species at all stages of disk evolution with solar compositions.  The ice condensation front is located at 5 AU after $\sim 4.4 \times 10^5$ years of disk evolution. The troilite condensation front is always ahead of that for water ice and reaches the inner regions of the nebula (r < 5 AU) in less than $1 \times 10^5$ years.

Recent work suggests that large variations in major element chemistry may have occurred in the solar nebula. In particular, Cyr *et al.* (1998, 1999) suggest that the oxygen abundance in the inner nebula was depleted relative to solar as a result of diffusive water vapor redistribution, which is thought to overwhelm the inward drift of ice particles. The depletion of water vapor results in reduced oxygen abundances in the inner region of the nebula (dashed curves in figure 45) and affects the locations of these two condensation

Figure 45. The locations of condensation fronts of troilite and water ice with respect to time. Note that these condensation fronts use the condensation temperature at the start of condensation, not the 50% condensation temperature. As the early solar nebula cooled, the condensation fronts of both sulfur and water moved inwards. The locations of both fronts are dependent upon oxygen fugacity, as shown by the separate lines drawn for lower oxygen fugacities. With an oxygen removal greater than 30%, water ceases to appear in our calculations, and with an oxygen removal greater than 15%, troilite no longer condenses. Here we have shown the lower limits of the stability of these compounds.
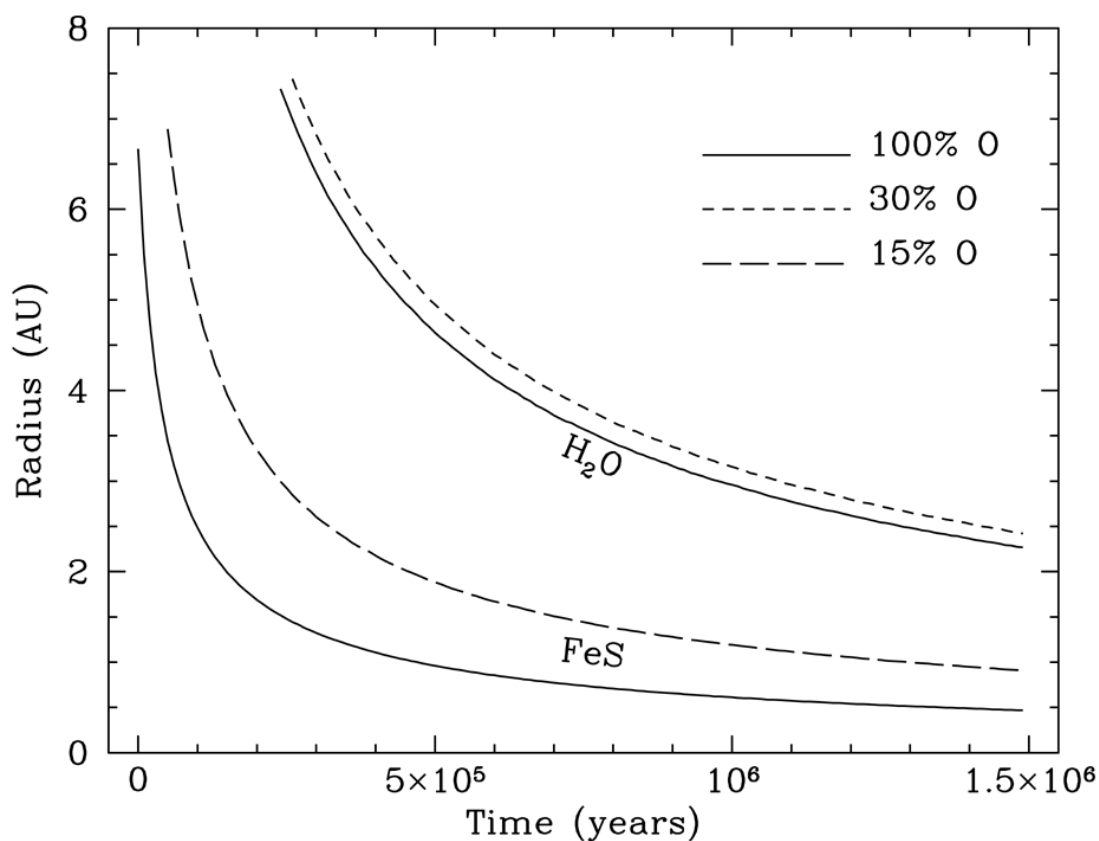
fronts. Gases other than water (like $CO_2$, $CH_4$, and CO) do not diffuse outwards as a result of the removal of water vapor, thus the amount of carbon in the system remains constant relative to a depletion in oxygen. These gases (CO, $CH_4$, and $CO_2$) condense at temperatures significantly lower than the water condensation point (i.e. their "sinks" occur further out in the radius of the nebula), thus diffusion is less significant because of lower concentration and temperature gradients. It is true that a minor pressure gradient will result from the removal of $H_2O$ vapor; however, the abundance of $H_2$ and He gases remain unaffected by water vapor redistribution and it is these gases that determine the total pressure of the nebula. Condensation of graphite may hypothetically occur as a result of the depletion of oxygen. However, our code assumes that any graphite that forms is in contact with the other equilibrium phases and is thus not removed from the system (i.e. in full equilibrium). In addition, the kinetics for the formation of graphite depend largely on the gaseous abundance of long chains of carbon (Salpeter 1974) and our equilibrium calculations and those of Larimer and Bartholomay (1979) do not suggest the abundance of these chemicals. These molecules are mainly a result of disequilibrium processes, thus the majority of C remains in the gaseous phase as $CH_4$. As a result, the C/O ratio resulting from the depletion of water remains dependent only on the amount of water removed from the system.

Our equilibrium calculations indicate that the condensation temperature for troilite is 690K for oxygen abundances above 25% of the solar oxygen abundance (or equivalently *C/O = 2*). The equilibrium constant for the troilite formation reaction,

$$Fe + H_2S\ (g) \rightarrow FeS + H_2\ (g) \tag{98}$$

is pressure independent since the number of moles of gas is the same on each side of the reaction. For lower oxygen abundances (or higher C/O ratios), the troilite condensation temperature drops because other sulfur species become more stable (specifically solid MgS). Figure 45 illustrates the effects of extreme oxygen depletion (15% solar O abundance or equivalently *C/O = 3.33*) on the location of troilite condensation front. In this case, the troilite condensation temperature varies between 400K (at a pressure of 5.6 $\times$ 10$^{-7}$ bars) at early times to 417K (at a pressure of 2.7 $\times$ 10$^{-6}$ bars) at later times. For oxygen abundances of <12.5-15% in a solar-composition gas (*C/O* $\geq$ 3.5-4), troilite is not present in an equilibrium mixture and MgS is the primary S-bearing solid.

The condensation temperature of water changes only slightly when the oxygen abundance is reduced. Under solar abundance conditions, the condensation temperature of ice varies between 151 K and 155 K. For cases where the O abundance is 30% solar (*C/O* = 1.66) as in figure 45, the ice condensation temperature varies from 143 K to 146 K. If the oxygen abundance is $\leq$25-30% solar (*C/O* $\geq$ 1.66-2), H$_2$O solid does not appear in an equilibrium mixture since all the oxygen is in the magnesium silicates (MgSiO$_3$ and Mg$_2$SiO$_4$). These calculations show that the temperature of ice condensation is relatively insensitive to the bulk O abundance.

The overall effect of depleted water on sulfur chemistry is illustrated in figure 46, in which we show the distribution of sulfur species in the nebula at t = 5 $\times$ 10$^5$ years for a range of radii and for four different oxygen fugacities. The vertical axis is effectively the log of the mixing ratio of that species since $N_{total}$ represents the total number of gas

Figure 46.  Graph showing the dependence of major sulfur-bearing species on relative oxygen abundance at a time of $5 \times 105$ years.  As oxygen is removed from the system (B, C, and D), SiS and MgS become the dominant S-bearing gas and solid respectively.  For reference, the temperatures in each panel at 0.5AU, 1.0AU, 1.5AU, 2.0AU, 2.5AU and 3.0AU are respectively 1180 K, 672 K, 509 K, 387 K, 308 K and 253 K.   A.)  100% of the initial oxygen.  B.) 33% of the initial oxygen.  C.)  20% of the initial oxygen.  D.) 10% of the initial oxygen.
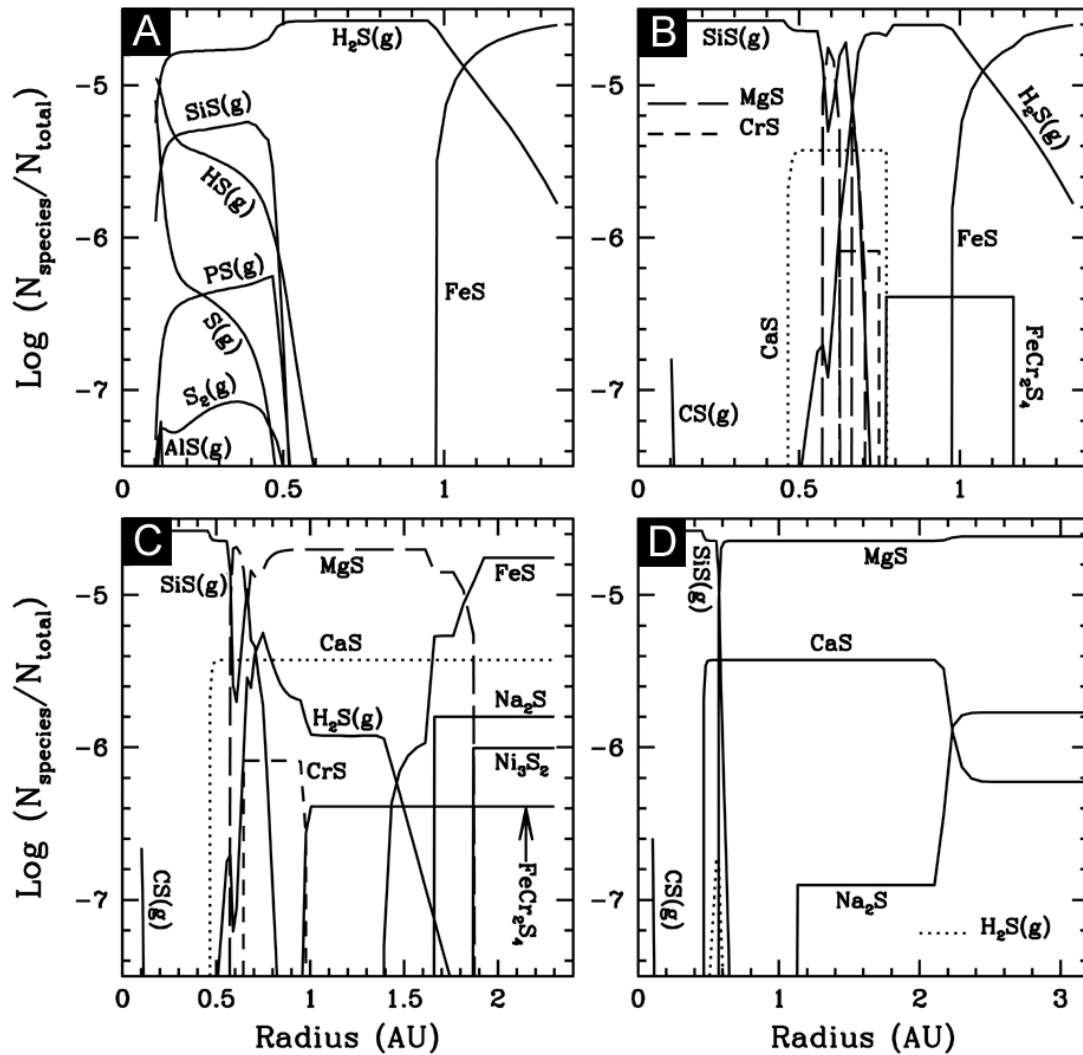
particles present at that pressure and temperature. We assume that the pressure and temperature are related by the ideal gas law. All species in the figure are solid phase species unless they are followed by a (g). The innermost radius for which we plot data in figure 46 is 0.1 AU, which is the innermost data point in the Hersant *et al.* (2001) profile.

$H_2S$ (g) is the dominant sulfur species throughout most of the nebula when the oxygen abundance is solar (figure 46a). At 0.98 AU (where $T = 690K$), troilite begins condensing. At larger radii all the sulfur is converted to troilite. Iron is twice as abundant as sulfur so it is theoretically possible for 100% of the sulfur to be converted into troilite. However there are dynamical issues that must also be considered. It is possible that the diffusion of $H_2S$ gas will alter the local abundance of sulfur. It is also possible that the reaction to produce troilite will occur too slowly to convert all the sulfur in $H_2S$ (g) into troilite in the lifetime of the nebula. These issues will be explored in more detail in sections 6.4.2 and 6.4.3. We emphasize here that these graphs display the equilibrium abundances ignoring all dynamical effects.

Our graphs are limited by certain features of our computer codes, especially at lower temperatures. The presence of many stable solids at lower temperatures makes finding a solution difficult. Under these conditions, the SOLGASMIX code is unable to determine the equilibrium mixture for temperatures below 559 K (r > 1.35 AU). Reducing the total number of species resolves some of these problems. The HSC code is able to find solutions at temperatures down to ~100 K.

The equilibrium distribution of sulfur is significantly affected by progressive depletion of $H_2O$ (g). When the inner nebula is depleted down to 33% of the original

solar O abundance ($C/O = 1.5$), a significant change in S chemistry occurs (figure 46b).

At temperatures above 920 K, SiS replaces $H_2S$ as the primary sulfur-bearing gas species.

Between 650 K and 920 K, $H_2S$ is the dominant sulfur gas species and the only other

sulfur gas phase species present in significant abundance is CS.  Below 650 K, troilite is

the dominant sulfur-bearing species. However, many other condensed sulfurous species

are also stable. Oldhamite (CaS) exists between 785 K and 1272 K and contains a large

proportion of the total Ca. Chromium and Mg are also chalcophilic under these

conditions, forming $FeCr_2S_4$, CrS and MgS. Under these conditions, MgS is abundant in

a narrow temperature range (between 900 and 1100 K) and becomes significantly more

abundant as the oxygen abundance is reduced even further.  As the abundance of O

decreases, Mg and Ca are both forced to enter sulfide phases as there is not enough O

available to form silicates, and this is a general trend we observe in our models.

Under these conditions the total mineralogy is significantly different.  Reduced

minerals such as cohenite and silicon carbide dominate at higher temperatures, replacing

silicates.  Clearly the equilibrium between enstatite and forsterite is affected, with

enstatite always present below ~1000 K.  The overall mineralogy is shown in figure 47.

The distribution of S changes even more dramatically when the O abundance is

reduced to 20% solar ($C/O = 2.5$) (figure 46c).  In section 6.4.3 we will show that such

conditions are unlikely for the solar nebula, but may be possible if water vapor

continuously diffuses out to the condensation front and the resulting condensates do not

migrate back inwards and increase the O abundance. Under these reducing conditions,

solving for chemical equilibrium at low temperatures is easier since fewer solid oxides

Figure 47. Equilibrium condensation sequence for a system at 10<sup>-5</sup> bar and with 33% of
starting O (as per figure 46B). Legends follow Wood and Hashimoto (1993).
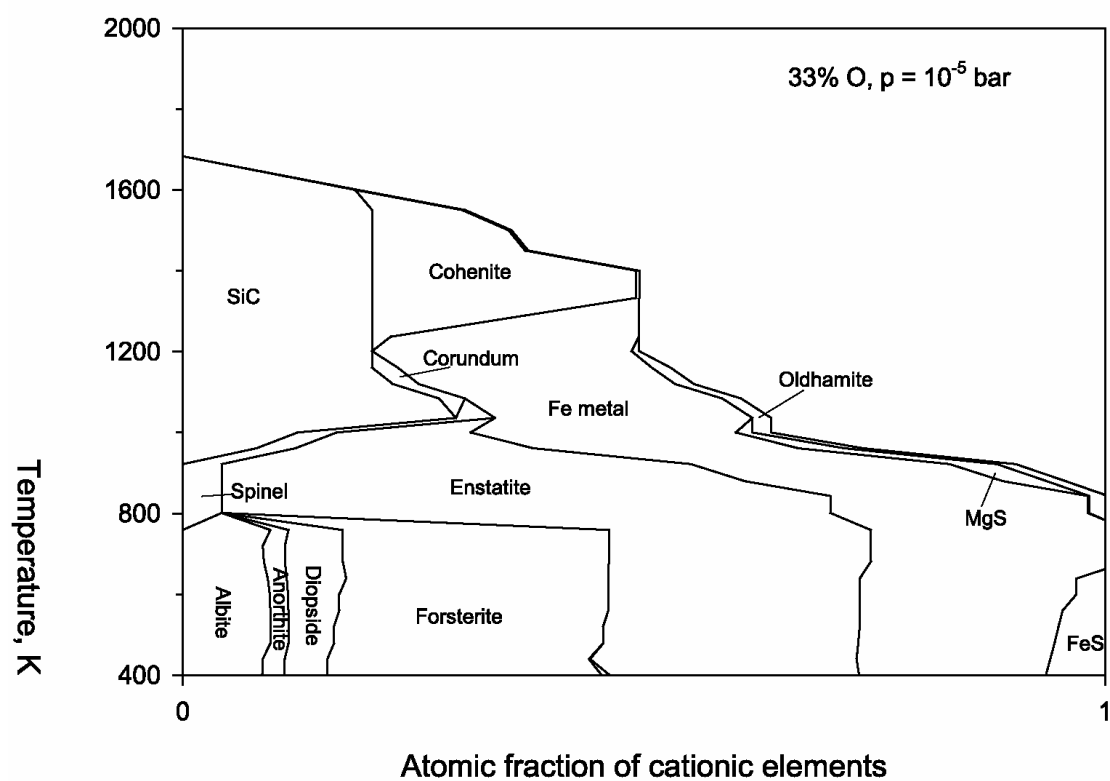
are stable. Thus, our calculations for these systems extend to larger radii (where $T \sim$ 336K). The intermediate temperature region is now dominated by MgS. Overall SiS (g), gS and troilite are the primary S-bearing phases as the system cools from high to low temperatures. $H_2S$ is a minor species in the gas phase. The troilite condensation front is at 1.4 AU, where T $\sim$ 547 K. Troilite equals MgS in abundance at ~1.8 AU ($T \sim$ 420K). At this low temperature, troilite formation kinetics may be too sluggish to allow for significant troilite production.

Two additional solids, $Na_2S$ and $Ni_3S_2$, are stable under these conditions (figure 46c). The stability of $Ni_3S_2$ is doubtful. The most abundant nickel-bearing sulfide in highly reduced meteorites is pentlandite [$(Fe,Ni)_9S_8$]. However, there are limited thermodynamic data for this phase and thus it is not considered in our calculations. The $Ni_3S_2$ phase is used as a proxy for pentlandite and its presence in our calculations indicates that a nickel sulfide mineral is likely to be stable and probably in solid solution with troilite. The solar abundances of sodium and nickel are both low enough that they play only a minor role in sulfur chemistry.

Troilite is not stable under the most reducing conditions that we studied, a nebula depleted to 10% solar O ($C/O = 5$, see figure 46d). The most abundant S-bearing gas under these conditions is SiS. MgS condenses at ~1000K. CaS and $Na_2S$ are also stable and together contain about 9% of the sulfur. Chromium condenses into the bulk metal and $Cr_2N$ is stable at lower temperatures. Our equilibrium calculations suggest that the sulfides MgS, $Na_2S$ and CaS dominate at these low temperatures. These extremely reducing conditions cannot occur in the diffusive model we describe below in section

6.4.3.  This is due to the limitation that the removal of oxygen can only proceed to the point where all water is removed from the system.  At a removal of about 80% of the total oxygen, the remainder of the oxygen is stored in silicate or solid oxide compounds. These compounds do not react with hydrogen gas to yield more water vapor, since the oxides and silicates are thermodynamically favored compared to water.  The only case where this would be a realistic approximation is in the case of carbon stars, where the initial C/O ratio is 5 or so.

One of the most significant changes in the equilibrium distribution of S that results from $H_2O$ depletion in the inner nebula is the transition from $H_2S$ to SiS as the dominant S-bearing gas. It is worth examining this transition in more detail (figure 48). At 80% O, $H_2S$ is more abundant than SiS in the high temperature regions. At 70% O, the abundance curves for $H_2S$ and SiS cross twice and overall both have similar abundances in the region $r \leq 0.63$ AU ($T \geq 950$K). At 60% O, SiS is the more abundant species. Thus, 70% O effectively represents the transition between $H_2S$ dominating at high temperatures and SiS dominating at high temperatures.

While the change from 80% O to 60% O dramatically changes the high-temperature chemistry, it has a negligible effect on the low-temperature chemistry. The stability fields of $H_2S$ (g) and troilite are similar in all three cases. The major difference is the Cr distribution. Six percent of total S is in $FeCr_2S_4$ at O abundances of 70% and 60% of solar, resulting in 6% less troilite. At an O abundance of 60% solar MgS is stable over a small temperature interval.

Figure 48. Graph demonstrating the $H_2S$/SiS transition with changing oxygen abundance at a time of $5 \times 10^5$ years. At solar oxygen, $H_2S$ is more abundant than SiS, but when the O abundance becomes less than 70% of solar, SiS becomes the major S- bearing gas species. The figure graphs the abundance of the most abundant species only ($H_2S$, SiS, troilite and MgS) for 80% O, 70% O and 60% O. Note that the vertical scale is different from that of figure 46.
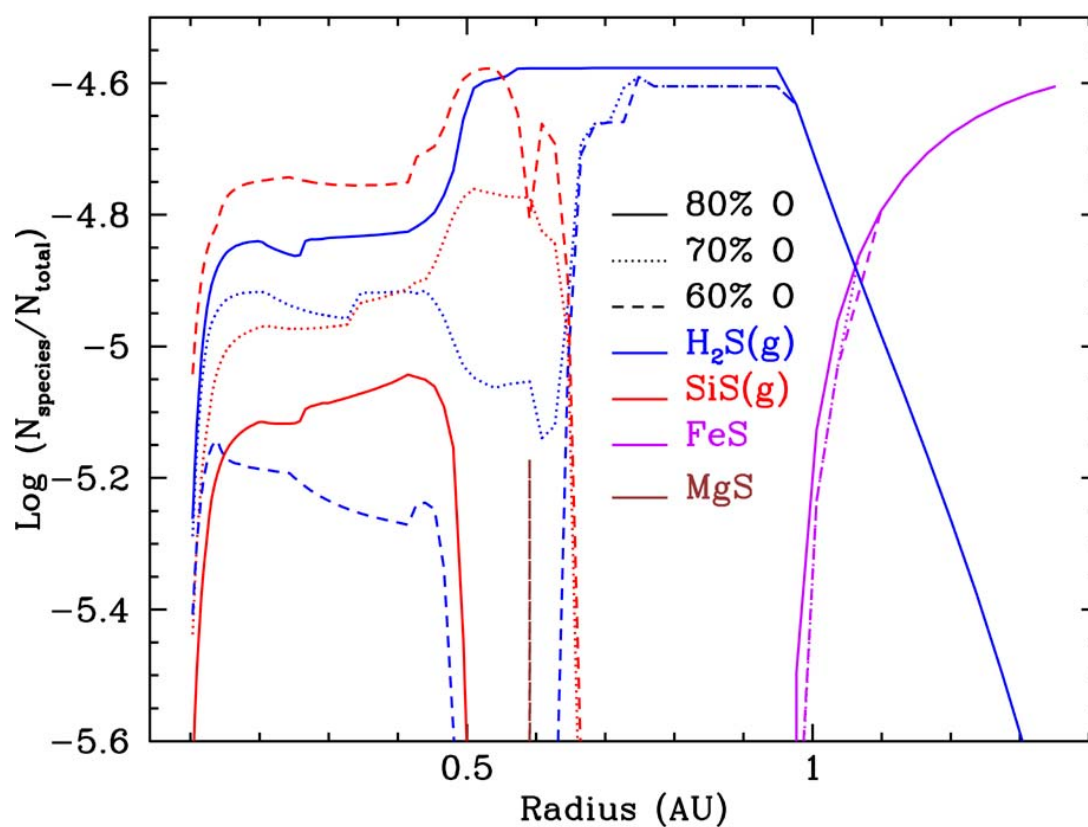
The calculations described above are specific to the "nominal" model from Hersant *et al.* (2001). We also performed calculations using the "warm" and "cold" models defined in their paper and illustrated here in figure 43. The condensation fronts occur at larger radii and the gas phase species extend to larger radii in any warmer model (and vice versa for any colder model). However, the general appearance of the sulfur distribution (as a function of oxygen percentage) does not change. Thus, the results described above qualitatively describe the equilibrium sulfur chemistry for a range of nebular models.

Our equilibrium calculations do not account for reaction kinetics. One of the most important reactions is FeS formation from the reaction of $H_2S$ gas with Fe metal. The gas-solid reaction kinetics are dependent on sulfur abundance, iron metal grain size, and temperature. We address the issue of kinetics in the following section.

6.4.2  Sulfide Formation Kinetics

Unlike $H_2O$, which condenses directly into the solid state, S is incorporated into solid material through the gas-solid reaction of iron with $H_2S$ (g) to form troilite. As a result of this reaction pathway, it is necessary to consider the kinetics of this reaction to compare the timescales for sulfur condensation to the evolution timescales of a protoplanetary accretion disk. We have performed these calculations in the context of a slowly cooling nebula whose inner regions are continuously depleted in $H_2O$ vapor as a result of diffusion out to the snow line. The reaction kinetics for sulfide formation have been

measured in a series of experimental studies (Lauretta *et al.* 1996, 1997, 1998). We use the results of these studies to estimate the timescales for S condensation.

Reaction kinetics were measured in $H_2S$-$H_2$ gas mixtures containing 25-10,000 ppm $H_2S$. The solar abundance of S suggests that $H_2S$ was present in the solar nebula at an abundance of 27 ppm (Lodders 2003). Experiments were performed both with pure Fe metal (Lauretta *et al.* 1996) and with meteoritic alloys (Lauretta *et al.* 1997 and 1998). These studies show that the rate of troilite formation varies as a function of temperature, $H_2S$ and $H_2$ partial pressures, metal composition, and metal grain size. For small metal grains the rate-limiting step in the solar nebula was either the delivery of $H_2S$ gas molecules to the metal surface or the dissociation of $H_2S$.

In the near-vacuum conditions of the solar nebula it is more likely that the supply of gas molecules to the metal surface is the rate-limiting step. This scenario can be modeled using the simple collision theory developed by Fegley (1988). The time to condense all S ($t_{chem}$) in seconds is:

$$t_{chem} = \frac{[H_2S]}{\left(\frac{2.635 \times 10^{25} \cdot P_{H_2S}}{\left(M_{H_2S} \cdot T\right)^{\frac{1}{2}}}\right) \cdot A_{Fe} \cdot \exp\left(\frac{-E_{act,FeS}}{RT}\right)} \tag{99}$$

In this equation [$H_2S$] is the abundance of $H_2S$ (g) in moles cm$^{-3}$, $P_{H_2S}$ is the partial pressure of $H_2S$ in bars, $M_{H_2S}$ is the molecular weight of $H_2S$ in g mole$^{-1}$, T is the temperature in K, $A_{Fe}$ is the surface area per unit volume of Fe metal grains in cm$^2$ per cm$^3$ of the solar nebula, which varies as a function of average metal grain size, $E_{act,FeS}$ is the activation energy for troilite formation in Joules / mole, and R is the gas constant

(8.314 J / mole K). The constant $2.635 \times 10^{25}$ has units of $(g\ K\ moles)^{1/2}\ cm^{-2}\ bar^{-1}\ s^{-1}$.
We use this equation to estimate the troilite formation timescales.

Experimental studies of Fe sulfurization in 100 ppm $H_2S$ (g) displayed Arrhenius
behavior and yielded an activation energy of 49 kJ/mole (Lauretta *et al.* 1996).
Sulfurization of both pure Fe and meteoritic metal in 50 ppm $H_2S$ did not display
Arrhenius behavior (Lauretta *et al.* 1996, 1998). Instead, in both studies it was observed
that the reaction rates at the lower temperatures (T < 613 K for pure Fe and T < 558 K for
the meteoritic metal) were larger than those at the higher temperatures. As a result a value
for the activation energy from these experiments was not easily obtained. However, the
studies of pure Fe sulfurization suggest an upper limit for the activation energy of 42
kJ/mole while those of meteoritic metal sulfurization in 50 ppm $H_2S$ yield an upper limit
of 50 kJ/mole. Thus, we use a value of 50 kJ/mole in our calculations. It is likely that the
activation energy for troilite formation is lower than this for the conditions expected in
the solar nebula. Thus this activation energy value will yield an upper limit for our
estimation for the timescale of troilite formation.

The results of our calculations are shown in figure 49. Three different Fe metal
grain sizes were considered: 10 nm, 10 μm, and 10 mm. These calculations show that the
smallest grains considered will sulfurize well within the estimated cooling time for the
solar nebula. Grains that are 10 μm or larger will completely sulfurize at 690 K, but S
condensation will be kinetically inhibited at lower temperatures (500 K) in the outer
regions of the nebula (>3 AU). The larger grains (10 mm) will remain relatively unaltered
throughout the early history of the solar nebula.

Figure 49. A graph of the dependence of H$_2$S-FeS reaction time on metal grain size and radius.  The solid line represents the time for the nebula to cool from 690 K to 500 K ($t_{cool}$) and represents our estimate of the amount of time available for S condensation. The dashed lines show the amount of time required to condense 100% of the sulfur in a solar composition system at 690K while the dotted lines show the same results at 500 K.   If $t_{cool}$>$t_{chem}$, then sulfurization of the metal can proceed.  For log time in years, subtract 7.5 from the y-axis.
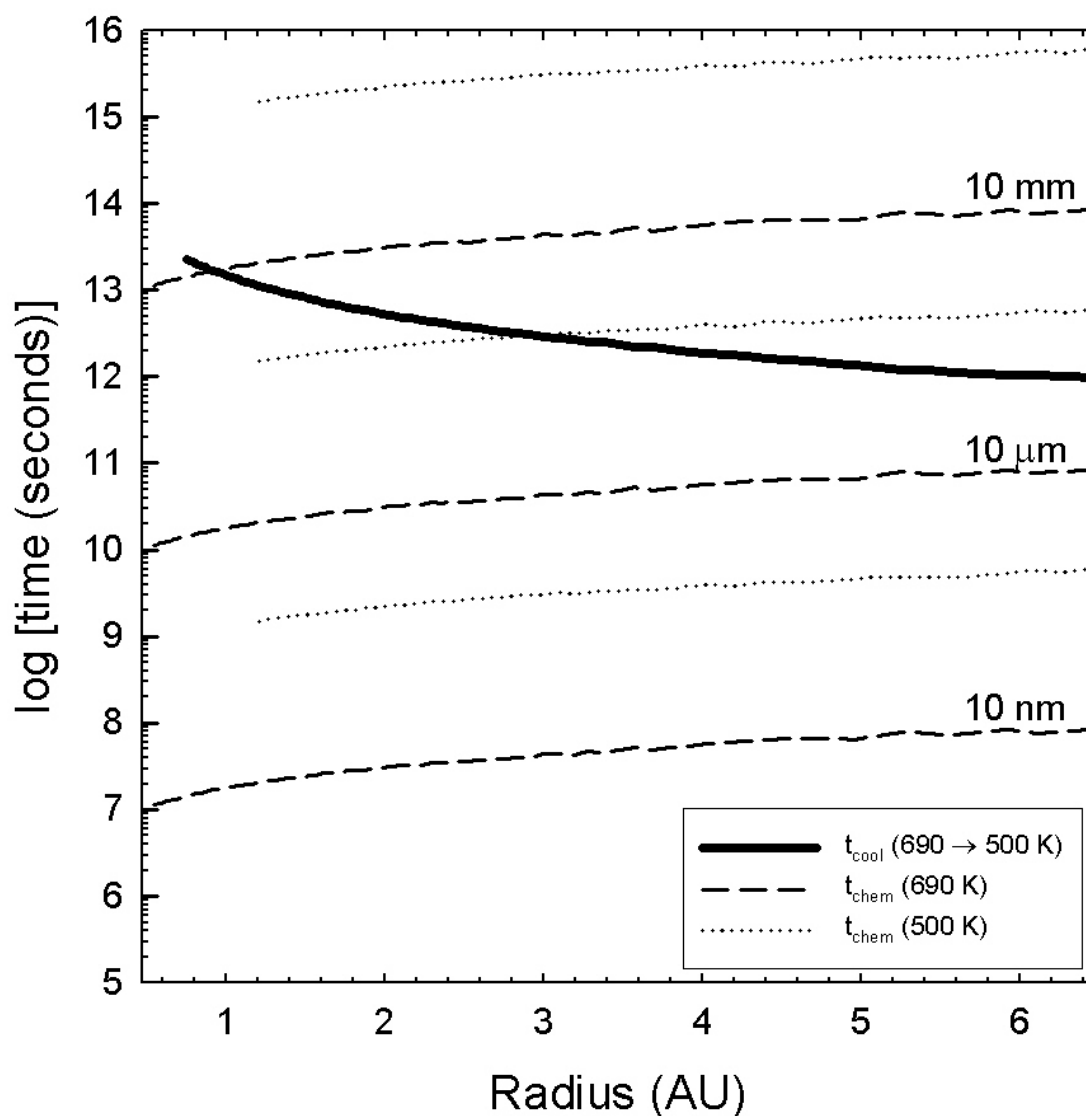
We apply the kinetic considerations determined in this section to a gas diffusion model in an attempt to discern the effect of having a large sulfur sink (in the form of FeS) on the distribution of sulfur in the early solar nebula in the next section. These calculations influence our overall sulfur distribution, especially in the region of planetary formation.

6.4.3 Sulfur Diffusion Calculations

As the solar nebula evolved, the molecular species in the gas were redistributed by diffusion (Pringle 1981). This idea was explored by Stevenson and Lunine (1988) and Cyr et al. (1998) in looking at the distribution of water vapor over time in the nebula. These authors found that the inner nebula would be rapidly depleted in water vapor over a time of $\sim10^5$ years as water diffused out to the snow line where it condensed forming water ice.

We have applied a model similar to the ones used by Stevenson and Lunine (1988) and Cyr et al. (1998) to study the distribution of the gases $H_2S$ and $H_2O$ in the nebula. $H_2S$ is assumed to be lost in the regions of the nebula where troilite forms. Troilite begins to form at a temperature of $\sim690$ K, though its formation may be kinetically inhibited at low temperatures (see section 6.4.2). To account for this in our model, we assume that $H_2S$ is removed from the gas phase in regions of the nebula that are between 500 and 690 K. Sunward of this region, troilite does not form because it is still too hot. On the anti-Sun side of this region, the kinetics of the reaction are assumed

to be too slow for $H_2S$ to form. At this temperature, 10 μm Fe grains (among the smallest

grains observed in meteorites) take roughly $10^5$ years to sulfurize, which is comparable to

the time it takes for there to be noticeable evolution of the nebula thermal profile. Thus,

this temperature is used as a lower limit for the reaction to be completed. Below

temperatures of ~110 K, $(NH_4)_2S$ is a potential sulfur-bearing condensate (Fegley and

Lewis 1980). At these low temperatures, diffusion occurs very slowly, so if these species

are present, they will not affect this diffusion calculation. Compounds related to these

species may be in comets. Water vapor is assumed to be lost as it condenses beyond the

snow line (temperatures below ~160 K) without any kinetic considerations.

To model the distribution of the two species, we use the two-dimensional

diffusion equation in cylindrical coordinates assuming azimuthal symmetry following

Stevenson and Lunine (1988) and Cyr et al. (1998):

$$\frac{\partial C}{\partial t} = \frac{1}{r}\frac{\partial}{\partial r}\left(rD(r)\frac{\partial C}{\partial r}\right) \qquad (100)$$

where C is the relative concentration of the molecular species of interest and D(r) is the

diffusion coefficient (note: Stevenson and Lunine (1988) and Cyr *et al.* (1998) used a

diffusion coefficient that did not vary with distance from the Sun). The diffusion

coefficient is found using local nebular parameters such that:

$$D(r) = \alpha \frac{c_s^2}{\Omega_K} \qquad (101)$$

where α is the viscous turbulence parameter (set to 0.009 to be consistent with the nebula

model used here), $c_s$ is the local speed of sound, and $\Omega_K$ is the local Keplerian angular

velocity. Note that a more detailed calculation would include consideration of the changing surface density with time. Such a consideration is beyond the scope of this paper. Here we attempt to show roughly how the two concentrations change with time.

We apply this model to a snapshot of the nebula at the instant when the water condensation front is at 5 AU. This occurs at a time of 0.44 Ma in the nominal nebula model. The initial conditions of the model are found by taking the nebular profile (pressure and temperature at the midplane as a function of distance from the Sun) and calculating the midplane hydrogen number density assuming an ideal gas. Initially, $H_2S$ and $H_2O$ are assumed to be distributed at the relative solar ratio given by Grevesse and Sauval (1998) and Supulver and Lin (2000). In the regions of the nebula where troilite and water ice are assumed to form, the relative concentrations of the respective species are set to zero. (This is an approximation since figure 46a illustrates that the $H_2S$ concentration gradually drops to a very low concentration. For our purposes, decreases in the concentrations by an order of magnitude are significant. Note that the axes of the plots in figure 50 are linear and not logarithmic). We also determine Fe grain size limitations based on the reaction kinetics which would be consistent with this initial sulfur distribution. Assuming that all FeS forms in the region between 1 and 1.6 AU, as shown in figure 50, the maximum allowable grain size is 10 mm or less near the Sun, and ~3 mm out at the edge of the reaction front. This is based on a comparison between the amount of time required for the reaction to occur and the cooling time of the nebula. We note that the local cooling rate in the nebula depends on nebular structure and

Figure 50. Graph of the diffusion of both A.) $H_2S$ and B.) $H_2O$, in the solar nebula, assuming a reaction zone for $H_2S$ from 500-690 K. The times marked represent the amount of time after the starting time of 0.44 Ma. Everything is normalized to its initial local abundance.
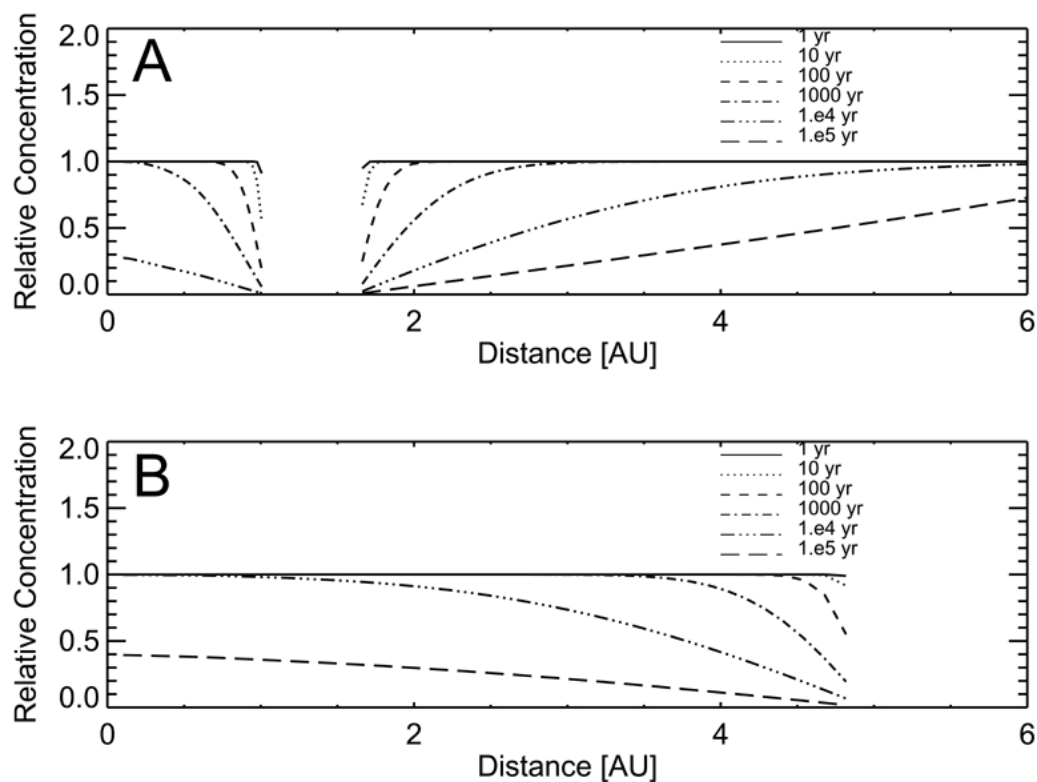
location, and models generally show that the outer nebula reaches low temperatures more rapidly than the inner nebula (Cassen 1994, Hersant et al. 2001).

We assume that the temperature structure of the nebula is constant during the time considered and that diffusion is the only method by which any molecular species is transported within the nebula (i.e. there was no migration or decomposition of troilite or water ice, and no significant advective flow of the gas). Lastly, we assume that the troilite formation is not inhibited by iron depletion in the region where it forms.

Figure 50 illustrates how the $H_2S$ and $H_2O$ profiles evolve with time, plotting the concentrations at different radii relative to what they were at the starting time (0.44 Ma) at that radius. Troilite forms between ~1.0 and ~1.6 AU (section 6.4.1 and 6.4.2), which is illustrated by the gaps in the profiles on the graph. $H_2S$ diffusion occurs more rapidly than $H_2O$ diffusion due to a larger concentration gradient. Note that the region interior to the gap where troilite forms is quickly depleted in $H_2S$ (in ~$10^4$ years), and this occurs before any significant $H_2O$ is lost in that region. Thus, the nebula is too oxidizing to allow significant MgS to form there. If we examine the nebula at a time later in its existence (~$10^5$ years), then regions of low O and S fugacities coexist as a result of diffusion. Our set of condensation calculations with realistic O depletions suggests that the only effect this has on the equilibrium chemistry is a lower condensation temperature of the sulfides MgS and CaS. The condensation temperature of FeS is unaffected.

We also performed similar calculations for nebula profiles when the water ice condensation front reached 4 AU and 3 AU. In these cooler profiles, the troilite formation zone was between 0.8 and 1.3 AU and 0.6 and 1.0 AU for those respective times. The

same general trend was seen in these calculations as in figure 50; those regions that rapidly lost $H_2S$ did not lose significant amounts of water vapor on the same timescale. Thus the major sulfide should still be FeS (as noted in figure 46). It should be noted that the time for the water ice condensation front to migrate from 5 AU to 4 AU was $1.9 \times 10^5$ years and for it to move from 4 AU to 3 AU took $3.7 \times 10^5$ years. Thus the diffusion profiles shown for $10^5$ years may not be valid since we required that the temperature of the nebula not change during the time considered. However, for times of $10^4$ years or less (thus the time it takes for the inner nebula to lose its $H_2S$), it is reasonable to assume that the temperature profile does not change significantly.

If we assume that the profiles shown at $10^5$ years are valid, even if the condensation front has migrated sunwards by some fraction of an AU, then there exist regions of depleted O concentrations. Such regions correspond to C/O values greater than 0.5. In these regions, a dual sink situation may be active, wherein both MgS and FeS form, removing $H_2S$ (g) from the system. More detailed calculations of such a system would depend on the kinetics of the formation of MgS, which are unknown.

6.5 Discussion

We have calculated the equilibrium condensation chemistry of sulfur coupled with the diffusion of water and sulfur in the nebula and with kinetic considerations for the dominant solid sulfide phase, troilite. We find that a solar-composition nebula is too oxidizing to form the reduced condensed sulfur-bearing species MgS and CaS in

significant amounts, consistent with meteoritic observations. We also demonstrate that the gas $H_2S$ is still present at temperatures lower than 500K, due to the slow reaction kinetics for the formation of troilite at these temperatures. We find that by varying oxygen fugacity, the major sulfur-bearing gas species changes from $H_2S$ at high O abundance to SiS at low O abundance. In addition, we find FeS to be the dominant S-bearing solid species at high oxygen fugacities, whereas MgS, CaS, and FeS are the major sulfide species at lower oxygen fugacities. We apply our results in a qualitative fashion to meteorites, Jupiter, and observations of protoplanetary disks beyond our own solar system.

6.5.1 Applications to Meteorites

The majority of meteorites are members of the ordinary chondrite class. These meteorites contain abundant magnesium silicates, iron metal, and FeS. The observed modal FeS to iron metal ratio is usually significantly less than 1, implying incomplete reaction of iron and sulfur. Our results are consistent with this, since the kinetics in section 6.4.2 suggest that there would not be time for the complete conversion of iron metal to troilite. FeS is by far the most common sulfur bearing mineral in primitive meteorites. However, the enstatite chondrites also possess several accessory sulfide minerals. Enstatite chondrites are a peculiar meteorite class whose mineralogy is dominated by enstatite ($MgSiO_3$) and which display evidence of formation in a very reducing environment. Enstatite chondrites are grouped into two classes: the EH chondrites are enstatite chondrites with high total

iron content, and the EL chondrites are those with low iron content. EH chondrites contain MgS, whereas EL chondrites contain the more ferroan alabandite, (Mn,Fe)S (Ehlers and El Goresy 1988). Enstatite chondrites also contain oldhamite (CaS) and silicon dissolved in iron metal.  Very few other meteorite classes contain these compounds, and as a result, they have been the subject of much study in an attempt to determine their origin.

Many different studies have been performed to see if it is possible to replicate the observed mineralogy of enstatite chondrites using condensation calculations. Larimer (1968) studied the presence and significance of oldhamite in meteorites and was among the first to suggest that in order to reproduce the observed mineralogy of enstatite chondrites, nebular heterogeneities were required. He suggested that a slight C/O fractionation may have occurred in certain regions of the solar nebula. Baedecker and Wasson (1975) outlined several potential mechanisms for the formation of enstatite chondrites, the first of which was the depletion of an oxidizing agent (like water) from the solar nebula. Herndon and Suess (1976) attempted to show that enstatite chondrite minerals could form in a solar nebula with pressures of approximately 1 bar. Larimer and Bartholomay (1979) addressed this proposed mechanism, finding that Herndon and Suess (1976) had omitted several important high temperature silicate condensates, and that these would form instead of the more reduced minerals suggested by Herndon and Suess (1976). Most recently, Hutson and Ruzicka (2000) replicated the mineralogy of enstatite chondrites by coupling the water depletion of Cyr *et al.* (1998) with a depletion of refractory components. This work supports Hutson and Ruzicka (2000), agreeing with

their suggestion that some of the minerals in enstatite chondrites formed through the heterogeneities resulting from the ice condensation front. According to our models, we suggest that between 50-70% of the oxygen was removed by diffusion to form these accessory sulfide minerals. We also calculate that the timescale for the formation of the these minerals is approximately $10^5$ years or more, based on the results portrayed in figure 50. The location of the formation of enstatite chondrites is more difficult to constrain with our model, but it must have been beyond the troilite condensation front, but before the water ice condensation front (as enstatite chondrites have no recorded aqueous alteration products). Thus we predict that the enstatite chondrites formed between ~1 and ~4 AU. This model does not explain all of the minerals or phases in enstatite chondrites (like CAIs or chondrules), but it provides an explanation for the sulfide phases consistent with the overall reduced character of these meteorites.

6.5.2 Applications to Jupiter

The abundance of elemental sulfur in Jupiter measured by the Galileo probe is approximately three times solar, in rough agreement with the noble gases and carbon- and nitrogen-bearing species (Atreya *et al.* 2003). One interpretation of this pattern is that it is a direct reflection of the abundance pattern in very cold planetesimals that entered Jupiter with little alteration from the molecular cloud (Owen *et al.* 1999). An alternative model is that planetesimals formed locally in the region of Jupiter, cooling slowly and accommodating volatiles by trapping them in the ice as clathrate hydrates (Gautier *et al.*

2001). This last model predicts an overabundance of sulfur in Jupiter, introduced as hydrogen sulfide, by a factor of two over what is observed. One possible way to reconcile this model with the Galileo measurements is to postulate a depletion of $H_2S$ in the region near Jupiter where planetesimals formed and then were accreted onto the giant planet. Our results suggest that such a depletion is possible as a result of the coupling between the oxygen-dependent sulfur chemistry, the FeS kinetics, and the nebular transport processes that affect both the water (hence oxygen) abundance via cold trapping and the sulfur abundance at and beyond the FeS boundary. More detailed numerical transport models are required to test this assertion and can be put on a firm footing using the thermochemical results and approximate kinetic considerations given here. Meanwhile, the two models for the origin of the heavy element enrichment in Jupiter can be definitively tested only with future missions that will measure the deep oxygen abundance of Jupiter (Lunine *et al.* 2003).

6.5.3 Applications to Protoplanetary Disks

The results of our calculations have important implications for future observations of molecular species in protoplanetary accretion disks surrounding low mass stars. Because sulfur is the most volatile of all the major rock-forming elements, it is likely to remain in the gas-phase for longer times and out to larger radii than the other abundant elements such as Mg, Fe, and Si.

An important transition in the distribution of sulfur-bearing species inward of 5 AU (figure 48) occurs when the inner nebula is depleted in oxygen by 30%. The most abundant gaseous species changes from $H_2S$ to SiS. Both of these molecules are observable using current astronomical facilities. Furthermore, future sub-mm interferometers such as ALMA will be capable of measuring chemical composition gradients in the inner regions of nearby protoplanetary accretion disks. Thus, determination of the $H_2S$/SiS ratio in these objects can provide evidence for the presence of a nebular snow line and can constrain the oxidation state and major element chemistry in the inner regions, where rocky planets are likely to form.

Acknowledgements

CHAPTER 7


CONCLUSIONS


Chapters 2-5 focused on experimental studies of phosphide corrosion, on the specific

reaction pathway that leads from the phosphide to inorganic and organic P compounds,

and on a statistical overview of meteorites and other extraterrestrial material as sources of

P and C. How does the corrosion of schreibersite compare to other models of prebiotic

phosphorylation?


7.1 Schreibersite Corrosion as a Source of Prebiotic P


Is the system described in chapter 2 even relevant? Are the experiments described

prebiotic, i.e. reasonable on the early Earth? I explore the nature of the phosphide

powder and the corrosion solutions in this next section to determine whether these

experiments could be described as "prebiotic."


7.1.1 Criteria for Prebioticity


For a system to be "prebiotic," the reaction conditions must be relevant for a system

without human intervention. They must occur naturally. For instance, the reaction at

160° C of:

$$\text{Uridine} + H_3PO_4 \rightarrow \text{Uridine-}PO_3 + H_2O \qquad\qquad (102)$$

has been claimed to be a prebiotic reaction (Ponnamperuma and Mack 1965). However, phosphoric acid is not a constituent of any known geochemical system, thus this reaction can not claim to be prebiotically relevant.

7.1.1.1 Phosphide Powder

The experiments described in chapters 2 and 4 used a synthetic iron phosphide powder instead of natural schreibersite. The powder consisted of mainly $Fe_3P$ but also had $Fe_2P$ as a minor constituent (~5%) of the powder. Both minerals are in meteorites, though schreibersite is much more common than $Fe_2P$ (barringerite). XRD data suggests that barringerite did not corrode in these experiments (figure 11, table 13), indicating the observed chemistry is solely a product of $Fe_3P$ corrosion.

The $Fe_3P$ powder is structurally identical to schreibersite based on XRD data. Like native schreibersite, the $Fe_3P$ powder is also strongly attracted to a magnet. The phosphide powder is chemically identical to iron-end member schreibersite based on EMPA data. The only difference in chemistry between the phosphide powder and schreibersite is in the amount of nickel in schreibersite. The abundance of nickel in meteoritic schreibersite ranges from ~50 atom % nickel (the mineral nickelphosphide) to <10% Ni in the schreibersite of some enstatite chondrites (Lin and El Goresy 2002). The addition of Ni to metal may decrease the weathering rate slightly as Ni has a lower oxidation potential than iron metal (0.22 V for Ni $\rightarrow$ Ni$^{2+}$ vs 0.44 V for Fe $\rightarrow$ Fe$^{2+}$).

However, this decrease in corrosion ability is relatively minor given the large oxidation potential of P, and chapter 3 demonstrates that schreibersite corrodes naturally.

A final difference between meteoritic schreibersite and the experimental powder is grain size / surface area. The surface area may affect reaction rates, though the extent of this effect is unclear. The $Fe_3P$ powder has a huge surface area compared to meteoritic schreibersite. With an average grain radius of ~5 μm, the phosphide powder has a surface area of about 0.086 $m^2$ per gram of powder. For a comparison, the average surface area (*SA*) of schreibersite in an iron meteorite is:

$$ SA \ (in \ \frac{m^2}{g}) = \frac{4\pi r^2 \times 0.1}{7,000,000 \frac{g}{m^3} \times \frac{4}{3} \pi r^3} = \frac{0.3}{7,000,000r} = \frac{0.3}{22,700 \times \sqrt[3]{M}} \tag{103} $$

where *r* is radius in meters, 0.1 is the volume fraction schreibersite and assumes 1 weight % P in the meteorite, 7,000,000 $g/m^3$ is the density of an iron meteorite, and *M* is its mass in grams, all assuming a perfectly spherical single mass. In general, smaller meteorites have more exposed schreibersite. A large fall with a radius of 10 m would have a phosphide surface area of 125 $m^2$, which on a per mass basis would be a factor ~5 × $10^{-8}$ less per gram compared to the experimental powder. However, most large falls break up on atmospheric entry. For example, Sikhote Alin generated >8,500 pieces during break up and impact. Assuming a mass vs. number distribution with a slope of -1 and perfect sphericity the total surface area would be 0.0001 $m^2$ exposed schreibersite area per gram of total meteorite, closer to the calculated value for the phosphide powder. When factors such as small fragments and non-sphericity are included, this number approaches the experimental phosphide value. Additionally, meteoritic kamacite and sulfides are the

first to corrode which in turn greatly increases the available phosphide surface area for future corrosion (Buchwald 1977).

The schreibersite corrosion region explored in chapter 3 demonstrates that schreibersite corrodes. The schreibersite corroded after the metal which had corroded to completion. This mineralogical evidence suggests schreibersite corrodes on geologically short timescales. The chemical and physical similarities between the phosphide powder and actual meteoritic schreibersite suggest that the differences between the two are not significant enough to necessitate the use of much rarer schreibersite in the experiments. The phosphide powder is an accurate proxy for meteoritic schreibersite.


7.1.1.2 Solution Chemistry


The experiments formed P compounds at room temperature and in deionized water. Deionized water is analogous to fresh water, which typically contains $<10^{-4}$ M of $Mg^{2+}$ or $Ca^{2+}$ (Berner and Berner 1986), too little to cause the precipitation of P-bearing salts and minerals.

Several experiments were performed under Ar gas. These experiments replicated an inert atmosphere (neither oxidizing nor reducing), consistent with the conditions presumed for the early Earth. The results from these experiments showed the same chemistry as those under an air atmosphere, albeit at lower total concentrations. An air atmosphere was employed for the majority of the experiments since the chemistry did not change significantly under air versus argon except for higher total yields, which

facilitated determination of the P chemistry by NMR.  Replicating these experiments

under a methane atmosphere could initiate Fischer-Tropsch type reactions producing

minor quantities of organics, though this effect was not investigated.

Solution molarities ranged from 0.025 to 1.2 M of organics or salts.  These

concentrations are necessarily high, as reaction yields correlated closely with mole

fractions of added compounds, and NMR needs relatively high concentrations of products

for accurate detection and identification.  Origins of life experiments have been plagued

by unreasonably high concentrations since its inception.  Yields of prebiotic reactions are

1-10% but start with molar concentrations on the order of unity.  The ocean would not

have had concentrations of constituents on the order of 0.01 M, much less 1.0 M and

more likely concentrations of organics would be ~$10^{-4}$ M.  Prebiotic chemists have

justified the use of higher concentrations by emphasizing environments in which

concentrations are boosted by natural processes like desert playas and polar regions.

The use of unreasonable concentrations of organic compounds is a problem for

prebiotic chemistry as a whole, as well as a problem for this research.  The crater-lake

described in chapter 5 could increase the concentration of organic compounds

substantially, overcoming this problem.

The organic compounds used in the experiments were mostly simple organic

species, with the exception of adenosine and EDTA.  Most species are 2-3 carbon

compounds with a range of functional groups.  The organic chemistries explored included

moderately reduced carbon species (ethanol, acetonitrile) to slightly oxidized species

(acetaldehyde, acetone) to fairly oxidized carbon species (glycolaldehyde, acetate,

pyruvate) to completely oxidized species (bicarbonate). Thus the experiments explored the range of possible solution chemistry. Many of these organic compounds have been detected in meteorites, including ethanol and acetate. The simplicity of these two carbon species is consistent with a prebiotic system.

Most solutions were made basic by the addition of NaOH at the end of each experiment, which facilitated peak identification and precipitated $Fe^{3+}$ complexes, freeing some P salts and allowing for determination by NMR. Without addition of NaOH, Fe complexes interfered with the magnetic properties of the solution and prevented detection by NMR. Solutions with a pH of ~13 are rare in geochemical systems, and hence are not likely to be prebiotic. However, there are several reasons to assume that the addition of NaOH to the solutions did not significantly affect solution chemistry. First and foremost, solutions which were not made alkaline by addition of NaOH did not demonstrate a significant change in chemistry. For instance, the addition of $NaHCO_3$ brought the solution to a pH of 9.5 and precipitated $Fe^{3+}$ complexes, allowing for easy determination by NMR. The addition of $NH_4OH$ brought the solution to a pH of ~8, and allowed for accurate determination of P species by TOF-MS. No addition of any salt allowed for detection of $\cdot PO_3^{2-}$ radicals by EPR. Thus, the addition of NaOH to each solution only allowed for determination by NMR, and did not appear to affect solution chemistry significantly.

7.1.1.3 Comparison to Other Prebiotic Experiments

Other prebiotic phosphorylation experiments were described and summarized in chapter 1. Compared to these earlier experiments, the phosphide corrosion system is much simpler, requiring less human interference. Unlike these proposed prebiotic phosphorylation pathways, this study does not use elevated temperatures ($>100 °$ C), unlikely P compound as starting materials like Na-phosphates, energetic P-N organics or organic P anhydrides, or energetic organic condensing agents. The experiments described in chapter 2 are simple, and hence prebiotic.

The phosphide powder is a suitable proxy for schreibersite and that the solution chemistries were similar to those possible on the early Earth excluding improvements to reaction chemistry to allow for detection by NMR hence the experiments described in chapter 2 are considered to be prebiotic. How would the P compounds produced in these experiments influence chemistry at the origin of life?

7.1.2 Inorganic Phosphorus Compounds Produced

A complex series of mixed-valence, multi-P-bearing molecules are synthesized from the corrosion of schreibersite. The four main inorganic species are orthophosphate, phosphite, hypophosphate, and pyrophosphate. Diphosphite is a common accessory P salt, and minor inorganic P species are common when chelating agents are added to the corroding schreibersite.

Orthophosphate is the main form of P on the surface of the Earth today. Life currently extracts P from orthophosphate minerals, or through eating organisms capable of extracting P. Orthophosphate is highly insoluble and its concentration is buffered by the solubility of apatite. The experiments in chapter 2 suggest that orthophosphate reaches molarities of $10^{-2}$ M, a factor of $10,000\times$ over the solubility of apatite. The phosphate molarity approaches the concentration of phosphate employed by many prebiotic phosphorylations.

Pyrophosphate is extensively generated in modern biochemical systems as a byproduct of the reaction:

$$ATP \rightarrow AMP + PPi \tag{104}$$

which overcomes large energy barriers associated with some biochemical reactions. Other biological uses of pyrophosphate include as a phosphorylating agent and a food source for ancient organisms (Baltscheffsky 1971). Pyrophosphate also aids in photosynthesis (Forti and Rosa 1974). Abiotic formation of condensed phosphate has been extremely difficult in lab settings, and requires elevated temperatures, or artificial phosphate minerals (Rabinowitz et al. 1968), or energetic compounds (e.g., Weber 1982; Hermes-Lima and Vieyra 1989, de Zwart et al. 2004).

Polyphosphates are produced in small (nM- mM) quantities through a series of radical propagation and termination reactions. Polyphosphates are abundant in some biochemical systems, especially plant cell vacuoles, and in nerve cells. Their biological purpose is unclear at present.

Hypophosphate compounds have been incompletely explored in the prebiotic / biochemical literature as they are encountered very infrequently in chemical synthesis. However, hypophosphate mimics pyrophosphate in some biological compounds (Lauquin and Vignais 1973) and may be used as a prebiotic phosphorylation agent if the P-P bond can be cleaved.

7.1.2.1 Organophosphonates as Precursors to Organophosphates?

The prebiotic potential of phosphite has been investigated historically, and alternate biologies utilizing C-P or P-H linkages have been proposed. Our experiments show that phosphite ($HPO_3^{2-}$) is an abundant (>100 μM concentrations) component of all aqueous corrosion experiments. This intriguing result suggests that phosphite was as abundant in primordial aqueous systems as orthophosphate and that the phosphate world may have been preceded by a phosphonate world. Phosphonates are biochemically active P-bearing molecules that contain direct P-C bonds. Phosphonic acids are not widespread in biology, although they are used by sea anemones (Horiguchi & Kandatsu 1959) and some bacteria. The most abundant of these molecules is aminoethylphosphonate [$NH_2CH_2CH_2PO_3^{2-}$], which forms phosphonolipids as part of some cell membranes. Phosphonolipids are resistant to enzymatic hydrolysis and enable organisms to withstand extreme conditions (Engel 1977, Hilderbrand and Henderson 1983). Modern biochemical systems have developed around the use of phosphate, hence phosphonates are occurrence now relatively rare.

The idea of an early phosphonate-based life was first developed by Schwartz (1997) who proposed an alternate biochemistry based on sugar-phosphonates and a DNA analog containing pyrophosphonate linkages (figure 51). Alternative linkages of sugar-$OPHO_2$-sugar have been proposed by Peyser and Ferris (2001, figure 51) and experimentally investigated (de Graaf and Schwartz 2005). Phosphite readily form organics in the presence of UV radiation (de Graaf et al. 1995), and the P-C bond is especially resistant to hydrolysis under a wide range of pH and temperature.

These proposed biochemistry have advantages compared to the phosphate biochemistry as phosphonates are more stable, phosphite is more soluble than orthophosphate, and phosphonates are readily produced from organics and phosphite irradiated by UV light. Later organisms would probably have replaced phosphonates with phosphates due to the ease of translating phosphates and the energetic favorability of phosphate-based ATP.
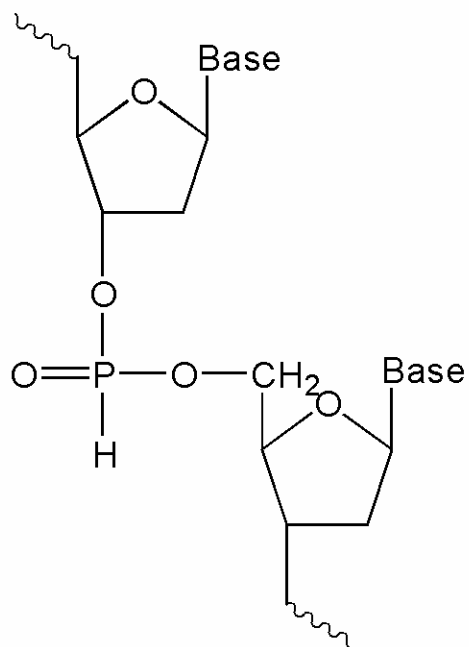
The inorganic corrosion products of iron phosphide are potentially useful for early biochemical systems. The production of organic P compounds is intriguing, as these compounds are formed through an abiotic process.

Figure 51.  Phosphonates as precursors to phosphates.

<u>Schwartz (1998)</u>
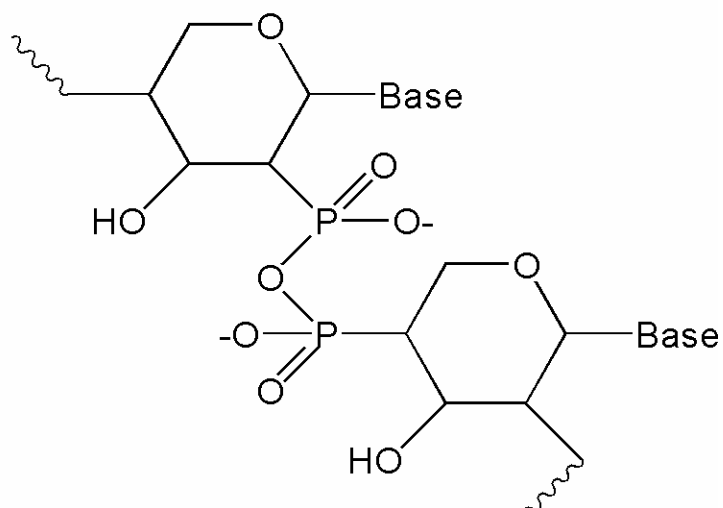


<u>Peyser and Ferris (2001)</u>

7.2 Implications of Organic Phosphorus Compounds

Organic P compounds are produced at a ratio of 1-5% of the total P compounds, according to NMR and MS. The organic P compounds produced include species with P-C linkages and species with P-O-C linkages. These compounds are synthesized through a series of radical reactions:

$$\cdot PO_3^{2-}, \cdot OPO_3^{2-} + \cdot R \rightarrow R\text{-}PO_3^{2-}, ROPO_3^{2-} \tag{105}$$
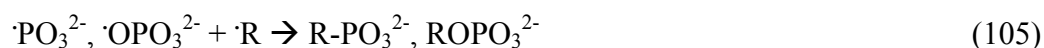
These reactions have implications for meteoritics and for origins of life studies.

7.2.1 Meteoritic Implications

The suite of meteorite organics includes several phosphonic acid species in low (nM) concentrations. The proposed origin of these species ranges from C-P interstellar precursors (Cooper et al. 1992) to UV photolysis of phosphite followed by radical termination with organics (de Graaf et al. 1995). The reaction pathway described in chapter 4 is similar but not equivalent to the de Graaf et al. (1995) model.

The total abundance of phosphonic acid species in Murchison is ~2 ppm, and the total P abundance is ~1000 ppm. Thus ~0.2 % of all P in Murchison is in organic P compounds. Solutions of phosphide and organics will generate phosphonic acids at ~2% of the total P abundance. If all the phosphide in the Murchison parent body corroded away through aqueous corrosion, and given that phosphide is the P carrier for ~10% of the total P in a meteorite, then the observed organic P abundance in Murchison is

consistent with the yields from the aqueous corrosion of schreibersite in organic-rich fluids.

The corrosion experiments do not produce the phosphonic acid series observed in Murchison, but the starting solution did not set out with this goal in mind. Meteorites have a much larger variety of organic compounds, including insoluble organic matter, hydrocarbons, alcohols, and aromatic compounds. The solution studied in depth only incorporated acetate. In order to produce the organic P compounds, the starting solution would likely be much more complex. Methyl radicals and other hydrocarbon radicals combined with phosphite radicals could terminate to form the organic P series of Murchison.

Alternatively, the organic P series could have been altered from the starting composition. No hypophosphate, pyrophosphate, or phosphite salts have ever been detected in the matrix of meteorites. These species are stable over several years, but are not stable over geologic timescales. They oxidize and hydrolyze to form orthophosphate. The same may be true of some organic P species. Compounds like hydroxylmethylphosphonate are exposed to highly reducing conditions in a meteorite (due to corrosion of metal and serpentinization), which has the net result of removing O from organics. Perhaps some of these organic P compounds underwent the same reaction, losing O to form hydrocarbon-$PO_3$ species.

7.2.2 Relevance to the Origin of Life

Two broad classes of organophosphorus molecules were formed in these experiments. The formation of C-P linkages suggests that the early Earth may have been seeded with abundant C-P molecules, and that the first organisms may have used these in addition to phosphate as P biomolecules (discussed above).

The C-P linkage is strong and resistant to hydrolysis, hence it is stable and long-lived. However, organophosphonates are hard to synthesize compared to organophosphates since they require a radical-type reaction as opposed to a simple dehydration/phosphate transfer reaction. If organophosphonates were used at all, early life coopted organophosphonates from its environment as a limiting nutrient, and used phosphates/organophosphates for the majority of metabolic work. Organophosphonates may have fulfilled other functions, like the formation of lipids where they are currently employed, or replication and information transfer molecules.

The presence of P-O-C linkages formed at room temperature from the corrosion of schreibersite indicates that this functional group may have been readily produced on the early Earth. The production of P-O-C linkages proceeds not by dehydration reactions, but through radical termination reactions, which overcomes many of the difficulties traditionally associated with their formation. The molecules formed include phosphoglycolate and phosphonomethylphosphate.

Phosphoglycolate is one of the molecules generated by the corrosion of phosphide, and is part of the glycolate pathway in modern biochemistry, which turns

sugars to amino acids. The formation of this compound may indicate that the production

of biologically-useful compounds could proceed through pathways similar to the pathway

that generated this molecule. For instance, 2-phosphoglycerate could be produced from

the oxidation of 3-hydroxylpropanoic acid:



(106)
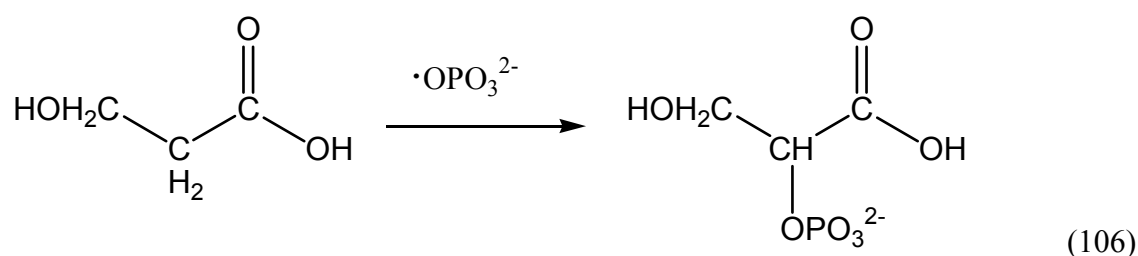
This research suggests that carboxylic acids are easier to phosphorylate than

sugars. Sugar phosphates are not likely products of phosphorylation reactions by

schreibersite corrosion. Schreibersite corrosion generates a substantial amount of

dissolved $Fe^{2+}$ and $Fe^{3+}$ which can catalyze the polymerization of sugars and other

aldehydes. For instance, the propagation of a glycolaldehyde radical



(107)
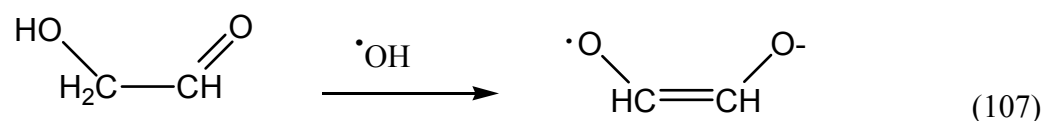
forms a diol radical, a molecule that readily reacts with itself to form tar. Aldolizations

are also catalyzed by $Fe^{2+}$ and $Fe^{3+}$ (see chapter 4), which is problematic for more

prebiotic hypotheses.

Ionic organic compounds like carboxylic acids are the most likely compounds to

be phosphorylated in this environment. These compounds are stabilized by keto-enol

tautomerization and by the negatively charged carboxylic acid functional group. In the

absence of other mechanisms like stabilization through organosulfide formation, the

likely first organic P compounds consisted of phosphorylated carboxylic acids.

Subsequent reactions could lead to biologically useful products. For instance,

decarboxylation of 3,4-dihydroxylbutanoic acid could lead to 1-phosphoglycerol:

$$\cdot OPO_3^{2-} \quad \xrightarrow{\phantom{xxxx}} \quad -CO_2$$

(108)
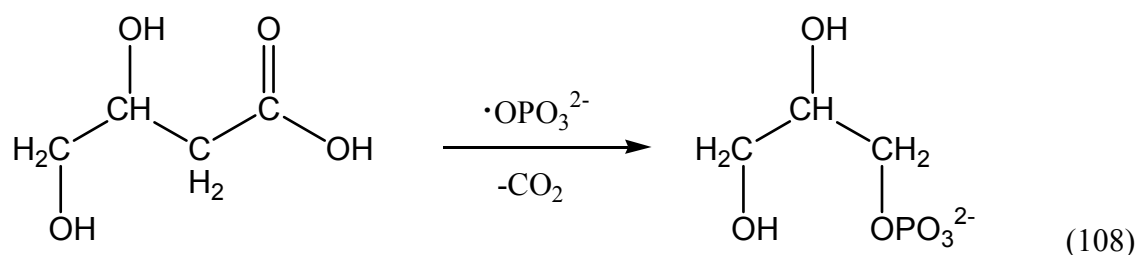
which is the critical organophosphate species in all lipids.

It is very difficult to phosphorylate complex organic species like adenosine

through a radical mechanism simply due to the number of possible locations at which

adenosine could be phosphorylated. Thus the phosphorylation of simple compounds

probably preceded the phosphorylation of complex molecules.

These reaction pathways carry intriguing results for the origin of phosphorylated

biomolecules. This phosphorylation pathway proceeds at low temperatures under simple

conditions and suggests that meteoritic material played a major role in the origin of life.

This is further supported by the flux of material that fell to the Earth early in its history.

7.3 Meteorites versus Other Reactive Phosphorus Sources

Iron meteorites were the most likely source of schreibersite on the early Earth. Our

experiments used the same amount of schreibersite present in an iron meteorite of 10-20

g. The current flux of metallic P is $1.5 \times 10^3$ kg / year. During the late heavy

bombardment period, the impact rate may have been as much as $10^5 \times$ larger, for a total

flux of 2-3 $\times 10^8$ kg of P per year. Correspondingly, organophosphorus compounds

would be produced at a total amount of $10^6$-$10^7$ kg per year assuming identical rates to

these experiments. Large impactors may have increased the local concentration of

reactive P to ~1 kg per m$^2$, a huge concentration. How do these values compare with

terrestrial values?

Yamagata et al. (1991) proposed volcanism as a feasible source of

polyphosphates, which could then react to form organophosphates, as per reactions

described by Rabinowitz et al (1968) and Schwartz and Ponnamperuma (1968). Using the

ideal situation (used by Keefe and Miller 1995 to show why volcanoes do not provide

enough P for phosphorylation reactions), one would expect ~$10^9$ kg of P would be

released by volcanoes per year. Measurements of the polyphosphate concentration of the

fumarole waters of Mount Usu suggest that the actual polyphosphate yield is actually

closer to 1%, and the actual amount released might be several orders of magnitude less

than this amount (which would counteract a higher rate of volcanism on the early Earth).

Phosphorylation of organics would be much lower, given that these energetic

polyphosphates are in aqueous systems and the condensation reaction would be inhibited

by the prodigious amount of water (with yields perhaps at $\sim 10^{-3}$). Taking the low yield of polyphosphates and the low yield of condensation reactions, organophosphates may be produced at $\sim 10^4$ kg/year, as a maximum estimate.

Lightning has been proposed as a source of reduced P compounds (Glindemann et al. 1999). The system described consists of phosphate minerals being heated to high temperatures by lightning, and reduced to phosphite. Yields were maximized ($\sim 5\%$) with Na-phosphates on a clay matrix. The maximum localized accumulation is estimated $\sim 10^{-5}$ mols per m$^2$ per year by this pathway.

Orgel (2004) outlines three major restrictions for any system to be considered important in prebiotic evolution: 1) the starting materials must be present in adequate amounts at the site of synthesis; 2) reactions must occur in water or in the absence of a solvent; and 3) the yield of the product must be significant. In all three cases, the proposed meteoritic P source has the upper hand compared to the volcanic and lightning models. A meteorite may deliver huge quantities of highly reactive P to a single location, whereas volcanoes and lightning do not. Furthermore, IDPs fall evenly across the surface of the Earth. Additionally, volcanic activity is transient, lasting for short geologic timescales; whereas a single large meteorite (such as a $10^8$ kg meteorite like the one that formed Meteor Crater, AZ) would provide a long-lived source of P through corrosion, especially if confined to a crater-lake.

7.4 What was the First Phosphorus Biomolecule?

These experiments inform us on the nature of the first P biomolecules, and thereby the history of the origin of life, if we assume that the schreibersite corrosion pathway described above was the pathway through which the first P biomolecules were formed. How does this information compare and inform views on the origin of life?

Was P even involved in the first life?  Given the difficulties associated with prebiotic phosphorylation, some say no (see chapter 1).  However, given the dominance of P in metabolism, it is hard to see how life would have "changed horses" from non P-based metabolism and replication to P-based metabolism and replication.  The phosphorus problem is plausibly overcome by using P radicals generated through the corrosion of schreibersite.

7.4.1 Clues from Biochemistry

The "strong" RNA world posits the spontaneous formation of nucleotides through the phosphorylation of nucleosides, followed by the activation of nucleotides and resulting in the formation of a strand of an RNA polymer.  In this view, complex phosphorylated biomolecules preceded the origin of life.  It is due to this complexity that the "strong" RNA world is unlikely.  The chemistry of this system requires exacting specificity of placement for many of the components of RNA.  For one, the nucleobases must be linked to the ribose at the first carbon of the sugar through a dehydration reaction, which also

must be produced in abundance through abiotic processes. Ribose is difficult to produce

through prebiotic chemistry, as are all sugars (Ricardo et al. 2004). Orthophosphate must

then link to the fifth carbon of ribose, and must be activated by adding two more

orthophosphates, all through a series of dehydration reactions. Finally, the activated

nucleotide must link together through the fifth and third carbons of ribose, forming a

chain. Each of these events is unlikely and the multiplication of unlikely events results in

an extremely unlikely total event (Shapiro 1986).

A more advantageous way to look at the origin of P organics is to analyze the P

species in the categories defined in chapter 1. What was the first energetic P

biomolecule? What was the first stable P biomolecule? For the first, we examine

metabolism since phosphate bond energy is key to life. Next, we analyze replication and

structural P biomolecules.


7.4.1.1 Phosphorus Metabolism


Understanding the order in which biochemical components arose aids our understanding

of the origin of life. For instance, consider the molecule ATP. What was the first

purpose of ATP? Was ATP first used in metabolic processes as the main energy carrier

of life or was it first used to construct RNA? The chemistry of ATP suggests the latter.

For one, ATP is chemically identical to the adenosine nucleotide in RNA, except for the

presence of a polyphosphate. The nature of the ribose sugar in the adenosine nucleotide

is specific to the formation of RNA, i.e. the 3 and 5 carbons in ribose are specific to

forming a bridging polymer. This stereospecificity is not utilized in metabolic reactions involving ATP, and the specification of this stereochemistry would be detrimental for early biochemistry as it would require a very specialized chemical pathway. Specificity is unlikely for early metabolism. ATP is also not the only energy carrying nucleotide in life. Other nucleotide triphosphates like CTP and GTP have specific, albeit minor roles as energy carriers. Together these lines of evidence suggest that the RNA world preceded ATP-centered metabolism. It is likely that some other metabolic carrier of energy preceded ATP, and that ATP produced primarily for RNA synthesis was coopted into this role as had chemical properties that made it useful for metabolism (like an intermediate energeticity and low concentrations of cellular ADP). ATP-based metabolism likely followed the origin of life by several million years.

Possible metabolic precursors to ATP include simple sugar polyphosphates, polyphosphates, and perhaps P-N compounds (figure 52). Sugar polyphosphates are less specific than ATP and stereochemistry-specific synthesis of sugar phosphates would be less critical for these compounds. Perhaps metabolic energy was first stored by less specific phosphorylations of sugar in cells, and that this was later coopted by RNA synthesis. P-N compounds are used today for phosphate energy storage, and the dephosphorylation of these compounds is close in energy to the dephosphorylation of ATP. Inorganic polyphosphates are present in many organisms today, and these have the potential to phosphorylate some organics, though the energy yield is lower than that for

Figure 52. Possible precursors to ATP.

## High energy sugar phosphates (glucose and ribose pyrophosphates)

$H_2C$ —$OP_2O_6^{3-}$
OH
O
OH
OH
OH

$^{3-}O_6P_2O$—$CH_2$
OH
O
OH   OH

## P-N Compounds (Phosphocreatine)

O
$NH_2^+$
-O
$H_2$
C
-O
P
$O^-$
N
C
N
C
H
O
$CH_3$
O
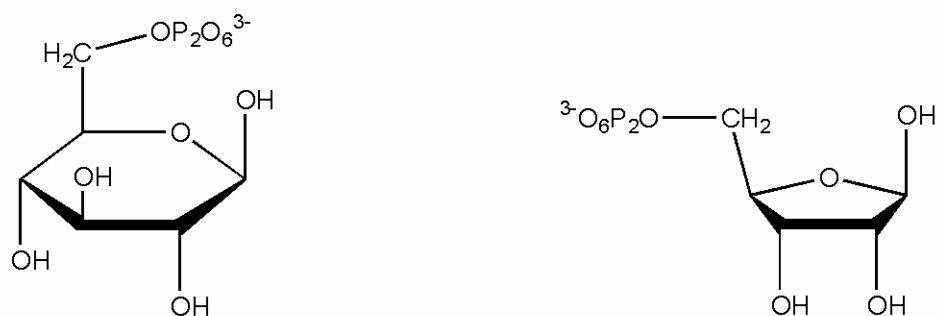
## Polyphosphates (triphosphate)

O          O          O
-O—P—O—P—O—P—O-
$O^-$       $O^-$       $O^-$
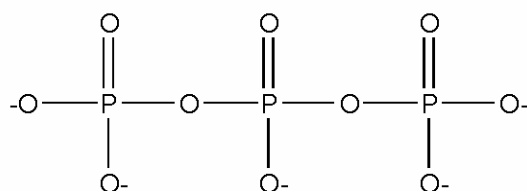
ATP.  Nonetheless, polyphosphates are fairly simple, and their abiotic production is well documented.

The corrosion experiments produce significant quantities of polyphosphate material, especially pyrophosphate.  The production of pyrophosphate and polyphosphate is relatively easy compared to organophosphate production. The very first energetic P biomolecule was probably an inorganic P species like pyrophosphate or a higher polyphosphate for this reason.  Subsequent evolution would have preferred sugar polyphosphates, P-N compounds, and eventually ATP because these compounds are all superior energy carriers than polyphosphates.  These later phosphate energy carriers are better at storing more energy from chemical reactions, thus allowing better energy extraction, and hence greater metabolic potential.  Given subsequent selective pressures from Darwinian evolution, organisms that used high energy organo(poly)phosphate compounds as metabolic energy carriers would be more fit and hence outbreed the polyphosphate metabolic energy carriers.

7.4.1.2 Metabolism and Replication

If polyphosphates preceded energetic organophosphates, then what was the first stable P biomolecule?  Was it involved in replication in RNA?  Table 1 shows the abundance of the biogenic elements H, C, O, N, S, and P in RNA, the metabolism core, lipids, and bulk bacteria.  The ratio of these biogenic elements in metabolism and in RNA is remarkably similar.  This similarity may indicate that these two processes are intricately linked, and

that either they arose together, or one was initially established and in turn resulted in the second. So which came first, metabolism or replication?

Replication is a metabolic process today, so it would seem obvious that metabolism arose first. Thus this question is partially an exercise in semantics, but comes down to the key discussion: A replicator could have been the first metabolic process to originate, and hence would in turn have led the chemistry of metabolism. However, given the complexity of all replicators compared to the mish-mash of reactions that define metabolism, this seems unlikely. Simple organics are more easily phosphorylated organics than are complex replicators, as detailed by the phosphide corrosion experiments. Pre-life or the first life probably consisted of a set of metabolic processes designed to extract, store, and utilize energy, and replication probably arose as a secondary process.

What does this entail for early life? Informational molecules code for proteins, which construct cell parts and catalyze reactions. Without an informational molecule, early life would have depended on the abiotic production or availability of key components. This sort of world could be termed a "Vitamin World," by comparison to modern life. Humans have lost the ability to synthesize vitamin C through metabolic reactions. The genes that code for vitamin C production have been corrupted and as a result, humans can no longer produce vitamin C. We must extract this vital nutrient from the food we eat. The "Vitamin World" implies that life was heterotrophic to begin with, and that informational molecules became necessary as the vitamins were removed. Perhaps the first informational molecules were used for energy storage or catalysis, and

their ability to drive replication became an advantageous secondary feature (later a primary feature) as conditions became less accommodating to the vitamin world.

7.4.1.3 Other Phosphorus Biomolecules

Another group of P biomolecules are the phospholipids. Section 7.2.2 describes a potential pathway for the origin of phosphoglycerol, the key organophosphate constituent of phospholipids. Lipids are critical to organisms as they provide a two dimensional surface for biochemical reactions. Removing one dimension is advantageous for chemical reactions and allows for greater reaction specificity and increased reaction rate. Many proteins are bound to membranes and catalyze chemical reactions, and lipids, proteins, carbohydrate metabolism, and many other cellular functions take place bound to membrane material (including the endoplasmic reticulum). The phosphate groups of phospholipids provide a charge matrix similar to a mineral surface, and enable the synthesis of many metabolic compounds.

Some (e.g. Cairns-Smith 1982, Smith 1998) have posited a mineral / mineral surface origin for early life based on these factors. Mineral surfaces, like lipid bilayers, are two dimensional and assist chemical reactions. Perhaps phospholipids did the same, providing a mineral-like surface on which metabolic chemical reactions could take place, in addition to provide a distinct boundary between cellular and non-cellular material. Perhaps phospholipids were the first organophosphate molecule?

The organic P compounds produced through schreibersite corrosion include several P-C compounds as well as P-O-C compounds similar to those found in modern phospholipids. Biologic P-C compounds are almost exclusively a constituent of lipid material. These modern characteristics of compounds similar to those produced through schreibersite corrosion may belie ancient biochemistry. Perhaps the phospholipids detail the original environment for life?

7.5 Sulfur in Biochemistry

Pasek et al. (2005) provided an overview of sulfur cosmochemistry in the Solar System, and discuss the effects of change C/O ratios due to water diffusion, the effects of sulfide removal from the formation of troilite, and the diffusion of sulfur. These concepts were placed in the planetary context of sulfur abundances in Jupiter, enstatite chondrite mineralogy, and extrasolar system gases. This paper was presented as chapter 6. Troilite (FeS) is the dominant sulfur mineral in most systems.

Troilite has been implicated in the origin of life process (Wachterhauser 1988a). Subsequent research has emphasized the role of sulfides in early metabolism or in prebiotic synthesis. There are two views of sulfur in the study of the origin of life- sulfides as a metabolic fuel, and sulfides as a catalyst.

Wachterhauser (1988b) proposed that troilite could be sulfidized by $H_2S$:

$$FeS + H_2S \rightarrow FeS_2 + H_2 \tag{109}$$

to form pyrite and release hydrogen gas. This reaction is exothermic and could have been an early pathway for metabolism. This is the pyrite-pulled metabolism described by Cody (2004). Some experiments with sulfides suggest that organic compounds are changed through pathways similar to metabolism, but a full description of the process is lacking.

Sulfides have been employed in catalysts for the synthesis of important biomolecules (Cody et al. 2000, 2001). In these experiments, sulfides like troilite reduce $CO_2$ and CO to form organic acids, a carbon-fixation pathway. The reactive site for these reactions appears to be the metal ion with sulfur stabilizing organic intermediates. The activity of sulfur in these systems better mimics the activity of sulfur in modern biochemistry.

Sulfur is a critical biochemical element. Unlike P, S fills only two distinct, but critical roles in biology. Sulfur is critical to catalytic and metabolic molecules.

Amino acids are the constituents of proteins, which are the catalytic molecules of life. Two of the twenty amino acids have sulfur- methionine and cysteine (figure 53). The amino acid cysteine is the major amino acid that controls the tertiary structure of proteins, which determines the shape of these molecules and hence their reactivity. Two cysteine amino acids form disulfide bonds which tie the protein together in certain locations. This linkage is called a cystine residue. Sulfur determines structure in this role, which in turn determines catalytic ability. Interestingly enough, the sulfide necessary for these amino acids in generated through a series of reductions from phosphate energy, implying a metabolic link between P and S (figure 54).

Figure 53. Sulfur biomolecules.

## S Aminoacids

### Methionine

NH₃+ ... structure

$$NH_3^+$$

HC—C—S—CH₃ with H₂ H₂ and COO-

### Cysteine

$$NH_3^+$$

HC—C—SH with H₂ and COO-

## Coenzyme A

HS—C(H₂)—C(H₂)—N(H)—C(=O)—C(H₂)—CH₂—HN—C(=O)—CH—OH—C(CH₃)(H₃C)—CH₂—O—P(=O)(O-)—O—P(=O)(O-)—Adenosine-3-Phosphate

## Rieske Center

Fe—S cluster structure (Fe, S cubane with four Fe and four S)
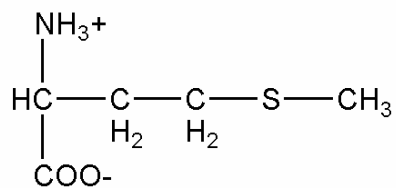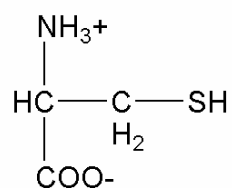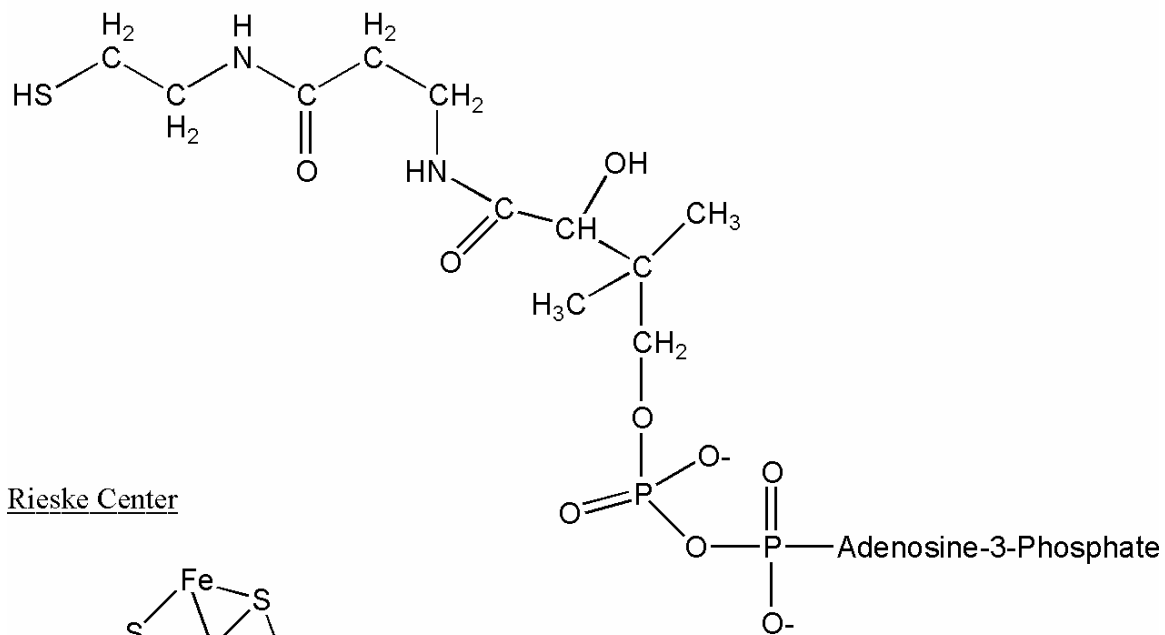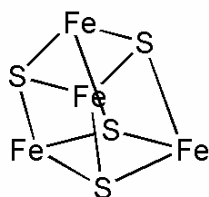
Figure 54.  The metabolic production of sulfide from sulfate using P organics.



$+ ATP$

$+ P_2O_7{}^{4-}$

Reduction x 2

$S^{2-} + AMP$
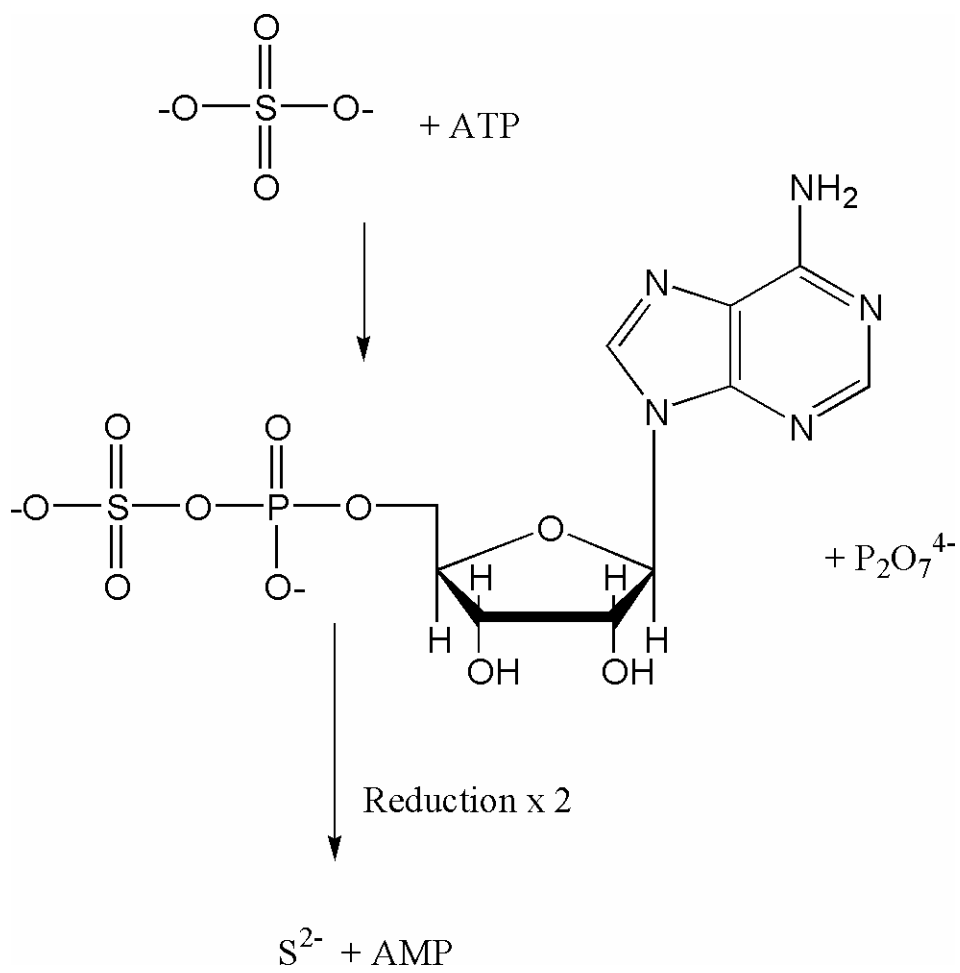
Sulfur plays a similar role in metabolism as it acts mainly as catalyst. Coenzyme A (CoA) is the primary workhorse for the citric acid cycle, and its reactivity is due to the reactive thiol group (figure 53). This thiol bonds through dehydration to carboxylic acids, allowing further reactions to take place. A final S molecule of relevance is the Rieske iron-sulfur proteins (figure 53). These compounds are the primary workhorses for mitochondrial electron transfer. Interestingly, all Rieske iron-sulfur proteins have the stoichiometric formula FeS, identical to the meteoritic mineral troilite.

Sulfur is a key element of metabolism, and it often acts in tandem with phosphate. For example, the enzyme glyceraldehyde 3-phosphate dehydrogenase uses a thiol bond to bind glyceraldehyde 3-phosphate, where it is oxidized, and phosphorylated to form an energetic phosphoanhydride (figure 55), which loses its phosphate group to provide energy for the phosphorylation of ADP to form ATP. Several other metabolic reactions involve the formation of a thioester followed by subsequent phosphorylation, including key reactions of the citric acid cycle.

Understanding the interplay of P and S in metabolism is a key to understanding the origin of life. Given that meteoritic schreibersite is an excellent source of prebiotic P, and that some of the metabolic workhorse molecules are stoichiometrically similar to meteoritic troilite, then understanding the cosmochemical behavior of S also informs our understanding of the origin of life.

Figure 55. P-S cooperative metabolism. The phosphorylation of 3-glyceraldehyde phosphate follows the formation of a thioester.
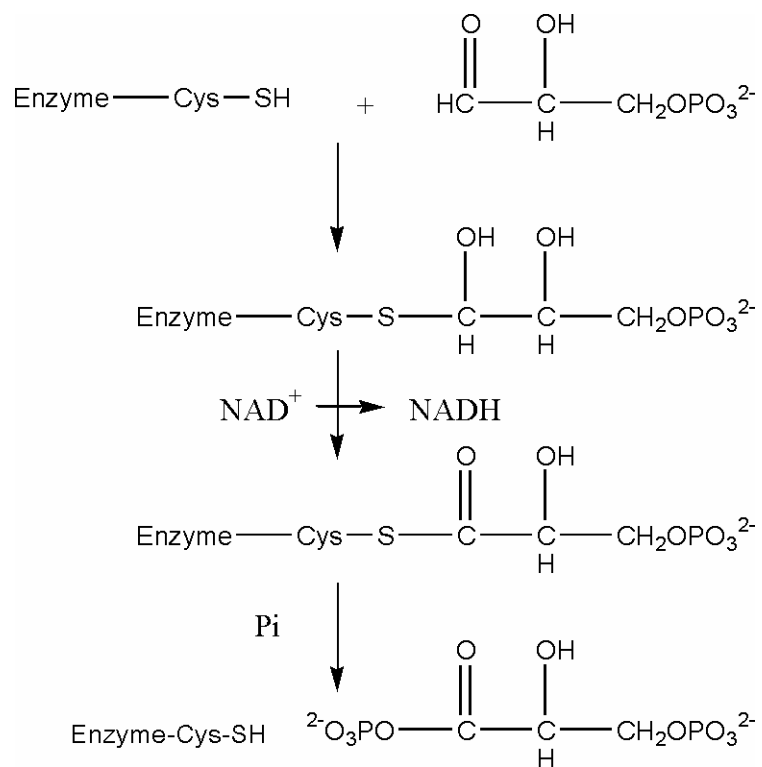
Phosphide / sulfide assemblages are common in meteorites, and sulfide nodules are frequently rimmed by sizable schreibersite layers.  This mineral assemblage is replicated in the sulfidization experiments of Lauretta et al. (1998).  The spatial relatedness of these two meteorite minerals coupled with the metabolic relatedness is intriguing, and warrants further study.

7.6 Speculation on the Origin of Life

A speculative scenario leading to the origin of life follows.

A large meteorite struck the early Earth.   It leaves a 5 km diameter crater from its collision, and a huge amount of metallic minerals, including schreibersite, cohenite, troilite (FeS), and simple iron nickel alloy.  Since the crater is a topographic low, it accumulates water which washes down its slopes, dissolving organics from IDP material and some material which has been produced endogenously.  The organic-laden water flows down the slope and gathers in a pool at the bottom of the crater.  Water evaporates from the crater, increasing the concentration of the non-volatile mineral salts and organics.

Simple chemical reactions begin to occur between the corroding metal and dissolved organics.  The cohenite corrodes to form a hydrocarbon oil slick on top of the crater-lake, which protects many of the organic compounds from damaging UV radiation. Some organic compounds are reduced from H· radicals, others are polymerized and oxidized from ·OH radicals.  Others bond to the sulfide minerals where they are protected

from attack. Still others gain phosphate and C-P linkages. The corroding metal and constant flux of organic material keeps the system in disequilibrium. Some chemical reactions counteract the disequilibrium by proceeding to thermodynamically preferred states. Other chemical reactions become coupled, and aid in increasing the diversity of the system by using the energy flux to produce a complex group of products.

Eventually the certain molecules in the system are preferentially formed compared to other molecules, and begin to form cycles wherein the members of the cycle are generated from simpler starting materials. Sulfides are major catalysts affecting the directed synthesis of species, and energetic phosphates provide the energy. At some point, the system starts to utilize the chemical energy of the corroding metal and organic solution to form the cycle members. Perhaps these reactions occur on the surface of a phosphate mineral grain, which has formed through the addition of weathered Ca and Mg salts to orthophosphate from corroded schreibersite. The phosphate catalyzes many reactions due to its charged nature and available surface area. Other reactions take place on sulfide grains, including many that are thermodynamically unfavorable. Due to the close proximity of these sulfide / P assemblages, these two chemistries become interlinked. Eventually, phospholipids become abundant enough that these chemical systems can leave the surface of the phosphate minerals enclosed in their own mineral-like membrane. Some capture sulfide grains which further increases their ability to produce cycle chemicals.

RNA may have originated as a chemical catalyst. The nucleobases of RNA are capable of stabilizing metabolic intermediates and encouraging reaction, though this

activity is currently performed by the amino acid hystidine in enzymes. Ribose in RNA may act to bind some energetic products by hydrolysis, acting in the same fashion as serine in modern catalytic intermediates. The phosphate in RNA can serve as an immediate source of P for chemical reactions. Thus original role of RNA could have been to encourage reactions by stabilizing energetic intermediates. The replicative and informational potential of RNA might have been coopted after this primary function.

Eventually, the suite of chemical reactions becomes very complex, and energy is stored in large polymers. Some of these polymers happen to catalyze other reactions, and other polymers are autocatalytic. The coupling of the chemical cycles with the autocatalytic molecules leads to a replicator, where the chemical cycles are used primarily to provide the materials necessary for the autocatalytic molecule to replicate. Replicators which are more efficient at replicating begin to dominate the system, eventually leading to biological evolution.

The crater begins to run low on the materials necessary for this early life. Some craters are destroyed by even larger impacts, stopping this primitive chemistry before it can get suitably started. Other craters are mercilessly heated and irradiated by the sun, polymerizing the organic compounds to the point of no biochemical utility. Some of these primitive organisms escape, either through destruction of their crater wall, or through a change in sea level. Some find security near volcanic fumaroles, where a steady source of phosphate, sulfide, and relatively quiescent conditions allow for proliferation and development. When the bombardment has slowed to a halt, some organisms return to the surface of the Earth where their biochemistries adapt to utilizing

solar energy.  With more time, these organisms evolve, diversify, and result in the life-

filled world of today.


7.7 Conclusion


The early Earth lacked reactive P compounds due to the stability of phosphate minerals.

Phosphorus has advantageous chemical properties which are utilized in modern day

biochemistry, but the life at the beginning would not have had a means of incorporating P

into its biochemical systems unless there was a source of reactive P on the early Earth.

Most proposed prebiotic mechanisms for the production of reactive P compounds are

flawed due to too much complexity or lack of a geochemical framework.

Meteoritic schreibersite corrodes to form a mixed valence set of P compounds.

The corrosion of schreibersite was demonstrated through a series of experimental studies

and a mineralogical study of corroded schreibersite in an aubrite meteorite.  Schreibersite

corrodes to form several P salts over relatively short geologic timescales.

Schreibersite corrodes to form a set of radicals.  The termination and propagation

reactions of these radicals results in the P compound chemistry observed in the

experimental studies.  Organic compounds are phosphorylated by these P radicals to form

P-C and P-O-C linkages.

Schreibersite is an abundant constituent of meteoritic metal.  Meteoritic metal was

readily available on the surface of the early Earth through large impacts by meteorites.

These large impacts delivered huge amounts of reduced P prior to the first evidence of

life, which indicates that biochemical systems were developed after the delivery of reduced P material.

Sulfur is an important biochemical element and is also delivered in large quantities by meteorites.  The cosmochemical behavior of sulfur was determined with changing O abundances.  Sulfur chemistry in turn informs studies of meteorites, Jupiter, and of early extrasolar disk material.

This work has shown the relevance of meteoritic material to the origin of life.  It is the first work to recognize the potential of reduced P as a source of reactive phosphorus for the origin of life.  The corrosion of schreibersite provides a ready route to the origin of biochemistry and metabolism. Assuming that schreibersite was the first source of P for life, this study also provides insight into the development of biochemical systems, including the temporal placement of the RNA world.

REFERENCES

Alexeev V.A., 2003, Meteorite ablation evaluated from data on the distribution of cosmogenic neon isotopes. *Solar System Research* **37**, 207-217.

Anders, E., 1989, Pre-biotic organic matter from comets and asteroids. *Nature* **342,** 255-257.

Atreya, S. K., Mahaffy, P., Niemann, H.B., Wong, M.H., and Owen, T., 2003, Comparison of the atmospheres of Jupiter and Saturn: Deep atmospheric composition, cloud structure, vertical mixing, and origin. *Planetary and Space Science* **47**, 1243- 262.

Baedecker, P. A. and Wasson, J.T., 1975, Elemental fractionations among enstatite chondrites. *Geochimica et Cosmochimica Acta* **39**, 735-765.

Baltscheffsky, H., 1971, In *Chemical Evolution and the Origin of Life*, (Buvet, R. and Ponnamperuma, C., eds.). North-Holland, Amsterdam, Netherlands, 466-474.

Barin, I., 1995, Thermochemical Data of Pure Substances. VCH Publishers, Weinheim, Germany.

Bean, H.D., Anet, F.A.L., Gould, I.R., and Hud, N.V., 2006, Glyoxylate as a backbone linkage for a prebiotic ancestor of RNA. *Origins of Life and Evolution of Biospheres* **36**, 39-63.

Beck, A., and Orgel, L.E., 1965, The formation of condensed phosphate in aqueous solution. *Proc. Natl. Acad. Sci. USA* **54**, 664-667.

Ben Omar, N., Gonzalez-Munoz, M.T., and Penalver, J.M.A., 1998, Struvite crystallization on Myxococcus cells. *Chemosphere* **36**, 75-481.

Berner, E.K. and Berner, R.A., 1996, Global environment. Water, Air, and Geochemical Cycles, Prentice Hall, Upper Saddle River, NJ, USA, 376 pp.

Bessman, T. M., 1977, SOLGASMIX-PV - A Computer Program to Calculate Equilibrium Relationships in Complex Chemical Systems, Oak Ridge National Laboratory Rep. TM-5775 (Oak Ridge: ORNL)

Bishop, M.J., Lohrmann, R., and Orgel, L.E., 1972, Prebiotic phosphorylation of thymidine at 65°C in simulated desert conditions. *Nature* **237**, 162-164.

Bjoraker, G.L., Larson, H.P., and Kunde, V.G., 1986, The gas-composition of Jupiter derived from 5μm airborne spectroscopic observations. *Icarus* **66,** 579-609

Bland, P.A. and Artemieva, N.A., 2003, Efficient disruption of small asteroids by Earth's atmosphere. *Nature* **424**, 288-291.

Bland, P.A., Berry, F.J., Smith, T.B., Skinner, S.J., and Pillinger, C.T., 1996, The flux of meteorites to the Earth and weathering in hot desert ordinary chondrite finds. *Geochimica et Cosmochimica Acta* **60**, 2053-2059.

Blaser, B. and Halpern, P., 1933, The oxidation of hypophosphoric acid by bromine. *Zeitschrift fur Anorganische und Allgemeine Chemie* **215**, 33-43.

Bockelée-Morvan, D., Crovisier, J., Mumma, M.J., and Weaver, H.A., 2004, In *Comets II* (Festou, M.C., Keller, H.U., and Weaver, H.A., eds.). University of Arizona Press, Tucson, AZ, USA, 391-423.

Bockelée-Morvan, D., Gautier, D., Hersant, F., Huré, J.-M., and Robert, F., 2002, Turbulent radial mixing in the solar nebula as the source of crystalline silicates in comets. *Astronomy and Astrophysics* **384**, 1107-1118

Boerio-Goates, J., Francis, M.R., Goldberg, R.N, Ribeiro da Silva, M.A.V., Ribeiro da Silva, M.D.M.C., and Tewarif, Y.B., 2001, Thermochemistry of adenosine. *J. Chem. Thermodynamics* **33**, 929–947.

Bogard, D.D. and Garrison, D.H., 2003, $^{39}$Ar-$^{40}$Ar ages of eucrites and thermal history of asteroid 4 Vesta. *Meteoritics & Planetary Science* **38,** 669-710.

Bohler, C., Nielsen, P.E., and Orgel, L.E., 1995, Template switching between PNA and RNA oligonucleotides. *Nature* **376**, 578-581

Brearley, A.J. and Jones, R.H., 1998, In *Planetary Materials: Reviews in Mineralogy, v. 36* (Papike, J.J., ed.). The Mineralogical Society of America, Washington DC, USA. Ch. 3.

Brearley, A.J., Saxton, J.M., Lyon, I.C., and Turner, G., 1999, Carbonates in the murchison CM chondrite: CL characteristics and oxygen isotopic compositions. *Lunar and Planetary Science Conference* **XXX**, 1301.

Britvin, S.N., Kolomenskii, V.D., Boldyreva, M.M., Bogdanova, A.N., Kretser, Yu.L., Boldyreva, O.N., and Rudashevskii, N.S., 1999, Nickelphosphide (Ni,Fe)$_3$P, the nickel analog of schreibersite. *Zapiski Vserossiiskogo Mineralogicheskogo Obshchestva* **128**, 64-72.

Britvin, S.N., Rudashevsky, N.S., Krivovichev, S.V., Burns, P.C., and Polekhovsky, Y.S., 2002, Allabogdanite, (Fe,Ni)$_2$P, a new mineral from the Onello meteorite: the occurrence and crystal structure. *American Mineralogist* **87**, 1245-1249.

Buchwald, V., 1975, The Handbook of Iron Meteorites. University of California Press, Berkeley, CA, USA, 1418 pp.

Buchwald, V.F., 1977, Mineralogy of the iron meteorites. *Phil. Trans. Royal Soc. London* **A286,** 453-491.

Burrows, A., and Sharp, C.M., 1999, Chemical equilibrium abundances in brown dwarfs and extrasolar giant planet atmospheres. *Astrophysical Journal* **512**, 843-863.

Buseck, P.R., 1969, Phosphide from metorites; barringerite, a new iron-nickel mineral. *Science* **165**, 169-71.

Buseck, P.R., 1977, Pallasite meteorites- mineralogy, petrology, and geochemistry. *Geochimica et Cosmochimica Acta* **41**, 711-740.

Cade-Menun, B.J., Liu, C.W., Nunlist, R., and McColl, J.G., 2002. Soil and litter phosphorus-31 nuclear magnetic resonance spectroscopy: Extractants, metals, and phosphorus relaxation times. *Journal of Environmental Quality* **31**, 457-465.

Cadogan, J.I.G., 1967, In *Advances in Free Radical Chemistry*, vol. 2 (Williams, G.H., ed.). Academic Press, New York, NY, USA.

Cairns-Smith, A.G., 1982, Genetic Takeover and the Mineral Origins of Life. Cambridge University Press, Cambridge, UK, 488 pp.

Cassen, P., 1994, Utilitarian models of the solar nebula. *Icarus* **112**, 405-429.

Cassen, P., 2001, Nebular thermal evolution and the properties of primitive planetary materials. *Meteoritics and Planetary Science* **36**, 671-700.

Cassidy, W.A. and Harvey, R.P., 1991, Are there real differences between Antarctic finds and modern falls meteorites? *Geochimica et Cosmochimica Acta* **55**, 99-104.

Cech, T.R., Zaug, A.J., and Grabowski, P.J., 1981, In vitro splicing of the ribosomal RNA precursor of tetrahymena: involvement of a guanosine nucleotide in the excision of the intervening sequence. *Cell* **27**, 487-496.

Chase, M.W., 1982, JANAF Thermodynamic Tables, Magnetic Tape Version. Dow Chemical Company, Midland.

Chase, M.W., 1998, NIST-JANAF Thermochemical Tables, 4th Ed. *J. Phys. Chem. Ref. Data Monogr.* **9**.

Cheng, C., Fan, C., Wan, R., Tong, C., Miao, Z., Chen, J., and Zhao, Y., 2002, Phosphorylation of adenosine with trimetaphosphate under simulated prebiotic conditions. *Origins of Life and Evolution of the Biosphere* **32,** 219–224.

Chyba, C.F. and Sagan, C., 1992, Endogenous production, exogenous delivery, and impact-shock synthesis of organic molecules- an inventory for the origins of life. *Nature* **355,** 125-132.

Clayton, D.D., 1988, in *Meteorites and the Early Solar System* (Kerridge, J.F. and Matthews, M.S., eds.). University of Arizona Press, Tucson, AZ, USA, 1021-1062.

Cody, G.D., 2004, Transition metal sulfides and the origins of metabolism. *Annu. Rev. Earth Planet. Sci.* **32**, 569-599.

Cody, G.D. and Alexander, C.M.O.D., 2005, NMR studies of chemical structural variation of insoluble organic matter from different carbonaceous chondrite groups. *Geochimica et Cosmochimica Acta* **69,** 1085–1097.

Cody, G.D., Alexander, C.M.O.D., and Tera, F., 2002, Solid-state ($^1$H and $^{13}$C) nuclear magnetic resonance spectroscopy of insoluble organic residue in the Murchison meteorites: A self-consistent quantitative analysis. *Geochim. Cosmochim. Acta* **66**, 1851-1865.

Cody, G.D., Boctor, N.Z., Filley, T.R., Hazen, R.M., Scott, J.H., and Yoder, H.S., 2000, Primordial carbonylated iron-sulfur compounds and the synthesis of pyruvate. *Science* **289,** 1337-1340.

Cody, G.D., Boctor, N.Z., Hazen, R.M., Brandes, J.A., Morowitz, H.J., and Yoder, H.S., 2001, Geochemical roots of autotrphic carbon fixation: hydrothermal experiments in the system citric acid, $H_2O$-($\pm$FeS)-($\pm$NiS). *Geochim. Cosmochim. Acta* **65**, 3557-3576.

Cohen, B.A., Swindle, T.D., and Kring, D.A., 2000, Support for the Lunar cataclysm hypothesis from lunar meteorite impact melt ages. *Science* **290,** 1754-1756.

Cohen, B.A., Swindle, T.D., and Kring, D.A., 2005, Geochemistry and $^{40}$Ar-$^{39}$Ar geochronology of impact-melt clasts in feldspathic lunar meteorites: Implications for Lunar bombardment history. *Meteoritics and Planetary Science* **40**, 755-778.

Cook, D.L., Walker, R.J., Horan, M.F., Wasson, J.T., and Morgan, J.W., 2004, Pt-Re-Os systematics of group IIAB and IIIAB iron meteorites. *Geochimica et Cosmochimica Acta* **68,** 1413-1431.

Cooper, G.W., Onwo, W.M., and Cronin, J.R., 1992, Alkyl phosphonic-acids and sulfonic-acids in the Murchison meteorite. *Geochimica et Cosmochimica Acta* **56,** 4109-4115.

Crick, F.H.C., 1968, The origin of the genetic code. *Journal of Molecular Biology* **38**, 367-379.

Cronin, J.R., Pizzarello, S., and Cruikshank, D.P., 1988, In *Meteorites and the Early Solar System* (Kerridge, J.F. and Matthews, M.S., eds.). University of Arizona Press, Tucson, Arizona, USA, 819-857.

Cyr, K. E., Sears, W.D., and Lunine, J.I., 1998, Distribution and evolution of water ice in the solar nebula: implications for solar system body formation. *Icarus* **135**, 537-548.

Cyr, K. E., Sharp, C.M., and Lunine, J.I., 1999, Effects of the redistribution of water in the solar nebula on nebular chemistry. *Journal of Geophysical Research* **104**, 19,003-19,014.

De Duve, C., 1998, in *Molecular Origins of Life,* (Brack, A., ed.). Cambridge University Press, Cambridge, UK, 219-236.

de Graaf, R.M. and Schwartz, A.W., 2005, Thermal synthesis of nucleoside H-phosphonates under mild conditions. *Origins of Life and Evolution of Biospheres* **35,** 1-10

de Graaf, R.M., Visscher, J., and Schwartz, A.W., 1995, A plausibly prebiotic synthesis of phosphonic acids. *Nature* **378**, 474-477.

de Graaf, R.M., Visscher, J., and Schwartz, A.W., 1997, Reactive phosphonic acids as prebiotic carriers of phosphorus. *Journal of Molecular Evolultion* **44**, 237-241.

de Zwart, I.I., Meade, S.J., and Pratt, A.J., 2004, Biomimetic phosphoryl transfer catalysed by iron(II)-mineral precipitates. *Geochimica et Cosmochimica Acta* **68,** 4093-4098.

Devouard, B. and Buseck, P.R., 1997, P-rich Fe, Ni sulfides in CM2 chondrites: condensation or alteration products?  *Meteoritics and Planetary Science* **32**, A34-A35.

Doan, A.S. Jr. and Goldstein, J.L., 1969, In *Meteorite Research* (Millman, P.M., ed.) D. Reidel Pub. Co., Boston, MA, USA, 763.

Drouart, A., Dubrulle, B., Gautier, D., and Robert, F., 1999, Structure and transport in the solar nebula from constraints on deuterium enrichment and giant planets formation. *Icarus* **140**, 129-155.

Dulick, M., Bauschlicher, C.W. Jr., Burrows, A., Sharp, C.M., Ram, R.S., and Bernath, P., 2003, Line intensities and molecular opacities of the FeH $F^4\Delta_i$ - $X^4\Delta_i$ Transition.  *The Astrophysical Journal* **594,** 651-663.

Dutrey, R. M., Guilloteau, S., and Guelin, M., 1997, Chemistry of protosolar-like nebulae: The molecular content of the DM Tau and GG Tau disks. *Astronomy and Astrophysics* **317**, L55-L58.

Ebel, D.S. and Grossman, L., 2000, Condensation in dust-enriched systems.  *Geochimica et Cosmochimica Acta* **64**, 339-366.

Ehlers, K. and El Goresy, A., 1988, Normal and reverse zoning in niningerite: a novel key parameter to the thermal histories of EH chondrites. *Geochimica et Cosmochimica Acta* **52**, 877-887.

Emsley, J., 2000., The 13th Element: The Sordid Tale of Murder, Fire, and Phosphorus. John Wiley & Sons, New York, NY, USA 327 pp.

Engel, R., 1977, Phosphonates as analogues of natural phosphates. *Chemical Reviews* **77**, 349-367.

Eriksson, G. and Rosé, E., 1973, Thermodynamic studies of high-temperature equilibria.8. General equations for calculation of equilibria in multiphase systems. *Chem. Scripta* **4**, 193.

Fegley B., Jr. 1988, Cosmochemical trends of volatile elements in the solar system. In *Workshop on the Origins of Solar Systems* (Nuth, J.A. and Sylvester, P.J., eds.). LPI Technical Report No. 88-04, 51-60.

Fegley, B. and Lewis, J.S., 1980, Volatile element chemistry in the solar nebula: Na, K, F, Cl, Br, and P. *Icarus* **41**, 439-455.

Ferris, J.P. and Ertem G., 1993, Oligomerization reactions of ribonucleotides - the reaction of the 5'-phosphorimidazolide of adenosine with diadenosine pyrophosphate on montmorillonite and other minerals. *Origins of Life and Evolution of the Biosphere* **23,** 229-241.

Ferris, J.P., Yanagawa, H., Dudgeon, P.A., Hagan, W.J. Jr., and Mallare, T.E., 1984, The investigation of the HCN derivative diiminosuccinonitrile as a prebiotic condensing agent. The formation of phosphate esters. *Origins of Life and Evolution of Biospheres* **15,** 29-43.

Forti, G. and Rosa, L., 1974, Mechanism of stimulation of photosynthesis by pyrophosphate. *Plant Science Letters* **2,** 95-100.

Frei, R. and Rosing, M.T., 2005, Search for traces of the late heavy bombardment on Earth-Results from high precision chromium isotopes. *Earth and Planetary Science Letters* **236**, 28-40.

French, B. M., 1998, Traces of Catastrophe: A Handbook of Shock-Metamorphic Effects in Terrestrial MeteoriteImpact Structures. LPI Contribution No. 954, Lunar and Planetary Institute, Houston, TX, USA, 120 pp.

Frossard, E., Brossard, M.B., Hedley, M.J., and Metherell, A., 1998, In *Phosphorus in the Global Environment: Transfers, Cycles and Management* (Tiessen, H., ed.). Wiley, Chichester, UK, 107–137.

Gabel, N.W., 1968, Abiotic formation of phosphoric anhydride bonds in dilute aqueous conditions. *Nature* **218,** 354.

Gao, K. and Orgel, L.E., 2000, Polyphosphorylation and non-enzymatic template-directed ligation of oligonucleotides. *Origins of Life and Evolution of the Biosphere* **30,** 45–51.

Gautier, D., Hersant, F., Mousis, O., and Lunine, J.I., 2001, Enrichments in volatiles in Jupiter: A new interpretation of the Galileo measurements. *Astrophysical Journal (Letters)* **550**, L227-L230 (erratum **559**, L183).

Gilbert, W., 1986, Origin of life- the RNA world. *Nature* **319**, 618.

Gillham, R.W. and O'Hannesin, S.F., 1994, Enhanced degradation of halogenated aliphatics by zero-valent iron. *Ground Water* **32**, 958-967.

Glavin, D.P. and Bada, J.L., 2001, Survival of amino acids in micrometeorites during atmospheric entry. *Astrobiology* **1**, 259-269.

Glindemann. D., de Graaf, R.M., and Schwartz, A.W., 1999, Chemical reduction of phosphate on the primitive Earth. *Origins of Life and Evolution of the Biosphere* **29,** 555-561.

Gomberg, M., 1900, An instance of trivalent carbon triphenylmethyl. *Journal of the American Chemical Society* **22**, 757-771.

González-Toril, E., Martínez-Frías, J., Gómez, J.M.G., Rull, F., and Amils, R., 2005, Iron meteorites can support the growth of acidophilic chemolithoautotrophic microorganisms. *Astrobiology* **5**, 406-414.

Goreva, J.S. and Lauretta D.S., 2004, Phosphate minerals in Semarkona. *Lunar and Planetary Science Conference* **XXXV**, 2065.

Grady, M.M., 2000, The Catalogue of Meteorites. Cambridge University Press, Cambridge, UK, 696 pp.

Grevesse, N. and Sauval, A.J., 1998, Standard solar composition. *Space Science Reviews*, **85,** 161-174.

Guerrier-Takada, C., Gardiner, K., Marsh, T., Pace, N., and Altman, S., 1983, The RNA moiety of ribonuclease P is the catalytic subunit of the enzyme. *Cell* **35**, 849-857.

Gulick, A., 1955, Phosphorus as a factor in the origin of life. *American Scientist* **43,** 479-489.

Gurvich, L. V., Veyts, I.V., and Alcock, C.B., 1994, Thermodynamic Properties of Individual Substances, 4th Ed., Vol. 3, Hemisphere Publishing, New York, NY, USA.

Halliday, I., Blackwell, A.T., and Griffin A.A., 1989, The flux of meteorites on the Earth's surface. *Meteoritics* **24**, 173-178.

Hallstedt, B., 1990, Assessment of the CaO-Al$_2$O$_3$ system. *Journal of the American Ceramics Society* **73**, 15-23.

Halmann, M., Sanchez, R.A., and Orgel, L.E., 1969, Phosphorylation of D-ribose in aqueous solution. *J. Org. Chem.* **34**, 3702-3703.

Halmann, M. and Schmidt, H-L., 1970, Cyanogen-induced synthesis of $^{18}$O-labelled B-ribofuranose-1-phosphate and its acid catalysed hydrolysis. *J. Chem. Soc.* **C**, 1191-1193.

Handschuh, G.J. and Orgel, L.E., 1973, Struvite and prebiotic phosphorylation. *Science* **179,** 483-484.

Hartmann, L. Calvet, N., Gullbring, E., and D'Alessio, P., 1998, Accretion and the evolution of T Tauri disks. *Astrophysical Journal* **495**, 385-400.

Hartmann, W.K., 2003, Megaregolith evolution and cratering cataclysm models- lunar cataclysm as a misconception (28 years later). *Meteoritics and Planetary Science* **38**, 579-594.

Harvey, R.P. and Cassidy, W.A. 1989. A statistical comparison of Antarctic finds and modern falls - mass frequency-distributions and relative abundance by type. *Meteoritics* **24**, 9-14.

Hawthorne, F.C., Cooper, M.A., Green, D.I., Starkey, R.E., Roberts, A.C., and Grice, J. D., 1999,  Wooldridgeite, $Na_2CaCu_2^{2+}(P_2O_7)_2(H_2O)_{10}$: a new mineral from Judkins Quarry, Warwickshire, England.  *Mineralogical Magazine* **63**, 13-16.

Hazen, R.M., 2005, Gen-e-sis: The Scientific Quest for Life's Origins.  Joseph Henry Press, Washington, D.C., USA, 339 pp.

Hegedus, L., Forsterling, H-D., Kokai, E., Pelle, K., Taba, G., Wittman, M., and Nozticzuas, Z., 2000, Chemical mechanism of the radical feedback loop in the classical BZ reaction. Malonyl bromite and oxalic acid as flow-through intermediates. *Phys. Chem. Chem. Phys.* **2**, 4023-4028.

Hermes-Lima, M. and Vieyra, A., 1989, Pyrophosphate formation from phospho(enol)pyruvate adsorbed onto precipitated orthophosphate: a model for prebiotic catalysis of transphosphorylations. *Origins of Life and Evolution of the Biosphere* **19,** 143-152.

Herndon, J. M. and Suess, H.E., 1976, Can enstatite meteorites form from a nebula of solar composition? *Geochimica et Cosmochimica Acta* **40**, 395-399.

Hersant, F., Gautier, D., and Hure, J., 2001, A two-dimensional model for the primordial nebula constrained by D/H measurements in the solar system: Implications for the formation of giant planets. *Astrophysical Journal* **554**, 391-407.

Hilderbrand, R.L. and Henderson, T.O.,1983, In *The Role of Phosphonates in Living Systems*, (Hilderbrand, R.L., ed.). CRC Press, Boca Raton, Florida, USA, 5-30.

Horiguchi, M. and Kandatsu, M., 1959, Isolation of 2-Aminoethane phosphonic acid from Rumen protozoa. *Nature* **184**, 901-902.

Howard, J.A., 1972, In *Advances in Free Radical Chemistry,* v. 4 (Williams, G.H., ed.). Academic Press, New York, NY, USA.

Hulshof, J. and Ponnamperuma, C., 1976, Prebiotic condensation-reactions in an aqueous-medium - review of condensing agents. *Origins of Life and Evolution of the Biosphere* **7,** 197-224.

Huré, J.-M., 2000, On the transition to self-gravity in low mass AGN and YSO accretion discs. *Astronomy and Astrophysics* **358**, 378-394.

Huss, G.R., 1991, Meteorite mass distributions and differences between Antarctic and non-Antarctic meteorites. *Geochimica et Cosmochimica Acta* **60**, 105-111.

Hutson, M.A. and Ruzicka, A., 2000, A multi-step model for the origin of E3 (enstatite) chondrites. *Meteoritics and Planetary Science* **35**, 601-608.

Ibanez, J.D., Kimball, A.P., and Oro, J., 1971, Possible prebiotic condensation of mononucleotides by cyanamide. *Science* **173,** 444-445.

Ikeda, Y. and Kimura, M., 1992, Mass-distribution of Antarctic ordinary chondrites and the estimation of the fall-to-specimen ratios. Meteoritics **27,** 435-441.

Ivanov, A.V., 1989, The Kaidun meteorite: composition and history. *Geochemistry International* **26**, 84-91.

Ivanov, A.V., Kononkova, N.N., and Guseva, Ye.V., 1993, Hydrothermal alteration of schreibersite and metallic iron in Kaidun III meteorite (EH5). *Geochemistry International* **30**, 11-19.

Ivanov, A.V., Zolensky, M.E., Saito, A., Ohsumi, K., Yang, S.V., Kononkova, N.N., Mikouchi, T., 2000, Florenskyite, FeTiP, a new phosphide from the Kaidun meteorite. *American Mineralogist* **85**, 1082-1086.

Joo, S.H., Feitz, A.J., Sedlak, D.L., and Waite, T.D., 2005, Quantification of the oxidative capacity of nanoparticulate zero valent iron. *Environmental Sci. Tech.* **39**, 1263-1268.

Joo, S.H., Feitz, A.J., and Waite, T.D., 2004, Oxidative degradation of the carbothioate herbicide, molinate, using nano-scale zero valent iron. *Environmental Sci. Tech.* **38**, 2242-2247.

Kakegawa, T., Noda, M., and Nannri, H., 2002, Geochemical cycles of bio-essential elements on the early Earth and their relationships to the origin of life. *Resource Geology*, 52(1), 83-89.

Kanavarioti, A., 1997, Dimerization in highly concentrated solutions of phosphoimidazolide activated mononucleotides. *Origins of Life and Evolution of the Biosphere* **27**, 357–376.

Kargel, J.S. and Lewis, J.S., 1993, The composition and early evolution of Earth. Icarus **105,** 1-25.

Kassel, L.S., 1933, Thermodynamic calculations from spectral data. *Phys. Rev.* **43**, 364-365.

Kassel, L.S., 1933, Mathematical methods for computing thermodynamic functions from spectral data. *J. Chem. Phys.* **1**, 576-585.

Keefe, A.D. and Miller, S.L., 1995, Are polyphosphates or phosphate esters pre-biotic reagents? *Journal of Molecular Evolution* **41,** 693-702.

Keefe, A.D. and Miller, S.L., 1996, Potentially prebiotic syntheses of condensed phosphates. *Origins of Life and Evolution of the Biosphere* **26,** 15-25.

Knacke, O., Kubaschewski, O., and Hesselmann, K., 1991, Thermochemical Properties of Inorganic Substances, Springer-Verlag, Heidelberg, Germany.

Koeberl, C., Reimold, W.U., McDonald, I., and Rosing, M., 2000, Search for petrographic and geochemical evidence for the late heavy bombardment on Earth in early Archean rocks from Isua, Greenland. *Lecture Notes in Earth Sciences* **91**, 73-97.

Kolb, V, Zhang, S.B., Xu, Y., and Arrhenius, G., 1997, Mineral-induced phosphorylation of glycolate ion- a metaphor in chemical evolution. *Origins of Life and Evolution of the Biosphere* **27**, 485-503.

Kongjiang, W., Zhifang, C., and Xianming, P., 1999, Enhanced photolysis of nucleic acid monomers by pyrophosphate in the simulated primitive soup. *Origins of Life and Evolution of the Biosphere* **29,** 261–272.

Kring, D.A. and Cohen, B.A., 2002, Cataclysmic bombardment throughout the inner solar system 3.9-4.0 Ga. *Journal of Geophysical Research* **107(E2)**, 1-6.

Krishnamurthy, R., Arrhenius, G., and Eschenmoser, A., 1999, Formation of glycolaldehyde phosphate from glycolaldehyde in aqueous solution. *Origins of Life and Evolution of the Biosphere* **29,** 333–354.

Krishnamurthy, R., Pitsch, S., and Arrhenius, G., 1999, Mineral induced formation of pentose-2,4-bisphosphates. *Origins of Life and Evolution of the Biosphere* **29,** 139–152,

Kruger, K. Grabowski, P.J., Zaug, A.J., Sands, J., Gottschling, D.E., and Cech, T.R., 1982, Self-splicing RNA: autoexcision and autocatalyzation of the ribosomal RNA intervening sequence of Tetrahymena. *Cell* **31**, 147-157.

Kyte, F.T. and Wasson, J.T., 1986, Accretion rate of extraterrestrial material: iridium deposited 33 to 67 million years ago. *Science* **232**, 1225-1229.

Lange H.C. and Heijnen, J.J., 2001, Statistical reconciliation of the elemental and molecular biomass composition of Saccharomyces cerevisiae. *Biotechnology and Bioengineering* **75,** 334-344.

Larimer, J. W., 1968. An experimental investigation of oldhamite CaS; and the petrologic significance of oldhamite in meteorites. *Geochimica et Cosmochimica Acta* **32**, 965-982.

Larimer, J.W. and Bartholomay, M., 1979, The role of carbon and oxygen in cosmic gases: some applications to the chemistry and mineralogy of enstatite chondrites. *Geochimica et Cosmochimica Acta* **43**, 1455-1466.

Lauquin, G. and Vignais, P.V., 1973, Adenine-nucleotide translocation in yeast mitochondria effect of inhibitors of mitochondrial biogenesis on ADP-translocase *Biochim. Biophys. Acta* **305,** 534-556.

Lauretta, D.S., Kremser, D.T., and Fegley, B.J., 1996, The rate of iron sulfide formation in the solar nebula. *Icarus* **122**, 288-315.

Lauretta, D.S., Lodders, K., and Fegley, B., 1997, Experimental simulations of sulfide formation in the solar nebula. *Science* **277**, 358-360.

Lauretta, D. S., Lodders, K., and Fegley, B., 1998, Kamacite sulfurization in the solar nebula. *Meteoritics and Planetary Science* **33**, 821-833.

Lin, C., Fu, H., Zhao, Y., and Cheng, C., 2005, Synthesis of nucleoside n-phosphoamino acids and peptide formation. *Origins of Life and Evolution of Biospheres* **35,** 11–17.

Lin, Y. and El Goresy, A., 2002, A comparative study of opaque phases in Qingzhen (EH3) and MacAlpine Hills 88136 (EL3): Representatives of EH and EL parent bodies.

*Meteoritics and Planetary Science* **37**, 577-599.

Lodders, K., 1999, Revised Thermochemical Properties of Phosphinidene (PH), Phosphine ($PH_3$), Phosphorus Nitride (PN), and Magnesium Phosphate ($Mg_3P_2O_8$). *Journal of Physical Chemistry Reference Data* **28**, 1705-1712.

Lodders, K., 2003, Solar system abundances and condensation temperatures of the elements. *Astrophysical Journal* **591**, 1220-1247.

Lodders, K. and Fegley, B., 1998, The Planetary Scientist's Handbook. Oxford University Press, Oxford, UK, 371 pp.

Lohrmann, R. and Orgel, L.E., 1968, Prebiotic synthesis: phosphorylation in aqueous solution. *Science* **171**, 64-66.

Love, S.G. and Brownlee, D.E., 1993, A direct measurement of the terrestrial massaccretion rate of cosmic dust. *Science* **262**, 550-553.

Lunine, J. I., Coradini, A., Gautier, D., Owen, T., and Wuchterl, G., 2003. In *Jupiter* (Bagenal, F. ed.). Cambridge University Press, London, UK, 748 pp.

Lunine, J. I., Owen, T.C., and Brown, R.H., 2000, In *Protostars and Planets IV* (Mannings, V., Boss, A.P., and Russel, S., eds.). University of Arizona Press, Tucson, AZ, USA, 1055-1080.

Macià, E., 2005, The role of phosphorus in chemical evolution. *Chem. Soc. Rev*. **34**, 1-14.

Macià, E., Hernández, M.V., and Oró, J., 1997, Primary sources of phosphorus and phosphates in chemical evolution. *Origins of Life and Evolultion of the Biosphere* **27,** 459-480.

Mackinnon, I.D.R. and Zolensky, M.E., 1984, Proposed structures for poorly characterized phases in C2M carbonaceous chondrite meteorites. *Nature* **309**, 240-242.

Makalkin, A.B. and Dorofeyeva, V.A., 1991, Temperatures in the protoplanetary disk: Models, constraints and consequences for the planets. *Izv. Earth Phys.* **27**, 650-664.

McGrath, J.W., Ternan, N.G., and Quinn, J.P., 1997, Utilization of organophosphonates by environmental microorganisms. *Letters in Applied Microbiology* **24**, 69-73.

Meibom, A. and Clark, B.E., 1999, Evidence for the insignificance of ordinary chondritic matter in the asteroid belt. *Meteoritics and Planetary Science* **34**, 7-24.

Mendeleyev, D.I., 1891, The Principles of Chemistry. Longmans, Green, London, UK 611 pp.

Miller, S.L., 1953, A production of amino acids under possible primitive Earth conditions. *Science* **117**, 528-529.

Miller, S.L. and Parris, M., 1964, Synthesis of pyrophosphate under primitive earth conditions. *Nature* **204,** 1248-1250.

Mittlefehldt, D.W., McCoy, T.J., Goodrich, C.A., and Kracher, A., 1998, In *Planetary Materials, Reviews in Mineralogy v.36* (Papike, J.J., ed.).  Mineralogical Society of America, Washington, D.C. USA, Ch. 4.

Moggi-Cecchi, V., Bindi, L., and Pratesi, G., 2005, A new iron-nickel phosphide from the Northwest Africa 1054 Meteorite. *Meteoritics and Planetary Science* **40**, A5308.

Monnard, P-A., Apel, C.L., Kanavarioti, A., and Deamer, D.W., 2002, Influence of ionic inorganic solutes on self-assembly and polymerization processes related to early forms of life: Implications for a prebiotic aqueous medium. *Astrobiology* **2**, 139-152.

Moore, C.B., Lewis, C.F., Gibson, E.K., and Nichiporuk, W., 1970, Total carbon and nitrogen abundances in lunar samples. *Science* **167** 495-497.

Moore, C.B., 1971, In *Handbook of Elemental Abundances in Meteorites*, (Mason, B., ed.). Gordon and Breach Science Publishers, New York, NY, USA, 131-136.

Morfill, G. E. and Volk, H.J., 1984, Transport of dust and vapor and chemical fractionation in the early protosolar cloud. *Astrophysical Journal* **287**, 371-395.

Munroe, M. 2004.,  Molecular Weight Calculator v. 6.37. http://www.alchemistmatt.com

Nazarov, M.A., Brandstaetter, F., and Kurat, G., 1998, Phosphorian sulfides and phosphides in CM chondrites. *Geokhimiya* **36**, 415-424.

Nelson, D.L., and Cox, M.M., 2005, Lehninger's Principles of Biochemistry, Fourth Edition. W.H. Freeman and Company, New York, New York, USA, 1100 pp.

Noguchi, Y., Nakai, Y., Shimba, N., Toyosaki, H., Kawahara, Y., Sugimoto, S., and Suzuki, E., 2004, The energetic conversion competence of Escherichia coli during aerobic respiration studied by $^{31}$P NMR using a circulating fermentation system. *Journal of Biochemistry* **136**, 509–515.

Norton, O.R., 2002, The Cambridge encyclopedia of meteorites. Cambridge University Press, Cambridge, UK, 374 pp.

Olsen E.J., Kracher A., Davis A.M., Steele I.M., Hutcheon I.D., and Bunch T.E., 1999, The phosphates of IIIAB iron meteorites. *Meteoritics and Planetary Science* **34,** 285-300.

Oparin, A.I., 1938, The Origin of Life. Translated by Sergius Morgulis. Dover Publications, Inc., New York, New York, USA. 270 pp.

Orgel, L.E., 1968, Evolution of the genetic apparatus. *Journal of Molecular Biology* **38**, 381-393.

Orgel, L.E., 2004, Prebiotic chemistry and the origin of the RNA world. *Critical Reviews in Biochemistry and Molecular Biology* **39**, 99-123.

Oró, J., 2002, In *Life's Origin* (Schopf, J.W., ed.). University of California Press, Berkeley, California, USA, 7-45.

Osterberg, R. and Orgel, L.E., 1972, Polyphosphate and trimetaphosphate formation under potentially prebiotic conditions. *J. Mol. Evol* **1**, 241-248.

Owen, T., Mahaffy, P., Niemann, H.B., Atreya, S.K., Donahue, T.M., Bar-Nun, A., and de Pater, I., 1999, A new constraint on the formation of giant planets. *Nature* **402**, 269-270.

Ozawa, T. and Hanaki, A., 1987, Spin-trapping of phosphorus-containing inorganic radicals by a water-soluble spin-trap, 3,5-dibromo-4-nitrosobenzenesulfonate. *Chemistry Letters* **1987**, 1885-1888.

Ozawa, T. and Hanaki, A., 1989, Spin trapping of short-lived phosphorus-containing inorganic radicals. *Nippon Kagaku Kaishi* **8**, 1408-1411.

Paillou, P., Barkooky, A.E., Barakat, A., Malezieux, J-M., Reynard, B., Dejax, J., and Heggy, E., 2004, Discovery of the largest impact crater field on Earth in the Gilf Kebir region, Egypt. *C.R. Geoscience* **336**, 1491-1500.

Parsons, A.F., 2000, An Introduction to Free Radical Chemistry. Blackwell Sciences Ltd., Oxford, UK, 238 pp.

Pasek, M.A. and Lauretta, D.S., 2005, Aqueous corrosion of phosphide minerals from iron meteorites: a highly reactive source of prebiotic phosphorus on the surface of the early Earth. *Astrobiology* **5**, 515-535.

Pasek, M.A., Milsom, J.A., Ciesla, F.J., Lauretta, D.S., Sharp, C., and Lunine, D.S., 2005, Sulfur chemistry in protoplanetary nebulae with time-varying oxygen abundances. *Icarus* **175**, 1-14.

Pasek, M.A., Smith, V.D., and Lauretta, D.S., 2004, A quantitative NMR analysis of phosphorus in carbonaceous and ordinary chondrites. *Lunar and Planetary Science Conference* **XXXV**, 1703.

Peacor, D.R., Dunn, P.J., Simmons, W.B., and Wicks, F.J., 1985, Canaphite, a new sodium calcium phosphate hydrate from the Paterson area, New Jersey. *Mineralogical Record* **16**, 467-468.

Petaev, M.I., Lavrukhina, A.K., and Khodakovskiy, I.L., 1986, Genesis of minerals of enstatite meteorites. *Geokhimiya* **9**, 1219-1232.

Peyser, J.R. and Ferris, J.P., 2001, The rates of hydrolysis of thymidyl-3',5'-thymidine-H-phosphonate: The possible role of nucleic acids linked by diesters of phosphorous acid in the origins of life. *Origins of Life and Evolution of the Biosphere* **31,** 363-380.

Pierazzo, E., and Chyba, C.F., 1999, Amino acid survival in large cometary impacts. *Meteoritics and Planetary Science* **34**, 909-918.

Pitsch, S., Pombovillar, E., and Eschenmoser, A., 1994, Chemistry of α-aminonitriles.13. Formation of 2-oxoethyl phosphates (glycolaldehyde phosphates) from *rac*-oxiranecarbonitrile and on (formal) constitutional relationships between 2-oxoethyl phosphates and oligo(hexopyranosyl and pentopyranosyl) nucleotide backbones. *Helvetica Chimica Acta* **77 ,** 2251-2285.

Pizarello, S., 2006, In *Meteorites and the Early Solar System*, v. 2.  In press.

Ponnamperuma, C., and Chang, S., 1971, In *Chemical Evolution and the Origin of Life,* (Buvet, R. and Ponnamperuma, C., eds.). North-Holland, Amsterdam, Netherlands.

Ponnamperuma, C. and Mack, R., 1965, Nucleotide synthesis under possible primitive Earth conditions.  *Science* **148**, 1221-1223.

Popova, V.I., Popov, V.A., Sokolova, E.V., Ferraris, G., and Chukanov, N.V., 2002, Kanonerovite, $MnNa_3P_3O_{10}(H_2O)_{12}$, first triphosphate mineral (Kazennitsa pegmatite, Middle Urals, Russia).   *Neues Jahrbuch fuer Mineralogie, Monatshefte* **3**, 117-127.

Prabahar, K.J. and Ferris, J.P., 1997, Effect of dinucleoside pyrophosphates on the oligomerization of activated mononucleotides on $Na^+$-montmorillonite: reaction of 5'-phosphoro-4-(dimethylamino)pyridinium [4-$(CH_3)_2$NPYPA] with A5'ppA. *Origins of Life and Evolution of the Biosphere* **27,** 513–523.

Prieto, C.A., Lambert, D.L., and Asplund, M., 2001, The forbidden abundance of oxygen in the sun. *Astrophysical Journal* **556,** L63-L66.

Prieto, C.A., Lambert, D.L. and Asplund, M., 2002, A reappraisal of the solar photospheric C/O ratio. *Astrophysical Journal* **573,** L137-L140.

Pringle, J.E., 1981, Accretion discs in astrophysics. *Annual Review of Astronomy and Astrophysics* **19**, 137-162.

Rabinowitz, J., Chang, S., and Ponnamperuma, C., 1968, Phosphorylation on the primitive Earth. *Nature* **218**, 442-443.

Ramdohr, P., 1963, The opaque minerals in stony meteorites. *Journal of Geophysical Research* **68**, 2011-2036.

Redfield, A.C., 1958, The biological control of chemical factors in the environment. *American Scientist* **46**, 205-221.

Reed, S.J.B., 1968, Perryite in the Kota-Kota and South Oman enstatite chondrites. *Mineralogical Magazine and Journal of the Mineralogical Society* **36**, 850-854.

Reimann, R. and Zubay, G., 1999, Nucleoside phosphorylation: a feasible step in the prebiotic pathway to RNA. *Origins of Life and Evolution of the Biosphere* **29,** 229–247.

Ricardo, A., Carrigan, M. A., Olcott, A. N., and Benner, S. A., 2004, Borate minerals stabilize ribose. *Science* **303,** 196.

Rietmeijer, F.J.M., 1989, Ultrafine-grained mineralogy and matrix chemistry of olivine-rich chondritic interplanetary dust particles. *Proc. Lunar Planet. Sci. Conf.* **19**, 513-521.

Rietmeijer, F.J.M., 1998, In *Planetary Materials: Reviews in Mineralogy, v. 36* (Papike, J.J., ed.). The Mineralogical Society of America, Washington DC, USA, Ch. 2.

Robitaille, P-M. L., Robitaille, P.A., Brown, G.G. Jr., and Brown, G.G., 1991, An analysis of the pH-dependent chemical-shift behavior of phosphorus-containing metabolites. *Journal of Magnetic Resonance* **92**, 73-84.

Roche Applied Science, 2005/2006, Chemical data for $Na_2ATP \cdot 3H_2O$. *Roche Applied Science Data* **2005/2006**, 112.

Ryder, G., 2003, Bombardment of the Hadean Earth: wholesome or deleterious? *Astrobiology* **3**, 3-6.

Rytting, E., Lentz, K.A., Chen, X-Q., Qian, F., and Venkatesh, S., 2005, Aqueous and cosolvent solubility data for drug-like organic compounds. *The AAPS Journal* **7**, E78-E105.

Sales, B.C., Chakoumakos, B.C., Boatner, L.A., and Ramey, J.O., 1992, Structural evolution of the amorphous solids produced by heating crystalline MgHPO$_4$·3H$_2$O. *J. Mater. Res.* **7**, 2646-2649.

Salpeter, E.E., 1974, Nucleation and growth of dust grains. *Astrophysical Journal* **193**, 579-584.

Sankarapandi, S. and Zweier, J.L., 1999, Evidence against the generation of free hydroxyl radicals from the interaction of copper, zinc-superoxide dismutase and hydrogen peroxide. *Journal of Biological Chemistry* **274**, 34576–34583.

Satre, M., Martin, J-B., and Klein, G., 1989, Methyl phosphonate as a ^{31}P-NMR probe for intracellular pH measurements in Dictyostelium amoebae. *Biochimie* **71,** 941-948.

Saygin, O., 1981, Nonenzymatic photophosphorylation with visible light.  A possible mode of prebiotic ATP formation.  *Naturwissenschaften* **68**, 617-619.

Saygin, O., 1983, Nonenzymatic photophosphorylation of acetate by carbamyl phosphate. A model reaction for prebiotic activation of carboxyl groups. *Origins of Life and Evolution of the Biosphere* **13,** 43-48.

Schmidt, G., Palme, H., and Kratz, K.-L., 2005, Chemical evidence of asteroidal fragments (iron meteorites and/or pallasites) in the earth's upper continental crust? *Meteoritics and Planetary Science* **40**, A5015.

Schoenberg, R., Kamber, B.S., Collerson, K.D., and Moorbath, S., 2002, Tungsten isotope evidence from ~3.8-Gyr metamorphosed sediments for early meteorite bombardment of the Earth. *Nature* **418**, 403-405.

Schwartz, A.W., 1972, In *Molecular Evolution Prebiological and Biological* (Rohlfing, D.L. and Oparin, A.I., eds.) Plenum Press, New York, New York, USA, 129-140.

Schwartz, A.W., 1997, Prebiotic phosphorus chemistry reconsidered. *Origins of Life and Evolution of the Biosphere* **27,** 505-512.

Schwartz, A.W. and Ponnamperuma, C., 1968, Phosphorylation on the primitive earth. Phosphorylation of adenosine with linear polyphosphate salts in aqueous solution. *Nature* **218,** 443.

Schwartz, A.W. and Van der Veen, M., 1973, Synthesis of hypophosphate by ultraviolet irradiation of phosphite solutions. *Inorg. Nucl. Chem. Lett.* **9**, 39-41.

Schwartz, A.W., Van der Veen, M., Bisseling, T., and Chittenden, G.J.F., 1975, Prebiotic nucleotide synthesis- demonstration of a geologically plausible pathway. *Origins of Life and Evolution of the Biosphere* **6**, 163-168.

Shakura, N.I. and Sunyaev, R.A., 1973, Black holes in binary systems. Observational appearance. *Astronomy and Astrophysics* **24**, 337-355.

Shapiro, R., 1986, A Skeptic's Guide to the Creation of Life on the Earth. Summit Books, New York, NY, USA, 332 pp.

Shapiro, R., 2000, A replicator was not involved in the origin of life. *IUBMB Life* **49,** 173-176.

Sharp, C.M. and Huebner, W.F., 1990, Molecular equilibrium with condensation. *Astrophysical Journal Supplement Series* **72**, 417-431.

Sharp, C.M. and Huebner, W.F., 1993, Molecular equations of state with condensation (MESC) for astrophysical applications. *Southwest Research Institute Report* **93-1**.

Sherwood, E. and Oro, J., 1977, Cyanamide mediated syntheses under plausible primitive earth conditions II. The polymerization of deoxythymidine 5'-triphosphate. *J. Mol. Evol.* **10**, 183-192.

Shock, E.L. and Schulte, M.D., 1990, Amino-acid synthesis in carbonaceous meteorites by aqueous alteration of polycyclic aromatic-hydrocarbons. *Nature* **343**, 728-731.

Shu, F.H., Tremaine, S., Adams, F.C., and Ruden, S.P., 1990, Sling amplification and eccentric gravitational instabilities in gaseous disks. *Astrophysical Journal* **358**, 495-514.

Smith, J.V., 1998, Biochemical evolution. I. Polymerization on internal, organophilic silica surfaces of dealuminated zeolites and feldspars. *Proc. Natl. Acad. Sci.* **95**, 3370–3375.

Spikakov, B.Ya., Maryutina, T.A., and Muntau, H. (1999) Phosphorus speciation in water and sediments. *Pure Appl. Chem.,* 71(11), 2161-2176.

Srinivasan, V. and Morowitz, H.J., 2004, Intermediary metabolism in the early assembly of cellular life. Abstracts of Papers, 228th ACS National Meeting 2004.

Steinman, G., Lemmon, R.M., and Calvin, M., 1964, Cyanamide: a possible key compound in chemical evolution. *Proc. Natl. Acad. Sci. USA* **52**, 27-30.

Steinman, G., Kenyon, D.H., and Calvin, M., 1965, Dehydration condensation in aqueous solution. *Nature* **206**, 707-708.

Stevenson, D.J. and Lunine, J.I., 1988, Rapid formation of Jupiter by diffuse redistribution of water vapor in the solar nebula. *Icarus* **75**, 146-155.

Supulver, K.D. and Lin, D.N.C., 2000. Formation of icy planetesimals in a turbulent solar nebula. *Icarus* **146**, 525-540.

Sweeny, K.H., 1981, The reductive treatment of industrial waters: I Process description. *American Institute of Chemical Engineers, Symposium Series, Water-1980* **77,** 72-78.

Swindle, T.D., Kring, D.A., Olson, E.K., and Isachsen, C.E., 2006, Ar-Ar dating of shock-melted ordinary chondrites: chronology of asteroidal impacts. *Lunar and Planetary Science Conference* **XXXVII**, 1454.

Terelli, E. and Wheeler, S.F., 1993, Formation of esters, especially phosphate esters, under 'dry' conditions and 'mild' pH. *Chem. Industry* **1993**, 164-165.

Thomas, K. L., Blandford, G. E., Keller, L. P., Klock, W., and McKay, D. S., 1993, Carbon abundance and silicate mineralogy of anhydrous interplanetary dust particles. *Geochim. Cosmochim. Acta* 57, 1551-1566.

Valsami-Jones, E., 2004, In *Phosphorus in Environmental Technology: Principles and Applications* (Valsami-Jones, E., ed.). IWA Publishing, London, UK, 20-50.

Van Wazer, J.R., 1958, Phosphorus and Its Compounds, vol. 1. Interscience, New York, NY, USA, 954 pp.

Wächtershäuser, G., 1988a, Before enzymes and templates: theory of surface metabolism. *Microbiol. Rev.* **52**, 452-484.

Wächtershäuser, G., 1988b, Pyrite formation, the first energy source for life: a hypothesis. *Syst. Appl. Microbiol.* **10**, 207-210.

Wachtershauser, G., 1992, Groundworks for an evolutionary biochemistry - the iron sulfur world. *Progress in Biophysics & Molecular Biology* **58**, 85-201.

Wagner, E., Xiang, Y.B., Baumann, K., Guck, J., and Eschenmoser, A., 1990, Chemistry of α-aminonitriles-aziridine-2-carbonitrile, a source of racemic O3-phosphoserinenitrile and glycolaldehyde phosphate. *Helvetica Chimica Acta* **73,** 1391-1409.

Walling, C., 1976, Fenton's reagent revisited. *Accounts of Chemical Research* **8**, 125-131.

Walling, C. and Padwa, A., 1963, Positive halogen compounds .7. Intramolecular chlorinations with long chain hypochlorites. *J. American Chem. Soc.* **85**, 1597-1601.

Wang, W.F., Schuchmann, M.N., Schuchmann, H.P., and von Sonntag, C., 2001, The importance of mesomerism in the termination of α-carboxymethyl radicals from aqueous malonic and acetic acids. *Chem. Eur. J.* **7**, 791-795.

Weaver, B.L. and Tarney, J., 1984, in *Physics and Chemistry of the Earth* (Pollack, H.N. and Murthy, V.R., eds.), v. 15.  Pergamon, Oxford, UK, 39-68.

Weber, A.L., 1981, Formation of pyrophosphate, tripolyphosphate, and phosphorylimidazole with the thioester, N,S-diacetylcysteamine, as the condensing agent. *J. Mol. Evol.* **18**, 24-29.

Weber, A.L., 1982, Formation of pyrophosphate on hydroxyapatite with thioesters as condensing agents. *Biosystems* **15,** 183-189.

Weber, A. L., 2001, The sugar model: catalysis by amines and amino acid products. *Origins of Life and Evolution of the Biosphere* **31**, 71-86.

Weck, P.F., Schweitzer, A., Stancil, P.C., Hauschildt, P.H. and Kirby, K., 2003, The molecular line opacity of MgH in cool stellar atmospheres. *The Astrophysical Journal* **582**, 1059-1065.

Wedepohl, K.H., 1995, The composition of the continental-crust. *Geochimica et Cosmochimica Acta* **59,** 1217-1232.

Westheimer, F.H., 1987, Why nature chose phosphate. *Science* **235**, 1173-1178.

White, W.B., Johnson, S.M., and Dantzig, G.B., 1958, Chemical equilibrium in complex mixtures. *Journal of Chemical Physics* **28**, 751-755.

Whittaker, R. H., 1970, Communities and Ecosystems. Macmillan, Toronto, ON, CA, 83.

Whittet, D.C.B., 1997, Is extraterrestrial organic matter relevant to the origin of life on the Earth? *Origins of Life and Evolution of the Biosphere* **27**, 249-262.

Willis, J., 1980, The bulk composition of iron meteorite parent bodies. Ph.D. Dissertation, University of California at Los Angeles, 208 pp.

Wlotzka, F., 1993, A weathering scale for the ordinary chondrites. *Meteoritics* **28**, A460.

Wood, J.A. and Hashimoto, A., 1993, Mineral equilibrium in fractionated nebular Systems. *Geochimica et Cosmochimica Acta* **57**, 2377-2388.

Wright, I.P. and Gilmour I., 1990, Meteoritics - origin of organic materials. *Nature* **345**, 110-111.

Wolf, D., and Palme, H., 2001, The solar system abundances of phosphorus and titanium and the nebular volatility of phosphorus. *Meteoritics and Planetary Science* **36**, 559-571.

Yamagata, Y., 1999, Prebiotic formation of ADP and ATP from AMP, calcium phosphates and cyanate in aqueous solution. *Origins of Life and Evolution of the Biosphere* **29,** 511–520.

Yamagata, Y. and Inomata, K., 1997, Condensation of glycylglycine to oligoglycines with trimetaphosphate in aqueous solution II: catalytic effect of magnesium ion. *Origins of Life and Evolution of the Biosphere* **27**, 339–344.

Yamagata, Y., Matsukawa, T., Mohri, T., and Inomata, K., 1979, Phosphorylation of adenosine in aqueous-solution by electric-discharges. *Nature* **282**, 284-286.

Yamagata, Y. and Mohri, T., 1982, Formation of cyanate and carbamyl phosphate by electric discharges of model primitive gas. *Origins of Life and Evolution of Biospheres* **12,** 41-44.

Yamagata, Y., Mohri, T., Yamakoshi, M., and Inomata, K., 1981, Constant AMP synthesis in aqueous solution by electric discharges. *Origins of Life and Evolution of Biospheres* **11,** 233-235.

Yamagata, Y., Watanabe, H., Saitoh, M., and Namba, T., 1991, Volcanic production of polyphosphates and its relevance to prebiotic evolution. *Nature* **352**, 516-519.

Yang, C-W., Williams, D.B., and Goldstein, J.I., 1996, A revision of the Fe-Ni phase diagram at low temperatures (<400 °C). *J. Phase Equilibria* **17**, 522-531.

Yoza, N. and Ohashi, S., 1965, Oxidation of red phosphorus with hydrogen peroxide and isolation of disodium dihydrogen hypophosphate. *Bulletin of the Chemical Society of Japan* **38,** 1408-1409.

Yoza, N., Ueda, N., and Nakashima, S., 1994, pH-dependence of P-31-NMR spectroscopic parameters of monofluorophosphate, phosphate, hypophosphate, phosphonate, phosphinate and their dimers and trimers. *Fresen. J. Anal. Chem.* **348**, 633-638.

Zaitsev, A.I., Dobrokhotova, Z.V., Litvina, A.D., and Mogutnov, B.M., 1995, Thermodynamic properties and phase equilibria in the Fe-P system. *Journal of the Chemical Society: Faraday Transactions* **91**, 703-712.

Zolensky, M.E. and Lindstrom, D., 1992, Mineralogy of 12 large chondritic interplanetary dust particles. *Proc. Lunar Planet. Sci.* **22**, 161-169.